



**MONASH** University

**The Role of MHCII Quality and Quantity  
in Determining CD8 T cell  
Development, Survival and Function**

*Yi Xiong, Xavier Sng*

*Doctor of Philosophy*

**A thesis submitted to Monash University  
In fulfilment of the requirements for the degree of  
Doctor of Philosophy**

**December 2019**

**Department of Biochemistry and Molecular Biology  
School of Biomedical Sciences  
Faculty of Medicine, Nursing and Health Sciences**

## Copyright Notice

© Yi Xiong, Xavier Sng (2019).

## Abstract

The major histocompatibility complex class I (MHCI) molecule is essential for the development, homeostatic maintenance, and activation of CD8 T cells. While it is clear that MHCI molecules are crucial in these processes, it is not clear how the similarities and differences between MHCI molecules and gene dosage influences the resulting CD8 T cell population.

Alloreactive CD8 T cells recognize and are activated by alternative MHCI molecules that were not expressed during thymic development and these cells can comprise up to 10% of the CD8 T cell population. It is not clear precisely how instruction on one MHC determines the number and quality of CD8 T cells specific for an alternative MHC. In my BSc. (Hons) project, I had characterized a population of alloreactive H-2D<sup>b</sup>PA<sub>224</sub>-specific CD8 T cells that were selected on the mismatched H-2K<sup>b</sup> molecule in H-2D<sup>b/-</sup> mice. Here, I further demonstrated that alloreactive H-2D<sup>b</sup>PA<sub>224</sub>-specific T cells have lower affinity for H-2D<sup>b</sup>PA<sub>224</sub> and are poorly responsive to stimulation *in vivo*. When I attempted the reciprocal experiment, isolating alloreactive CD8 T cells in H-2K<sup>b/-</sup> mice, I detected a peptide-independent, pan-H-2K-reactive population of CD8 T cells, characterised by the expression of memory markers, including the NK cell receptor Ly49C. *In vitro* analysis illustrated that H-2K<sup>b</sup> tetramers can interact with Ly49C and I therefore propose a model where Ly49C is mediating the non-specific binding to H-2K tetramers. This model also implies a novel mechanism, whereby the function of conventional memory phenotype CD8 T cells is regulated by the inhibitory NK receptor.

To investigate the impact of MHCI gene dosage on the generation and survival of polyclonal CD8 T cell populations, I generated MHCI hemizygous knockout mice expressing a single allele of one MHCI gene. Hemizygous mice expressed half the level of MHCI molecules and had half the level of circulating naïve CD8 T cells ( $T_N$ ). Despite this, hemizygous mice had normal thymic generation and output of  $T_N$  cells, suggesting that MHCI expression in the thymus is in excess of what is required for optimal CD8 T cell development. In the periphery,  $T_N$  cells retained in hemizygous mice exhibited higher levels of self-reactivity and were superior in cytokine production during infection. This highlights the importance of MHCI molecules in delimiting the size of the CD8  $T_N$  pool and it suggests an additional mechanism by which MHC heterozygosity confers a biological advantage over MHC homozygosity.

Finally, I investigated the effect of immunodomination by one MHCI-restricted population on another during infection, by infecting H-2K<sup>b-/-</sup> and H-2D<sup>b-/-</sup> mice with influenza A virus and analysing epitope-specific CD8 T cell responses after infection. Analyses revealed that immunodominant responses have an improved capacity to compensate for the loss of an MHCI-restricted response by, in part, increasing recruitment of high avidity cells from the naïve pool. Subdominant responses remained unchanged despite the loss of an MHCI gene, suggesting that subdominant CD8 T cells were less flexible in the magnitude of their responses.

Altogether, this thesis has expanded our understanding of MHCI determinants regulating CD8 T cell selection, maintenance and activation.

## **Declaration**

This thesis is an original work of my research and contains no material which has been accepted for the award of any other degree or diploma at any university or equivalent institution and that, to the best of my knowledge and belief, this thesis contains no material previously published or written by another person, except where due reference is made in the text of the thesis.

Signature:

Print Name: Yi Xiong, Xavier Sng

Date: 26<sup>th</sup> December 2019

## Communications

My research degree has resulted in the following communications:

### Journal articles

Prier J.E., Li J, Gearing L.J., Olshansky M, Sng YX.X, Hertzog P.J., Turner S.J. 2019. Early T-BET expression ensures an appropriate CD8<sup>+</sup> lineage-specific transcriptional landscape after influenza A virus infection. *Journal of Immunology* 203(4): 1044-1054.

Wu T, Guan J, Handel A, Tschärke D.C., Sidney J, Sette A, Wakim L.M., Sng YX.X, Thomas P.G., Croft N.P., Purcell A.W., La Gruta N.L. 2019. Quantification of epitope abundance reveals the effect of direct and cross-presentation on influenza CTL responses. *Nature Communications* 10(1): 2846-2859.

Quinn K.M., Fox A, Harland K.L., Russ B.E., Li J, Nguyen TH.O, Loh L, Olshansky M, Naeem H, Tsyganov K, Wide F, Webster R, Blyth C, Sng YX. X, Tiganis T, Powell D, Doherty P.C., Tuner S.J., Kedzierska K, La Gruta N.L. 2018. Age-related decline in primary CD8<sup>+</sup> T cell responses is associated with the development of senescence in virtual memory CD8<sup>+</sup> T cells. *Cell Reports* 23(12): 3512-3524.

Gras S, Chadderton J, Del Campo C.M., Farenc C, Wiede F, Joseph T.M., Sng YX.X, Mirams M, Watson K.A., Tiganis T, Quinn K.M., Rossjohn J, La Gruta N.L. 2016. Reversed T cell receptor docking on a major histocompatibility class I complex limits involvement in the immune response. *Immunity* 45(4): 749-760.

Quinn K.M., Zaloumis S.G., Cukalac T, Kan W.T., Sng YX.X, Mirams M, Watson K.A., McCaw J.M., Doherty P.C., Thomas P.G., Handel A, La Gruta N.L. 2016. Heightened self-reactivity associated with selective survival, but not expansion, of naïve virus-specific CD8<sup>+</sup> T cells in aged mice. *Proceedings of the National Academy of Sciences USA* 113(5): 1333-1338.

### **Manuscripts in preparation**

Sng YX.X, Li J, Zareie P, Assmus L, Lee J, Jones C.M., Turner S.J., Daley S.R., Quinn K.M., La Gruta N.L. The impact of MHC class I dose on development and maintenance of the polyclonal naïve CD8<sup>+</sup> T cell repertoire (**Submitted**).

Sng YX.X, Zareie P, Li J, Morey A, Turner S.J., Quinn K.M., La Gruta N.L. Positive selection of an alloreactive epitope-specific CD8 T cell population on an allogeneic MHCI molecule impairs TCR-dependent functionality.

Li J, Hardy K, Olshansky M, Barugahare A, Gearing L.J., Prier J.E., Sng YX.X, Nguyen M.L.T., Piovesan D, Russ B.E., La Gruta N.L., Hertzog P.J., Rao S, Turner S.J. KDM6B-dependent chromatin remodelling underpins effective virus-specific CD8<sup>+</sup> T cell differentiation.

Wirasinha R.C., Davies A.R., Srivastava M, Sheridan J.M., Sng YX.X, Loh K.L., Delmonte O.M., Rowe J.J., Miosge L.A., Lee C.E., Chand R, Chan A, Yap JY, Goodnow C.C., Keller M.D., Chen K, Reid H.H., Rossjohn J, Notarangelo L.D., La Gruta N.L., Gray D.H.D., Cook M.C., Daley S.R. NF- $\kappa$ B2 processing regulates thymic tolerance and prevents human autoimmune disease.

Assmus L, Guan J, Wu T, Zareie P, Nguyen A, Sng YX.X, Rossjohn J, Thomas P.G., Gras S, Croft N.P., Purcell A.W., La Gruta N.L. Overlapping peptides elicit distinct T cell responses during influenza A virus infection.

## **Oral presentations**

Sng YX.X, Li J, Zareie P, Assmus L, Lee J, Turner S.J., Daley S.R., Quinn K.M., La Gruta N.L. 2019. MHCI expression level delimits naïve CD8 T cell population size and quality. *17<sup>th</sup> International Congress of Immunology*, China National Convention Center, Beijing, China.

Sng YX.X, Li J, Zareie P, Assmus L, Lee J, Turner S.J., Daley S.R., Quinn K.M., La Gruta N.L. 2019. MHCI expression level delimits naïve CD8 T cell population size and quality. *2019 Influenza Program Retreat*, RACV Healesville Country Club, Victoria, Australia.

Sng YX.X, Li J, Zareie P, Assmus L, Lee J, Jones C.M., Turner S.J., Daley S.R., Quinn K.M., La Gruta N.L. 2018. MHCI expression level delimits naïve CD8 T cell population size and quality. *2018 Influenza Program Retreat*, Rydges on Swanston Conference Facility, Victoria, Australia.

Sng YX.X, Li J, Zareie P, Assmus L, Lee J, Turner S.J., Daley S.R., Quinn K.M., La Gruta N.L. 2018. MHCI expression level delimits naïve CD8 T cell population size and quality. *Australasian Society of Immunology 47<sup>th</sup> Annual Scientific Meeting*, Pan Pacific Hotel, Perth, Australia.

Sng YX.X, Li J, Zareie P, Assmus L, Turner S.J., Daley S.R., Quinn K.M., La Gruta N.L. 2018. MHCI expression level delimits naïve CD8 T cell population size and quality. *24<sup>th</sup> Annual Immunology Group of Victoria Meeting*, Werribee Mansion, Victoria, Australia (Awarded best PhD speaker).

Sng YX.X, Li J, Zareie P, Assmus L, Lee J, Turner S.J., Daley S.R., Quinn K.M., La Gruta N.L. 2018. MHCI expression level delimits naïve CD8 T cell population size and quality. *Monash Biomedical Rising Stars Series*, Monash University, Victoria, Australia.

Sng YX.X, Li J, Zareie P, Assmus L, Lee J, Turner S.J., Quinn K.M., La Gruta N.L. 2017. The impact of MHCI availability on the compensatory shifts in flu-specific responses during infection. *2017 Influenza Program Retreat: 3-minute thesis competition*, Rydges on Swanston Conference Facility, Victoria, Australia (Awarded runner-up best speaker).

Sng YX.X, Quinn K.M., La Gruta N.L. 2017. Characterization of MHC-reactive TCRs that appear to escape negative selection. *23<sup>rd</sup> Annual Immunology Group of Victoria Meeting: 3-minute thesis competition*, Balgownie Estate, Yarra Valley, Victoria, Australia.

Sng YX.X, Quinn K.M., La Gruta N.L. 2016. How TCR-pMHC interactions in the thymus shape the peripheral TCR repertoire. *Monash and Melbourne University Structural Immunology Meeting*, Monash University, Victoria, Australia.

Sng YX.X, Quinn K.M., La Gruta N.L. 2016. Effect of MHCI diversity on development of an epitope-specific CD8 T cell population. *2016 Influenza Program Retreat*, Rydges on Swanson Conference Facility, Victoria, Australia.

Sng YX.X, Quinn K.M., La Gruta N.L. 2016. Alloreactive flu-specific CD8 T cells have lower affinity for the mismatched MHCI and are less functional. *2016 Influenza Program Retreat*, Rydges on Swanson Conference Facility, Victoria, Australia.

### **Poster presentations**

Sng YX.X, Li J, Zareie P, Assmus L, Lee J, Turner S.J., Daley S.R., Quinn K.M., La Gruta N.L. 2019. DoI2019 Breaking News: Scientists discover link between mouse survival and mouldy hard cheese. *Day of Immunology*, Peter Doherty Institute Auditorium, The University of Melbourne, Victoria, Australia.

Sng YX.X, Li J, Zareie P, Assmus L, Lee J, Turner S.J., Daley S.R., Quinn K.M., La Gruta N.L. 2018. *Australasian Society of Immunology 47<sup>th</sup> Annual Scientific Meeting: BD Communications Session*, Pan Pacific Hotel, Perth, Australia.

Sng YX.X, Daley S.R., Quinn K.M., La Gruta N.L. 2018. MHCI expression delimits naïve CD8 T cell population size and quality, *Monash University Biomedicine Discovery Institute Student Symposium*, Monash University, Victoria, Australia.

## Thesis Including Published Works Declaration

I hereby declare that this thesis contains no material which has been accepted for the award of any other degree or diploma at any university or equivalent institution and that, to the best of my knowledge and belief, this thesis contains no material previously published or written by another person, except where due reference is made in the text of the thesis.

This thesis includes one submitted publication. The core theme of the thesis is to investigate the influence of MHCI quality and quantity on CD8 T cell selection, maintenance and effector functions. The ideas, development and writing up of all the papers in the thesis were the principal responsibility of myself, the student, working within the Department of Biochemistry and Molecular Biology, School of Biomedical Sciences, Faculty of Medicine, Nursing and Health Sciences, under the supervision of Nicole L. La Gruta, Kylie M. Quinn and Stephen S. Daley.

In the case of **Chapter Four**, my contribution to the work involved the following:

<b>Thesis Chapter</b>	<b>Publication Title</b>	<b>Status</b> <i>(published, in press, accepted or returned for revision, submitted)</i>	<b>Nature and % of student contribution</b>	<b>Co-author name(s) Nature and % of Co-author's contribution</b>	<b>Co-author(s), Monash student Y/N*</b>
Four	The Impact of MHC Class I Dose on Development and Maintenance of the Polyclonal Naïve CD8 T cell Repertoire	Submitted	80%. Performed experiments, analysed data, wrote first draft	Nicole La Gruta 5% - Designed study, supervised research Kylie Quinn 5% - Designed study, supervised research Jasmine Li 2% - Performed experiments Pirooz Zareie 1% - Performed experiments Claerwen Jones 1%- Performed experiments Jason Lee 1% - Performed experiments Lisa Assmus 1% - Performed experiments Stephen Daley 2% - Provided conceptual feedback Stephen Turner 2% - Provided conceptual feedback	No

I have / ~~have not~~ renumbered sections of submitted or published papers in order to generate a consistent presentation within the thesis.

**Student name:** Yi Xiong, Xavier Sng

**Student signature:**

**Date:** 26<sup>th</sup> December 2019

I hereby certify that the above declaration correctly reflects the nature and extent of the student's and co-authors' contributions to this work. In instances where I am not the responsible author I have consulted with the responsible author to agree on the respective contributions of the authors.

**Main Supervisor name:** Nicole L. La Gruta

**Main Supervisor signature:**

**Date:** 26<sup>th</sup> December 2019

## Acknowledgements

Undertaking my PhD program at the Biomedical Discovery Institute in Monash University have been a fulfilling and enjoyable journey. I am truly grateful to be given this opportunity where I developed and grew both as a scientist and as an individual. This journey would not be so smooth sailing without the constant support and guidance of many colleagues, friends and family, who have stood by me at both my lowest and highest points, keeping me on track throughout the duration of my degree.

First and foremost, I would like to thank Prof. Nicole La Gruta for taking me under your wing back in 2015 at the University of Melbourne. You have given me the opportunity to actualize my aspiration to be an immunologist, and it has been my greatest pleasure to be in your lab. I cannot be luckier to be in the La Gruta lab, and I cannot thank you enough for the lessons you have taught me throughout these five years.

To “only THE BEST co-supervisor” anyone could possibly wish for: Dr. Kylie Quinn. Thank you so much for nurturing me both in and out of the lab. My laboratory and analytical expertise, writing, presentation and critical-thinking skills would not be sharp without your constant feedback and supervision. I wish you all the very best in the Quinn Lab at RMIT, and I am confident that your lab will excel with your leadership standards of research.

To Dr. Stephen Daley for giving me the opportunity to be a part of the Daley Lab. Thank you very much for tolerating my random pop-ins into your office and allowing

me to be a part of a fantastic project. I wish you all the very best in Queensland, and it has been my pleasure to work with you.

My PhD journey would not have been stimulating and enjoyable without the members of the La Gruta and Turner labs. To Prof. Stephen Turner for always providing critical feedback in the progress of all my projects. To Dr. Pirooz Zareie (PeeZee) and Dr. Jasmine Li (Jazzy) for keeping the fun in and out of work. To Dr. Claerwen Jones for always ensuring that the lab runs smoothly (and keeping our tummies full). To the rest of the “La Turner” lab members past and present, thank you all very much for your support and guidance throughout my PhD journey.

A big thank you to my virology lecturer, panel member and mentor Prof. Lorena Brown. Thank you so much for your guidance and supervision since 2014. It has been my honour to sit through your virology lectures in my undergraduate years and thank you very much for your support through my PhD journey. Our biannual catch-ups at the annual flu retreats and my yearly reviews have been monumental in keeping my drive to complete my degree.

To the rest of my PhD supervisory committee members: Prof. Tony Purcell, Dr. Stephen Daley, Prof. Mibel Aguilar and Prof. Mariapia Degli-Esposti. Thank you all so much for your invaluable feedback and support in the growth of my PhD projects throughout the years.

To Elizabeth Kemp and Amelia Morrison from the postgraduate department for the constant reminders to ensure a timely completion and, to A/Prof. Priscilla Johanesen

and Sherrie Young from the Microbiology Department for always being around and providing assistance in times of need. The administrations of my degree would not be smooth without the assistance of a fantastic administrative team.

To Dr. Jie Lin in the Brooks lab at the Peter Doherty Institute for the generation of monomers used in this study. Chimeric monomers used in this study were gifts from Dr. Lucy Sullivan at the Peter Doherty Institute.

To A/Prof. Frank Alderuccio, Dr. Kim Murphy, Dr. Maria Demaria and Dr. Anita Barry from the immunology teaching department. Thank you all for giving me the opportunity to nurture the next generation of immunologists, and I look forward to working with all of you again in the future.

To my rock-climbing buddies: Sara and Rhea. Thank you for being my lead-climbing partners and getting me out of the house when I needed it.

To Jed and Wai: You have both been monumental in providing life advices and the hard truths when I needed it. Thank you both for keeping me grounded and focused through this journey.

To my League of Legends guild #KKB: Aeon, Tongers, Leon and Sean. My thesis-writing guilt would have taken me at “first blood” without your support. Our gaming sessions through the night really kept me sane and alive. Special thanks to Aeon, for whipping up a nightly feast for dinner throughout my thesis-writing period. I wish you all the very best in the (gaming) future.

To my friends from Singapore: Joseph, Dahlia, Charlene (Bird), WeiJie, MeiQi and Keifer. Thank you all so much for keeping me sane through these years away from home. All of you have a way of keeping me grounded and focused despite being thousands of miles away.

A big and special thanks to my partner Sean and my puppy Nike for being my pillar of support all these years. Both your constant excitements and enthusiasms have made this journey a joy to ride and I cannot thank you both enough for the adventures you have brought me.

Last but never least, to my family: mom, dad, JieMin and JieYi. Thank you for the immeasurable support throughout these six years abroad. I would like to thank in particular my mom and dad for the weekly phone calls to ensure my well-being all these years, for without, I would never be what I am today.

# Table of Contents

## 1. Introduction

1.1. The adaptive immune system.....	1
1.2. CD8 T cells .....	3
1.3. The T cell receptor.....	4
1.3.1. TCR diversity.....	4
1.3.2. TCR/CD3 structure.....	7
1.3.3. Expression of TCRs during T cell development.....	10
1.4. Major Histocompatibility Complex (MHC).....	14
1.4.1. Human Leukocyte Antigen (HLA) locus in humans.....	14
1.4.2. Histocompatibility-2 (H-2) locus in mice .....	15
1.4.3. MHC structure .....	16
1.4.4. Antigen presentation .....	18
1.4.4.1. MHCII antigen processing and presentation pathway .....	18
1.4.4.2. MHCI antigen processing and presentation pathway .....	19
1.5. TCR recognition of pMHCI and downstream signaling.....	21
1.5.1. The TCR-pMHCI interaction.....	21
1.5.2. Signal transduction upon TCR recognition of pMHCI .....	23
1.6. TCR-pMHCI interactions: importance in T cell biology.....	24
1.6.1. Thymic selection and MHC restriction.....	24
1.6.2. Homeostatic maintenance of naïve CD8 T cells .....	26
1.6.3. Activation of CD8 T cells for immune protection .....	27
1.7. CD8 T cell immunodominance.....	29

1.7.1. Determinants of immunodominance .....	29
1.7.2. Precursor frequency .....	29
1.7.3. TCR affinity for antigen .....	31
1.7.4. Antigen abundance and peptide presentation.....	33
1.7.5. Immunodomination.....	35
1.8. The C57BL/6 model of influenza A virus infection .....	38
1.9. Specific aims of this study .....	40

## **2. Materials and Methods**

2.1. Mice .....	41
2.2. Viruses .....	42
2.3. Infection and immunization of mice .....	42
2.4. Tissue sampling, processing and lymphocyte counting.....	43
2.4.1. Lungs .....	43
2.4.2. Spleen and peripheral lymph nodes.....	44
2.4.3. Thymus .....	44
2.4.4. Bone marrow .....	45
2.4.5. Viable lymphocyte counts .....	45
2.5. Cell lines .....	46
2.5.1. 2.4G2 hybridoma cell line.....	46
2.5.2. Ag8.653 hybridoma cell line for GM-CSF.....	46
2.5.3. HEK 293T cells .....	47
2.6. Tetramers .....	48
2.7. Tetramer and surface antibody staining .....	50
2.8. Tetramer-based magnetic enrichment of epitope-specific naïve CD8 T cells .....	51

2.9. Peptide re-stimulation of antigen-specific CD8 T cells and intracellular cytokine staining .....	53
2.10. Flow cytometric acquisition and analysis.....	54
2.11. Isolation of Single Cells by Fluorescence Activated Cell Sorting (FACS)...	54
2.12. Single-cell proliferation assay .....	55
2.13. Carboxyfluorescein Succinimidyl Ester (CFSE) and Cell Trace Violet (CTV) labelling of cells .....	56
2.14. Adoptive transfer of splenocytes.....	57
2.15. Multiplexed single cell Reverse Transcriptase Polymerase Chain Reaction (Multiplex RT-PCR) .....	57
2.15.1. Reverse transcription of cDNA .....	57
2.15.2. External PCR.....	58
2.15.3. Internal PCR.....	59
2.15.4. Agarose gel electrophoresis .....	60
2.15.5. PCR product purification.....	60
2.15.6. Sequencing reaction.....	60
2.15.7. Terminator removal .....	61
2.15.8. Sequencing.....	62
2.16. DC vaccination.....	62
2.17. NK Cell Depletion using PK136 mAb Administration.....	63
2.18. 5-bromo-2'-deoxyuridine (BrdU) administration to track cell division <i>in vivo</i> ..	63
.....	63
2.19. In vivo labelling of Recent Thymic Emigrants (RTEs).....	65
2.20. Statistical analyses .....	66

### 3. Characterization of Enhanced H-2K Binding by T cells from H-2K<sup>b/-</sup> mice

3.1. Introduction .....	67
3.2. Results .....	70
3.2.1. Alloreactive CD8 T cells in the H-2D <sup>b/-</sup> mouse model.....	70
3.2.2. Alloreactive H-2D <sup>b</sup> PA <sub>224</sub> CD8 T cells are bona fide CD8 T cells specific for H-2D <sup>b</sup> PA <sub>224</sub> .....	74
3.2.3. Alloreactive H-2D <sup>b</sup> PA <sub>224</sub> -specific CD8 T cells are non-responsive after BMDC vaccination in vivo .....	77
3.2.4. Identification of H-2K <sup>b</sup> -reactive T cells in H-2K <sup>b/-</sup> and DKO, but not WT and H-2D <sup>b/-</sup> mice .....	80
3.2.5. Increased binding of H-2K MHC I occurs independently of CD8 co- receptor and H-2K allele .....	86
3.2.6. TCR repertoire analysis showed NKT cell repertoire bias in CD4, and no V-region bias in CD8 T cells .....	92
3.2.7. TCRs on H-2K-reactive T cells cannot bind H-2K <sup>b</sup> tetramers .....	101
3.2.8. H-2K-reactive CD8 and CD4 T cells express markers of T <sub>MEM</sub> and NKT cells, respectively .....	103
3.2.9. H-2K-reactive NK cells persist in $\beta_2m^{-/-}$ mice, suggesting a non-TCR- mediated interaction.....	105
3.2.10. H-2K <sup>b</sup> tetramers simultaneously bound Ly49C expression in CHO cell line .....	107
3.2.11. Ly49C/I/F/H blocking antibody failed to abrogate binding of H-2K- reactive cells .....	
110	
3.3. Discussion .....	112



## **5. Analysis of Immunodomination in Anti-Viral CD8 T cell Responses During**

### **IAV Infection**

5.1. Introduction .....	155
5.2. Results .....	159
5.2.1. Modest compensation in the magnitude of H-2D <sup>b</sup> NP <sub>366</sub> response after HKx31 virus infection .....	159
5.2.2. Compensation by the immunodominant H-2D <sup>b</sup> NP <sub>366</sub> and H-2K <sup>b</sup> Ova <sub>257</sub> CD8 T cell responses in mice lacking the alternative MHC gene, after primary acute infection with IAV-Ova virus .....	169
5.2.3. Impaired IAV-specific CD8 T cell memory formation in mice lacking H- 2D <sup>b</sup> , but not H-2K <sup>b</sup> .....	174
5.2.4. The H-2K <sup>b</sup> Ova <sub>257</sub> -specific CD8 T cell response is markedly augmented in H-2D <sup>b/-</sup> mice after secondary challenge with PR8-Ova virus .....	178
5.2.5. Quality of compensatory H-2D <sup>b</sup> NP <sub>366</sub> and H-2K <sup>b</sup> Ova <sub>257</sub> responses are similar to those observed in WT mice following IAV-Ova infection .....	182
5.2.6. Diminished capacity of H-2K <sup>b</sup> Ova <sub>257</sub> -specific CD8 T cells in H-2D <sup>b/-</sup> mice is not influenced by the proportion of MPECs and SLECs.....	188
5.2.7. Unaltered H-2K <sup>b</sup> Ova <sub>257</sub> presentation with the lack of H-2D <sup>b</sup> .....	191
5.2.8. The compensatory increase in the H-2K <sup>b</sup> Ova <sub>257</sub> -specific CD8 T cell response is driven by augmented recruitment of naïve cells in H-2D <sup>b/-</sup> mice..	193
5.3. Discussion .....	197
<b>6. Concluding Remarks .....</b>	<b>204</b>
<b>7. Bibliography .....</b>	<b>220</b>
<b>8. Appendices.....</b>	<b>270</b>

# List of Figures

## Chapter One

- Figure 1 Genomic organization and somatic recombination of TCR $\alpha$  and TCR $\beta$  in humans and mice.
- Figure 2 Schematic diagram of the conventional interactions between TCR CDR loops and pMHCI, the CD3 signalling complex and the CD8 co-receptor.
- Figure 3 Gene map of the HLA and H-2 locus in humans and mice respectively.
- Figure 4 Schematic diagram of the structure and MHCI and MHCII molecules.

## Chapter Two

- Figure 5 Gating strategy to identify epitope-specific tetramer binding cells following tetramer-based magnetic enrichment.

## Chapter Three

- Figure 6 Alloreactive H-2D<sup>b</sup>PA<sub>224</sub>-specific CD8 T cells can be selected on the H-2K<sup>b</sup> molecule, but have lower affinity for H-2D<sup>b</sup>PA<sub>224</sub>, altered TCR repertoire and impaired TCR-dependent functionality.
- Figure 7 A putative alloreactive H-2D<sup>b</sup>PA<sub>224</sub>-specific TCR binds H-2D<sup>b</sup>PA<sub>224</sub> tetramer but at a lower MFI than 6218 TCR.
- Figure 8 Responsiveness of naïve H-2D<sup>b</sup>PA<sub>224</sub>-specific CD8 T cells to BMDC vaccination.
- Figure 9 Inflated population of H-2K<sup>b</sup> tetramer staining cells in mice lacking H-2K<sup>b</sup>.
- Figure 10 H-2K<sup>b</sup>-reactive CD8 and CD4 T cells in the absence of H-2K<sup>b</sup>.
- Figure 11 Elevated numbers of H-2K<sup>b</sup>B8R<sub>20</sub>-specific CD8 T cells following tetramer-based magnetic enrichment in H-2K<sup>b</sup><sup>-/-</sup> and DKO mice.

- Figure 12 Schematic representation of the WT and chimeric H-2K<sup>b</sup> monomer.
- Figure 13 H-2K<sup>b</sup>-reactive cells bound chimeric H-2K<sup>b</sup> tetramers, and its interaction is independent of CD8 co-receptor binding.
- Figure 14 H-2K<sup>b</sup>-reactive CD8 T cells are cross-reactive with H-2K<sup>d</sup>.
- Figure 15 TRAV and TRBV usage for the global non-antigen specific CD8 T cell population, and the H-2K-reactive CD8 and CD4 cell-derived TCRs binding simultaneously to H-2K<sup>b</sup>NS2<sub>114</sub> and H-2K<sup>b</sup>PB1<sub>703</sub> from H-2K<sup>b</sup><sup>-/-</sup> mice.
- Figure 16 Representative dot plots showing TCR $\beta$  expression and tetramer staining of TCRs identified from H-2K-reactive CD8 and CD4 TCRs from H-2K<sup>b</sup><sup>-/-</sup> mice.
- Figure 17 Phenotypic characterization of H-2K-reactive CD8 and CD4 T cells in H-2K<sup>b</sup><sup>-/-</sup> mice.
- Figure 18 H-2K-reactive cells are present in the NK cell population from a  $\beta_2m$ <sup>-/-</sup> mouse.
- Figure 19 Binding of H-2K<sup>b</sup>NS2<sub>114</sub> and H-2K<sup>b</sup>PB1<sub>703</sub> tetramers to Ly49C-expressing CHO cell line.
- Figure 20 H-2K-reactive cells bound H-2K<sup>b</sup> tetramers despite the presence of a blocking anti-Ly49C/I/F/H mAb (clone: 14B11).

## Chapter Four

- Figure 21 Expression of MHCI genes is independently regulated and dependent on gene dosage.
- Figure 22 MHCI expression level delimits naïve CD8<sup>+</sup> T cell number in the periphery but not CD8<sup>+</sup> T cell development or thymic output.
- Figure 23 MHCI expression level influences the composition of the peripheral naïve CD8<sup>+</sup> T cell repertoire.
- Figure 24 Reduced MHCI expression leads to alterations in IAV-specific naïve CD8<sup>+</sup> T cell repertoires and IAV-specific CD8<sup>+</sup> T cell immune responses.

- Figure 25 MHC I expression level does not influence peripheral CD4<sup>+</sup> T cell population.
- Figure 26 Gating strategy for perivascular CD8<sup>+</sup> thymocytes.
- Figure 27 MHC I expression level influences the composition of the peripheral naïve CD8<sup>+</sup> T cell repertoire.
- Figure 28 MHC I expression level influences the composition of the peripheral naïve CD4<sup>+</sup> T cell repertoire.

## Chapter Five

- Figure 29 Absolute numbers of CD8 T cells in IAV-infected WT, H-2K<sup>b</sup><sup>-/-</sup> and H-2D<sup>b</sup><sup>-/-</sup> mice at day 10 post-infection.
- Figure 30 Magnitude of epitope-specific CD8 T cell responses after intranasal (i.n.) infection with 10<sup>4</sup> pfu of HKx31 virus.
- Figure 31 Cytokine production by epitope-specific Cd8 T cells at 10 days after i.n. infection with 10<sup>4</sup> pfu HKx31 virus.
- Figure 32 Timeline and weight loss following i.n. primary and i.n. secondary challenge with HKx31-Ova and PR8-Ova IAV, respectively.
- Figure 33 Magnitude of epitope-specific CD8 T cell responses after i.n. infection with 10<sup>4</sup> pfu of HKx31-Ova virus.
- Figure 34 Magnitude of epitope-specific memory CD8 T cell populations 60 days after i.n. primary acute infection with 10<sup>4</sup> pfu of HKx31-Ova virus.
- Figure 35 Magnitude of epitope-specific CD8 T cell responses after i.n. prime and i.n. challenge with 10<sup>4</sup> pfu of HKx31-Ova and 10<sup>4</sup> pfu of PR8-Ova viruses, respectively.
- Figure 36 Cytokine production by epitope-specific CD8 T cell responses after i.n. infection with 10<sup>4</sup> pfu of HKx31-Ova virus.
- Figure 37 MFI of IFN $\gamma$  production by H-2K<sup>b</sup>Ova<sub>257</sub>- and H-2D<sup>b</sup>NP<sub>366</sub>-specific CD8 T cells after Ova<sub>257</sub> and NP<sub>366</sub> peptide stimulation respectively.

- Figure 38 Kinetics of H-2K<sup>b</sup>Ova<sub>257</sub>-specific CD8 T cell response after IAV infection.
- Figure 39 Proportion of MPECs and SLECs in the H-2K<sup>b</sup>Ova<sub>257</sub>-specific CD8 T cell population 10 days after i.n. primary acute infection with 10<sup>4</sup> pfu of HKx31-Ova.
- Figure 40 Similar presentation of H-2K<sup>b</sup>Ova<sub>257</sub> on DCs from WT and H-2D<sup>b</sup><sup>-/-</sup> mice following HKx31-Ova infection.
- Figure 41 Schematic of BrdU treatment strategy.
- Figure 42 Increased recruitment of H-2K<sup>b</sup>Ova<sub>257</sub>-specific CD8 T cells in the absence of H-2D<sup>b</sup>.

## Chapter Six

- Figure 43 Schematic diagram of alloreactive H-2D<sup>b</sup>PA<sub>224</sub>-specific TCR in complex with H-2D<sup>b</sup>PA<sub>224</sub>.
- Figure 44 Heterozygosity and homozygosity at the HLA locus impacts the quality of peripheral naïve CD8 T cells.

## List of Tables

### Chapter One

Table 1	Expression of CD44, CD25, CD4 and CD8 at the various stages of thymic development
---------	---

### Chapter Two

Table 2	Mouse strains used in the studies described in this thesis.
Table 3	Tetramers used in the studies described in this thesis.
Table 4	H-2K <sup>b</sup> chimeric tetramers used in the studies described in this thesis.
Table 5	Stimulation antibody concentrations for well coating for single-cell proliferation assay.
Table 6	Reverse transcriptase master-mix for cDNA synthesis.
Table 7	Reverse transcriptase reaction conditions for cDNA synthesis.
Table 8	External PCR master-mix for multiplex RT-PCR reaction.
Table 9	PCR conditions for external and internal multiplex RT-PCR.
Table 10	Internal PCR master-mix for multiplex RT-PCR reaction.
Table 11	Sequencing reaction master-mix for multiplex RT-PCR reaction.
Table 12	Sequencing reaction conditions for multiplex RT-PCR.

### Chapter Three

Table 13	<i>Ex vivo</i> analysis of paired and unpaired TCR CDR3 amino acid residues in the H-2K-reactive CD8 T cell population from H-2K <sup>b/-</sup> mice using multiplex RT-PCR.
Table 14	<i>Ex vivo</i> analysis of paired and unpaired TCR CDR3 amino acid residues in the total CD8 T cell population from H-2K <sup>b/-</sup> mice using multiplex RT-PCR.

Table 15 *Ex vivo* analysis of paired and unpaired TCR CDR3 amino acid residues in the H-2K-reactive CD4 T cell population from H-2K<sup>b-/-</sup> mice using multiplex RT-PCR.

## Chapter Five

Table 16 Amino acid sequences and MHCI restriction of IAV-derived epitopes investigated in this study.

## Appendices

Table 17 Peptides used in the studies described in this thesis.

Table 18 Mouse-specific antibodies used for flow cytometry analyses.

Table 19 Mouse multiplex primer sequences for amplifying CDR3 $\alpha$  region by single-cell multiplex RT-PCR.

Table 20 Mouse multiplex primer sequences for amplifying the CDR3 $\beta$  region by single-cell multiplex RT-PCR.

Table 21 *Ex vivo* analysis of paired and unpaired TCR CDR3 amino acid residues from naïve H-2D<sup>b</sup>PA<sub>224</sub>-specific CD8 T cells from H-2D<sup>b-/-</sup> mice.

## Abbreviations

Aa	Amino acid
Ab	Antibody
AIRE	Autoimmune regulator
APC	Antigen presenting cell
AP-1	Activator protein-1
BCR	B cell receptor
BMDC	Bone marrow derived dendritic cells
BrdU	5-bromo-2'-deoxyuridine
$\beta_2m$	Beta-2-microglobulin
CD	Cluster of differentiation
CDR	Complementarity-determining regions
CFSE	Carboxyfluorescein succinimidyl ester
cTEC	Cortical thymic epithelial cell
CTV	Cell tracker violet
DAMPs	Danger associated molecular patterns
DC	Dendritic cell
DKO	Double knockout
DN	Double negative
DP	Double positive
DRiPs	Defective ribosomal products
GM-CSF	Granulocyte-macrophage colony-stimulating factor
GvHD	Graft <i>versus</i> host disease
GvL	Graft <i>versus</i> leukemia
H-2	Histocompatibility-2

HA	Haemagglutinin
HIV	Human immunodeficiency virus
HLA	Human leukocyte antigen
HSCT	Haematopoietic stem cell transplant
IAV	Influenza A virus
IFN $\gamma$	Interferon-gamma
IL	Interleukin
i.n.	Intranasal
ITAM	Immunoreceptor tyrosine-based activation motif
i.v.	Intravenous
LFA	Leukocyte
LIP	Lymphopenia-induced proliferation
mAb	Monoclonal antibody
MFI	Median fluorescence intensity
MHCI	Major histocompatibility complex class I
MHCII	Major histocompatibility complex class II
MPEC	Memory precursor effector cells
mTEC	medullary thymic epithelial cell
NA	Neuraminidase
NF- $\kappa$ B	Nuclear factor kappa B
NP	Nucleoprotein
Ova	Ovalbumin
PA	Acidic polymerase
PAMPs	Pattern associated molecular patterns
PB1	Basic polymerase protein 1

PB1-F2	Basic polymerase protein 1 – Frameshift 2
PCR	Polymerase chain reaction
pfu	Plaque forming units
pMHC	Peptide-MHC
PRR	Pattern recognition receptors
RAG	Recombination-activating gene
RT-PCR	Reverse transcriptase PCR
SLEC	Short-lived effector cells
SP	Single positive
SPR	Surface plasmon resonance
S1P	Sphingosine 1-phosphate
TAP	Transporter associated with antigen processing
TCR	T cell receptor
Tdt	Terminal deoxynucleotidyl transferase
TNF	Tumour necrosis factor
TRA	T cell receptor alpha
TRB	T cell receptor beta
WT	Wildtype



## **1. Introduction**

### **1.1. The adaptive immune system**

The immune system plays a critical role in protecting the host against infections and diseases from microorganisms, such as parasites, bacteria and viruses. It is made up of multiple, highly specialised cell populations and molecules that mediate defence against invading pathogens. The immune system can be partitioned into two major arms: the innate and adaptive immune systems.

The innate immune system is our first line of defence against invading pathogens. Broadly, the innate immune system encompasses all aspects of the host's defence mechanisms that are encoded by the germline genes of the host. This includes physical barriers such as epithelial cells that form tight cell-cell interactions, mucus layers lining the internal cavities of the body, and innate immune cells that survey the circulation for foreign pathogens. Innate immune cells express Pattern Recognition Receptors (PRRs) that recognize conserved structures common to many pathogens, but not self, known as Pathogen-Associated Molecular Patterns (PAMPs; reviewed in (1)). During an infection, damage to tissue or cell death can also result in the production of Damage-Associated Molecular Pattern (DAMP) molecules to induce potent inflammatory responses (reviewed in (2)). PAMPs and DAMPs are recognized by PRRs on stromal cells and innate immune cells, and this can trigger inflammation *via* multiple pathways, such as the inflammasome pathway (3, 4). Upon activation, the

innate immune response attempts to control the infection, providing the host with immediate, non-specific recognition and control or elimination of pathogen. The innate immune response can also generate inflammatory cytokines that augment subsequent activation of adaptive immune cells (reviewed in (5)).

In contrast to innate immune cells, adaptive immune cells demonstrate exquisite specificity toward pathogen-encoded protein antigens, and they are capable of forming a pool of memory cells to more effectively clear pathogens following subsequent re-infection. Specificity is imparted by antigen-specific receptors expressed on B and T lymphocytes, known as B cell receptors (BCRs) and T cell receptors (TCRs), respectively. The sequence and binding sites of these antigen-specific receptors are incredibly diverse and the mechanisms generating this diversity will be described below. The combination of a diverse range of receptors with high specificity for individual foreign antigens means that individual lymphocytes can specifically control and clear infections by distinct pathogens and eliminate tumours while preserving normal tissue integrity.

B cells provide humoral immunity through the secretion of antibodies that bind soluble antigen or antigens on the surface of pathogens and other targets. Once bound, these antibodies can mediate a number of effector functions, such as complement fixation (6). T cells, on the other hand, provide cellular immunity, and conventional T cells can be further subdivided into CD4 (helper) T cells and CD8 (killer) T cells. CD4 T cells play a number of key roles during the adaptive immune responses, predominantly *via* the production of soluble cytokines (7). They can shape the quality of B cell and CD8 T cell responses, by promoting B cell class switching, CD8 T cell activation, and

memory formation, and CD4 T regulatory cells also play a key role in suppressing immune responses (8). In addition to cytokine production, CD4 T cells have also been shown to secrete granzymes and perforin to mediate direct cytotoxicity (reviewed in (9)).

## 1.2. CD8 T cells

In contrast to CD4 T cells, CD8 T cells play a critical role in controlling and facilitating clearance of intracellularly infected or malignant cells (reviewed in (10)). CD8 T cells are activated in the lymph node following the specific recognition, *via* the TCR, of a peptide epitope presented by the major histocompatibility complex class I molecule (MHCI) on the surface of a professional antigen presenting cell (APC).

Once activated through their TCR, effector CD8 T cells migrate into the periphery and engage multiple molecular mechanisms to target and kill any cell that presents their cognate peptide + MHCI (pMHCI) antigen. Activated CD8 T cells can engage two pathways to induce direct lysis of target cells; the intrinsic pathway and the extrinsic pathway. The extrinsic pathway is mediated by ligation of death receptors, such as CD95L (FasL), which can interact with CD95 (Fas) on target cells to initiate apoptosis of target cells through the caspase cascade (11, 12). However, the intrinsic pathway is the main mechanism by which CD8 T cells kill target cells. Activated CD8 T cells produce and store perforin and granzymes, a family of serine proteases, in cytoplasmic granules. Upon detection of cognate pMHCI antigen, these granules are released, and perforin assembles into multimeric pores in the target cell membrane to permit a targeted delivery of granzymes (13, 14). This induces cytolysis of the target

cell by triggering an intrinsic pathway of apoptosis resulting in DNA fragmentation (15). Activated CD8 T cells can also secrete cytokines such as interferon-gamma ( $\text{IFN}\gamma$ ) and tumour necrosis factor (TNF) to control pathogen replication and activity (16, 17). CD8 T cells therefore possess a number of potent immunological mechanisms for control of infection and malignancy. Critically, these mechanisms could cause damage to normal, healthy tissue, necessitating the tight regulation of CD8 T cell activation, in part by the requirement for the T cell to specifically recognize peptide-MHCI (pMHCI) ligands *via* their cell surface expressed TCR.

### **1.3. The T cell receptor**

T cells develop in the thymus, where they first express a TCR required for the recognition of pMHC ligands. Each T cell expresses a unique TCR that recognises a specific peptide epitope, which gives rise to a highly diverse repertoire of clonally expressed TCRs in the T cell population. Indeed, the TCR repertoire must be extremely diverse to increase the likelihood that a TCR will be available to recognise and respond to the wide array of peptide antigens encoded by various pathogens and presented on MHC molecules.

#### **1.3.1. TCR diversity**

The remarkable diversity of TCRs is generated during T cell development through somatic recombination of multiple gene elements at the  $\text{TCR}\alpha$  (TRA) and  $\text{TCR}\beta$  (TRB) loci. The TRA locus is made up of TCR Variable (V), Junction (J) and Constant (C)

region genes. In humans, there are 47 TRAV genes, 61 TRAJ genes and a single TRAC gene. In mice, there are 98 TRAV genes, 60 TRAJ genes and a single TRAC gene (**Figure 1A**) (18). The TRB locus is also comprised of TCR V-, J- and C-region genes and it has an additional set of Diversity (D) genes, further amplifying variability. In humans, there are 54 TRBV, 2 TRBD, 14 TRBJ and 2 TRBC genes. In mice, there are 35 TRBV, 2 TRBD, 14 TRBJ and 2 TRBC genes (**Figure 1B**) (18).

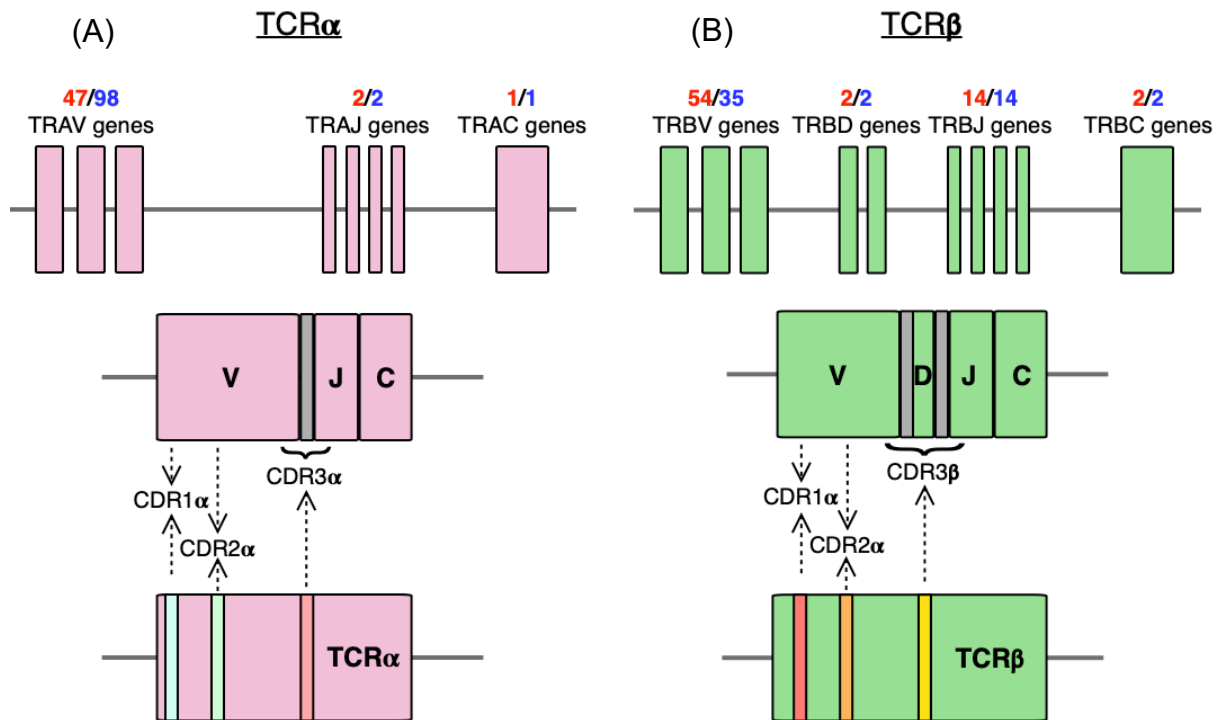


**Figure 1:** Genomic organization and somatic recombination of (A) TCR $\alpha$  and (B) TCR $\beta$  in humans and mice. CDR1 and CDR2 are encoded by TRAV and TRBV gene segments of TCR $\alpha$  and TCR $\beta$  respective, and the CDR3 encompasses the junction of V and J (for TCR $\alpha$ ) or V, D and J regions (for TCR $\beta$ ). Non-template encoded nucleotide (N nucleotide) insertions are represented by grey boxes between V and J for TCR $\alpha$  or between VD and DJ for TCR $\beta$ . The number of TRAV, TRAD, TRAJ and TRAC gene segments in humans and mice are highlighted in red and blue, respectively. This image was adapted from (19).

TCR diversity is facilitated during T cell development through the expression of the recombination-activating gene (RAG) -1 and RAG-2 enzymes, which is triggered during T cell development and the enzymes then mediate the process of somatic, or VDJ, recombination. This is the random splicing and reassembly of individual TRAV, TRAJ and TRAC gene (**Figure 1A**) segments with each other, alongside that of the TRBV, TRBD, TRBJ and TRBC gene segments (**Figure 1B**) (20). The random permutations and combinations of the V-, D- and J-genes can generate substantial

diversity in the resulting TCRs. In addition, the imprecise joining of gene segments results in overhanging ends of DNA that are repaired by the random insertion of non-template encoded nucleotides (*N* nucleotides) by the terminal deoxynucleotidyl transferase (Tdt) enzyme, contributing up to 90% of the diversity in TCRs (21). Finally, the independently recombined TCR $\alpha$  and TCR $\beta$  chains are randomly paired to give rise to the final  $\alpha\beta$ TCR heterodimer. Collectively, the multiple mechanisms of germline diversity, somatic recombination, non-template encoded addition of nucleotides, and  $\alpha\beta$  chain pairing translate to a theoretical diversity of up to  $10^{21}$  different TCRs in humans and  $10^{15}$  TCRs in mice (22). However, only  $2.5 \times 10^7$  distinct TCRs are found in the mature peripheral T cell repertoire following thymic development (22–24).

### 1.3.2. TCR/CD3 structure

The structure of the TCR is essential to its function. TCRs on CD4 and CD8 T cells are expressed as transmembrane  $\alpha\beta$  heterodimers ( $\alpha\beta$ TCR). The  $\alpha\beta$ TCR is generated during T cell development, with each chain consisting of a variable and a constant region (reviewed in (25)). The constant regions of both the  $\alpha$ - and  $\beta$ -chains anchor the TCR to the cell membrane *via* their transmembrane domain (26) and the heterodimer is held together by a disulphide bond located extracellularly but adjacent to the transmembrane domain. The three complementarity-determining regions (CDRs) of the TCR  $\alpha$  and  $\beta$  chains are highly variable loops within each of the TCR $\alpha$  and  $\beta$  chains. The CDR are the most variable regions of the TCR and so make the contacts with the pMHC1 complex (**Figure 2**; reviewed in (27)). CDR1 and CDR2 are germline encoded by individual TCR  $\alpha$  and  $\beta$  variable genes (TRAV and TRBV, respectively)

and typically mediate most of the contacts with MHC molecules. By contrast, the CDR3 regions span the VJ and VDJ gene junctional regions, are therefore highly diverse and typically play a dominant role in peptide recognition (28).

The recognition by the TCR of its cognate pMHC complex is crucial for T cell activation. However, the TCR alone lacks the intracellular domains required for signalling transduction and must associate with the CD3 complex (CD3) to trigger signalling (**Figure 2**; discussed in **Section 1.5.1**). The CD3 complex consists of three dimers made up of the  $\gamma$ ,  $\delta$ ,  $\epsilon$ ,  $\zeta$  subunits (29, 30); the CD3 $\epsilon\gamma$  heterodimer, CD3 $\epsilon\delta$  heterodimer and the CD3 $\zeta\zeta$  homodimer, each of which contains intracellular immunoreceptor tyrosine-based activation motifs (ITAMs). The ITAMs contain tyrosine rich domains that can be phosphorylated during the engagement of the TCR with the pMHC molecule, leading to the downstream signaling cascade and T cell activation. A recent study by Dong et al (2019) resolved the structure of the TCR in complex with the various CD3 chains using cryo-electron microscopy, revealing the precise interactions mediated between the CD3 complex and the  $\alpha\beta$ TCR (31). Here, they demonstrated the importance of the CD3 complex to provide structural support for the TCR *via* physical interactions with the constant regions of both TCR  $\alpha$  and  $\beta$  chains at the extracellular and transmembrane domains.

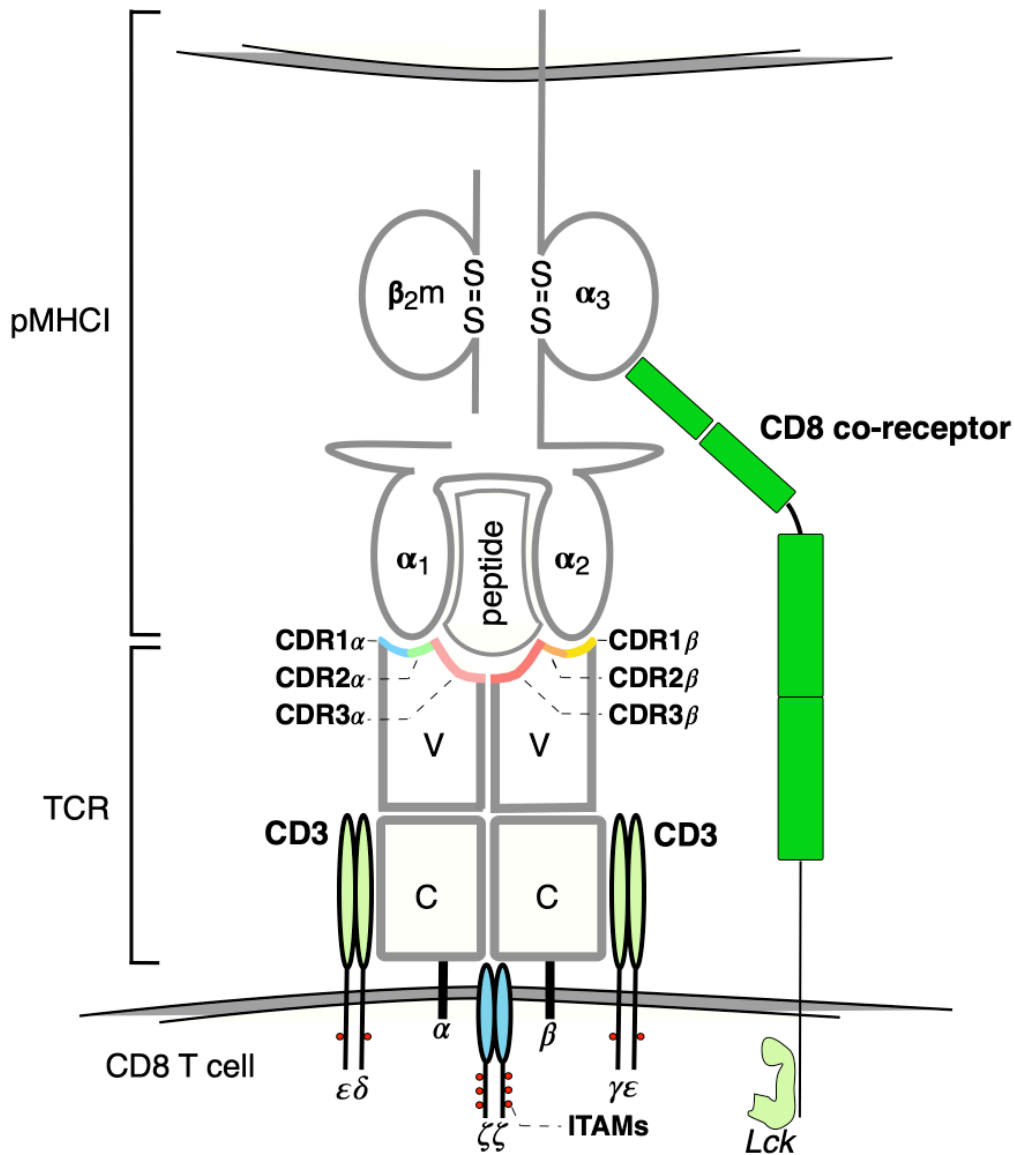


**Figure 2:** Schematic diagram of the conventional interactions between the TCR CDR loops and pMHC I, and the recruitment of CD3 signalling complex and CD8 co-receptor. The CDR1 and CDR2 domains of both TCR $\alpha$  and TCR $\beta$  typically contact the MHC I molecule, while the CDR3 $\alpha$  and CDR3 $\beta$  loops interact with the peptide. Upon TCR-pMHC I binding, the CD8 co-receptor brings the signalling molecule Lck into close proximity with the ITAMs on CD3 cytoplasmic tails to mediate signalling.

### 1.3.3. Expression of TCRs during T cell development

T cells develop in the thymus from common lymphoid progenitor cells that migrate from the bone marrow to the thymus to become thymocytes (reviewed in (32, 33)). The thymus provides a microenvironment for T cell development and the stages of T cell development can be broadly categorized into four main stages based on the expression of co-receptors CD4 and CD8 (34). Thymocytes that lack the expression of both CD4 and CD8 (termed double-negative; DN) are further subdivided into four stages (DN1 to DN4) based on expression of CD25 and CD44 (**Table 1**; reviewed in (35)).

At the DN1 stage (**Table 1**), thymocytes have recently arrived the thymus from the bone marrow and they have the potential to give rise to multiple different T cell lineages, including  $\alpha\beta$  and  $\gamma\delta$  T cells (35). The cell fate decision into  $\alpha\beta$  or  $\gamma\delta$  T cell lineages is mediated by Notch signalling, which inhibits rearrangement of the  $\gamma\delta$  TCR loci but promotes rearrangement the  $\alpha\beta$  TCR loci (36–38).

At DN2, thymocytes upregulate the expression of CD25, migrate into the thymic cortex and somatic recombination is initiated through upregulation of RAG-1 and RAG-2 enzymes. Initially, these enzymes are recruited to mediate gene rearrangement of the TRB locus, one allele at a time (**Table 2**). The rearranged TCR $\beta$  chain is then expressed, and it forms a heterodimer with an invariant pre-TCR $\alpha$  chain in complex with CD3 (39, 40), generating a complex known as the pre-TCR.

At DN3, somatic recombination at the TRB locus continues and signalling from the pre-TCR is tested. If the pre-TCR is capable of signalling, either by self-pMHC recognition, self-dimerization, or both, the thymocyte receives a survival signal and it progresses into the following stages of thymic development (41, 42). In addition, rearrangement of the second TCR $\beta$  allele is inhibited, in a process known as allelic exclusion. This represents a key mechanism that supports the T cell clonal selection theory, where a T cell expresses only a single type of receptor with unique specificity (43). If the pre-TCR fails to recognize self-pMHC, it cannot permit TCR signalling, indicating that the rearranged TCR $\beta$  chain is non-functional. If this occurs, the second allele at the TRB locus then undergoes rearrangement and it is tested for functionality in the pre-TCR. If the second TCR $\beta$  chain is still non-functional, the thymocyte undergoes apoptosis (39). If the pre-TCR can permit TCR signalling, then the rearranged TCR $\beta$  chain is functional and the thymocyte undergoes several rounds of division to generate more progenitors, in a process known as  $\beta$ -selection (39).

At DN4, thymocytes that express a functional TCR $\beta$  chain can initiate the rearrangement of the TCR $\alpha$  locus. These cells can then start to upregulate the expression of both CD4 and CD8 co-receptors to become double-positive (DP) thymocytes (**Table 1**).

**Table 1:** Expression of CD44, CD25, CD4 and CD8 at the various stages of thymic development.

Developmental stage	Marker Expression				Anatomical location	Key processes
	CD44	CD25	CD4	CD8		
DN1	+	-	-	-	Cortex	
DN2	+	+	-	-	Cortex	$\beta$ -chain rearrangement
DN3	-	+	-	-	Cortex	$\beta$ -chain testing $\beta$ selection
DN4	-	-	-	-	Cortex	$\alpha$ -chain rearrangement
DP (CD4+CD8+)	-	-	+	+	Cortex	$\alpha$ -chain rearrangement $\alpha$ -chain testing (Positive selection)
SP (CD4+CD8-)	-	-	+	-	Cortex/ Medulla	Negative selection
SP (CD4-CD8+)	-	-	-	+	Cortex/ Medulla	Negative selection

At the DP stage, the TRA loci undergo further rearrangement and testing of the TCR $\alpha$  chain (**Table 1**). Unlike the TCR $\beta$  chain, genomic allelic exclusion does not apply to the TCR $\alpha$  chain, where both TRA loci can undergo rearrangement (44). Once rearranged, the TCR $\alpha$  chain is tested for functionality by pairing it with the functional TCR $\beta$  chain. At this point, both rearranged TCR $\alpha$  chains compete for TCR $\beta$  pairing; where the TCR $\alpha$  chain with higher pairing affinity for the rearranged TCR $\beta$  chain outcompetes the other TCR $\alpha$  chain (45). The paired TCR $\alpha\beta$  chain is tested for its functionality by binding to self-pMHC. The formation of a functional TCR $\alpha\beta$  leads to the down-regulation of the unpaired TCR $\alpha$  chain, and the retention of the functional TCR $\alpha$  chain on the cell surface (46). If the paired TCR $\alpha\beta$  chain is non-functional, the

other TCR $\alpha$  chain is paired with the TCR $\beta$  chain for a second round of testing. If there is still no signalling, then the thymocyte undergoes apoptosis in a process known as death by neglect. The productive rearrangement of a functional  $\beta$ - and  $\alpha$ -chains ensures that the T cells that survive express a TCR that can bind and recognize MHC molecules with a reasonable affinity, in a process known as selection (**Section 1.6.1**).

## 1.4. Major Histocompatibility Complex (MHC)

### 1.4.1. Human Leukocyte Antigen (HLA) locus in humans

In humans, the MHC genes are encoded at the human leukocyte antigen (HLA) locus, which is positioned on chromosome 6, distal from the beta-2-microglobulin ( $\beta_2m$ ) gene on chromosome 15 (47, 48). The HLA locus is comprised of genes encoding three classical MHC class I (MHC Ia) molecules (HLA-A, -B and -C) and three classical MHC class II (MHC II) molecules (HLA-DP, -DQ and -DR) (**Figure 3A**). Of note, the HLA locus also encodes four non-classical MHC class I (MHC Ib) molecules (HLA-E, -F, -G and -H), but these are not a major focus of this work and will not be discussed further. Humans can inherit three MHC Ia molecules, as well as three MHC II  $\alpha$  chains and four MHC II  $\beta$  chains with multiple isoforms from each parent. Given that MHC II  $\alpha$  and  $\beta$  chains can, in some cases, pair independently for each molecule, then a heterozygote individual can co-dominantly express six MHC Ia molecules and up to twelve MHC II molecules. In addition to the polygenicity of HLA genes, there is massive allelic variation at each of these genes across the human population: 17,191 HLA Class I and 6,716 HLA Class II alleles have been characterised to date (49). This theoretically results in vastly different complements of HLA molecules between any two individuals. The polygenicity and polymorphism of MHC genes allow the presentation of a larger repertoire of peptides, conferring better protection against a variety of pathogens that an individual can be exposed to throughout their lifespan (50).

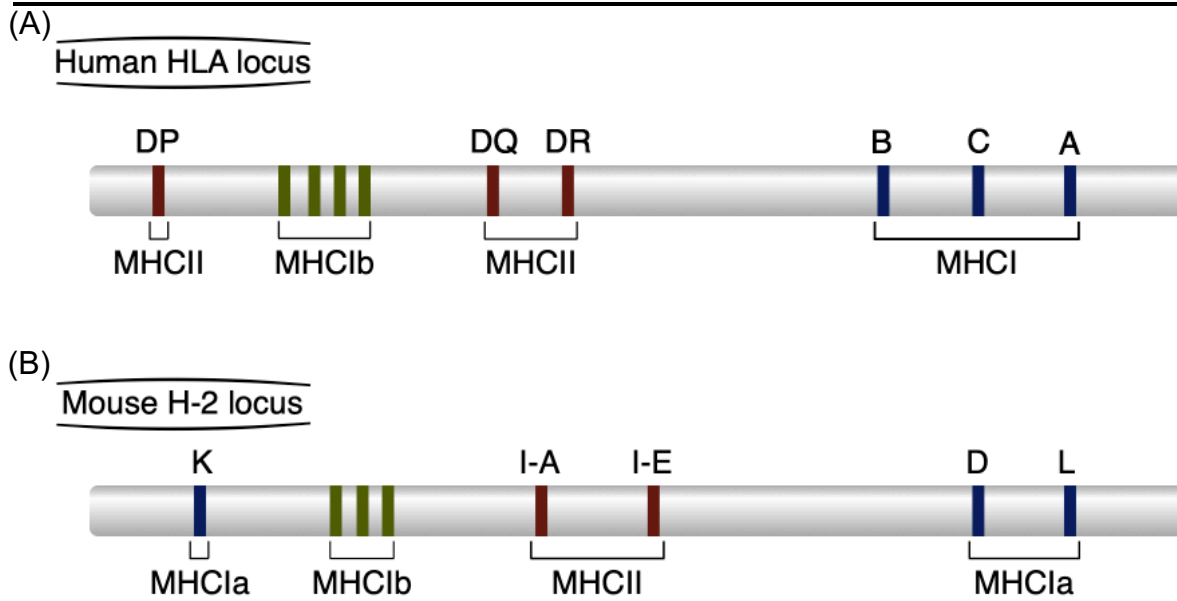


**Figure 3:** Gene map of the HLA and H-2 locus in humans and mice respectively. (A) The human HLA locus encodes three MHCIIa (HLA-A, -B and -C), four MHCIIb (HLA-E, -F, -G and -H) and three MHCII (HLA-DP, -DQ and -DR) molecules. (B) The mouse H-2 locus encodes three MHCIIa (H-2K, -D and -L), three MHCIIb (H-2M, -T and -Q) and two MHCII (I-A and I-E) molecules.

#### 1.4.2. Histocompatibility-2 (H-2) locus in mice

In mice, the MHC genes are encoded at the histocompatibility-2 (H-2) locus, which is positioned at a single locus on chromosome 17, distal from the  $\beta_2m$  gene on chromosome 2 (51, 52). The H-2 locus contains genes for three classical MHCIIa (H-2K, -D and -L), three non-classical MHCIIb (H-2M, -T and -Q) and two MHCII (I-A and I-E) molecules (**Figure 3B**). Like the HLA locus, the H-2 locus can encode a diverse array of allelic variants at each of these genes in wild and outbred mice.

In inbred strains, mice are homozygous for a specific allelic variant at each gene and strain-specific MHCII alleles have been well-characterised. The nomenclature for these

alleles is based on the original strains they were characterized in (53). For example, the C3H/HeJ mouse strain is defined as having the *k*-haplotype at the H-2 locus, where all MHC genes have the *k* allele, while the C57BL/6 mouse strain is defined as having the *b*-haplotype, where all MHC genes have the *b* allele.

Of note, the C57BL/6 mice is a natural knockout for the H-2L gene (53). As a result, a wildtype C57BL/6 mouse will express only two MHCI molecules: H-2D<sup>b</sup> and H-2K<sup>b</sup> while the C3H/HeJ mouse will express three MHCI molecules: H-2D<sup>k</sup>, H-2K<sup>k</sup> and H-2L<sup>k</sup>. These inbred mouse models are therefore useful tools for studying MHC and T cell biology in a highly controlled system, given that polymorphism at the H-2 locus is limited and can be manipulated through breeding.

### 1.4.3. MHC structure

MHC molecules are essential to present peptides to T cells to mediate their maturation, survival and activation (reviewed in (54)). The MHCI molecule is expressed on all nucleated cells and presents antigen to CD8 T cells, while the MHCII molecule is expressed on APCs and presents antigen to CD4 T cells.

The structure of the MHC molecule is crucial for its function. The MHCI molecule is a heterodimer of a large  $\alpha$ -chain polypeptide (the heavy chain) (55, 56), which is non-covalently bound to  $\beta_2m$  (the light chain) (57). The MHCI  $\alpha$ -chain contains three domains:  $\alpha_1$ ,  $\alpha_2$  and  $\alpha_3$ , with the peptide loading cleft positioned between  $\alpha_1$  and  $\alpha_2$  domains (**Figure 4A**). The  $\beta_2m$  functions to provide physical support to the peptide-

binding groove. In contrast, the MHCII molecule is a heterodimer of  $\alpha$  and  $\beta$  chain polypeptides (**Figure 4B**) (58). Both the  $\alpha$  and  $\beta$  chains are made up of two regions: the  $\alpha_1$  and  $\alpha_2$ , and  $\beta_1$  and  $\beta_2$  respectively, with the peptide-binding cleft localized between and  $\alpha_1$  and  $\beta_1$  domains.

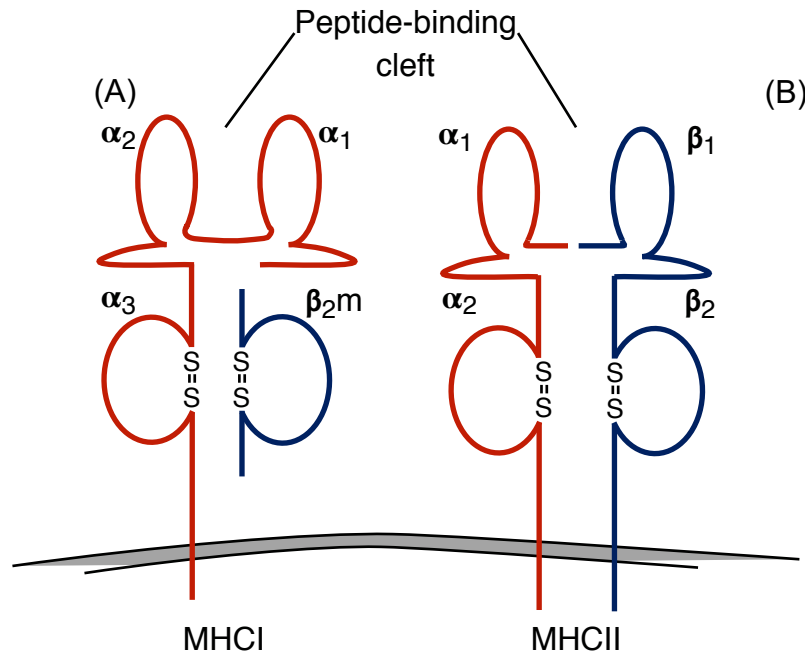


**Figure 4:** Schematic diagram of the structure of MHC I and MHC II molecules. The MHC I is made up of the  $\alpha$ -chain, stabilized by the  $\beta_{2m}$ , while the MHC II is made up of an  $\alpha$ - and  $\beta$ -chain. The peptide-binding cleft lies between the  $\alpha_1$  and  $\alpha_2$  domains and between the  $\alpha_1$  and  $\beta_1$  domains of MHC I and MHC II, respectively.

The peptide-binding cleft of both MHC I and MHC II share a similar structure to accommodate peptides for presentation. The domains proximal to the peptide-binding cleft ( $\alpha_1$  and  $\alpha_2$  for MHC I,  $\alpha_1$  and  $\beta_1$  for MHC II) form a curved  $\beta$ -sheet as a base and two  $\alpha$ -helices above, with the peptide-binding cleft between the two  $\alpha$ -helices (59). This cleft can accommodate a polypeptide from the target antigen. For MHC I, the cleft is closed at both ends by tyrosine residues, resulting in the binding of shorter peptides of ~8-10 amino acid (a.a.) (60). For MHC II, the cleft is open-ended, allowing longer

peptides of 13-25 a.a. in length to bind and be presented (60). While the binding of peptides to an MHC molecule is affected by the characteristics of a given MHC allele, each MHC allele can accommodate a wide repertoire of different peptides, as long as residues at certain positions can anchor the peptide into the peptide-binding cleft (61).

#### **1.4.4. Antigen presentation**

##### ***1.4.4.1. MHCII antigen processing and presentation pathway***

Peptide fragments presented by MHC molecules can either be sourced exogenously (extracellular environment), or endogenously (intracellular environment), and processed by distinct pathways. The exogenous pathway is used primarily by APCs to load peptides onto MHCII molecules for CD4 T cell activation (62). MHCII is expressed on APCs, including DCs, macrophages and B cells, as these cells can endocytose proteins from their extracellular environment. After endocytosis, exogenous proteins are degraded in early endosomes into peptide fragments by proteases (62). While the antigen is being degraded, the MHCII molecule is assembled in the endoplasmic reticulum (ER) and loaded with the Class II-associated li peptide (CLIP) to ensure stability of the molecule (63, 64). The stabilised MHCII molecule is then transported to the early endosome in a vesicle, which fuses with the endosome to give MHCII access to the exogenous antigen-derived peptides. The CLIP peptide is then displaced from the MHCII molecule by a chaperone protein called HLA-DM in humans and H-2M in mice, and replaced by an exogenous antigen-derived peptide (39). Once assembled, the peptide-loaded MHCII molecule (pMHCII) is exported onto the cell surface for presentation to CD4 T cells.

#### **1.4.4.2. MHC I antigen processing and presentation pathway**

In contrast to MHCII, the endogenous pathway is utilized by all nucleated cells to load endogenously-derived peptides into MHCI molecules (65). These proteins can be degraded during normal cell homeostasis by cytosolic proteasomes and are continuously presented on the cell surface by MHCI. After degradation, endogenously-derived peptides are further trimmed by aminopeptidases to generate peptides of the appropriate length (8-10 a.a. long) for loading onto the MHCI molecule (61). Once processed, peptide fragments are translocated into the ER by the transporter associated with antigen presentation (TAP) protein. MHCI molecules are expressed in the ER but must be loaded with peptide in order to exit the ER (66). As a result, newly assembled MHCI molecules are stabilized by the chaperone molecules ERp57, tapasin and calreticulin until an endogenously derived peptide can be loaded, at which point TAP will interact with tapasin to displace the chaperone molecules and permit peptide binding (67). Once the peptide is loaded onto MHCI, the peptide-loaded MHCI molecule (pMHCI) is transported to the cell surface for presentation (68).

Importantly, protein degradation can be altered during an infection. Infection-induced IFN $\gamma$  signalling upregulates the expression of specialized proteasome subunits that can integrate into the proteasome to form the immunoproteasome (69). Compared to constitutive proteasomes, immunoproteasomes preferentially cleave proteins into peptide fragments with amino acid residues that favour binding to the MHCI molecule (69–71). The loss of the immunoproteasome alters the repertoire of pathogen-derived peptides presented during an infection, which implies that the immunoproteasome influences the quality of antigenic peptides loaded on the MHCI molecule (72). In

addition, recent evidence suggests that the immunoproteasome also enhances the abundance of antigenic peptides presented on MHCI to promote a robust immune response during infection (73–75).

## 1.5. TCR recognition of pMHCI and downstream signaling

### 1.5.1. The TCR-pMHCI interaction

The interaction between the TCR and the pMHCI is highly conserved and it is critical for the selection, maintenance and activation of CD8 T cells (discussed in **Section 1.6**). The precise mechanisms that underpin TCR-pMHC recognition and signalling events have been extensively investigated with technological advances driving significant developments in our knowledge of the biology (reviewed in (19)).

The engagement of the TCR with its cognate pMHCI complex leads to the physical recruitment of the CD8 co-receptor to the signalling complex, where it binds to the  $\alpha_3$  domain of the MHC molecule (**Figure 2**) (76). This recruitment brings the CD8 co-receptor into close proximity with the TCR to 1) stabilize the interaction between TCR and pMHC, and 2) localize the Src family tyrosine kinase, Lck, to the CD3 signaling complex (discussed in **Section 1.5.2**). Studies using surface plasmon resonance (SPR) analysis have demonstrated that, in order to transduce a signal, TCRs typically exhibit an affinity for pMHCI within the range of  $K_D = 1\text{-}50\mu\text{M}$  (77, 78). The fact that such low affinity interactions are able to support signal transduction highlights the crucial role of the CD8 co-receptor in stabilizing the TCR-pMHCI complex (79).

The docking topology of the TCR over the pMHCI complex is highly conserved. The TCR conventionally docks diagonally above the pMHCI complex, with the  $\alpha_2$  and  $\alpha_3$  domain of the TCR positioned over the  $\alpha_1$  and  $\alpha_2$  helices of the MHCI, respectively (**Figure 2**). The CDR1 and CDR2 regions on the TCR are usually positioned directly

above the MHCI molecule, with the CDR3 region typically making prominent contacts with the loaded peptide (80, 81). This conventional docking topology permits the most variable region of the TCR to interact with the diverse repertoire of peptides that may be loaded into the MHCI molecule. It is also thought to facilitate optimal localization of CD8-associated Lck with the ITAMs of CD3 for effective phosphorylation and, thereafter, CD8 T cell activation (82, 83) (discussed in **Section 1.5.2**). It should be noted, however, that recent structural studies have demonstrated that a TCR can also dock in non-conventional, 180° reversed orientations with the MHC molecule, but this recognition modality does not appear to be conducive to signal transduction (84, 85).

While there are general guidelines for TCR-pMHCI interactions, there are no absolute rules governing CDR loop interactions with the peptide and MHC molecule. Multiple studies have demonstrated that certain TCRs position over the pMHCI complex in such a way that the CDR3 residues contact the MHC molecule, while germline-encoded CDR1 and CDR2 residues contribute to peptide interactions (28, 86, 87). This indicates that there is a level of flexibility in the TCR-pMHCI interaction and suggests that a TCR can utilize various binding strategies to provide optimal TCR-pMHCI interactions for CD8 T cell development, maintenance and activation (27).

### 1.5.2. Signal transduction upon TCR recognition of pMHC1

Upon TCR recognition of pMHC1 and engagement of the CD8 co-receptor, the Src kinase, Lck, which is associated with the intracellular domains of the CD8 co-receptor, is brought into proximity with the CD3 complex. Lck then phosphorylates the ITAM motifs on the CD3 chains, resulting in the recruitment and phosphorylation of signalling kinases, including zeta-chain associated protein kinase 70 (Zap-70), and propagation of the signalling cascade. TCR/CD3 signaling ultimately results in the activation of a number of transcription factors, including nuclear factor of activated cells (NFAT), nuclear factor  $\kappa$ B (NF- $\kappa$ B), and activator protein 1 (AP-1) (reviewed in (88)). These transcription factors translocate into the nucleus of T cells to regulate gene transcription for T cell activation.

## 1.6. TCR-pMHC interactions: importance in T cell biology

### 1.6.1. Thymic selection and MHC restriction

The fate of a thymocyte undergoing development is strongly dependent on the affinity of its TCR for self-pMHC complexes in the thymus (reviewed in (32, 89)). Thymocytes are “educated” at discrete points in their development in a process known as thymic selection.

Positive selection is a checkpoint where thymocytes are tested to determine whether their rearranged TCR is able to recognize and bind self-pMHC expressed on cortical thymic epithelial cells (cTECs) (reviewed in (90)). If the thymocyte does not express a functional TCR or express a TCR that does not bind to MHC with sufficient affinity, the thymocyte dies by apoptosis in a process known as death by neglect. At this stage, up to 90% of thymocytes express a non-functional TCR that cannot recognize self-pMHC and are removed from the peripheral repertoire (reviewed in (91)). If the rearranged TCR is capable of recognizing self-pMHC in the thymus, the TCR-pMHC interaction delivers a survival signal to the thymocyte that up-regulates the pro-survival molecule, Bcl-2 (92). Of note, DP thymocytes can differentiate into CD4+CD8- or CD4-CD8+ single-positive (SP) thymocytes (discussed in **Section 1.3.3**). This decision is guided by whether the TCR on the differentiating thymocyte binds to either MHCII or MHCI, respectively, during positive selection. Positive selection ensures that mature T cells express a TCR that is capable of interacting with its selecting MHC molecule in a phenomenon known as MHC restriction. The concept of MHC restriction was first proposed by Peter Doherty and Rolf Zinkernagel in 1974, when they demonstrated that effector CD8 T cells could only lyse virus-infected cells that expressed an MHC

allele present during their development in the thymus (93). They proposed that these cells were restricted in the periphery to interact with the MHC that they were positively selected on during thymic development.

Negative selection eliminates thymocytes that express TCRs that bind too strongly to self-pMHC. Recent evidence has shown that negative selection can occur in both the thymic cortex and the medulla. In the cortex, TCRs that interact with self-pMHC loaded with ubiquitous self-antigens on cortical DCs are first removed from the repertoire (94, 95). Following negative selection in the cortex, SP thymocytes migrate into the thymic medulla where the TCR is tested again by medullary thymic epithelial cells (mTECs). To access the full complement of self-antigen, mTECs express the transcription factor, autoimmune regulator (AIRE), which permits expression of all peripheral-tissue antigens (PTA; reviewed in (96)). PTA-derived peptides can then be presented on MHC I and MHC II directly by mTECs, or indirectly by thymic DCs, to developing SP thymocytes (reviewed in (97, 98)). It is proposed that a further 30-50% of all positively selected thymocytes are deleted by negative selection (99). Thus, only around 3% of all thymocytes that enter the thymus develop into mature peripheral T cells (100, 101).

### 1.6.2. Homeostatic maintenance of naïve CD8 T cells

After mature T cells emerge from the thymus, the maintenance of CD8 T cells in the periphery is governed by complex homeostatic mechanisms. For naïve CD8 T cells, homeostasis is maintained by 1) the homeostatic cytokine, IL-7 (102, 103), 2) sphingosine-1-phosphate (S1P) signalling (104) and 3) the transient but repeated contact of the TCR with self-pMHC, which is termed tonic signalling (105, 106).

Tonic signalling refers to the sub-threshold signals driven by the interaction of the TCR with self-pMHC that do not trigger canonical TCR activation (107), but maintain the expression of the anti-apoptotic Bcl-2 and other Bcl-2 family members such as Mcl-1 to promote the survival of naïve CD8 T cells (108). Adoptive transfers of naïve CD8 T cells into  $\beta_2m^{-/-}$  recipient mice prevented the survival of transferred cells, implying that the continuous TCR contact with self-pMHC ligands is absolutely crucial for the survival of naïve CD8 T cells (105). Furthermore, studies using transgenic mouse models have demonstrated that tonic signalling is mediated by the same peptide ligand and MHC molecule that mediated positive selection of that T cell during thymic development, suggesting that tonic signalling occurs in both a peptide- and MHC-restricted manner (109).

The interaction between a TCR and self-pMHC in addition to IL-7 signalling in the periphery can mediate either the homeostatic turnover or rapid proliferation of circulating T cells. Under conditions of CD8 T cell lymphopenia, residual naïve CD8 T cells undergo rapid lymphopenia-induced proliferation (LIP) and expand to repopulate the periphery (106, 109–112). LIP of naïve CD8 T cells has largely been studied using

adoptive transfer of a small population of naïve T cells (usually transgenic CD8 T cells) into T cell deficient recipients (RAG<sup>-/-</sup>, SCID or irradiated hosts) to simulate a lymphopenic environment and its effect on LIP. Under lymphoreplete conditions on the other hand, CD8 T cells undergo a slow homeostatic turnover to maintain the number of naïve CD8 T cells at steady state. Multiple studies using complex mathematical modelling and BrdU incorporation have determined that the rate of homeostatic turnover of naïve T cells occurs at the slow rate of 5 divisions over a period of 2 weeks (113–115).

### **1.6.3. Activation of CD8 T cells for immune protection**

Naïve antigen-specific CD8 T cells are activated in the lymph node draining the site of infection, where infected or cross-presenting DCs present pathogen-derived peptides loaded into MHCI on their cell surface (discussed in **Section 1.4.4**). The activation, expansion and differentiation of naïve CD8 T cells to acquire effector functions requires priming by DCs, as demonstrated by experiments depleting DCs *in vivo* (116–118). The process of activation requires three critical signals: 1) TCR recognition of pMHCI on DCs, 2) co-stimulatory interactions and 3) cytokine signalling.

The signal 1 is delivered through the physical interaction of the TCR with the pMHCI complex presented on DCs. Signals 2 and 3 are also required for full activation of CD8 T cells to enhance the magnitude of response, but they also shift qualitative aspects of the response, such as improving memory formation or changing the type of effector functions engaged (119, 120). Signal 2 is delivered by a triad of co-stimulatory molecules expressed on professional APCs for effective T cell activation: B7-1 (CD80),

B7-2 (CD86), ICAM-1 (CD54) and Lymphocyte Function-Associated Antigen 3 (LFA-3; CD48) (121), where these interactions are prerequisites for T cell activation, and promote T cell proliferation and cytokine production (122–124). The absence of co-stimulatory signals, when T cells are presented with signal 1 only, results in T cell anergy (a state of unresponsiveness), implying the importance of signal 2 to promote effective T cell activation (122).

Signal 3 is delivered by cytokines such as interleukin 12 (IL-12), interferon  $\alpha$  (IFN $\alpha$ ) and IFN $\beta$  (125, 126). The presence of these cytokines is critical to promote T cell clonal expansion alongside the development of effector functions, such as the production of cytokines (IFN $\gamma$ , TNF, IL-2 and others) and cytotoxicity (reviewed in (126)). In the absence of signal 3, CD8 T cells survive poorly, fail to develop optimal effector functions and do not form a robust memory population (125–127).

Together, these three signals trigger the full activation of naïve CD8 T cells, leading to clonal expansion and differentiation into effector CD8 T cells that can produce cytokines and lyse target cells during an infection.

## **1.7. CD8 T cell immunodominance**

### **1.7.1. Determinants of immunodominance**

Following infection, only a small proportion of pathogen-derived epitopes can elicit CD8 T cell responses. Of those responses, the magnitudes of these epitope-specific CD8 T cell responses fall into a highly reproducible hierarchy known as an immunodominance hierarchy (reviewed in (128)). A relatively large CD8 T cell response is described as being immunodominant, while a smaller response is known as a subdominant response.

The CD8 T cell immunodominance hierarchy is shaped by a number of determinants. These determinants can be broadly grouped into those that influence the CD8 T cells, such as the frequency of naïve precursor CD8 T cells and the affinity of their TCRs for antigen, and those that affect antigen presentation, such as antigen dose (128). In addition, the phenomenon of immunodomination, where the presence of an immunodominant CD8 T cell response can suppress a subdominant CD8 T cell response, has also been shown to influence the immunodominance hierarchy (129, 130).

### **1.7.2. Precursor frequency**

The frequency of naïve epitope-specific CD8 T cells is considered to be one of the critical determinants of immunodominance (131, 132). The size of an endogenous antigen-specific CD8 T cell population is highly reproducible and can range from 1 to

89 cells per million naïve CD8 T cells per mouse (133), which makes detection and enumeration of naïve epitope-specific CD8 T cells challenging. There have been several studies that have demonstrated a close correlation between the naïve CD8 T cell frequency and immune response magnitude. For instance, in the vaccinia virus model, CD8 T cell responses against the H-2K<sup>b</sup>B8R<sub>20-27</sub> and H-2K<sup>b</sup>A47<sub>138-146</sub> epitopes are reproducibly large (immunodominant) after infection (134). The precursor frequencies of naïve H-2K<sup>b</sup>B8R<sub>20-27</sub>- and H-2K<sup>b</sup>A47<sub>138-146</sub>-specific CD8 T cells correlates with the response magnitude following infection, at ~1,000 and ~120 cells per mouse, respectively (133–135).

More recently, several studies have demonstrated that the correlation between naïve CD8 T cell precursor frequency and response magnitudes is not absolute (136–140). In the C57BL/6 model of influenza A virus (IAV) infection, CD8 T cell responses to nucleoprotein peptide (NP<sub>366-374</sub>) and acidic polymerase peptide (PA<sub>224-233</sub>) are immunodominant (141). However, naïve H-2D<sup>b</sup>NP<sub>366-374</sub>- and H-2D<sup>b</sup>PA<sub>224-233</sub>-specific CD8 T cell populations are relatively small, at ~36 and ~64 cells per mouse, respectively (133, 137). In contrast, the naïve CD8 T cell populations specific for the subdominant epitopes – namely those derived from non-structural protein 2 (NS<sub>2114-121</sub>) or polymerase B subunit 1 (PB1<sub>703-711</sub>) bound to H-2K<sup>b</sup>, or that derived from a shifted framework polymerase B 1 protein (PB1-F<sub>262-70</sub>) bound to H-2D<sup>b</sup> – are substantially larger, at ~282, ~308 and ~225 cells per mouse, respectively (133, 136, 137). In a separate model of respiratory syncytial virus (RSV) infection in adult CB6F1 hybrid mice (142), the H-2K<sup>d</sup>M<sub>282-90</sub>-specific CD8 T cell response is immunodominant, comprising up to 40% of total effector CD8 T cell numbers, while the subdominant H-2D<sup>b</sup>M<sub>187-195</sub>-specific CD8 T cells make up only 10% of effector CD8 T cells after RSV

infection. However, the precursor frequencies of both H-2K<sup>d</sup>M2<sub>82-90</sub>- and H-2D<sup>b</sup>M<sub>187-195</sub>-specific naïve CD8 T cells are similar, at ~400 cells in naive mice (142), demonstrating another disparity between precursor frequency and immunodominance hierarchy.

These studies demonstrate that, while the size of a naïve epitope-specific CD8 T cell population is highly reproducible from individual to individual, the size of this population is not the sole determinant of immune response magnitude following infection. Importantly, our understanding of how the size of the naïve epitope-specific CD8 T cell population integrates with other determinants is wholly unclear.

### 1.7.3. TCR affinity for antigen

A second determinant that plays a role in dictating the immunodominance hierarchy following a viral infection is the intrinsic affinity of the TCR for the pMHC complex. Analyses of both CD4 and CD8 T cell responses suggested that the relative expansion of particular clones during antigen-specific responses may correlate with the TCR affinity for the pMHC complex, where precursors with low avidity for antigen proliferate to a lesser extent than those with higher avidity (143–145).

This notion was elegantly demonstrated in a novel study by Zehn et al (2009) where C57BL/6 mice were infected with the *Listeria monocytogenes* bacteria expressing variants of the H-2K<sup>b</sup>Ova<sub>257</sub> peptide with varying affinities for the H-2K<sup>b</sup>Ova<sub>257</sub>-specific TCR (OTI) (146). While OTI transgenic T cells responding to the WT N4 (SIINFEKL) peptide, the moderately lower affinity Q4 (SIIQFEKL) peptide, or the markedly

diminished affinity V4 (SIIVFEKL) variant, were all capable of the same initial rate of proliferation, the affinity of TCR-pMHC recognition was significantly associated with the extent of division. Thus, the final CD8 T cell response magnitude correlated with TCR-pMHC affinity (N4 < Q4 < V4).

In the C57BL/6 model of IAV infection, subdominant responses against H-2D<sup>b</sup>PB1-F2<sub>62</sub> and H-2K<sup>b</sup>NS2<sub>114</sub> have been correlated with lower affinity TCR (147), supporting the idea that low TCR affinity can restrict CD8 T cell response magnitude. In addition, affinity maturation of TCRs has been observed previously, where CD8 T cells bearing higher affinity TCRs have been shown to selectively expand during infection, giving rise to a narrower repertoire of TCRs with increased overall affinity over the course of infection (148). The affinity of TCR clonotypes utilized in the immune response has been well-documented in C57BL/6 model of IAV infection (149). The immunodominant CD8 T cell responses against H-2D<sup>b</sup>NP<sub>366</sub>- and H-2D<sup>b</sup>PA<sub>224</sub>-epitopes predominantly utilize TRBV13-1 and TRBV29, respectively, after IAV infection. Both TRBV13-1 and TRBV29 have been shown to bind their cognate antigen (H-2D<sup>b</sup>NP<sub>366</sub> and H-2D<sup>b</sup>PA<sub>224</sub>, respectively) with higher affinity than other TRBVs in the antigen-specific CD8 T cell population, and therefore preferentially expand during the immune response against IAV (80, 149, 150). Affinity may also impact on the lifespan of effector T cells, as T cells with lower affinity TCRs have been seen to undergo early apoptosis regulated by the pro-apoptotic molecules BIM, NOXA and Mcl1 (151, 152). Altogether, there is strong evidence in current literature to support the hypothesis that the intrinsic affinity of TCR for pMHC is a strong determinant of the primary CD8 T cell response magnitude during infection and the longevity of those cells.

#### 1.7.4. Antigen abundance and peptide presentation

The relative abundance of peptide-antigen presented during infection to stimulate a given CD8 T cell population is another parameter that influences the magnitude of response. Several studies have demonstrated a positive correlation between antigen abundance and the magnitude of CD8 T cell responses, by altering the abundance of specific epitopes using various strategies, such as 1) infections with increasing doses of viruses or 2) employing recombinant viruses with the expression of target epitopes under the control of differentially expressed genes (153–155). However, it should be noted, that the immunogenicity of antigen plateaus with increasing abundance and increasing the amount of antigen beyond that level can thereafter reduce the magnitude of the CD8 T cell response (156). This suggests that although antigen abundance correlates well with CD8 T cell response magnitude, there is a homeostatic mechanism at play to curtail the expansion of CD8 T cells when extreme levels of antigen are presented.

In addition, defective ribosomal products (DRiPs) derived from viral-derived proteins contribute, in part, to early T responses during infection. During an infection, the rapid (immuno)proteasomal processing of viral proteins inevitably gives rise to misfolded or prematurely terminated polypeptides (157). CD8 T cell responses to DRiP antigens have been identified across various infection models (134, 158), although the relationship between DRiP abundance and CD8 T cell magnitude is still unclear.

The level of antigen presentation is not necessarily predictive of the size of the CD8 T cell response. A recent study by Ting et al (2019) elegantly demonstrated the relative

abundance and mode of antigen presentation using mass spectrometry and immunopeptidomics in the IAV model of infection (75). Although the H-2D<sup>b</sup>PA<sub>224</sub> epitope was poorly presented, it was capable of eliciting an immunodominant CD8 T cell response, demonstrating that the abundance of antigen presented is not predictive of the magnitude of the CD8 T cell response. In addition, they identified novel peptides that were presented at adequate levels but were unable to generate a CD8 T cell response, further illustrating the discrepancy between antigen abundance and CD8 T cell response magnitude.

Altogether, there have been multiple studies performed to correlate the level of antigen abundance and mode of presentation with the magnitude of CD8 T cell responses, there is still a substantial lack of evidence to predict the immunodominance hierarchy using antigen dose as a primary determinant.

### 1.7.5. Immunodomination

Immunodomination describes the phenomenon where the presence of an epitope-specific response suppresses other T cell responses. It is commonly thought of as immunodominant CD8 T cell responses suppressing subdominant CD8 T cell responses. However, within an epitope-specific CD8 T cell population, we can also observe individual CD8 T cell clones outcompeting other clones after activation (129, 130, 159). Immunodomination therefore impacts CD8 T cells within an antigen-specific population but it can also influence CD8 T cells across different epitope specificities. Immunodomination is proposed to be a consequence of multiple mechanisms, including individual naïve CD8 T cells competing for access to APCs, preferential presentation of certain epitopes on MHCI, suppression of APCs by early effector responses to inhibit subsequent priming, and the rapid activation of certain responses that results in poor activation of slower CD8 T cell responses (reviewed in (128)).

The phenomenon of immunodomination occurring within an epitope-specific CD8 T cell population was demonstrated by the transfer of naïve transgenic T cells into recipients prior to infection, to result in the suppression of endogenous epitope-specific CD8 T responses cells during infection. For example, Kedl et al (2000) adoptively transferred transgenic ovalbumin (Ova<sub>257</sub>)-specific (OT-I) naïve CD8 T cells into naïve C57BL/6 mice before infection with an Ova-expressing vaccinia virus (160). They observed the preferential expansion of transferred OT-I cells compared to endogenous H-2K<sup>b</sup>Ova<sub>257</sub>-specific CD8 T cells. Similarly, the transfer of transgenic lymphocytic choriomeningitis virus (LCMV)-derived H-2D<sup>b</sup>GP<sub>33-41</sub>-specific CD8 T cells impeded the endogenous H-2D<sup>b</sup>GP<sub>33</sub> responses (161). However, the presence of transferred H-

2D<sup>b</sup>GP<sub>33-41</sub> transgenic cells failed to inhibit another immunodominant CD8 T cell response following LCMV infection, suggesting that there are various mechanisms at play between CD8 T cells within and across distinct specificities.

The effect of immunodomination across CD8 T cells of different specificities is most easily demonstrated by the impact of 1) the removal of prominent virally-encoded epitopes, or 2) the introduction of novel epitopes into a virus, on existing CD8 T cell responses. The removal of the immunodominant H-2D<sup>b</sup>NP<sub>366</sub> and H-2D<sup>b</sup>PA<sub>224</sub> epitopes during IAV resulted in a compensatory increase of the otherwise subdominant H-2K<sup>b</sup>PB1<sub>703</sub>-specific response, suggesting that the H-2K<sup>b</sup>PB1<sub>703</sub>-specific response is suppressed by the presence of the two immunodominant responses (162). On the other hand, the introduction of an epitope not usually present during a viral infection can also modulate the immunodominance hierarchy. The inclusion of the Ova<sub>257</sub> epitope into IAV resulted in an unaltered immunodominant H-2D<sup>b</sup>NP<sub>366</sub>-specific response but it diminished the magnitude of the co-dominant H-2D<sup>b</sup>PA<sub>224</sub>-specific CD8 T cell response, relative to WT IAV virus (163). Altogether, these studies suggest that although immunodomination does occur across CD8 T cell populations with different specificities, some specificities are more sensitive to immunodomination than others.

Overall, studies in the field of CD8 T cell immunodomination have shown disparate observations in various models using techniques such as TCR transgenic mouse models and reverse genetics to create viruses with the removal or introduction of epitopes. However, the rules governing immunodomination are unclear, warranting

further investigation to better understand the role of immunodomination in determining an effective CD8 T cell response during infection.

## 1.8. The C57BL/6 model of influenza A virus infection

The IAV infection in the C57BL/6 mouse is a well-characterized experimental system for the analysis of CD8 T cell responses. Primary intranasal infection causes a transient, localized acute pneumonia cleared by day 10 with no evidence of persistent viral antigen (164). Experimentally, the two strains of viruses that are most commonly used to study immunity against IAV infection are the HKx31 (H3N2) and PR8 (H1N1) virus. The use of serologically distinct strains allows the analysis of primary and secondary CD8 T cell responses in the absence of pre-formed neutralizing antibodies (165).

A distinct advantage of this model for the study of anti-viral CD8 T cell responses is the fact that IAV infection of C57BL/6 mice induces a number of CD8 T cell responses that have been extremely well-characterised with respect to 1) epitope specificity (166), 2) the frequency of naïve epitope specific CD8 T cells (133, 136, 137), 3) response magnitude after infection (167–171) and 4) the TCR clonotypic repertoire of naïve and immune epitope-specific CD8 T cells (28, 136, 149, 172–177). Following IAV infection of C57BL/6 mice, the most dominant and well-studied epitopes include the previously mentioned H-2D<sup>b</sup>NP<sub>366</sub>, H-2D<sup>b</sup>PA<sub>224</sub>, H-2D<sup>b</sup>PB1-F2<sub>62</sub>, H-2K<sup>b</sup>PB1<sub>703</sub> and H-2K<sup>b</sup>NS2<sub>114</sub> epitopes. After primary IAV infection, H-2D<sup>b</sup>NP<sub>366</sub> and H-2D<sup>b</sup>PA<sub>224</sub> are immunodominant, making up the largest CD8 T cell populations, while all other responses, including those directed at H-2D<sup>b</sup>PB1-F2<sub>62</sub>, H-2K<sup>b</sup>NS2<sub>114</sub> and H-2K<sup>b</sup>PB1<sub>703</sub>, make up smaller subdominant populations (137). There is, therefore, a distinct IAV-specific CD8 T cell immunodominance hierarchy in C57BL/6 mice. Naïve CD8 T cell populations specific for each IAV-derived epitope have been enumerated

in C57BL/6 mice and are highly reproducible across individual mice (136, 137). As mentioned, the repertoire of TCRs that comprise the naïve and immune CD8 T cell population has been well-defined for these influenza epitopes. Analysis of TCR repertoires from several of these epitope-specific populations have revealed that TCRs within an epitope specificity share remarkably consistent and characteristic features between individual mice. This reproducibility of pMHC1-specific CD8 T cell frequency and immunodominance hierarchy and the detailed characterization of qualitative aspects of the IAV-specific CD8 T cell response, provides an ideal model with which to study the determinants driving an effective CD8 T cell response during virus infection.

## 1.9. Specific aims of this study

This thesis is a continuation of my BSc. (Hons) work, with the broad aim of investigating how both the nature and amount of MHCI expression determines CD8 T cell selection, homeostatic maintenance and activation. In particular, this thesis addresses how the CD8 T cell response to viral infection is able to compensate in the absence of either the H-2D<sup>b</sup> or H-2K<sup>b</sup> MHCI molecule. It also investigates how alterations in the level of MHCI gene expression influence CD8 T cell generation and homeostatic maintenance, and the efficiency with which a non-restricting MHCI molecule, either H-2K<sup>b</sup> or H-2D<sup>b</sup>, influences CD8 T cell selection and activation. Using a well characterized mouse model of IAV infection in C57BL/6 mice, this thesis addresses the following aims:

1. To more deeply characterise the functional capacity of alloreactive CD8 T cells in response to cognate antigen.
2. To identify and characterise a T cell ligand that uniquely binds H-2K<sup>b</sup> in mice lacking H-2K<sup>b</sup>.
3. To examine the impact of physiological MHCI expression levels on the homeostatic maintenance of naïve CD8 T cells.
4. To assess the effect of immunodomination on CD8 T cells, and the relative capacity of CD8 T cell populations to compensate for the loss of individual MHCI molecules during infection.

Collectively, this thesis aims to provide an improved understanding of the key determinants underpinning the development, survival and responsiveness of the peripheral repertoire of CD8 T cells.

## 2. Materials and Methods

### 2.1. Mice

All mice used in this thesis (**Table 2**) were bred and housed under SPF conditions in the Animal Research Laboratory (ARL) in Monash University, Victoria, Australia. C57BL/6 mice were sourced from the Monash Animal Research Platform (MARP). Mice infected with IAV were housed in the QC2 quarantine facility at the ARL. All animal experimental protocols used in this thesis were approved by Monash University Ethics Committee. At the commencement of each experiment, mice were aged between 6 and 12 weeks and mice used within each experiment were age- and sex-matched.

**Table 2:** Mouse strains used in the studies described in this thesis.

Strain	Background	MHCIIa haplotype	MHCIIa genes expressed
C57BL/6 MARP	C57BL/6	<i>b</i>	2 copies of D gene 2 copies of K gene Natural knockout of L gene
H-2D <sup>b-/-</sup> K <sup>b+/+</sup> (D <sup>b-/-</sup> )	C57BL/6	<i>b</i>	0 copies of D gene 2 copies of K gene Natural knockout of L gene
H-2D <sup>b-/-</sup> K <sup>b+/-</sup> (K <sup>b+/-</sup> )	C57BL/6	<i>b</i>	0 copies of D gene 1 copy of K gene Natural knockout of L gene
H-2D <sup>b+/+</sup> K <sup>b-/-</sup> (K <sup>b-/-</sup> )	C57BL/6	<i>b</i>	2 copies of D gene 0 copies of K gene Natural knockout of L gene
H-2D <sup>b+/-</sup> K <sup>b-/-</sup> (D <sup>b+/-</sup> )	C57BL/6	<i>b</i>	1 copy of D gene 0 copies of K gene Natural knockout of L gene
H-2D <sup>b-/-</sup> K <sup>b-/-</sup> (DKO)	C57BL/6	<i>b</i>	0 copies of D gene 0 copies of K gene Natural knockout of L gene

## 2.2. Viruses

Two strains of influenza A virus were used in this study: A/Puerto Rico/8/34 (PR8, H1N1) and A/Hong Kong/X31 (HKx31, H3N2) (165). These two strains of IAV differ in their surface glycoproteins (haemagglutinin (HA) and neuraminidase (NA)) but share other internal viral proteins (nucleoprotein (NP), acidic polymerase (PA), non-structural proteins (NS1 and NS2), polymerase B1 (PB1 and PB2)). The use of serologically distant viruses allows the investigation of secondary T cell responses without interference from cross-protective neutralising antibody responses.

Recombinant HKx31 and PR8 viruses expressing an epitope from ovalbumin (HKx31-Ova and PR8-Ova, respectively) were used in some experiments. The Ova epitope (peptide sequence: SIINFEKL; Ova<sub>257-264</sub>) was inserted into the NA stalk of both HKx31 and PR8 (163). This insertion introduces an immunodominant H-2K<sup>b</sup>-restricted CD8 T cell response directed against Ova during IAV infection.

## 2.3. Infection and immunization of mice

For primary infection, mice were anaesthetised by inhalation of isoflurane and infected intranasally (i.n.) with  $1 \times 10^4$  plaque forming units (PFU) of influenza A virus (IAV), either WT strain HKx31 or HKx31-Ova in 30  $\mu$ L of PBS. For secondary infections, mice primed with the above method were re-challenged i.n. 60 days post-primary infection with  $1 \times 10^4$  PFU of PR8 or PR8-Ova virus in 30  $\mu$ L of PBS.

For DC vaccination, mice were intravenously (i.v.) immunized with  $1 \times 10^6$  activated bone marrow derived dendritic cells (BMDCs) that had been pulsed with the IAV-derived PA<sub>224</sub> peptide in 200  $\mu$ L of PBS.

## 2.4. Tissue sampling, processing and lymphocyte counting

### 2.4.1. Lungs

For isolation of lymphocyte populations from the lung parenchyma, mice were killed *via* CO<sub>2</sub> asphyxiation. Immediately after death, the abdominal section of the vena cava was cut and lungs were perfused through the right ventricle with 10 mL phosphate buffered saline (PBS) containing 2 mM ethylenediaminetetraacetic acid (EDTA). Lungs were harvested into 1 mL of complete Roswell Park Memorial Institute (cRPMI) (**Appendix 8.3**) before being cut into small fragments and digested with lung digestion media (**Appendix 8.3**) at 37°C, 5% CO<sub>2</sub> for 30 mins. Following digestion, lung homogenates were mechanically disrupted and passed through a 70  $\mu$ m filter (BD Falcon, BD Biosciences, Bedford, MA, USA). Collagenase activity was quenched with 20ml of cRPMI. Lungs cells were pelleted (515 x *g*, 6 mins, 4°C), resuspended in cRPMI and filtered through a 70  $\mu$ m sieve. The cell suspension was underlaid with 70% Percoll (**Appendix 8.3**) and centrifuged at 800 x *g* for 20 mins at room temperature with minimum deceleration. Density separated lymphocytes at the interface were harvested into 10 ml of cRPMI, centrifuged (800 x *g*, 6 mins, 4°C) and resuspended at the optimal density as required for experiments.

#### **2.4.2. Spleen and peripheral lymph nodes**

For the isolation of lymphocyte populations in secondary lymphoid tissues, pooled spleen and major lymph nodes (axillary, brachial, cervical, inguinal, mesenteric), or mediastinal (mLN) were harvested into cRPMI. Tissues were mechanically disrupted with a 3 mL syringe plunger and passed through a 70 µm filter. Cells were then pelleted (515 x *g*, 6 mins, 4°C) and resuspended at the optimal density for experiments.

For spleen samples, red blood cells were lysed with Red Blood Cell Lysing Buffer Hybri-Max™ (Sigma-Aldrich, St. Louis, Missouri, USA) for 2 mins at room temperature (RT). The lysing reaction was quenched with cold Hanks balanced salt solution (HBSS), centrifuged at 515 x *g* for 6 mins at 4°C and resuspended at the optimal density for experiments.

#### **2.4.3. Thymus**

For the isolation of thymocytes from the thymus, mice were killed *via* CO<sub>2</sub> asphyxiation. Immediately after death, the abdominal section of the vena cava was cut, and the thymus was perfused through the left ventricle with 10mL PBS containing 2 mM EDTA. Thymi were harvested into 4 mL of cRPMI, mechanically disrupted with a 3 mL syringe plunger and passed through a 70 µm filter. Thymocytes were then pelleted (515 x *g*, 6 mins, 4°C) and resuspended at the optimal density for experiments.

#### **2.4.4. Bone marrow**

For the isolation of bone marrow to generate BMDCs, mice were killed *via* CO<sub>2</sub> asphyxiation and the skin around the limbs were removed to harvest the femur and humerus into sterile HBSS. Excess muscle tissue surrounding the bones was removed and bone marrow was harvested by removing each end of the bone and expelling the marrow with 5 mL of PBS containing 2% fetal calf serum (FCS) in a 22-gauge needle. The bone marrow was mechanically disrupted with a 3 mL syringe plunger, passed through a 70 µm filter and pelleted (300 x g, 8 mins, 27°C). Red blood cells were lysed with Red Blood Cell Lysing Buffer Hybri-Max™ for 2 mins at RT. The lysing reaction was quenched with cold cRPMI, cell were pelleted again and resuspended at the optimal density for cell culturing.

#### **2.4.5. Viable lymphocyte counts**

Viable lymphocyte counts were determined for tissues by trypan blue exclusion. Aliquots of cells were diluted in 0.1% solution of Trypan Blue dye (Gibco, Waltham, Massachusetts, USA) in PBS, and 10 µL was loaded onto a haemocytometer (Hirschmann, Neckartenzlingen, Germany). Cells were examined under a light microscope (Leica Microsystems, Wetzlar, Germany). The viable cell count represents the number of live lymphocytes with the exclusion of dead cells. The total cell number was determined by the equation:

$$\text{Average count} \times \text{dilution factor} \times \text{total volume of sample (ml)} \times 10^4$$

## 2.5. Cell lines

### 2.5.1. 2.4G2 hybridoma cell line

2.4G2 supernatant was used to block non-specific binding of fluorescently labelled antibodies to Fc $\gamma$  receptors. 2.4G2 cells are a B cell hybridoma cell line that produces a monoclonal antibody specific for a common epitope between CD16 (Fc $\gamma$ RIII) and CD32 (Fc $\gamma$ RII). 2.4G2 cells were seeded into 175 cm<sup>2</sup> tissue culture flasks in cRPMI and cultured at 37°C with 5% CO<sub>2</sub> until spent. The supernatant was recovered following centrifugation (515G for 6 mins) and filtered through a 0.22 $\mu$ m vacuum filter. Aliquots of 2.4G2 hybridoma supernatant were stored at -80°C until use.

### 2.5.2. Ag8.653 hybridoma cell line for GM-CSF

GM-CSF was used to culture bone marrow derived dendritic cells (BMDCs) for DC vaccination. Ag8.653 is a commercially available myeloma cell line transfected with the GM-CSF gene to constitutively produce the GM-CSF cytokine. Ag8.653 hybridoma cells were seeded into 175 cm<sup>2</sup> tissue culture flask in cIMDM containing 1mg/mL of antibiotic geneticin (G418 sulfate, Gibco) to select for hybridoma cells that have retained the GM-CSF gene. Cells were cultured at 37°C with 5% CO<sub>2</sub> until confluent. Once confluent, cells were harvested and washed with fresh cIMDM without geneticin to remove all traces of antibiotics. Cells were reseeded into fresh 175 cm<sup>2</sup> in cIMDM without geneticin and cultured at 37°C with 5% CO<sub>2</sub> until spent. The supernatant was recovered following centrifugation (515G for 6 mins at 4°C) and filtered through a 0.22 $\mu$ m vacuum filter. The concentration of GM-CSF in supernatant was quantified

using the ELISA MAX™ Standard Set Mouse GM-CSF kit (Biolegend, San Diego, California, USA). GM-CSF supernatant aliquots were stored at -80°C until use.

### **2.5.3. HEK 293T cells**

HEK 293T cells are an easily transfected human kidney cell line used to express TCRs that are identified through multiplex RT-PCR. These cells were grown in cDMEM at 37°C with 10% CO<sub>2</sub>, passaged when confluent and then transfected with plasmid constructs encoding for TCR  $\alpha$  and  $\beta$  chains, as well as the chains of the CD3 complex and CD8 co-receptors. Successfully transfected cells were used to study the binding capacity of a TCR against its cognate pMHC I molecule using tetramer staining.

## 2.6. Tetramers

Monomeric biotinylated MHCI complexes were refolded with peptides at the Monomer Facility at the University of Melbourne. All monomers were mouse MHCI molecules stabilized non-covalently with human  $\beta_2m$ . 10  $\mu\text{g}$  of monomers ( $1\mu\text{g}/\mu\text{L}$ ) were tetramerized with either 15  $\mu\text{g}$  of PE- or 10 $\mu\text{g}$  of APC-conjugated streptavidin (both at 1  $\mu\text{g}/\mu\text{L}$ , Invitrogen, Carlsbad, California, USA) in 6 additions at 10 min intervals, with incubations on ice in the dark. Tetramers were topped up with PBS to a final volume of 30  $\mu\text{L}$  and left overnight at 4°C in the dark. Tetramers (0.3  $\mu\text{g}/\mu\text{L}$ ; **Table 3**) were stored in the dark at 4°C until required for tetramer staining of antigen-specific CD8 T cells (**Section 2.7**).

**Table 3:** Tetramers used in the studies described in this thesis<sup>1</sup>.

Monomers	Fluorophore conjugate
<i>Influenza A virus tetramers</i>	
H-2D <sup>b</sup> NP <sub>366-374</sub>	PE
H-2K <sup>d</sup> NP <sub>147-155</sub>	PE
H-2D <sup>b</sup> PA <sub>224-233</sub>	PE
H-2D <sup>b</sup> PB1-F2 <sub>62-70</sub>	PE
H-2K <sup>b</sup> NS2 <sub>114-120</sub>	APC, PE
H-2K <sup>b</sup> PB1 <sub>703-711</sub>	APC, PE
<i>Vaccinia virus tetramer</i>	
H-2K <sup>b</sup> B8R <sub>20-27</sub>	PE
<i>HIV virus tetramer</i>	
H-2K <sup>d</sup> AMQ <sub>197-205</sub>	APC
<i>Others</i>	
H-2K <sup>b</sup> Ova <sub>257-263</sub>	APC, PE

<sup>1</sup> All monomers were made by Dr. Jie Lin from the Monomer Facility at the Peter Doherty Institute at The University of Melbourne

Chimeric H-2K<sup>b</sup> monomers were refolded with H-2K<sup>b</sup>-restricted peptides but the MHCI heavy chain contained mouse  $\alpha_1$  and  $\alpha_2$  domains from H-2K<sup>b</sup> and the  $\alpha_3$  domain from H-2D<sup>b</sup> (**Table 4**). Chimeric monomers were tetramerized and stored similar to wildtype tetramers as described above.

**Table 4:** H-2K<sup>b</sup> chimeric tetramers used in the studies described in this thesis<sup>1</sup>

Chimeric monomers	Fluorophore conjugate
<i>Influenza A virus tetramers</i>	
H-2K <sup>b</sup> NS2 <sub>114-120</sub>	APC, PE
H-2K <sup>b</sup> PB1 <sub>703-711</sub>	APC, PE
<i>Vaccinia virus tetramer</i>	
H-2K <sup>b</sup> B8R <sub>20-27</sub>	PE
<i>Others</i>	
H-2K <sup>b</sup> Ova <sub>257-263</sub>	APC, PE

<sup>1</sup> All chimeric monomers were gifts of Dr. Lucy Sullivan at The University of Melbourne

## 2.7. Tetramer and surface antibody staining

Cells were stained for tetramer in 96-well U-bottom plates (CoStar<sup>®</sup> Corning, NY, USA). For each sample,  $1 \times 10^6$  cells were aliquoted into plates and then incubated with specific peptide-MHCI tetramers (0.825 ng/ $\mu$ L) conjugated to either PE or APC fluorophores (**Table 3 and 4**). Cells were stained in a final volume of 50  $\mu$ L in magnetic activating cell-sorting (MACS) buffer for 1 hr at RT in the dark and then washed twice in 200  $\mu$ L of MACS buffer prior to antibody staining described below.

Cells were also stained for surface markers in 96-well U-bottom plates (CoStar<sup>®</sup> Corning). For each sample,  $1 \times 10^6$  cells were aliquoted into plates and cells were stained with antibodies (**Appendix 8.2**). Cells were stained in a final volume of 50  $\mu$ L in MACS buffer for 30 mins at 4°C in the dark. Cells were then washed twice in 200  $\mu$ L of MACS buffer and prepared for flow cytometric analysis (**Section 2.10**).

## 2.8. Tetramer-based magnetic enrichment of epitope-specific CD8 T cells

For the identification and isolation of low frequency epitope-specific CD8 T cells from naïve mice or early timepoints following IAV infection, spleen and major LNs were individual mice harvested, pooled and processed into a single cell suspension (**Section 2.4.2**). Cells were resuspended in Fc block (**Appendix 8.3**) to prevent non-specific binding of antibodies to Fc receptors expressed on neutrophils, monocytes, macrophages, DCs and B cells (178). Cells were then stained with 1 µg of PE- or APC-labelled tetramers (**Section 2.6**) for 1hr at room temperature in the dark. Cells were then washed with cold MACS buffer and resuspended in 400 µL of MACS buffer with 50 µL of anti-PE or anti-APC conjugated microbeads (Miltenyi Biotec, Gladbach, Germany), and incubated at 4°C for 30 mins in the dark. Cells were washed twice in cold MACS buffer, passed through a 70 µm filter, resuspended in 3 mL of MACS buffer and passed through a LS column in a QuadroMACS magnet (Miltenyi Biotec). The flow-through was collected and passed through the column again, followed by three additional 3 mL washes with cold MACS buffer. Column-bound cells were eluted in 5 mL of MACS buffer, centrifuged (515 x g, 6 mins, 4°C) and stained with a panel of antibodies for flow cytometry (**Appendix 8.2**).

For the analysis of epitope-specific CD8 T cell precursors from naïve mice, cells were stained with: anti-B220:FITC, anti-CD11b:FITC, anti-CD11c:FITC, anti-NK1.1:FITC, anti-F4/80:FITC, anti-CD4:PerCP-Cy5.5, anti-TCRβ:APC-Cy7, anti-CD44:PE-Cy7, anti-CD8:BUV394 antibodies and Live/dead fixable violet dead cell stain (viability

stain; Invitrogen) (**Appendix 8.2**). For the detection of epitope-specific CD8 T cells at early timepoints post-infection, anti-CD11b:FITC, anti-CD11c:FITC and anti-NK1.1:FITC antibodies were omitted from the panel as activated CD8 T cells may express these markers. I-A<sup>b</sup>:FITC antibody was substituted to identify MHCII-expressing cells. After antibody staining, cells were washed twice in MACS buffer and resuspended in FACS buffer for enumeration of epitope-specific cells by analysis of the entire sample by flow cytometry (**Section 2.10**) or FACS sorting (**Section 2.11**).

The gating strategy was designed to exclude cells that have bound non-specifically to the magnetic column. *Bona fide* naïve epitope-specific CD8 T cells are identified as B220<sup>-</sup> CD11b<sup>-</sup> CD11c<sup>-</sup> NK1.1<sup>-</sup> F4/80<sup>-</sup> TCRβ<sup>+</sup> CD4<sup>-</sup> CD8<sup>+</sup> tetramer<sup>+</sup> (**Figure 5**). Antigen-experienced epitope-specific CD8 T cells from mice early after infection are identified as I-A<sup>b</sup><sup>-</sup> B220<sup>-</sup> F4/80<sup>-</sup> TCRβ<sup>+</sup> CD4<sup>-</sup> CD8<sup>+</sup> CD44<sup>hi</sup> tetramer<sup>+</sup>.

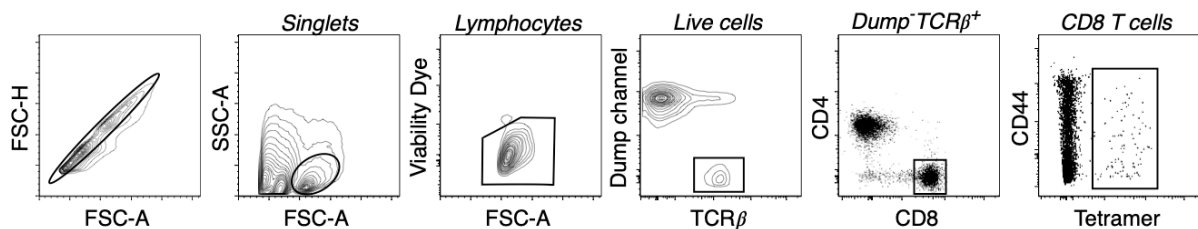


**Figure 5:** Gating strategy to identify epitope-specific tetramer binding cells following tetramer-based magnetic enrichment. Gating tree identifies live singlets, lymphocytes, dump<sup>-</sup>, TCRβ<sup>+</sup> CD4<sup>-</sup>, CD8<sup>+</sup> tetramer<sup>+</sup> cells.

## 2.9. Peptide re-stimulation of antigen-specific CD8 T cells and intracellular cytokine staining

To identify antigen-specific T cells through cytokine production, single cell suspensions of lymphocytes isolated from spleens and lungs of immune mice (**Section 2.4.1, 2.4.2**) were aliquoted at  $1-2 \times 10^6$  cells/well in a 96-well U-bottom tissue culture plates. Cells were incubated at 37°C for 5 hrs in the absence of peptide as a control, or in the presence of 1  $\mu$ M of IAV-specific peptides (**Appendix 8.1**), along with 10 U/mL of human recombinant IL-2 (rh-IL-2; Roche Diagnostics, Basel Switzerland) and 1  $\mu$ L/mL brefeldin A (BD Biosciences) in cRPMI. Cells were stained for surface markers (**Appendix 8.2**), followed by fixation and permeabilization using the BD Cytofix/Cytoperm Kit (BD Biosciences). Briefly, cells were fixed with 100  $\mu$ L of BD Cytofix/Cytoperm buffer for 30 mins at 4°C and then washed twice in 1x BD Perm/Wash buffer. Subsequently, cells were stained intracellularly with a combination of antibodies specific for intracellular cytokines: anti-IFN $\gamma$ :FITC, anti-TNF:APC and anti-IL-2:PE (**Appendix 8.2**) in 1x BD Perm/Wash buffer for 30 mins at 4°C. To remove all unbound antibodies, cells were washed twice in 200  $\mu$ L of 1x BD Perm/Wash buffer, twice in 200  $\mu$ L of MACS buffer and resuspended in the desired amount of sort buffer for analysis by flow cytometry (**Section 2.10**). Background levels of intracellular cytokine staining were defined using control samples incubated without peptide and background was subtracted from statistics (frequency of cytokine<sup>+</sup> cells) obtained from samples incubated with peptides.

## 2.10. Flow cytometric acquisition and analysis

Samples were acquired on a BD Fortessa X-20 with FACSDiva software (BD Immunocytometry Systems, San Jose, CA, USA). For the high-throughput sampler (HTS; BD Biosciences), samples were resuspended in 200 µL of MACS buffer in 96-well U-bottom or V-bottom (CoStar® Corning) plates for acquisition. The HTS was programmed to resuspend the samples prior to acquisition and acquire 150 µL of sample at a flow-rate of 150 µL/min. To prevent contamination across samples, the flow cell was flushed with 800 µL of sheath fluid prior to acquiring the next sample. Data were analysed with FlowJo version 9.9.6 (Tree Star Inc., Ashland, Oregon, USA).

## 2.11. Isolation of Single Cells by Fluorescence Activated Cell Sorting (FACS)

Following tetramer-based magnetic enrichment (**Section 2.8**) and/or antibody staining, lymphocytes were resuspended at  $4 \times 10^7$  cells/mL in sort buffer. Cells were passed through a 40 µm filter into 5 mL polypropylene FACS tubes (BD Falcon) for FACS. Single cell FACS was performed by staff at the Monash FlowCore facility (Monash University, Clayton campus) using a BD Influx (BD Biosciences). Cells were sorted directly into 5 mL polypropylene FACS tubes, 96-well twin.tec PCR plates (Eppendorf, Hamburg, Germany), or 96-well Nunclon cell culture plates (Nunc, Roskilde, Denmark).

## 2.12. Single-cell proliferation assay

To polyclonally expand single-sorted naïve CD8 T cells, 96-well Nunclon round bottom plates (Nunc, Roskilde, Denmark) were coated with anti-CD3 $\epsilon$ , anti-CD8 $\alpha$  and anti-LFA-1 mAbs (**Table 5**), incubated overnight at 4°C to allow mAbs to bind, and excess mAbs were removed by washing 3x with cold sterile PBS. Coated wells were prepared prior to FACS sorting (**Section 2.11**) with 200  $\mu$ L of cRPMI with 10 U/mL of rh-IL-2. Following FACS single-cell sort, cells were incubated at 37°C with 5% CO<sub>2</sub> for 9 days.

**Table 5:** Stimulating antibody concentrations for well coating for single-cell proliferation assay.

Reagent	Concentration ( $\mu$ g/mL)	Volume per well ( $\mu$ L)
Anti-CD3 $\epsilon$	10	0.50
Anti-CD8 $\alpha$	10	0.50
Anti-LFA-1	5	0.25
Sterile PBS	-	48.75
Final Volume		50.00

## 2.13. Carboxyfluorescein Succinimidyl Ester (CFSE) and Cell Trace Violet (CTV) labelling of cells

To track lymphocyte division, lymphocytes that were sorted into 5mL polypropylene FACS tubes (**Section 2.11**) were transferred into 50 mL falcon tubes for CFSE or CTV labelling.

For CFSE staining, sorted cells were washed with warm PBS to remove excess protein and then stained with 1  $\mu$ M of CFSE in PBS at 37°C for 10 mins in the dark. The reaction was quenched with cold PBS and incubated for a further 5 mins on ice. Cells were washed twice, and centrifuged at 550 x g for 6 mins at 4°C and resuspended into desired volume for further analyses.

For CTV labelling, sorted cells were washed with warm PBS to remove excess protein and then stained with 1  $\mu$ M of CTV in PBS at 37°C for 20 mins in the dark. The reaction was quenched with 20 mL of cRPMI and cells were further incubated in warm cRPMI at 37°C for 5 mins to permit modification of the CTV dye. CTV-labelled cells centrifuged at 550 x g for 6 mins at 27°C were washed in twice in warm cRPMI and resuspended into a desired volume for further analyses.

## 2.14. Adoptive transfer of splenocytes

CFSE or CTV labelled cells were resuspended at the desired number of cells in 200  $\mu$ L of warm sterile PBS. Recipient mice were placed under a heat lamp for approximately 10mins until the tail vein was dilated and visible. Cells for adoptive transfer were administered intravenously in the tail vein using a 27-gauge needle.

## 2.15. Multiplexed single cell Reverse Transcriptase Polymerase Chain Reaction (Multiplex RT-PCR)

### 2.15.1. Reverse transcription of cDNA

The nested multiplex RT-PCR used to amplify TCR CDR3 $\alpha$  and CDR3 $\beta$  from individually sorted T cells was first described by Dash et al (2011) (179). cDNA was synthesized from individual sorted T cells in 96-well twin.tec PCR plates (**Section 2.11**; Eppendorf, Hamburg, Germany) for use in the nested multiplex PCR reactions using a SuperScript<sup>TM</sup> VILO<sup>TM</sup> cDNA Synthesis Kit (Invitrogen<sup>TM</sup>, Carlsbad, California, US). The reverse transcriptase master mix (**Table 6**) was prepared and dispensed into individual wells containing single sorted cells. Plates were centrifuged at 1,160 x g for 1 min at 4°C and reverse transcription was performed using conditions in **Table 7** using an Eppendorf (Model 5345) PCR machine (Eppendorf).

**Table 6:** Reverse transcriptase master-mix for cDNA synthesis

Reagents	Volume (µL) per sample
5x VILO™ reaction mix	0.5
10x Superscript® RT (200 U/µL)	0.25
10% Triton X-100	0.275
HPLC Water	1.5

**Table 7:** Reverse transcriptase reaction conditions for cDNA synthesis

Steps	Temperature (°C)	Duration (mins)
Primer annealing	25	10
Elongation	42	120
RT enzyme denaturation	85	5
End of reaction	16	Hold

### 2.15.2. External PCR

Following cDNA synthesis, plates were centrifuged at 1160 x *g* for 1 min at 4°C. External PCR master-mix (**Figure 8**) was dispensed into individual wells. Plates were centrifuged at 1160 x *g* for 1 min at 4°C and the external PCR reaction was performed as in **Table 9**.

**Table 8:** External PCR master-mix for multiplex RT-PCR reaction

Reagents	Volume (µL) per sample
10x PCR buffer + MgCl <sub>2</sub>	2.5
dNTP mix (10mM)	0.5
TRAV external primers (5 pmol/µL) <sup>†</sup>	0.5
TRAC external primers (5 pmol/µL) <sup>†</sup>	0.5
TRBV external primers (5 pmol/µL) <sup>†</sup>	0.5
TRBV external primers (5 pmol/µL) <sup>†</sup>	0.5
Taq DNA polymerase (5 U/µL)	0.15
HPLC Water	17.35

<sup>†</sup> Primer sequences are available in **Appendix 8.4**

**Table 9:** PCR conditions for external and internal multiplex RT-PCR

Steps	Temperature (°C)	Duration
Initial denaturation	95	5 mins
Denaturation	95	5 secs
Primer annealing	52	5 secs
Elongation	72	45 secs
Final extension	72	7 mins
End of PCR cycling	16	Hold

### 2.15.3. Internal PCR

Following the external PCR reaction, plates were centrifuged at 1160 x g for 1 min at 4°C prior to the internal PCR reaction. Amplified external PCR product (2.5 µL) was added into two new 96-well twin.tec PCR plates, in order to amplify the TCR $\alpha$  and  $\beta$  chains separately. Internal master mix  $\alpha$  and  $\beta$  (**Table 10**) were dispensed into corresponding plates, centrifuged at 1160 x g for 1 min at 4°C and the internal PCR reaction was performed with the same conditions as external PCR reaction (**Table 9**).

**Table 10:** Internal PCR master-mix for multiplex RT-PCR reaction

Reagents	$\alpha$ chain mix Volume (µL) per sample	$\beta$ chain mix Volume (µL) per sample
10x Coral load PCR buffer	2.5	2.5
dNTP mix (10mM)	0.5	0.5
TRAV internal primers (5 pmol/µL) <sup>†</sup>	0.5	-
TRAC internal primers (5 pmol/µL) <sup>†</sup>	0.5	-
TRBV internal primers (5 pmol/µL) <sup>†</sup>	-	0.5
TRBV internal primers (5 pmol/µL) <sup>†</sup>	-	0.5
Taq DNA polymerase (5 U/µL)	0.15	0.15
HPLC water	18.35	18.35

<sup>†</sup> Primer sequences are available in **Appendix 8.4**

#### 2.15.4. Agarose gel electrophoresis

Following internal PCR, plates were centrifuged at 1160 x *g* for 1 min at 4°C. 5µL of samples were loaded onto a 2% agarose gel with SybrSafe (Invitrogen) for electrophoresis to identify successful amplification reactions. Electrophoresis was performed at 100V for 30 mins and visualized on a UV transilluminator.

#### 2.15.5. PCR product purification

DNA from positive samples, indicated by a positive band following gel electrophoresis, was purified and prepared for sequencing. In a new 96-well twin.tec PCR plate, 5 µL of internal PCR products were added to 1 µL of ExoSAP-IT PCR Product Cleanup Reagent (Applied Biosystems, Waltham, Massachusetts, USA) and incubated at 37°C for 15 mins followed by 80°C for another 15 mins.

#### 2.15.6. Sequencing reaction

Plates containing purified PCR product were centrifuged at 1160 x *g* for 1 min at 4°C. Sequencing reaction master mix (**Table 11**) was prepared separately and added into the corresponding plates –  $\alpha$  and  $\beta$ . Plates were centrifuged again at 1160 x *g* for 1 min at 4°C and sequencing was performed as in **Table 12**.

**Table 11:** Sequencing reaction master-mix

Reagents	$\alpha$ chain mix Volume ( $\mu\text{L}$ ) per sample	$\beta$ chain mix Volume ( $\mu\text{L}$ ) per sample
Big Dye	1	1
5x dilution buffer	4	4
DMSO	1	1
TRAC internal primers (5 pmol/ $\mu\text{L}$ ) <sup>†</sup>	1	-
TRBC internal primers (5 pmol/ $\mu\text{L}$ ) <sup>†</sup>	-	1
HPLC water	7	7

<sup>†</sup> Primer sequences are available **Appendix 8.4**

**Table 12:** Sequencing reaction conditions

Steps	Temperature ( $^{\circ}\text{C}$ )	Duration
Initial activation	95	5 mins
Denaturation	95	5 secs
Primer annealing	52	5 secs
Elongation	72	45 secs
Final extension	72	7 mins
End of PCR cycling	16	Hold

### 2.15.7. Terminator removal

Excess terminator residues were removed using a DyeEx 96 kit (Qiagen, Hilden, Germany). A DyeEx 96 plate was centrifuged at 1160 x *g* for 3 mins at 4 $^{\circ}\text{C}$  to remove storage buffer, then placed onto a half-skirt PCR microplate (Axygen, Corning, NY, USA). Sequencing reaction products were centrifuged at 1160 x *g* for 1 min at 4 $^{\circ}\text{C}$ , then 20  $\mu\text{L}$  of amplified products were added directly to the centre of the DyeEx 96 plate column. The plate was centrifuged at 1160 x *g* for 3 mins at 4 $^{\circ}\text{C}$  to elute the purified sample, which was then dried on a heat block at 95 $^{\circ}\text{C}$  for 30 mins.

### 2.15.8. Sequencing

Sanger sequencing was performed by Monash Micromon Platform Facility at Monash University (Clayton campus), Clayton, VIC, Australia.

### 2.16. DC vaccination

To stimulate alloreactive cells *in vivo*, we used a DC vaccination approach. To generate BMDCs for DC vaccination, the bone marrow of mice was harvested (**Section 2.4.4**). Bone marrow cells were grown in granulocyte-macrophage colony-stimulating factor (GM-CSF) to promote BMDC differentiation as previously described (180, 181). Briefly, bone marrow cells were cultured in cRPMI with 20 ng/mL of GM-CSF (**Section 2.5.2**) for 12 days with regular replenishment of media and GM-CSF at days 1, 3, 6, 8, 10 and 11. Following culture, BMDCs were activated with cRPMI containing 1 µg/mL of lipopolysaccharide and 20 ng/mL of GM-CSF for 16 hrs. Activated BMDCs were pulsed with 1 µM of PA<sub>224</sub> peptide for 2 hrs at 37°C, washed and resuspended in PBS to 1 x 10<sup>6</sup> cells/mL for administration. For DC vaccination, each mouse received 1 x 10<sup>6</sup> of peptide-pulsed BMDCs in 200 µL intravenously. Activated alloreactive cells were recovered 5 days post-vaccination for analysis.

## 2.17. NK Cell Depletion using PK136 mAb Administration

To avoid a mixed lymphocyte reaction after DC vaccination, the endogenous NK cell population was depleted prior to adoptive transfer of peptide-pulsed BMDCs (182). Anti-NK1.1 (Clone PK136) monoclonal antibody was purchased from the Walter and Eliza Hall Institute (WEHI) antibody facility. To initially deplete NK cells, mice received 2 doses of 100 µg anti-NK1.1 mAb intraperitoneally at a 2-day interval (day -2 and day 0) prior to DC vaccination (**Section 2.16**). Mice also received depleting antibodies at 2-day intervals for the duration of the experiment after DC vaccination.

## 2.18. 5-bromo-2'-deoxyuridine (BrdU) administration to track cell division *in vivo*

To track IAV antigen-specific CD8 T cells dividing *in vivo* during IAV infection, mice were fed *ad libitum* 0.8 mg/mL of BrdU (Sigma-Aldrich) in drinking water from day 5 post-infection. Mice were then euthanised at day 7 post-infection, and spleens and all major lymph nodes including the mLN were pooled for processing (**Section 2.4.2**). IAV antigen-specific CD8 T cells were isolated using tetramer-based magnetic enrichment (**Section 2.8**) prior to intranuclear staining for BrdU. Proliferating cells that had incorporated BrdU into their DNA were identified using a BrdU Flow Kit (BD Pharmingen, Franklin Lakes, New Jersey, USA). Briefly, cells were fixed and permeabilized with 200 µL of BD Cytofix/Cytoperm buffer for 30 mins at 4°C and then washed twice in 1 mL of 1x BD Perm/Wash buffer. Subsequently, cells were permeabilized with 200 µL of BD Cytoperm Permeabilization Buffer Plus for 10 mins

on ice and wash twice with 1 mL of 1x Perm/Wash buffer. Cells were re-fixed with 200  $\mu$ L of BD Cytfix/Cytoperm buffer for 5 mins at 4°C. To make DNA-incorporated BrdU more accessible for antibody staining, cells were treated with 100  $\mu$ L of 300  $\mu$ g/mL DNaseI for 1 hr at 37°C, then washed twice in 1 mL of 1x BD Perm/Wash buffer. Exposed BrdU was stained with either anti-BrdU:FITC or anti-BrdU:APC antibodies in 1x BD Perm/Wash buffer for 30 mins at 4°C. Cell were then washed twice in 1 mL of 1x BD Perm/Wash buffer, twice in 1 mL of MACS buffer and resuspended in FACS buffer for flow cytometric analysis (**Section 2.10**).

## 2.19. *In vivo* labelling of Recent Thymic Emigrants (RTEs)

To assess the rate of thymocyte egress from the thymus, mice were administered 1 µg of PE-conjugated anti-CD8 $\alpha$  antibody (clone 53-6.7) in 200 µL of PBS by intravenous (i.v.) injection. Control mice received 200 µL of PBS by i.v. injection. Mice were then euthanized 3 mins later *via* CO<sub>2</sub> asphyxiation and the thymus was perfused to remove CD8 T cells in the vasculature, harvested and processed (**Section 2.4.3**).

To isolate the low-frequency of RTEs in the perivascular space exposed to i.v. administered anti-CD8 $\alpha$ :PE antibody, single-cell suspensions were incubated with 50 µL of anti-PE microbeads (Miltenyi Biotec) for 30mins at 4°C in the dark. Samples were washed twice in cold MACS buffer, filtered through a 70µm filter, resuspended in 3mL of MACS buffer and passed through an LS column loaded on a QuadroMACS magnet (Miltenyi Biotec) as described in **Section 2.8**.

To distinguish newly matured RTEs in the perivascular space from other SP CD8 thymocytes, samples were stained with a panel of antibodies including an anti-CD8 $\beta$ :PE-Cy7 (Clone: YTS156.7.7) and anti-CD103 antibodies (Clone: 2E7). RTEs were identified by co-staining with both anti-CD8 $\alpha$ :PE and anti-CD8 $\beta$ :PE-Cy7 antibodies, and are CD103<sup>hi</sup>, while SP CD8 thymocytes only stained positive for anti-CD8 $\beta$ : PE-Cy7 antibodies and are CD103<sup>lo</sup>.

## 2.20. Statistical analyses

Data analyses were performed using the software GraphPad Prism (v8.2.1; San Diego, CA), Pestle (v1) and SPICE (v5.35; both Mario Roederer and Joshua Nozzi, National Institute of Health, Bethesda, Maryland, USA). Normal distribution of variation was not assumed within experimental groups, hence statistical analyses in this thesis were performed using a non-parametric two-tailed unpaired Students' t-test (Mann Whitney test) unless stated otherwise. A p value of <0.05 was taken to indicate a significant difference. For all data representation, graphs represent mean  $\pm$  standard error of the mean (SEM).

## Chapter Three

### **3. Characterization of Enhanced H-2K Binding by T cells from H-2K<sup>b</sup><sup>-/-</sup> mice**

#### **3.1. Introduction**

The phenomenon of MHC restriction was first described in 1974 (93). It dictates that a T cell is restricted in the periphery to interact with the same MHC molecule that it was positively selected on during thymic development. However, exceptions to this rule exist, and alloreactive T cells can recognize and become activated by peptide presented by allogeneic MHC molecules that were not present during thymic selection. Alloreactive T cells are present at a high precursor frequency of (1 in 10<sup>3</sup>-10<sup>4</sup> T cells), which is 100- to 1000-fold more frequent than any single foreign-peptide-self-MHC complex (183, 184). In an individual, alloreactive cells can constitute up to 10% of mature T cells (185). The identification of alloreactive T cells therefore highlights that MHC restriction is not an absolute phenomenon.

Alloreactivity is physiologically relevant in humans, as it is responsible for clinical consequences such as graft rejection, as well as graft vs host disease (GvHD) and graft vs leukemia (GvL) (reviewed in (186, 187)). In GvHD and GvL, donor T cells selected on a particular donor-derived HLA haplotype are activated in the presence of an alternative host-derived HLA haplotype, resulting in the graft's rejection of the host cells (188). Therefore, HLA matching between donor and recipient is of paramount

importance during transplantation, especially during haematopoietic stem-cell transplant (HSCT).

The mechanisms mediating alloreactivity have been a subject of longstanding debate in the field (reviewed in (189)). One model suggests that, over millions of years of co-evolution, the TCR chains and MHC molecules have evolved to recognise one another through highly conserved interactions between the TCR and the MHC molecule, to permit a degree of TCR-pMHC binding that is independent of the loaded peptide (190–195). Another more recent model suggests that an alloreactive TCR requires the co-recognition of both the MHC molecule and the loaded peptide (196–199). Indeed, structural studies indicated that the extent to which the TCR interacts with self- and allogeneic-pMHC complexes is generally comparable, with no unusual interactions occurring during allorecognition, and both the allogeneic MHC molecule and the bound peptide contribute to the pMHC surface exposed to the TCR. Thus, these data tend to favour the model of co-recognition of peptide+MHC in alloreactive TCR-pMHC interactions.

The capacity of an alternative MHCII molecule to mediate the selection of an MHCII-restricted population of alloreactive T cells has been investigated in mouse models. A seminal study by Jenkins and colleagues used the I-A<sup>b</sup> (MHCII from C57BL/6 mice) tetramer loaded with the immunogenic epitope 2W1S to isolate alloreactive CD4 T cells in allomorphic mouse strains expressing allelic variants of the H-2 locus (200). In this study, they identified a high frequency of I-A<sup>b</sup>:2W1S-specific CD4 T cells in various mouse strains expressing allelic variants of the I-A<sup>b</sup> molecule, compared to C57BL/6 mice. They also demonstrated that the alloreactive I-A<sup>b</sup>:2W1S-specific CD4 T cells

found in BALB/c mice were specific for I-A<sup>b</sup> loaded with unknown self-peptides, suggesting that these cells were highly cross-reactive T cells. Furthermore, these cells were less-responsive to stimulation when stimulated by I-Ab:2W1S *in vivo*. This study suggests that allelic variants of the H-2 genes can mediate the selection of I-A<sup>b</sup>-reactive CD4 T cells, although the qualitative response to I-A<sup>b</sup> loaded with peptide may be impaired.

Although alloreactive cells are clearly generated *in vivo*, the impact of selection on one MHCI molecule on the ability of CD8 T cells to respond to peptide presented by another MHCI molecule remains unclear. In the first part of this chapter, I aimed to extend the analyses performed in my BSc. (Hons) year by assessing the functionality of alloreactive H-2D<sup>b</sup>PA<sub>224</sub>-specific CD8 T cells that were selected on the alternative H-2K<sup>b</sup> molecule; in particular the ability to respond to cognate antigen *in vivo*, compared to syngeneic H-2D<sup>b</sup>PA<sub>224</sub>-specific CD8 T cells. In the second part of this chapter, my aim was to evaluate the reverse scenario; namely the ability of the non-restricting H-2D<sup>b</sup> molecule to mediate the selection of two H-2K<sup>b</sup>-restricted CD8 T cell populations, H-2K<sup>b</sup>NS<sub>214</sub>- and H-2K<sup>b</sup>PB<sub>1703</sub>-specific CD8 T cells, with the ultimate aim of defining generalisable characteristics attributable to alloreactive antigen-specific CD8 T cells.

## 3.2. Results

### 3.2.1. Alloreactive CD8 T cells in the H-2D<sup>b</sup><sup>-/-</sup> mouse model

In work performed during my BSc. (Hons) year, I investigated the relative ability of one MHC I molecule (H-2K<sup>b</sup>) to mediate the selection and peripheral maintenance of CD8 T cells specific for an epitope restricted by a distinct MHC I molecule (H-2D<sup>b</sup>). To this end, I used tetramer-based magnetic enrichment to isolate H-2D<sup>b</sup>PA<sub>224</sub>-specific T cells from H-2D<sup>b</sup><sup>-/-</sup> mice, with the aim of enumerating and characterising the phenotype and function of these alloreactive cells. Here, I will briefly summarize the findings of that unpublished work, which provide an experimental basis for the study outlined in this chapter.

The number of naïve H-2D<sup>b</sup>PA<sub>224</sub>-specific CD8 T cells has been well-characterized in WT mice, with an average of 68 +/- 18 cells per mouse (137). This result was reproduced in the analysis of WT and H-2K<sup>b</sup><sup>-/-</sup> mice (**Figure 6A**), consistent with the fact that naïve H-2D<sup>b</sup>PA<sub>224</sub>-specific CD8 T cells are selected on the H-2D<sup>b</sup> molecule in both of these strains. In contrast, there was a significantly reduced, but consistently detectable population of naïve H-2D<sup>b</sup>PA<sub>224</sub>-specific CD8 T cells in H-2D<sup>b</sup><sup>-/-</sup> mice (**Figure 6A**), suggesting that these cells could be selected on an MHC I molecule distinct from H-2D<sup>b</sup>. The absence of H-2D<sup>b</sup>PA<sub>224</sub>-specific CD8 T cells in DKO mice (**Figure 6A**), lacking both H-2D<sup>b</sup> and H-2K<sup>b</sup>, suggested that the small number of alloreactive naïve H-2D<sup>b</sup>PA<sub>224</sub>-specific CD8 T cells in H-2D<sup>b</sup><sup>-/-</sup> mice were being selected on the H-2K<sup>b</sup> molecule. Deeper analyses revealed that alloreactive naïve H-2D<sup>b</sup>PA<sub>224</sub>-specific CD8 T cells in H-2D<sup>b</sup><sup>-/-</sup> mice exhibited a significantly and consistently lower median fluorescent intensity (MFI) of tetramer staining (**Figure 6B**) despite

expressing similar levels of TCR (data not shown), indicative of a lower affinity for H-2D<sup>b</sup>PA<sub>224</sub>.

The TCR $\alpha\beta$  repertoire of naïve H-2D<sup>b</sup>PA<sub>224</sub>-specific CD8 T cells from WT mice has been recently characterized by Cukalac et al, where a strong bias in variable gene usage for both TCR $\alpha$  (TRAV) and TCR $\beta$  (TRBV) chains was observed (149). For the TCR $\alpha$  chain, there was an equal and preferential bias for TRAV6, TRAV9 and TRAV12, while TRBV29 was predominantly used for the TCR $\beta$  chain (**Figure 6C**) (149, 150). While TCR repertoire analysis of alloreactive H-2D<sup>b</sup>PA<sub>224</sub>-specific CD8 T cells selected in H-2D<sup>b</sup><sup>-/-</sup> mice showed a retention of relatively dominant TRAV6, TRAV9 and TRAV12 usage, the TRBV29 was significantly reduced ( $p=0.006$ ; Wilcoxon signed-rank sum test). Thus, the selection of H-2D<sup>b</sup>PA<sub>224</sub>-specific CD8 TCRs on the H-2K<sup>b</sup> molecule resulted in a modified TCR repertoire that could account for a lowered TCR affinity for the cognate H-2D<sup>b</sup>PA<sub>224</sub> molecule.

Given that alloreactive naïve H-2D<sup>b</sup>PA<sub>224</sub>-specific CD8 T cells exhibited an altered TCR repertoire and potentially lower TCR binding affinity, I then assessed the intrinsic functionality and epitope-driven functionality of these alloreactive cells. To determine whether selection of alloreactive CD8 T cells on H-2K<sup>b</sup> impacted on their intrinsic functionality, I polyclonally expanded single sorted naïve H-2D<sup>b</sup>PA<sub>224</sub> CD8 T cells using stimulation with plate bound anti-CD3, -CD8 and -CD11a mAb. When the clonal burst size of H-2D<sup>b</sup>PA<sub>224</sub> CD8 T cells was assessed after 5 days of stimulation, there was no significant difference across the three mouse strains (**Figure 6D**), suggesting that the intrinsic proliferative capacity of H-2D<sup>b</sup>PA<sub>224</sub>-specific CD8 T cells was unaltered by their selecting ligand. To assess epitope-driven functionality, I rested the

expanded cells and then re-stimulated them with the PA<sub>224</sub> peptide loaded on WT splenocytes. As the concentration of PA<sub>224</sub> peptide was increased, the frequency of cytokine-producing H-2D<sup>b</sup>PA<sub>224</sub>-specific CD8 T cells from WT and H-2K<sup>b</sup><sup>-/-</sup> mice also increased (**Figure 6E**). In contrast, H-2D<sup>b</sup>PA<sub>224</sub>-specific CD8 T cells from H-2D<sup>b</sup><sup>-/-</sup> mice failed to respond at any concentration of the PA<sub>224</sub> peptide, although they did produce cytokine after stimulation by PMA/Ionomycin.

These data suggest that although H-2D<sup>b</sup>PA<sub>224</sub>-specific CD8 T cells can be selected on the allomorphic H-2K<sup>b</sup> molecule, they have 1) an intrinsically lower TCR affinity for H-2D<sup>b</sup>PA<sub>224</sub>, 2) altered TCR $\beta$  usage and 3) impaired responsiveness when stimulated by cognate H-2D<sup>b</sup>PA<sub>224</sub> antigen.

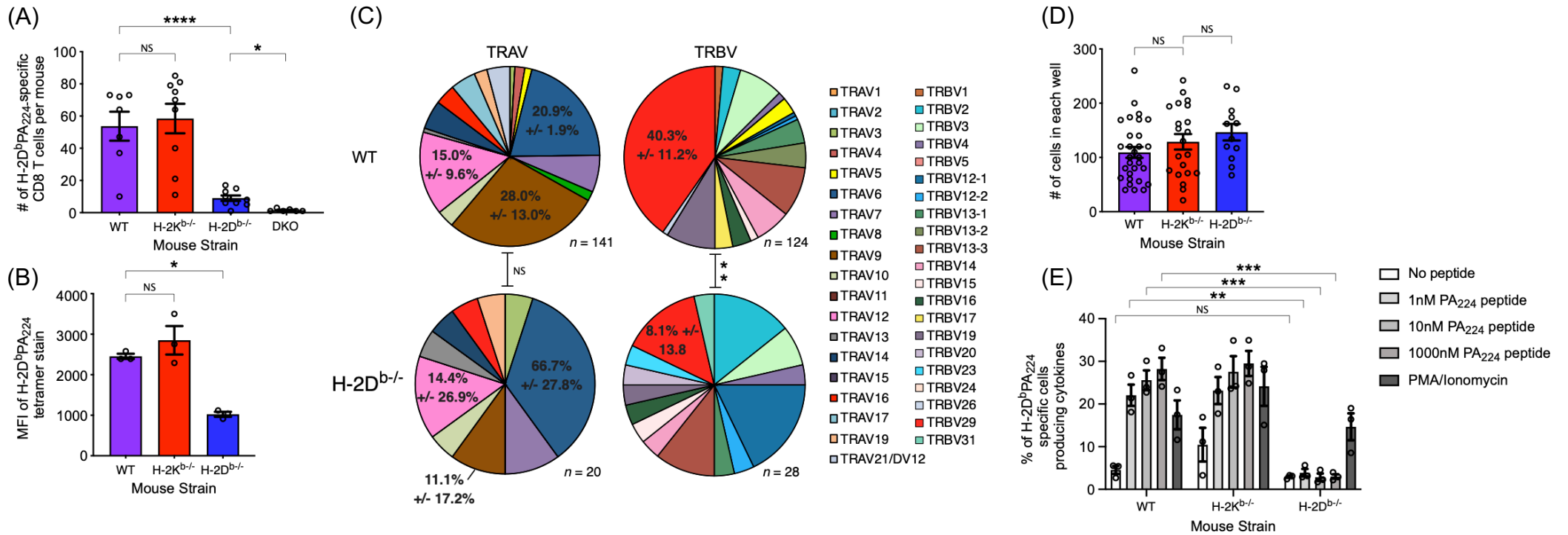


**Figure 6:** Alloreactive H-2D<sup>b</sup>PA<sub>224</sub>-specific CD8 T cells can be selected on the H-2K<sup>b</sup> molecule, but have lower affinity for H-2D<sup>b</sup>PA<sub>224</sub>, altered TCR repertoire and impaired TCR-dependent functionality. (A) Number and (B) tetramer MFI of H-2D<sup>b</sup>PA<sub>224</sub>-specific CD8 T cells in WT (purple), H-2K<sup>b</sup> (red), H-2D<sup>b</sup> (blue) and DKO (grey) mice following tetramer-based magnetic enrichment. (C). TRAV and TRBV usage for naïve H-2D<sup>b</sup>PA<sub>224</sub> TCRs from WT and H-2D<sup>b</sup> mice (TCR repertoire data for WT mice taken from (149)). (D) Clonal burst size of single-cell sorted naïve H-2D<sup>b</sup>PA<sub>224</sub>-specific CD8 T cells 5 days after polyclonal expansion. (E) Frequency of cytokine producing cells (IFN $\gamma$ , and/or TNF, and/or IL-2) following stimulation by various concentrations of PA<sub>224</sub> peptides. \*\*\*\* indicates p < 0.0001, \*\*\* indicates p < 0.001, \*\* indicates p < 0.01, \* indicates p < 0.05, NS indicates P  $\geq$  0.05 (Mann-Whitney test). Statistical analysis for (C) was performed using Wilcoxon signed-rank sum test. Lines and error bars represent mean +/- SEM. Numbers in pie charts represent the frequency of respective TRAV and TRBV usage +/- standard deviation. These results are representative of 2-3 independent experiments. Data was generated and reproduced from my BSc. (Hons) work, for the purpose of providing background to the current study.

### 3.2.2. Alloreactive H-2D<sup>b</sup>PA<sub>224</sub> CD8 T cells are *bona fide* CD8 T cells specific for H-2D<sup>b</sup>PA<sub>224</sub>

The following work was performed during my PhD candidature. Naïve alloreactive H-2D<sup>b</sup>PA<sub>224</sub> CD8 T cells are present at an exceptionally low precursor frequency (~9 cells per H-2D<sup>b/-</sup> mouse) (**Figure 6A**), which is close to the limit of detection for the naïve tetramer-based magnetic enrichment assay. Therefore, it was critical to validate that the TCR sequences I had characterized from H-2D<sup>b/-</sup> mice were *bona fide* H-2D<sup>b</sup>PA<sub>224</sub>-specific TCRs.

From the TCR $\alpha\beta$  sequence database obtained from the TCR sequencing of H-2D<sup>b</sup>PA<sub>224</sub>-specific T cells from H-2D<sup>b/-</sup> mice (**Appendix 8.5**), I selected and expressed a putative alloreactive TCR, along with CD3 $\gamma\delta\epsilon\zeta$  subunits, in 293T cells and assayed for TCR expression and H-2D<sup>b</sup>PA<sub>224</sub> tetramer binding. I selected an alloreactive TCR that exhibited TCR characteristics that appeared to be largely unique to H-2D<sup>b/-</sup> mice, but not WT and H-2K<sup>b/-</sup> mice, consisting of the TRAV19-TRAJ48 (CDR3 $\alpha$  amino acid sequence: GSNYGNEKI) and TRBV12-1-TRBJ2-5 (CDR3 $\beta$  amino acid sequence: SLGLGQDTQ) gene segment combinations. As a positive control, I expressed a well-characterized canonical H-2D<sup>b</sup>PA<sub>224</sub>-specific TCR from WT C57BL/6 mice: “6218” that was previously shown to be highly specific for H-2D<sup>b</sup>PA<sub>224</sub> (80). The 6218 TCR consisted of the TRAV19-TRAJ53 (CDR3 $\alpha$  amino acid sequence: SGGSNYKL) and TRBV29-TRBJ2-7 (CDR3 $\beta$  amino acid sequence: SFGREQ). As a negative control, I expressed a TCR specific for an irrelevant H-2D<sup>b</sup>NP<sub>366</sub> epitope.

Both of the H-2D<sup>b</sup>PA<sub>224</sub>-specific TCRs were successfully expressed on the surface of 293T cells and both could bind the H-2D<sup>b</sup>PA<sub>224</sub> tetramer (**Figure 7A**). With increasing levels of TCR $\beta$  expression, I observed increasing staining with H-2D<sup>b</sup>PA<sub>224</sub> tetramer for both alloreactive and 6218 H-2D<sup>b</sup>PA<sub>224</sub>-specific TCRs. In contrast, the irrelevant H-2D<sup>b</sup>NP<sub>366</sub> TCR failed to bind H-2D<sup>b</sup>PA<sub>224</sub> at any level of TCR $\beta$  expression (**Figure 7A, B**). This demonstrated that the CD8 T cells identified by H-2D<sup>b</sup>PA<sub>224</sub> tetramer binding in H-2D<sup>b</sup><sup>-/-</sup> mice, were likely to be *bona fide* H-2D<sup>b</sup>PA<sub>224</sub>-specific CD8 T cells.

Deeper analysis of the MFI of H-2D<sup>b</sup>PA<sub>224</sub> tetramer binding revealed that the cells expressing the alloreactive TCR from H-2D<sup>b</sup><sup>-/-</sup> mice bound less tetramer than the 6218 WT TCR at a given level of TCR expression (**Figure 7A, B**). Collectively, these data indicate that both of the TCRs identified from WT or H-2D<sup>b</sup><sup>-/-</sup> mice are specific for H-2D<sup>b</sup>PA<sub>224</sub> but, in agreement with previous results (**Figure 6B**), they also suggest that selection on a mismatched MHCI (H-2K<sup>b</sup>) results in an intrinsically lower affinity for H-2D<sup>b</sup>PA<sub>224</sub> antigen.

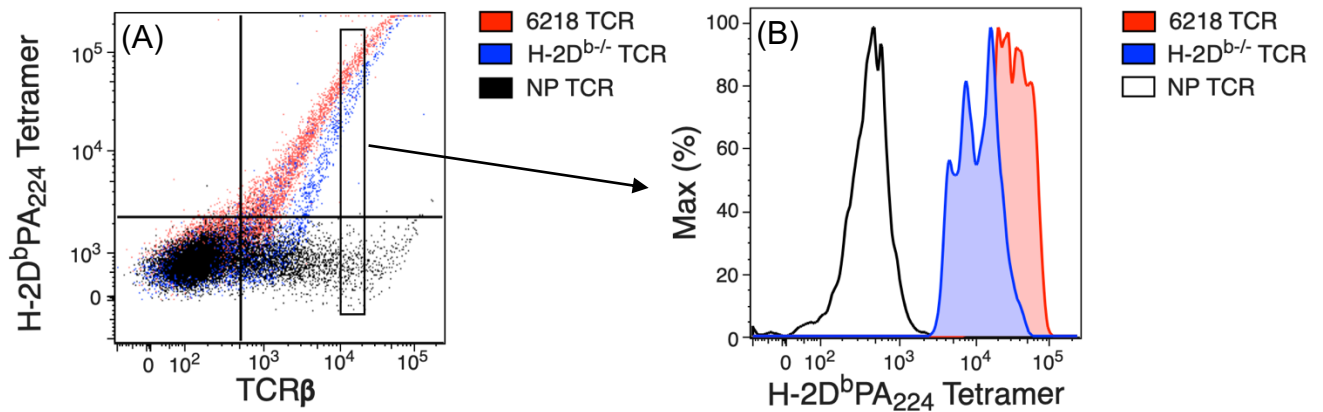


**Figure 7:** A putative alloreactive H-2D<sup>b</sup>PA<sub>224</sub>-specific TCR binds H-2D<sup>b</sup>PA<sub>224</sub> tetramer but at a lower MFI than 6218 TCR. (A) Representative tetramer and TCRβ staining on 293T cells expressing the 6218 (red), alloreactive (blue) H-2D<sup>b</sup>PA<sub>224</sub>-specific, and H-2D<sup>b</sup>NP<sub>366</sub> (black) TCRs. (B) Representative histogram showing H-2D<sup>b</sup>PA<sub>224</sub> tetramer binding for the designated level of TCR expression. An irrelevant TCR specific for the H-2D<sup>b</sup>NP<sub>366</sub> was used as a negative control (white). Results are representative of 2 independent experiments.

### 3.2.3. Alloreactive H-2D<sup>b</sup>PA<sub>224</sub>-specific CD8 T cells are non-responsive after BMDC vaccination *in vivo*

My previous *in vitro* analysis of the functionality of alloreactive T cells indicated a significantly inferior sensitivity to antigen relative to their CD8 T cell counterparts selected on H-2D<sup>b</sup> (**Figure 6E**). However, that assay relied on an initial polyclonal stimulation step, which may have caused the cells to become refractory to subsequent epitope-specific stimulation (201). Therefore, I developed a vaccination strategy with peptide-pulsed bone marrow-derived dendritic cells (BMDC) to assess the *in vivo* functional capacity of H-2D<sup>b</sup>PA<sub>224</sub>-specific CD8 T cells selected on a matched *versus* mismatched MHCI molecule. Bone marrow of WT mice was cultured in the presence of GM-CSF for 14 days to promote the differentiation of hematopoietic stem cells into BMDCs (180, 181). BMDCs were then LPS activated and loaded with PA<sub>224</sub> peptide, before being used to vaccinate WT, H-2K<sup>b</sup><sup>-/-</sup> and H-2D<sup>b</sup><sup>-/-</sup> mice. Epitope-specific CD8 T cell responses were analysed 5 days after vaccination. Prior to vaccination, recipient mice were depleted of NK cells using an anti-NK1.1 monoclonal antibody to prevent rapid rejection of transferred BMDCs upon transfer to H-2K<sup>b</sup><sup>-/-</sup> and H-2D<sup>b</sup><sup>-/-</sup> recipients (188, 202, 203).

At 5 days following vaccination, H-2D<sup>b</sup>PA<sub>224</sub>-specific CD8 T cells in both WT and H-2K<sup>b</sup><sup>-/-</sup> mice upregulated CD44 expression, indicating that the PA<sub>224</sub> peptide pulsed BMDCs were able to activate H-2D<sup>b</sup>PA<sub>224</sub>-specific CD8 T cells *in vivo* (**Figure 8A, B**). In contrast, alloreactive H-2D<sup>b</sup>PA<sub>224</sub>-specific CD8 T cells from H-2D<sup>b</sup><sup>-/-</sup> mice failed to upregulate CD44 (**Figure 8A, B**). Similarly, a modest expansion of H-2D<sup>b</sup>PA<sub>224</sub>-specific CD8 T cells in both WT and H-2K<sup>b</sup><sup>-/-</sup> mice, but not H-2D<sup>b</sup><sup>-/-</sup> mice, was observed

(**Figure 8C,D**). Of note, since H-2D<sup>b</sup>PA<sub>224</sub>-specific CD8 T cells in H-2K<sup>b</sup><sup>-/-</sup> mice were activated and expanded to the same degree as WT mice, this indicated that the rapid rejection of transferred cells as a result of foreign MHCI expression at this early stage, was not responsible for the lack of response observed in H-2D<sup>b</sup><sup>-/-</sup> mice (204, 205).

In summary, both *in vitro* and *in vivo* functional assays suggest that, while alloreactive H-2D<sup>b</sup>PA<sub>224</sub>-specific CD8 T cells may be able to bind H-2D<sup>b</sup>PA<sub>224</sub> tetramer, they are substantially less responsive to H-2D<sup>b</sup>PA<sub>224</sub> stimulation when compared to cells selected on the matched MHCI molecule. This impaired functionality is not due to an intrinsic defect in the proliferative capacity in these cells (**Figure 6D**), but is more likely to be mediated by the altered TCR repertoire of H-2D<sup>b</sup>PA<sub>224</sub> CD8 T cells from H-2D<sup>b</sup><sup>-/-</sup> mice, which appeared to be comprised of cells with a lower affinity for H-2D<sup>b</sup>PA<sub>224</sub>.

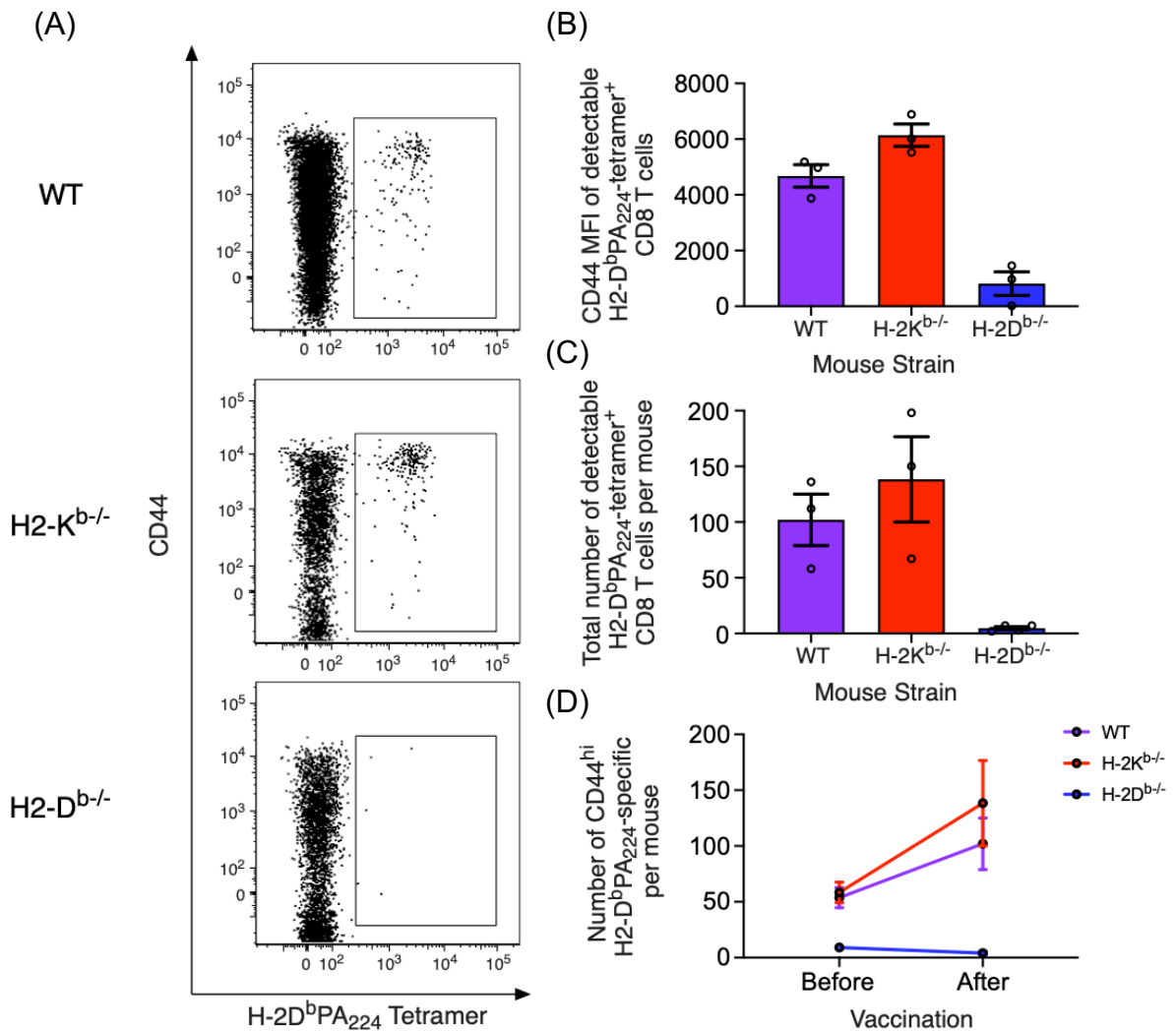


**Figure 8:** Responsiveness of naïve H-2D<sup>b</sup>PA<sub>224</sub>-specific CD8 T cells to BMDC vaccination. (A) Representative tetramer and CD44 staining plot and (B) CD44 MFI of detectable H-2D<sup>b</sup>PA<sub>224</sub>-specific CD8 T cells from WT (purple), H-2K<sup>b</sup>-/- (red) and H-2D<sup>b</sup>-/- (blue) mice. (C) Enumeration of H-2D<sup>b</sup>-PA-specific CD8 T cells from WT, H-2K<sup>b</sup>-/- and H-2D<sup>b</sup>-/- mice 5 days after administration with 10<sup>6</sup> PA<sub>224</sub> peptide-pulsed BMDC. (D) Numbers of detectable H-2D<sup>b</sup>PA<sub>224</sub>-specific CD8 T cells before and after peptide-pulsed BMDC vaccination. Cells (live, B220-, F4/80-, CD4-, TCRβ+, CD8+ lymphocytes) were isolated from spleen and peripheral lymph nodes following tetramer based magnetic enrichment. Lines and error bars represent mean +/- SEM. Results are from a single experiment with *n* = 3 mice per group.

### 3.2.4. Identification of H-2K<sup>b</sup>-reactive T cells in H-2K<sup>b</sup><sup>-/-</sup> and DKO, but not WT and H-2D<sup>b</sup><sup>-/-</sup> mice

From the results generated thus far, I have demonstrated the ability of the non-restricting H-2K<sup>b</sup> molecule to mediate the selection of an alloreactive H-2D<sup>b</sup>PA<sub>224</sub>-specific CD8 T cell population. Alloreactive H-2D<sup>b</sup>PA<sub>224</sub>-specific CD8 T cells selected on the mismatched H-2K<sup>b</sup> molecule appear to bind H-2D<sup>b</sup>PA<sub>224</sub> tetramer with an overall lower affinity, and have impaired functional capacity both *in vivo* and *in vitro* when stimulated with antigen, when compared to H-2D<sup>b</sup>PA<sub>224</sub>-specific CD8 T cells selected on the matched MHCI molecule.

Next, I investigated the reciprocal scenario by determining the capacity of H-2D<sup>b</sup> to mediate the selection of H-2K<sup>b</sup>-restricted CD8 T cell populations. For this work, I focused on the H-2K<sup>b</sup>NS<sub>2114</sub> and H-2K<sup>b</sup>PB<sub>1703</sub> epitopes, as naïve and antigen-experienced CD8 T cell populations specific for these epitopes have been well-characterized in C57BL/6 mice (136, 137). In addition, they have large precursor frequencies in C57BL/6 mice of ~282 H-2K<sup>b</sup>NS<sub>2114</sub>- and ~308 H-2K<sup>b</sup>PB<sub>1703</sub>-specific CD8 T cells per mouse but they generate subdominant immune responses (141, 169). To determine the capacity of H-2D<sup>b</sup> to mediate the selection of H-2K<sup>b</sup>NS<sub>2114</sub> and H-2K<sup>b</sup>PB<sub>1703</sub>-specific CD8 T cells, I used tetramer-based magnetic enrichment to isolate epitope-specific cells from naïve WT, H-2D<sup>b</sup><sup>-/-</sup>, H-2K<sup>b</sup><sup>-/-</sup> and DKO mice.

In both WT and H-2D<sup>b</sup><sup>-/-</sup> mice, I isolated similar numbers of naïve H-2K<sup>b</sup>NS<sub>2114</sub>- (283 and 255, respectively) and H-2K<sup>b</sup>PB<sub>1703</sub>-specific CD8 T cells (562 and 361, respectively), to those previously published (**Figure 9A-D**), and consistent with the

expression of H-2K<sup>b</sup> in both of these strains of mice (**Chapter 4, Figure 21C, D**). Intriguingly, when I stained cells from mice lacking H-2K<sup>b</sup> (H-2K<sup>b</sup><sup>-/-</sup> and DKO) with H-2K<sup>b</sup>NS2<sub>114</sub> and H-2K<sup>b</sup>PB1<sub>703</sub> tetramers, I identified large populations of tetramer+ CD8 T cells, with approximately 7,210 and 4,091 H-2K<sup>b</sup>NS2<sub>114</sub><sup>-</sup>, and 2,855 and 4,093 H-2K<sup>b</sup>PB1<sub>703</sub>-specific CD8 T cells in H-2K<sup>b</sup><sup>-/-</sup> and DKO mice, respectively (**Figure 9A-D**). This represented an up to 25-fold increase in frequency compared to WT mice and is well above the established range for MHC I-restricted precursor frequencies (0.8-10 cells per million CD8 or CD4 T cells) (133). In addition, the presence of H-2K<sup>b</sup> tetramer staining on cells from DKO mice implies that the tetramer was binding to a population of CD8 T cells selected on non-classical MHC Ib molecules, which was not observed for H-2D<sup>b</sup>PA<sub>224</sub>-specific cells in DKO mice (**Figure 6A**). These initial observations of hugely inflated precursor frequencies led me to hypothesise that this was a result of non-specific H-2K<sup>b</sup> tetramer binding. However, given that this population of tetramer binding cells was not observed in the presence of H-2K<sup>b</sup> (WT and H-2D<sup>b</sup><sup>-/-</sup> mice), it led us to further investigate the biology of this H-2K<sup>b</sup> tetramer interaction.

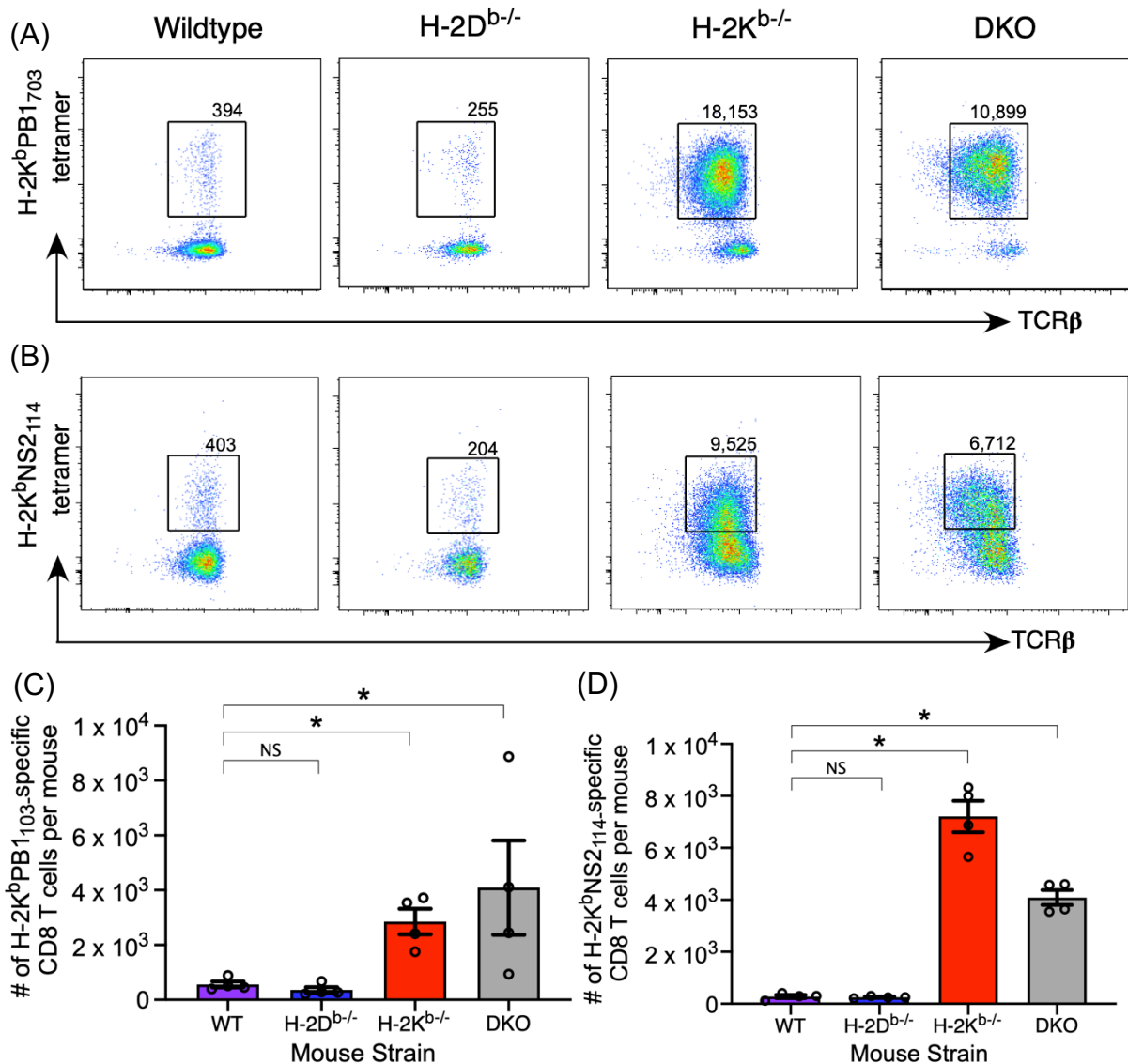


**Figure 9:** Inflated population of H-2K<sup>b</sup> tetramer staining cells in mice lacking H-2K<sup>b</sup>. (A, B) Representative tetramer and TCRβ staining, and (C, D) enumeration of (A, C) H-2K<sup>b</sup>PB1<sub>703</sub>- and (B, D) H-2K<sup>b</sup>NS2<sub>114</sub>-specific CD8 T cells following tetramer-based magnetic enrichment in WT, H-2K<sup>b</sup><sup>-/-</sup>, H-2D<sup>b</sup><sup>-/-</sup> and DKO mice. Cells are gated on live, B220<sup>-</sup>, CD11b<sup>-</sup>, CD11c<sup>-</sup>, F4/80<sup>-</sup>, NK1.1<sup>-</sup>, CD3<sup>+</sup>, TCRβ<sup>+</sup>, CD8 T lymphocytes. \* indicates  $p < 0.05$ , ns indicates  $p > 0.05$  (Mann-Whitney test). Lines and error bars represent mean  $\pm$  SEM. Results are representative of 3 independent experiment with  $n = 4$  mice per group.

To determine whether the populations that bound each of the H-2K<sup>b</sup> tetramers were distinct or the same population, I performed a dual tetramer-based magnetic enrichment, simultaneously identifying CD8 T cells that bound H-2K<sup>b</sup>NS2<sub>114</sub> and/or H-2K<sup>b</sup>PB1<sub>703</sub> tetramers.

In WT and H-2D<sup>b/-</sup> mice, the precursor frequencies of both H-2K<sup>b</sup>NS2<sub>114</sub>- and H-2K<sup>b</sup>PB1<sub>703</sub>-specific CD8 T cells (**Figure 10A, B**) were similar to those observed previously (**Figure 9C, D**) and those previously published (133, 136, 137). In H-2K<sup>b/-</sup> and DKO mice, I observed that the vast majority of CD8 T cells that bound the H-2K<sup>b</sup>NS2<sub>114</sub> tetramer simultaneously bound the H-2K<sup>b</sup>PB1<sub>703</sub> tetramer and *vice versa*, suggesting that the CD8 T cells were intrinsically “H-2K<sup>b</sup>-reactive” (**Figure 10C, D**). Notably, this phenomenon was only observed in the absence of H-2K<sup>b</sup> (H-2K<sup>b/-</sup> and DKO mice).

Of note, there was a population of CD8 T cells in H-2K<sup>b/-</sup> mice that bound exclusively to H-2K<sup>b</sup>NS2<sub>114</sub>, but not the H-2K<sup>b</sup>PB1<sub>703</sub>, tetramer, and this population of CD8 T cells was completely absent in DKO mice (**Figure 10C, D**). This suggested that H-2K<sup>b/-</sup> mice did contain a *bona fide* alloreactive CD8 T cell population selected by the non-restricted H-2D<sup>b</sup> molecule. However, the presence of the large numbers of H-2K<sup>b</sup>-reactive cells limited the ability to reliably resolve this potential alloreactive population and thus to characterise them further.

While I had previously focused on CD8 T cells, I noted that H-2K<sup>b</sup>-reactive cells were also present within the CD4 T cell population in H-2K<sup>b/-</sup> and DKO mice (**Figure 10G, H**) but not WT and H-2D<sup>b/-</sup> mice (**Figure 10E, F**), albeit at a significantly reduced

frequency compared to the CD8 T cell subset (**Figure 10I**). Within the CD8 T cell subset, the frequency of H-2K<sup>b</sup>-reactive CD8 T cells was approximately 1,700 H-2K<sup>b</sup>-reactive cells per million CD8 T cells, whilst there were only 173 H-2K<sup>b</sup>-reactive CD4 T cells per million CD4 T cells, 10-fold lower than the proportion of H-2K<sup>b</sup>-reactive CD8 T cells. Therefore, a small population of CD4 T cells was also capable of binding simultaneously to both H-2K<sup>b</sup> tetramers in the absence of H-2K<sup>b</sup>.

It is important to note that, in cells from mice lacking H-2K<sup>b</sup>, the phenomenon of pan-H-2K<sup>b</sup> reactivity was limited to this MHCI gene. Thus, cells from H-2K<sup>b</sup> deficient animals did not show an inflated number of H-2D<sup>b</sup> binding cells (**Figure 6A**). Indeed, the number of naïve H-2D<sup>b</sup>PA<sub>224</sub>-specific CD8 T cells was similar in WT and H-2K<sup>b</sup><sup>-/-</sup> mice, and negligible in DKO mice. This suggests that the phenomenon of pan-MHCI reactivity was exclusively directed at H-2K<sup>b</sup>.

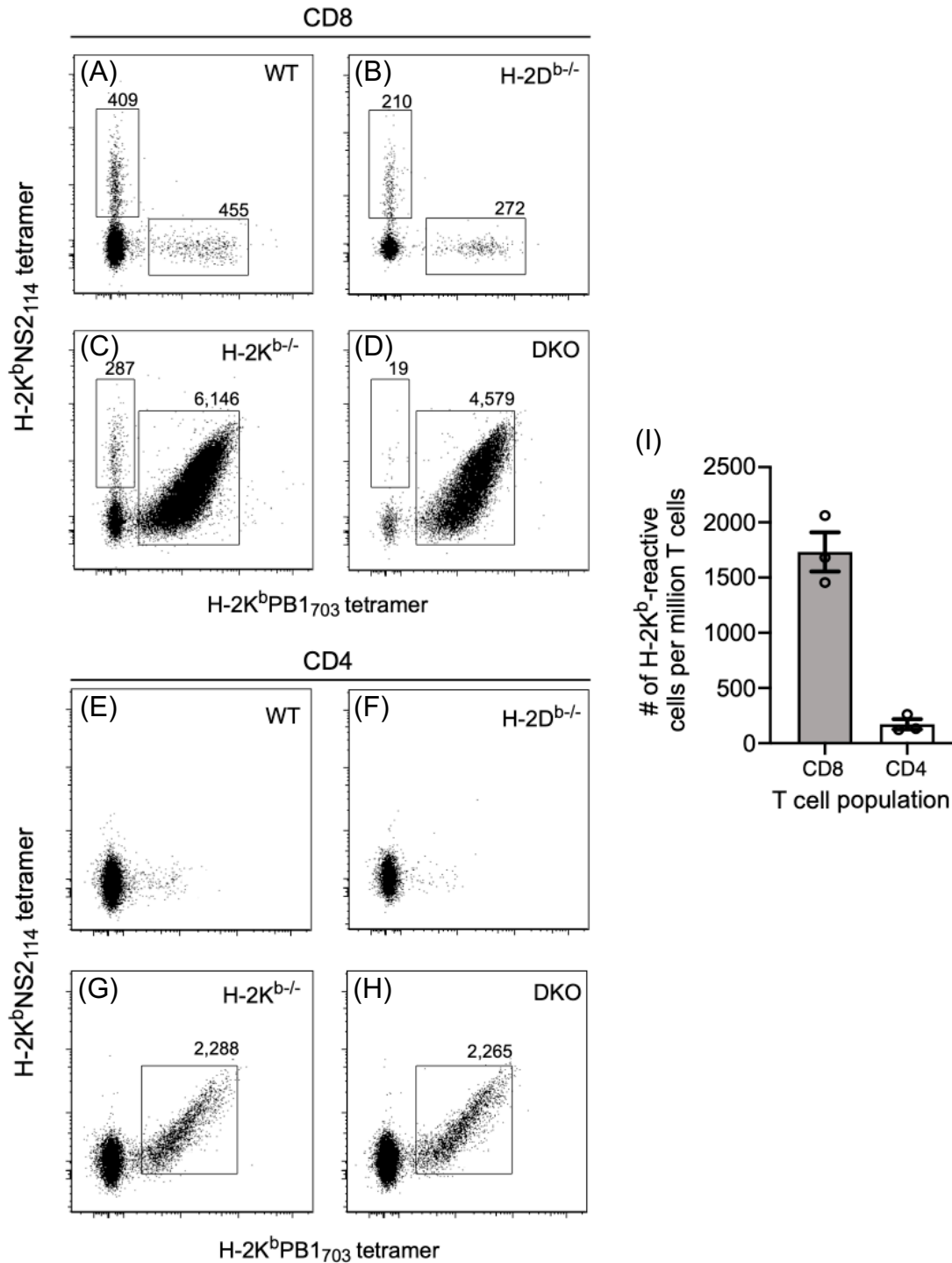


**Figure 10:** H-2K<sup>b</sup>-reactive CD8 and CD4 T cells in the absence of H-2K<sup>b</sup>. Representative dot plots of (A-D) CD8 and (E-F) CD4 T cells following dual tetramer-based magnetic enrichment with H-2K<sup>b</sup>NS2<sub>114</sub> and H-2K<sup>b</sup>PB1<sub>703</sub> tetramers from (A, E) WT, (B, F) H-2D<sup>b</sup>-/-, (C, G) H-2K<sup>b</sup>-/- and (D, H) DKO mice. Cells are gated on live, CD19<sup>+</sup>, F4/80<sup>+</sup>, CD11b<sup>-</sup>, CD11c<sup>-</sup>, NK1.1<sup>-</sup>, CD4<sup>-</sup>, TCRβ<sup>+</sup>, CD8<sup>+</sup> or CD4<sup>+</sup> lymphocytes. Results are representative of 3 independent experiments with *n* = 3 per group.

### 3.2.5. Increased binding of H-2K MHC I occurs independently of CD8 co-receptor and H-2K allele

I had identified a substantial population of H-2K<sup>b</sup>-reactive CD8 and CD4 T cells in mice that lacked H-2K<sup>b</sup>, which could be explained by two potential hypotheses. Firstly, it is possible that the absence of the H-2K<sup>b</sup> molecule has abrogated negative selection of T cells that are intrinsically reactive to H-2K<sup>b</sup>, resulting in the generation of a population of T cells with TCRs that bind to the H-2K<sup>b</sup> molecule independently of peptide. Secondly, it is possible that the binding of the H-2K<sup>b</sup> MHC I was being mediated by a ligand other than the TCR. For example, the CD8 co-receptor and Ly49 molecules, both expressed by T cells, are known to be bound by MHC I (206–209).

To firstly confirm that H-2K<sup>b</sup>-reactive TCRs were broadly reactive to all H-2K<sup>b</sup> tetramers independent of the peptide loaded, I performed tetramer-based magnetic enrichment using another H-2K<sup>b</sup> tetramer loaded with the vaccinia virus derived H-2K<sup>b</sup>B8R<sub>20</sub>-epitope. It has previously been shown that C57BL/6 mouse strains contain a remarkably large frequency of H-2K<sup>b</sup>B8R<sub>20</sub>-specific cells (~300-1,000 cells per mouse) (134).

I was able to isolate similar frequencies of naïve H-2K<sup>b</sup>B8R<sub>20</sub>-specific CD8 T cells from WT and H-2D<sup>b/-</sup> as compared to previous reports, at ~451 and ~546 cells per mouse, respectively. However, the loss of the H-2K<sup>b</sup> molecule once again led to a substantially inflated number of H-2K<sup>b</sup>B8R<sub>20</sub>-binding CD8 T cells in H-2K<sup>b/-</sup> and DKO mice (~16,269 and 9,116 CD8 T cells respectively), as I had previously observed for H-K<sup>b</sup>PB1<sub>703</sub> and H-2K<sup>b</sup>NS2<sub>114</sub> (**Figure 11**). This phenomenon of H-2K<sup>b</sup>-reactivity was again absent in

WT and H-2D<sup>b</sup><sup>-/-</sup> mice, which indicated that tetramer binding by H-2K<sup>b</sup>-reactive cells was mediated through the H-2K<sup>b</sup> molecule itself, independently of the loaded peptide.

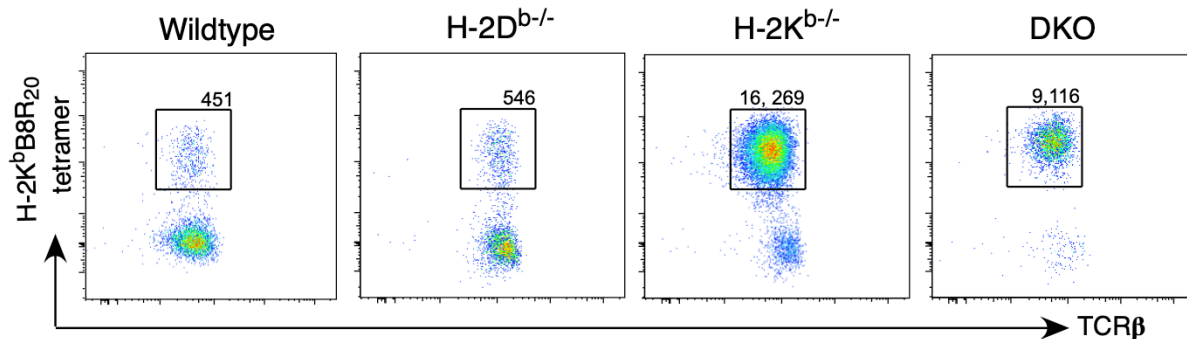


**Figure 11:** Elevated numbers of H-2K<sup>b</sup>B8R<sub>20</sub>-specific CD8 T cells following tetramer-based magnetic naïve enrichment in H-2K<sup>b</sup><sup>-/-</sup> and DKO mice. Representative dot plots showing H-2K<sup>b</sup>B8R<sub>20</sub> tetramer staining and TCRβ staining on live, CD19<sup>-</sup>, F4/80<sup>-</sup>, CD11b<sup>-</sup>, CD11c<sup>-</sup>, NK1.1<sup>-</sup>, CD4<sup>-</sup>, TCRβ<sup>+</sup>, CD8<sup>+</sup> T lymphocytes from naïve WT, H-2D<sup>b</sup><sup>-/-</sup>, H-2K<sup>b</sup><sup>-/-</sup> and DKO mice after tetramer-based magnetic enrichment. Results are representative of 2 independent experiments with  $n = 4$  per group.

The MHCI molecule is known to mediate a number of non-specific interactions with molecules other than the TCR (206–209). In particular, the  $\alpha_3$  domain of the MHCI molecule contains key bindings sites for the CD8 co-receptor (207, 208). Given the substantially increased binding of the tetramer by CD8 T cells in H-2K<sup>b</sup><sup>-/-</sup> and DKO mice, I considered the possibility that the tetramer may be binding directly to the CD8 co-receptor, independently of TCR. While the  $\alpha_3$  domain is highly homologous between H-2D<sup>b</sup> and H-2K<sup>b</sup> (31), it was clear that the H-2D<sup>b</sup>  $\alpha_3$  domain could not mediate this widespread T cell binding (**Figure 6A**). Therefore, I used a chimeric H-2K<sup>b</sup> tetramer, which contained the  $\alpha_3$  domain of H-2D<sup>b</sup> (gift of Lucy Sullivan and Andrew Brooks) (**Figure 12**).

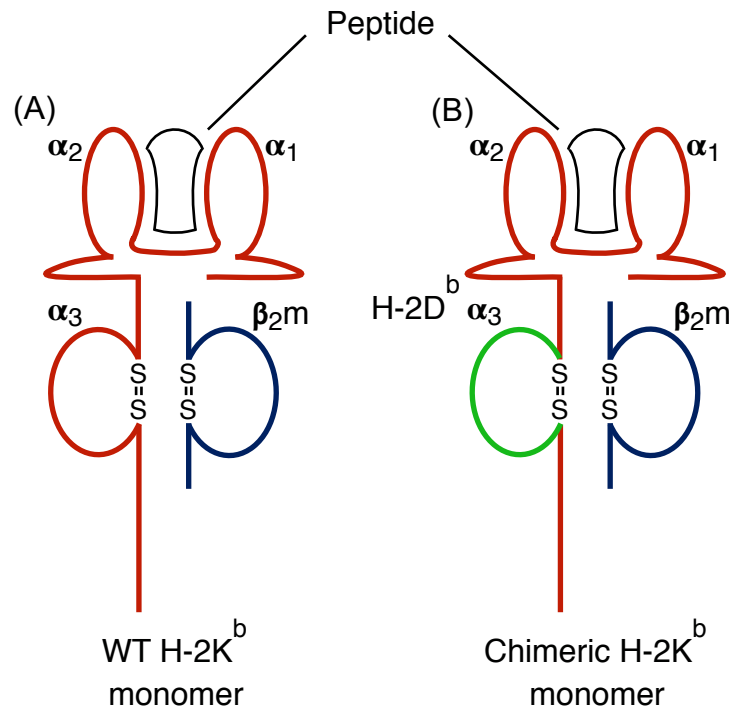


**Figure 12:** Schematic representation of the WT and chimeric H-2K<sup>b</sup> monomer. (A) The WT H-2K<sup>b</sup> monomer consists of the heavy α chain (red) comprising the α<sub>1</sub>, α<sub>2</sub> and α<sub>3</sub> domains and is stabilized by the β<sub>2</sub>m (blue). (B) The chimeric H-2K<sup>b</sup> monomer has the α<sub>3</sub> domain substituted with the H-2D<sup>b</sup> α<sub>3</sub> domain (green).

Tetramer-based magnetic enrichment using chimeric H-2K<sup>b</sup>NS2<sub>114</sub> and H-2K<sup>b</sup>PB1<sub>703</sub> tetramers yielded similar numbers of naïve antigen-specific CD8 T cells in WT mice, demonstrating that the substitution of the H-2K<sup>b</sup> α<sub>3</sub> domain with the H-2D<sup>b</sup> α<sub>3</sub> domain did not impact the detection of *bona fide* antigen-specific cells (**Figure 13A, B**). However, the chimeric tetramers failed to prevent binding of the H-2K<sup>b</sup>-reactive CD8 T cells in H-2K<sup>b</sup><sup>-/-</sup> mice, resulting in a similarly inflated population of CD8 T cells binding to both chimeric H-2K<sup>b</sup>NS2<sub>114</sub> and H-2K<sup>b</sup>PB1<sub>703</sub> tetramers, simultaneously (**Figure 13C**). This suggests that the region of the H-2K<sup>b</sup> that is being targeted by H-2K<sup>b</sup>-reactive cells lies outside the α<sub>3</sub> domain. In particular, it implicates the α<sub>1</sub>, and/or α<sub>2</sub>

domains of the H-2K<sup>b</sup> molecule, since the tetramers are routinely refolded with human  $\beta_2m$  to prevent non-specific binding and promote stability (210).

To further eliminate the possibility that H-2K<sup>b</sup> tetramer binding was mediated by the CD8 co-receptor, I blocked the ability of H-2K<sup>b</sup> tetramers to bind the CD8 co-receptor using an anti-CD8 $\beta$  mAb (Clone: 53-5.8), previously shown to block the interaction with MHCI (211). Since blocking the CD8-MHCI interaction decreases the stability of canonical TCR-pMHCI interactions, it can also result in substantially decreased conventional TCR-pMHCI binding. Consequently, addition of the anti-CD8 $\beta$  antibody almost completely abrogated the binding of H-2K<sup>b</sup>NS2<sub>114</sub> and H-2K<sup>b</sup>PB1<sub>703</sub> tetramers to CD8 T cells from WT mice (**Figure 13D**). Similarly, in H-2K<sup>b</sup><sup>-/-</sup> mice, inclusion of the anti-CD8 $\beta$  blocking antibody prevented the detection of epitope-specific CD8 T cells that bound exclusively to the H-2K<sup>b</sup>NS2<sub>114</sub> tetramer (**Figure 13E**), suggesting that the CD8-MHCI interaction was required for the tetramer-based identification of *bona fide* alloreactive cells, and that the addition of the antibody was blocking the CD8-MHCI $\alpha_3$  interaction. However, the addition of the CD8 $\beta$  blocking antibody failed to abolish the binding of the H-2K<sup>b</sup>-reactive CD8 T cells to H-2K<sup>b</sup> tetramers (**Figure 13E**). This implies both that the CD8 co-receptor does not facilitate tetramer binding by the H-2K<sup>b</sup>-reactive cells, and that these cells do not require CD8-MHCI association in order to bind the H-2K<sup>b</sup> tetramers.

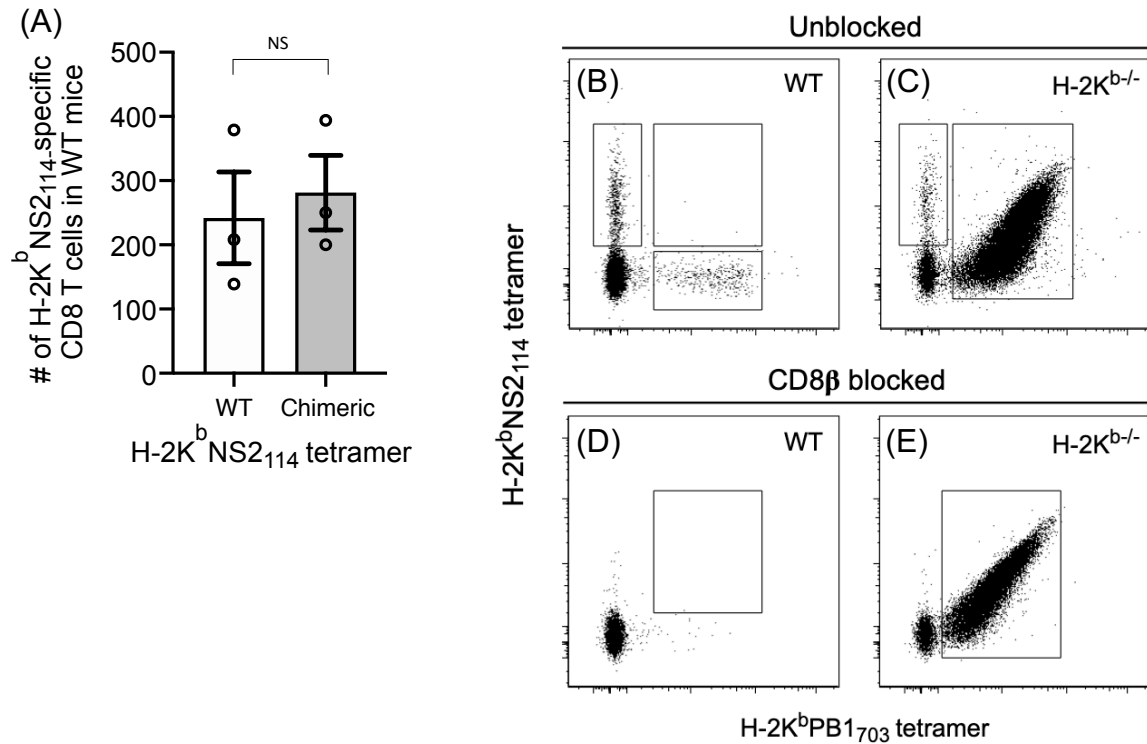


**Figure 13:** H-2K<sup>b</sup>-reactive cells bound chimeric H-2K<sup>b</sup> tetramers, and its interaction is independent of CD8 co-receptor binding. (A) The number of H-2K<sup>b</sup>NS2<sub>114</sub>-specific CD8 T cells in naïve WT mice following tetramer-based magnetic enrichment with WT or chimeric tetramer. Representative dot plots showing H-2K<sup>b</sup>NS2<sub>114</sub> and H-2K<sup>b</sup>PB1<sub>703</sub> staining in CD8 T cells from WT and H-2K<sup>b</sup><sup>-/-</sup> mice following magnetic enrichment in the absence (B, C) or presence (D, E) of blocking  $\alpha$ CD8 $\beta$  antibody. NS indicates  $p > 0.05$  (Student's t-test). Cells are gated on live, B220<sup>-</sup>, NK1.1<sup>-</sup>, F4/80<sup>-</sup>, CD11b<sup>-</sup>, CD11c<sup>-</sup> CD3<sup>+</sup>, TCR $\beta$ <sup>+</sup>, CD8<sup>+</sup> T lymphocytes. These results are representative of 3 independent experiments with  $n = 3$  per group.

Given the broad reactivity of H-2K<sup>b</sup>-reactive cells, I then aimed to determine if these cells were reactive to H-2K molecules regardless of the allelic variant. To address this, I performed tetramer-based magnetic enrichment of cells from WT and H-2K<sup>b</sup><sup>-/-</sup> mice using two H-2K<sup>d</sup> tetramers: the human immunodeficiency virus (HIV)-derived epitope H-2K<sup>d</sup>AMQ<sub>197</sub> and IAV-derived epitope H-2K<sup>d</sup>NP<sub>147</sub>.

In WT C57BL/6 mice, I detected a small number of uniquely H-2K<sup>d</sup>AMQ<sub>197</sub> and H-2K<sup>d</sup>NP<sub>47</sub>-specific CD8 T cells (13 and 23, respectively), as evidenced by their mutually exclusive tetramer staining (**Figure 14A**). These cells are likely to be *bona fide* alloreactive CD8 T cells selected on the H-2<sup>b</sup> allelic variant (unpublished data). By contrast, in H-2K<sup>b</sup><sup>-/-</sup> mice I detected the presence of a substantial H-2K<sup>d</sup>-reactive CD8 T cell population binding simultaneously to both H-2K<sup>d</sup> tetramers (**Figure 14B**), as I had observed for H-2K<sup>b</sup> tetramer binding.

To determine whether the H-2K<sup>d</sup>- and H-2K<sup>b</sup>-reactive cells were distinct or the same population, I performed a dual-enrichment using one H-2K<sup>d</sup> and one H-2K<sup>b</sup> tetramer on cells from an H-2K<sup>b</sup><sup>-/-</sup> mouse. My results show that H-2K<sup>b</sup>-reactive cells were indeed the same population that was cross-reactive to H-2K<sup>d</sup> tetramers (**Figure 14C**), suggesting that the population of H-2K<sup>b</sup>-reactive CD8 T cells that appear in the absence of H-2K<sup>b</sup> are broadly reactive to H-2K molecules.

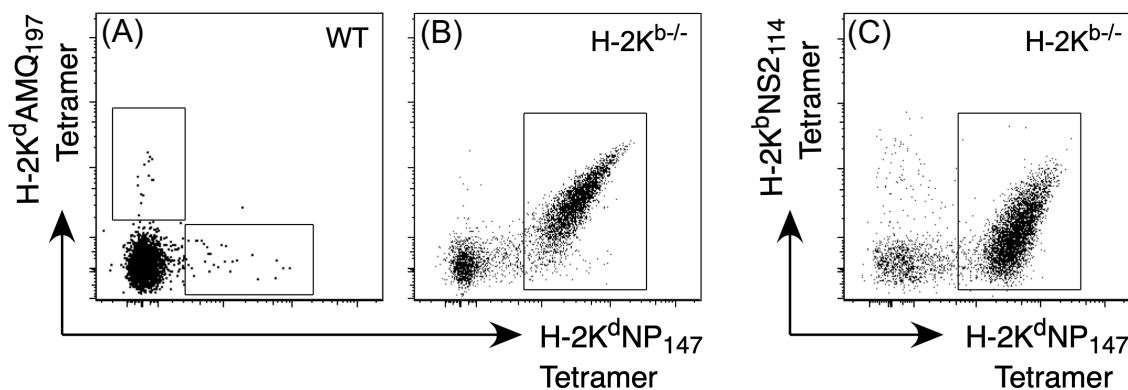


**Figure 14:** H-2K<sup>b</sup>-reactive CD8 T cells are cross-reactive with H-2K<sup>d</sup>. Representative dot plots of CD8 T cells following dual tetramer-based magnetic enrichment with (A, B) H-2K<sup>d</sup>AMQ<sub>197</sub>- and H-2K<sup>d</sup>NP<sub>147</sub> tetramers or (C) H-2K<sup>b</sup>NS<sub>2114</sub>- and H-2K<sup>d</sup>NP<sub>147</sub> tetramers in (A) WT and (B, C) H-2K<sup>b</sup><sup>-/-</sup> mice. Cells are gated on events that are live, B220<sup>-</sup>, NK1.1<sup>-</sup>, F4/80<sup>-</sup>, CD11b<sup>-</sup>, CD3<sup>+</sup>, TCRβ<sup>+</sup>, CD8<sup>+</sup> T lymphocytes. Results are representative of 3 independent experiments with *n* = 3 per group.

### 3.2.6. TCR repertoire analysis showed NKT cell repertoire bias in CD4, and no V-region bias in CD8 T cells

To investigate the possibility that H-2K-reactive T cells are a result of abrogated negative selection due to the absence of the H-2K<sup>b</sup> molecule, I analysed the paired TCR $\alpha\beta$  composition of H-2K-reactive CD4 and CD8 T cells in H-2K<sup>b</sup><sup>-/-</sup> mice. I cloned and sequenced TCR from H-2K-reactive cells and looked for specific characteristics that might confer binding to H-2K tetramers. I profiled the TCR repertoire using a multiplexed, nested RT-PCR (179) on individual sorted H-2K-reactive CD4 and CD8 T cells from H-2K<sup>b</sup><sup>-/-</sup> mice following dual H-2K<sup>b</sup>NS2<sub>114</sub> and H-2K<sup>b</sup>PB1<sub>703</sub> tetramer-based magnetic enrichment. I also sequenced the TCR $\alpha\beta$  repertoire of the global non-antigen-specific CD8 T cell population from H-2K<sup>b</sup><sup>-/-</sup> mice to define a baseline comparison for this analysis.

The TCR repertoire of the global CD8 T cell population in H-2K<sup>b</sup><sup>-/-</sup> mice revealed moderate biases in both the TCR $\alpha$  and TCR $\beta$  chain toward usage of TRAV6 (~22.0%), TRAV9 (~12.2%) and TRAV12 (19.5%) (**Figure 15A**), and TRBV13-3 (~17.1%), respectively (**Figure 15B**). When the H-2K-reactive CD8 T cell population was profiled, I observed broadly similar V-region usage for both the TCR $\alpha$  and TCR $\beta$  chain as compared to the total CD8 T cell population, possibly with modest increases in the TRBV29 and TRBV13-2 usage (**Figure 15C, D**). Moreover, clonotypic analysis of H-2K-reactive CD8 T cells (**Table 13**) revealed no CDR3 $\alpha$  or CDR3 $\beta$  sequences or motifs that were enriched relative to the background repertoire (**Table 14**), and that may have imparted preferential binding of H-2K<sup>b</sup> molecule. Thus, detailed analysis of

TCR characteristics in the H-2K-reactive CD8 T cell population offered no indication of features associated with H-2K binding.

In contrast, when the H-2K-reactive CD4 T cell population was profiled, I observed a dominant TRAV11 bias (~55%) in the TCR $\alpha$  chain and these TRAV11 TCRs consistently utilized the TRAJ18 gene and gave rise to a clonal CDR3 $\alpha$  sequence: GDRGSALGRL (**Table 15**). These TRAV11 TCRs also preferentially paired with TCR $\beta$  chains that used TRBV13-2 (~58%) (**Figure 15E, F**). Intriguingly, the TRAV11 (CDR3 $\alpha$ : GDRGSALGRL)-TRAJ18-TRBV13-2 TCR combination has been previously reported to be the semi-invariant TCR expressed by canonical NKT cells (212), indicating that the H-2K-reactive CD4 T cells are predominantly NKT cells. These data suggest that, at least for CD4 H-2K-reactive cells, the canonical NKT TCR is either well suited to H-2K binding, or that the expression of another ligand that is responsible for H-2K binding is preferentially expressed on NKT cells.

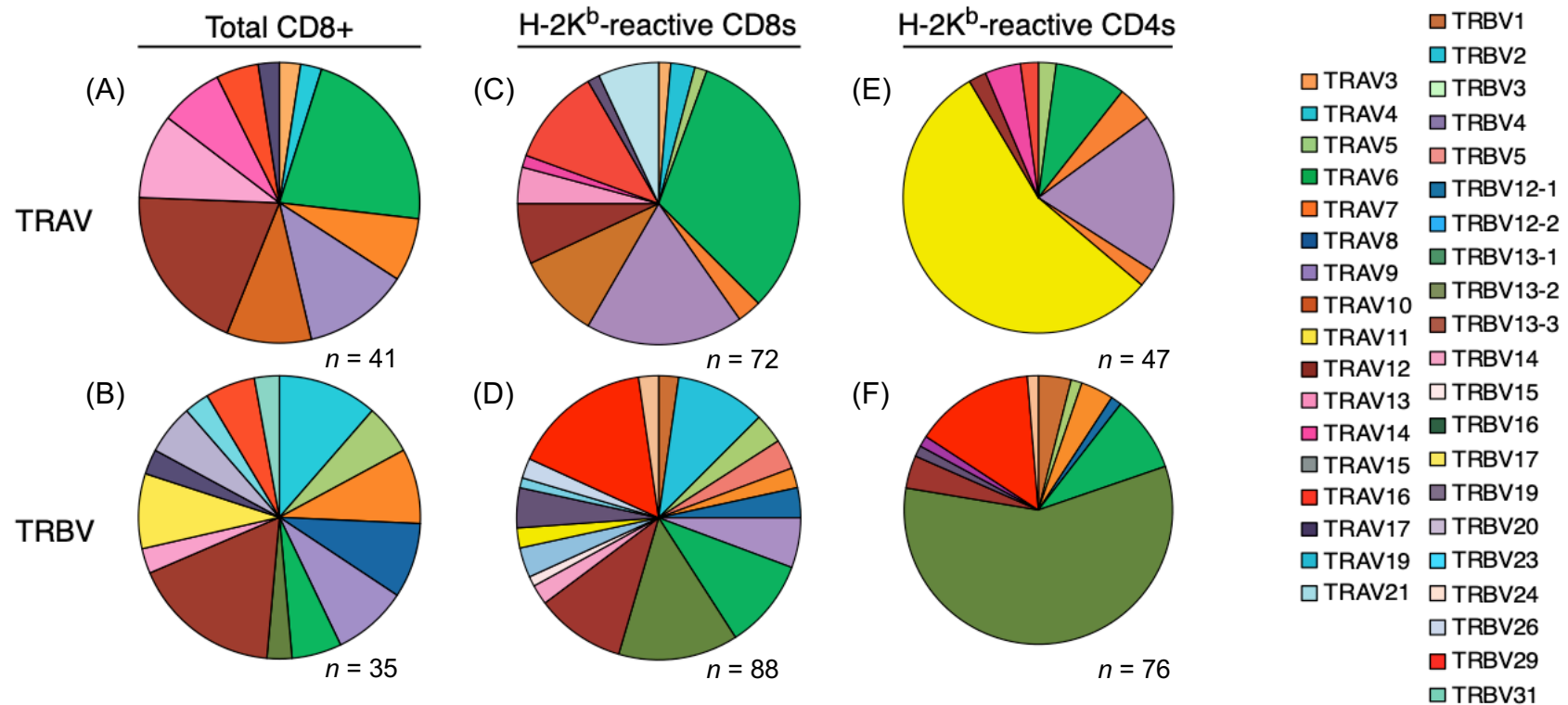


**Figure 15:** TRAV and TRBV usage for the global non-antigen specific CD8 T cell population, and the H-2K-reactive CD8 and CD4 cell-derived TCRs binding simultaneously to H-2K<sup>b</sup>NS<sub>2114</sub> and H-2K<sup>b</sup>PB<sub>1703</sub> from H-2K<sup>b/-</sup> mice. Individual cells were sorted and TCR $\alpha$  and  $\beta$  chains were sequenced, and gene usage assigned using IMGT (35). TRAV (A, C, E) and TRBV (B, D, F) usage represented as a proportion of the (A, B) global CD8 T cell population, (C, D) total H-2K-reactive CD8 T cells, and (E, F) H-2K-reactive CD4 T cells. Sequences for the data analysis of total CD8+ T cells were from a single H-2K<sup>b/-</sup> mouse, whereas data for H-2K-reactive CD4 and CD8 were generated from two H-2K<sup>b/-</sup> mice.

**Table 13:** *Ex vivo* analysis of paired and unpaired TCR CDR3 amino acid residues in the H-2K-reactive CD8 T cell population from H-2K<sup>b/-</sup> mice using multiplex RT-PCR.

TRBV	CDR3β	TRBJ	Length aa	TRAV	CDR3α	TRAJ	Length aa
1	SAGGLSL	1-3	7	9	SALAVVENS	44	9
1	SAGLGGGEQ	2	9	10	SMGGNTGKL	37	9
2	SQVTGGYAEQ	2-1	10	4	EDYGNEKI	48	8
2	SQDRDPPQGLGVNQDTQ	2-5	17	6	GTGGYKV	12	7
2	SQDLGGHAEQ	2	10	6	AANSGTYQ	13	8
3	SFRDRSSYEQ	2	10	16	REGLGNEKI	48	9
4	SFDWASNYAEQ	2-1	11	13	EGEYANKM	47	8
4	SPTENSDY	1-2	7	9	INNYAQGL	26	8
5	SQDSGLGDSQNTL	2	13	10	STNTGKL	27	7
14	SFRVPYEQ	2-7	8	21	RVGTGGNNKL	56	10
15	SRGRKDTQ	2-5	8	6	VPPNSGSYQ	13	10
16	SPRLGGRRQNTL	2-7	12	9	SAWLSGSFNKL	4	11
16	SLSGINTEV	1	9	17	ASGGSNYKL	53	9
17	SSPGLGGREQ	2-7	10	10	QGRAL	15	5
23	RDWGENTL	2-4	8	9	SMDNYAQGL	26	9
26	SLGTVSNERL	1-4	10	6	FNYAQGL	26	7
29	SLWGQGERL	1-4	9	16	RGPNYGNEKI	48	10
29	SSWGNTGQL	2	9	4	GGNTGYQNF	49	9
29	SYRGCTL	2-4	7	6	GDPSGGSNYKL	53	11
29	SPGTANSYD	1-2	9	6	SATNAYKV	30	8
29	SFADNSGNTL	1-3	10	6	DTNAYKV	30	7
29	SLWGDNSPL	1-6	9	7	TGYQNF	49	6
29	SRDKYEQ	2-7	7	9	SPEGADRL	45	8
29	RFNQDTQ	2-5	8	9	SMDNYAQGL	26	9
31	SFGRDEQ	2-1	7	5	SAYQGGRAL	15	9
31	SLEQGYNSPL	1-6	10	13	EPGANTGKL	52	9
13-1	SGRDNQDTQ	2-5	9	10	RNNYAQGL	26	8
13-1	SDWGGRRHEQ	2-7	9	9	SMFLSNYNVL	21	10
13-1	SDGTGGYEQ	2-7	9	16	RENYAQGL	26	8
13-1	SDRGGANDTQ	2-5	10	16	RGRDNNAGAKL	39	11
13-1	SEVGANTEV	1	9	16	RPYNAGAKL	39	9
12-2	SLGNQDTQ	2	8	2	TSNTNTGKL	27	9
12-2	SPNTGQL	2-2	9	9	SMDNYAQGL	26	9
12-2	SLRPNQDTQ	2-5	9	9	SMRRGTGSKL	58	10
12-2	SLRDRGYEQ	2	9	9	SASATGGNNKL	56	11
13-2	GDLGRGGQAP	1-5	10	6	GGPGGSNAKL	42	10
13-2	GDHEQ	2-7	5	6	SENYNQGKL	23	9
13-2	GDWGGEQ	2-7	7	9	SEASSFSKL	50	10
13-2	GDTGLGCGQNTL	2-4	12	9	PHTEGADRL	45	9
13-2	GDGGTKDTQ	2-5	9	16	RENYAQGL	26	08
13-3	SASGTK	2	6	6	RIASSGSWQL	22	10
13-3	SDAWGNQDTQ	2-5	10	6	SDGTGGYKV	12	9
13-3	TGNTEV	1	6	12	SDLGPGSWQL	22	11
2	SQGLGGPYEQ	2-7	10				
2	IQGLGGSEQ	2-7	9				
2	SHPGTGGNSDY	1-2	11				
2	SQGTGIHEQ	2	9				

Chapter Three – Alloreactivity and H-2K<sup>b</sup> Reactivity

2	SQEGQTNTEV	1	10			
2	SQDFSQGAGNTL	1	12			
3	SLDWGGDQNTL	2	11			
4	SWGHNSDY	1	8			
5	SQGLGAHQDTQ	2	11			
14	SFGRGYNSPL	1	10			
16	SLEVGGPNQDTQ	2-5	12			
16	SLEWGGNQDTQ	2-5	11			
17	SRWFNQDTQ	2	9			
19	SNRWDTQ	2-5	7			
19	SIPNTEV	1-1	7			
19	SILTGNNNQAP	1	11			
19	SIVGASERL	1	10			
26	SLGQGAAP	1-5	8			
29	SSGFNERL	1-4	8			
29	SLGPSGTGCTL	1	11			
29	SSEQ	2	4			
29	SPGQNSGNTL	1	10			
29	SRDRMYEQ	2	8			
29	SPGTAANSYD	1	10			
12-1	SGTGGTETL	2-3	9			
12-1	SRDWGFYAEQ	2	10			
12-1	SPADWGSETL	2	10			
12-2	SPWDRGYNSPL	1	11			
13-1	SDRVSYEQ	2-7	8			
13-1	SRSYEQ	2	6			
13-1	SDGLGSAETL	2	10			
13-1	SETGGPETL	2	9			
13-2	DATGDTGQL	2-2	9			
13-2	GVGGAETL	2-3	9			
13-2	GGTGGAITDQ	2-5	10			
13-2	GMWDNQAP	1-5	8			
13-2	GGPGSQDTQ	2	9			
13-2	GGYAEQ	2	6			
13-2	GDLGGSSYEQ	2	10			
13-3	SVGNTQ	2-5	6			
13-3	SDAGEV	1-1	6			
13-3	KSTNSDY	1	7			
13-3	SEGVAETL	2	8			
13-3	SDMGGLTGQL	2	10			
13-3	SNNQDTQ	2	7			
				2	TDIPYSNNRL	7 10
				3	SATQVVGQL	5 9
				6	GQGGRAL	15 7
				6	GASSFSKL	50 9
				6	GDWNSNNRI	31 9
				6	TPSSNTNKV	34 9
				6	GTGYQNF	49 7
				6	GASSGSWQL	22 9
				6	SADSGTYQ	13 8
				6	SAYNNAGAKL	39 10
				6	GATSSGQKL	16 9
				6	GTGYQNF	49 7

Chapter Three – Alloreactivity and H-2K<sup>b</sup> Reactivity

				6	GGAGSGGKL	44	9
				7	SERGNTGKL	37	9
				9	EGSNNRI	31	7
				10	SIGGGTGGNNKL	56	12
				10	ANYNTGNYKY	40	10
				10	SMTGSSGNKL	32	10
				12	SELSGSFNKL	4	10
				12	SGPCGSWQL	22	9
				12	SVPSGSWQL	22	9
				12	SDPSGSWQL	22	9
				13	GGGSWQL	22	7
				14	SEGLSGSFNKL	4	11
				16	REGVGSNNRI	31	10
				16	REGNTGKL	37	8
				16	RDYSNNRL	7	8
				21	RVGGGTGSKL	58	10
				21	RATGGNNKL	56	9

\* Sequences in red were selected for *in vitro* expression.

**Table 14:** *Ex vivo* analysis of paired and unpaired TCR CDR3 amino acid residues in the total CD8 T cell population from H-2K<sup>b/-</sup> mice using multiplex RT-PCR.

TRBV	CDR3 $\beta$	TRBJ	Length aa	TRAV	CDR3 $\alpha$	TRAJ	Length aa
2	SRDTLSAETL	2-3	10	6	GERNSGTYQ	13	9
2	SQDGWGS AETL	2-3	11	16	REGQQGTGSKL	58	11
3	SLDWGQDTQ	2-5	9	10	RTGYQNF	49	7
5	SQDPWGAYEQ	2-7	10	7	STD TNAYKV	30	9
5	SQDWGGADTGQL	2-2	12	12	SRNYAQGL	26	8
5	SAPTGYEQ	2-7	8	13	SGGNYKP	6	7
14	SLGGNQDTQ	2-5	9	10	SRSNNRI	31	7
17	SLDSSAETL	2-3	9	6	GESSGSWQL	22	10
17	SSRDWESSYEQ	2-7	11	6	SDGSNNRI	31	8
17	SSGDQNTL	2-4	8	16	REGAGYQNF	49	9
19	SIGGN YAEQ	2-1	9	12	SDRLATGGNNKL	56	12
20	RDGGAGNTL	1-3	9	6	RDTNKV	34	6
23	TTGLEQ	2-7	6	10	SNMGYKL	9	7
29	SWGNT EV	1-1	7	3	TGYQNF	49	6
29	STGVEQ	2-7	6	14	RGANKM	47	6
31	SLVWAPYEQ	2-7	9	6	SPMNYNQGKL	23	10
12-1	SLSGVTGQL	2-2	9	9	SLGTGGYKV	12	9
12-1	SLGGTNERL	1-4	9	9	SSTTASLGKL	24	10
12-1	FGGAREQ	2-7	7	13	SGGSNYKL	53	8
12-2	SLEGGGDTQ	2-5	9	6	GDNSGGSNYKL	53	11
12-2	SSSTGGARAEQ	2-1	11	7	SEPDRGSALGRL	18	12
13-2	GDGTGASYN SPL	1-6	12	6	GEANSAGNKL	17	10
13-3	NPDWGN YAEQ	2-1	11	6	G DATNAYKV	30	9
2	SQEKLGGDTQ	2-5	11				
2	SQDGWGGASEQ	2-7	11				
3	SPHWGGGQDTQ	2-5	11				
12-2	SRTGANTEV	1-1	9				

Chapter Three – Alloreactivity and H-2K<sup>b</sup> Reactivity

13-1	SDDWGVQDTQ	2-5	11				
13-1	SDTGGAYTGQL	2-2	11				
13-3	SGLGGREQ	2-7	8				
13-3	SDTGVEQ	2-7	7				
13-3	SEGWGTGQL	2-2	9				
13-3	SGDSYEQ	2-7	7				
13-3	SDAGEAETL	2-3	9				
20	REGQNSPL	1-6	7				
				4	LSGSFNKL	4	8
				6	ASSGSWQL	22	8
				7	SISTGYQNF	49	8
				9	SPLSSNTNKV	34	10
				9	SAEEAGNTGKL	37	11
				9	STSSSFSKL	50	9
				10	RDSNNRI	31	7
				12	SDPNNNNAP	43	9
				12	REVSSGSWQL	22	10
				12	SGLSSGSWQL	22	10
				12	TGGEGRAL	15	9
				12	SAPFRAQGL	26	9
				12	RHDTNAYKV	30	9
				13	EPNSGTQYQ	13	8
				13	ERGNYQL	33	7
				14	RASSGSWQL	22	9
				14	SAREATGGNNKL	56	12
				17	ENYGNEKI	48	8

**Table 15:** *Ex vivo* analysis of paired and unpaired TCR CDR3 amino acid residues in the H-2K-reactive CD4 T cell population from H-2K<sup>b/-</sup> mice using multiplex RT-PCR

TRBV	CDR3 $\beta$	TRBJ	Length aa	TRAV	CDR3 $\alpha$	TRAJ	Length aa
5	SHDNSQNTL	2-4	9	6	GAWNSNNRI	31	9
13-2	VPGRMSGNTL	1-3	10	6	GRGSALGRL	18	9
13-2	GDPWGGGEQ	2-7	9	7	SGSFNKL	4	7
13-2	GDWGKNTL	2-4	8	7	DRGSALGRL	18	9
13-1	SGGLGGRASAETL	2-3	13	9	SSPLQGTGSKL	58	11
13-2	GNTGQL	2-2	6	9	KGNMGYKL	9	8
13-2	GAYWGGSQNTL	2-4	11	9	SMLSAGNKL	17	9
13-2	GEWQGASGNTL	1-3	11	9	RSSGSFNKL	4	9
13-2	GDAGTNTGQL	2-2	10	9	RGNMGYKL	9	9
13-3	TARHTEV	1-1	7	9	SSNMGYKL	9	8
13-2	GDWRAGNTL	1-3	9	10	RSGSFNKL	4	8
1	SAEQGAGTL	2-4	9	11	GDRGSALGRL	18	10
29	SLRNHSGNTL	1-3	10	11	GDRGSALGRL	18	10
29	SSGAPTNERL	1-4	10	11	GDRGSALGRL	18	10
29	SLYRGAETL	2-3	10	11	GDRGSALGRL	18	10
13-2	GELGGRGDTQ	2-5	10	11	GDRGSALGRL	18	10
13-2	GDVQNQDTQ	2-5	9	11	GDRGSALGRL	18	10
13-2	GAPQGQYEQ	2-7	9	11	GDRGSALGRL	18	10
13-2	GDATGGGGTEV	1-1	11	11	GDRGSALGRL	18	10

Chapter Three – Alloreactivity and H-2K<sup>b</sup> Reactivity

13-2	GDRASSDY	1-2	8	11	GDRGSALGRL	18	10
13-2	GAAGTGGWNNQAP	1-5	13	11	GDRGSALGRL	18	10
13-2	GDAQGAYEQ	2-7	9	11	GDRGSALGRL	18	10
13-2	GETLTSNSDY	1-2	10	11	GDRGSALGRL	18	10
13-2	GDVEQ	2-7	5	11	GDRGSALGRL	18	10
13-2	WGDINQAP	1-5	8	11	VDRGSALGRL	18	10
13-2	GDWTGVSGNTL	1-3	11	11	GDRGSALGRL	18	10
13-2	GALDRGGAETL	2-3	11	11	GDRGSALGRL	18	10
13-2	GDAWGYSYEQ	2-7	10	11	GDRGSALGRL	18	10
13-2	GGTGGYAEQ	2-1	9	11	GDRGSALGRL	18	10
13-1	SEVWGGGSAETL	2-3	12	12	RRNNYAQGL	26	9
5	SQDWGSQNTL	2-4	10	14	GGTNSAGNKL	17	10
13-2	SGDRDWDQDTQ	2-5	10	14	RPFYTGNYKY	40	10
13-2	GDWGGAEQ	2-7	8	16	REGAGQGGRAL	15	11
1	SADVGAETL	2-3	9				
3	SRPGTGITGQL	2-2	11				
5	SQPGTGGPLAEQ	2-1	12				
19	TRLGGREQ	2-7	8				
20	RGTENTL	2-4	7				
29	TRTGRDTQ	2-5	8				
29	SLVRDRKNTL	2-4	10				
29	SLPGQKSSGNTL	1-3	12				
29	TSYAEQ	2-1	6				
29	SLPQGAYAEQ	2-1	10				
29	SWAGNEQ	2-7	7				
29	SLYGTGDNQAP	1-5	11				
29	SLSLTEV	1-1	6				
31	SRQGAFSGNTL	1-3	11				
12-1	SLGQPGNTL	1-3	9				
13-1	SGSGRYEQ	2-7	8				
13-1	SDVTISNERL	1-4	10				
13-1	SEWGGTEV	1-1	8				
13-1	SDPLGGRYAEQ	2-1	11				
13-1	SGRDFSSEQ	2-7	9				
13-2	GDVLGDTGQL	2-2	10				
13-2	GGTGGDYAEQ	2-1	10				
13-2	GDGGASSYEQ	2-7	10				
13-2	GGQGEEQ	2-7	7				
13-2	GDADWASSYEQ	2-7	11				
13-2	GDAQGGNTEV	1-1	10				
13-2	GDESTGISGNTL	1-3	12				
13-2	GDAAKNSDY	1-2	9				
13-2	GEWGGREQ	2-7	8				
13-2	GDALGRNQDTQ	2-5	11				
13-2	GETINQDTQ	2-5	9				
13-2	GDQDTQ	2-5	6				
13-2	GELGLGNIAEQ	2-1	11				
13-2	GTTGGNAETL	2-3	10				
13-2	GEGPGRHNSPL	1-6	11				
13-2	GDRWDWGNIAEQ	2-1	12				
13-2	GGETKEV	1-1	7				
13-2	GDHNSGNTL	1-3	9				
13-2	GEGRGYEQ	2-7	8				

Chapter Three – Alloreactivity and H-2K<sup>b</sup> Reactivity

13-2	GDAHWGGQNTL	2-4	11				
13-3	SRLGVYSYEQ	2-7	10				
				1	SADALGSSQNTL	2-4	2
				5	SIPGSFNKL	4	9
				6	GDQTGNTGKL	37	10
				6	GVSVTTASLGKL	24	12
				9	SAPFGGKL	27	8
				9	SMRYNQGKL	23	9
				9	RGNMGYKL	9	8
				11	GDRGSALGRL	18	10
				11	GDRGSALGRL	18	10
				11	GDRGSALGRL	18	10
				11	GDRGSALGRL	18	10
				11	GDRGSALGRL	18	10
				11	GDRGSALGRL	18	10
				11	GDRGSALGRL	18	10
				11	GDRGSALGRL	18	10
				11	GDRGSALGRL	18	10
				13-3	SPGTGGFYAEQ	2-1	2

\* Sequences in red were selected for *in vitro* expression.

\*\* Sequences boxed in red are the semi-invariant canonical NKT cell receptor  $\alpha$  chain TRAV11-TRAJ18 (212).

### 3.2.7. TCRs on H-2K-reactive T cells cannot bind H-2K<sup>b</sup> tetramers

Given that I had cloned paired TCR $\alpha$  and TCR $\beta$  chains from H-2K-reactive CD8 and CD4 T cells, I could now conclusively test whether the pan-H-2K interaction was mediated by a *bona fide* TCR binding with H-2K<sup>b</sup> tetramers. To do this, I transfected and expressed selected H-2K-reactive CD8 and CD4 TCRs (**Table 13, 15**, sequences in red), along with the CD3 $\gamma\delta\zeta$  complex, in 293T cells and tested their capacity to bind H-2K<sup>b</sup>NS2<sub>114</sub> and H-2K<sup>b</sup>PB1<sub>703</sub> tetramers. The 293T cell line is a human cell line that does not express other T cell-associated markers and will thus directly test TCR binding to tetramer by eliminating any non-TCR mediated tetramer binding. Based on the TCR clonotypic analysis described in **Section 3.2.6**, I selected three H-2K-reactive CD8 and two H-2K-reactive CD4 TCRs from H-2K<sup>b</sup><sup>-/-</sup> mice that were representative of the broader repertoire.

All of the H-2K-reactive CD8 and CD4 TCRs from H-2K<sup>b</sup><sup>-/-</sup> mice were successfully expressed on the surface of 293T cells, as evidenced by TCR $\beta$  staining (**Figure 16**). However, none of the TCRs could bind either H-2K<sup>b</sup>PB1<sub>703</sub> or H-2K<sup>b</sup>NS2<sub>114</sub> tetramers despite high levels of TCR expression (**Figure 16**). These data conclusively demonstrated that the interaction between the T cells from H-2K<sup>b</sup><sup>-/-</sup> mice and the H-2K<sup>b</sup> tetramer was not mediated by TCR recognition of the H-2K<sup>b</sup> molecule. It also indicates that the H-2K<sup>b</sup> tetramers are binding a molecule that is expressed on subsets of CD8 and CD4 T cells, and that is either upregulated, or becomes available for binding, only in the absence of the endogenous H-2K<sup>b</sup> molecule.

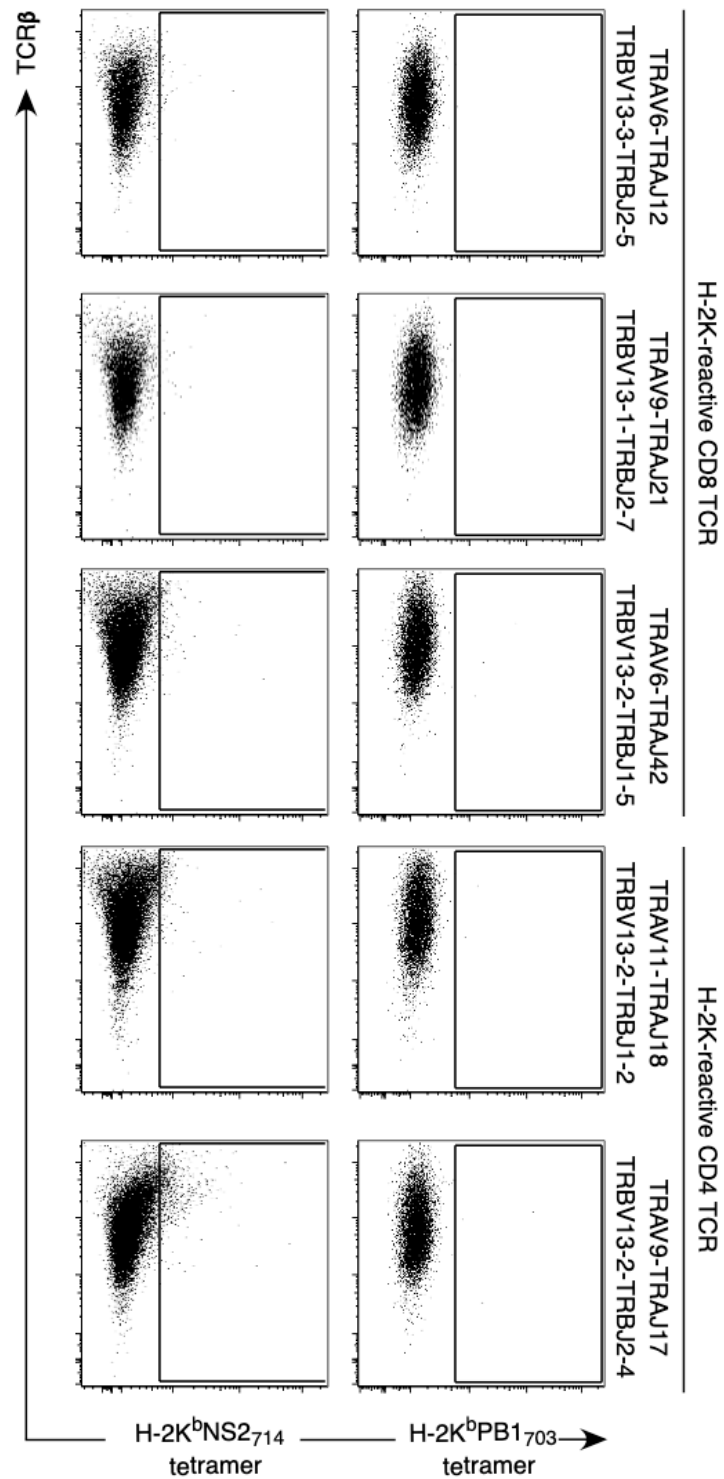


**Figure 16:** Representative dot plots showing TCR $\beta$  expression and tetramer staining of TCRs identified from H-2K-reactive CD8 and CD4 TCRs from H-2K<sup>b</sup><sup>-/-</sup> mice. Selected TCRs were transiently expressed, along with CD3 $\gamma\delta\epsilon$  and  $\zeta$  chains, in 293T cells. At 3 days after transfection, cells were stained with H-2K<sup>b</sup>PB1<sub>703</sub> and H-2K<sup>b</sup>NS2<sub>114</sub> tetramers and anti-TCR $\beta$  mAb. Cells are gated on live, GFP<sup>+</sup> 293T cells. These results are representative of 2 independent experiments.

### 3.2.8. H-2K-reactive CD8 and CD4 T cells express markers of T<sub>MEM</sub> and NKT cells, respectively

Given that the H-2K tetramer binding was not being mediated by the TCR, I wanted to further investigate the phenotypic characteristics of H-2K-reactive CD8 and CD4 T cells to see whether this could provide clues as to which ligand(s) might be mediating the H-2K interaction. To determine whether H-2K-reactive T cells were actually NKT cells, I characterized the expression level of several NK cell markers and activation markers. Specifically, I measured expression of CD8, TCR $\beta$  and CD44 on H-2K-reactive CD8 T cells, and NK1.1 on H-2K-reactive CD4 T cells from naïve H-2K<sup>b/-</sup> mice, comparing these expression levels to those seen on the total CD8 and CD4 T cell populations.

H-2K-reactive CD8 T cells had decreased expression of CD8 $\alpha$  and TCR $\beta$  (**Figure 17A, B**), but expressed higher levels of CD44 (**Figure 17C**) than total CD8 T cells, consistent with the phenotype of a previously activated CD8 T cell (213). This suggests that a receptor broadly expressed on activated or memory CD8 T cells may be binding H-2K<sup>b</sup> tetramers non-specifically. H-2K-reactive CD4 T cells consistently expressed the NK and NKT cell marker, NK1.1, as compared to total CD4 T cells, which did not express the marker (**Figure 17D**). This data was in line with my TCR clonotypic analysis, which showed a bias towards invariant NKT TCR usage.

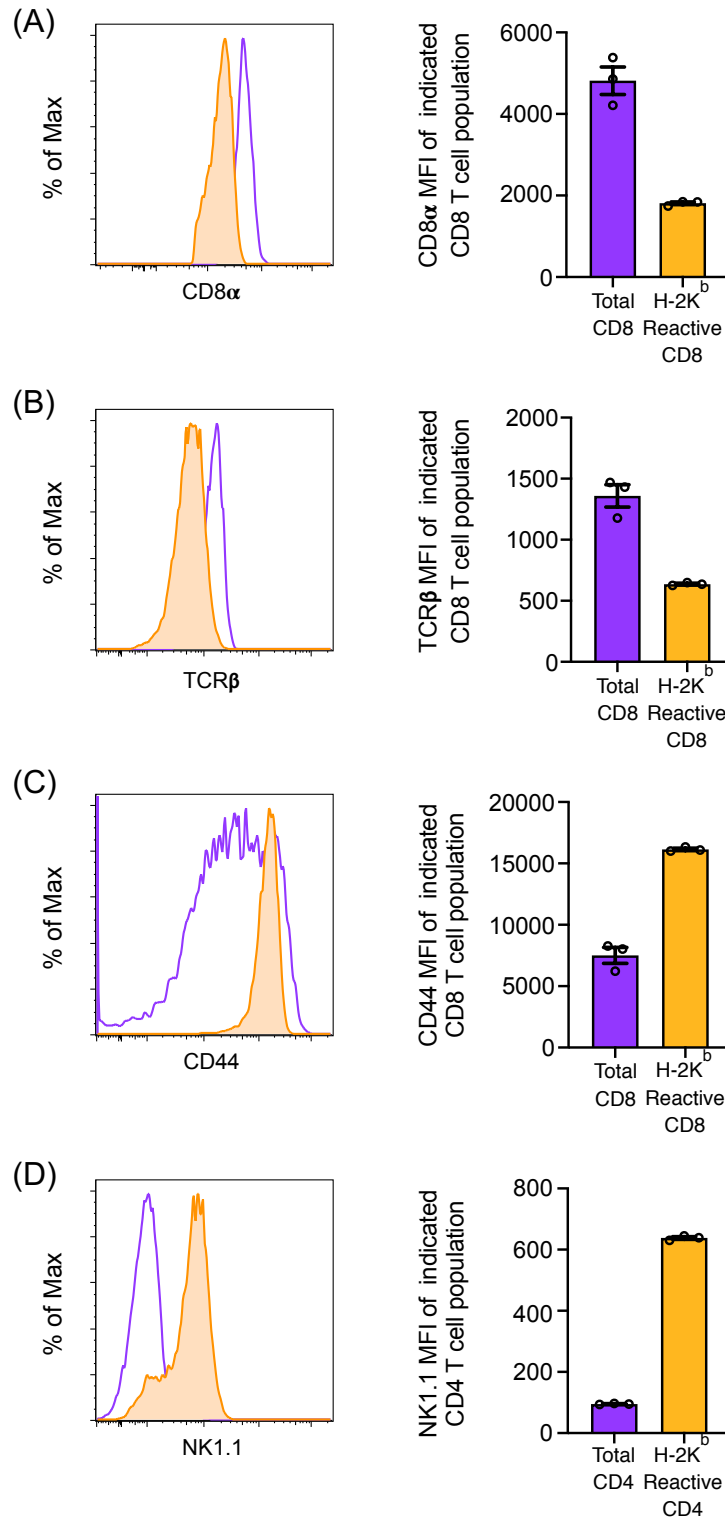


**Figure 17:** Phenotypic characterization of H-2K-reactive CD8 and CD4 T cells in H-2K<sup>b/-</sup> mice. Representative histograms and mean MFI of (A) CD8 $\alpha$ , (B) TCR $\beta$  and (C) CD44 expression on the total CD8 T cell (purple) and H-2K-reactive CD8 T cell population (orange) in H-2K<sup>b/-</sup> mice. (D) Representative histograms and mean MFI of NK1.1 expression on total CD4 T cells and H-2K-reactive CD4 T cells. These results are representative of 2 independent experiments with  $n = 3$  per group.

### 3.2.9. H-2K-reactive NK cells persist in $\beta_2m^{-/-}$ mice, suggesting a non-TCR-mediated interaction

Given that the major populations exhibiting the H-2K<sup>b</sup> binding appeared to be memory CD8 T cells and CD4<sup>+</sup> NKT cells, I used  $\beta_2m^{-/-}$  mice to eliminate both classical and non-classical MHC I molecules. The  $\beta_2m^{-/-}$  mice have a similar phenotype to DKO mice with a complete absence of MHC Ia, but  $\beta_2m^{-/-}$  mice additionally lack non-classical MHC Ib molecules, including the non-classical CD1d molecule required for NKT cell maturation (214). To evaluate whether MHC Ib was necessary for the generation of H-2K-reactive cells, I performed a dual H-2K<sup>b</sup> tetramer-based naïve magnetic enrichment in  $\beta_2m^{-/-}$  mice. In  $\beta_2m^{-/-}$  mice there was an almost complete absence of CD8 T cells, consistent with the dependence of CD8 T cell development on MHC Ia or MHC Ib molecules (**Figure 18A**). As a result, the H-2K-reactive CD8 population was also absent in  $\beta_2m^{-/-}$  mice. The total CD4 T cell population was still present in  $\beta_2m^{-/-}$  mice, but H-2K-reactive CD4 T cells were effectively absent (**Figure 18B**). Given that the vast majority of CD4 T cells are MHC II-restricted (and therefore unaffected in  $\beta_2m^{-/-}$  mice), this suggested that the H-2K-reactive cells within the CD4 population were limited to NKT cells or similar unconventional T cells that are dependent on MHC Ib for development. Further analysis in  $\beta_2m^{-/-}$  mice revealed the simultaneous binding of both H-2K<sup>b</sup>NS2<sub>114</sub> and H-2K<sup>b</sup>PB1<sub>703</sub> tetramers in the CD3<sup>-</sup> NK1.1<sup>+</sup> NK cell population (**Figure 18C**). This further demonstrates that the H-2K reactivity in mice lacking H-2K<sup>b</sup> is not likely to be mediated by specific TCR interactions but is instead likely to be mediated by other interactions, possibly an NK cell-related marker that is broadly

expressed on activated/memory CD8 T cells, NKT cells and NK cells, in the absence of H-2K<sup>b</sup>.

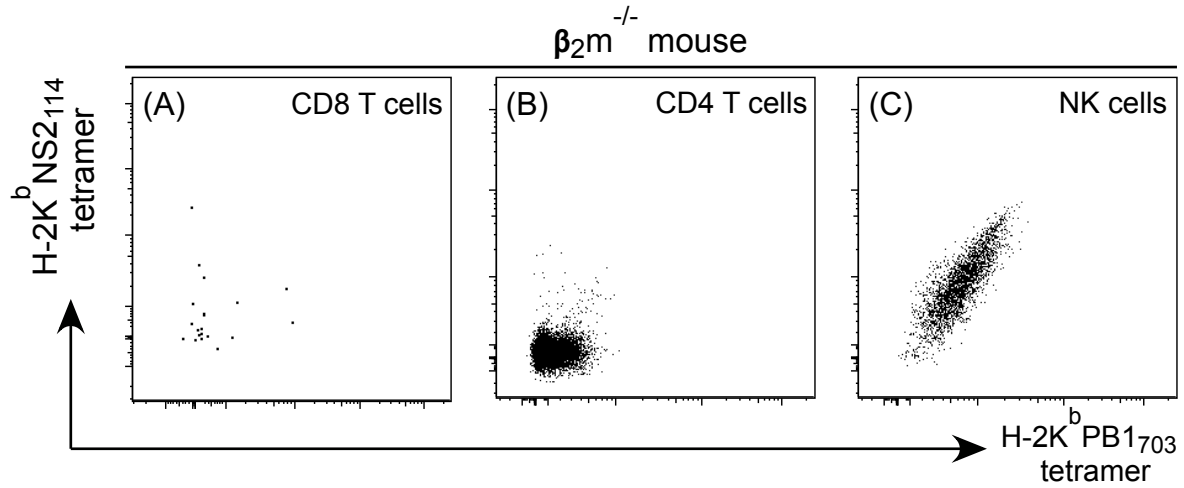


**Figure 18:** H-2K-reactive cells are present in the NK cell population from a  $\beta_2m^{-/-}$  mouse. Representative dot plots of H-2K-reactive (A) CD8, (B) CD4 T cells and (C) NK cells from  $\beta_2m^{-/-}$  mouse. Cells are gated on live, B220<sup>-</sup>, F4/80<sup>-</sup>, CD11b<sup>-</sup>, CD11c<sup>-</sup> lymphocytes. These results are representative of 2 independent experiments with  $n = 3$  per group.

### 3.2.10. H-2K<sup>b</sup> tetramers simultaneously bound Ly49C expression in CHO cell line

My analyses thus far indicate that the H-2K ligand in H-2K<sup>b</sup><sup>-/-</sup> mice is expressed on memory or activated CD8 T cells, NK cells and NKT cells. Analysis of the literature identified the Ly49 family of molecules as inhibitory receptors highly expressed on NK cells for the recognition of MHCI and MHCI-like molecules (206, 215, 216). In particular, Ly49C is a ligand for both H-2K<sup>b</sup> and H-2D<sup>b</sup> molecules but it binds H-2K<sup>b</sup> with a stronger affinity than H-2D<sup>b</sup> (206, 217). Ly49 molecules can bind MHCI in two orientations, namely in *cis* (on the same cell) and in *trans* (on different cells) (216). The interaction between Ly49 and MHCI occurs *via* the Ly49 molecule interacting with the  $\alpha_2$  and  $\alpha_3$  domains, and the  $\beta_2m$  molecule of the MHCI molecule (218–220). The interaction of Ly49 with MHCI in *cis* plays a predominantly inhibitory role to regulate NK cell activation (216, 221). In addition to *cis* binding, Ly49 and MHCI can interact in *trans*, where the binding is mediated by the same recognition sites as *cis* binding to enable the detection of alterations in the expression of self-MHCI molecule (215, 218). Thus, it is possible that, in the absence of H-2K<sup>b</sup>, Ly49C could bind H-2K tetramers through their unoccupied binding sites that would otherwise be occupied by H-2K<sup>b</sup> *cis* interactions.

Given that the H-2K<sup>b</sup> tetramers contained the  $\alpha_3$  domain from H-2D<sup>b</sup> and the human  $\beta_2m$  molecule, Ly49C might not be able to bind the chimeric H-2K<sup>b</sup> tetramers. To determine whether Ly49C could bind to H-2K<sup>b</sup> tetramers regardless of  $\alpha_3$  domain or  $\beta_2m$ , and regardless of the loaded peptide, I used a Ly49C-expressing Chinese

Hamster Ovary (Ly49C-CHO) cell line (gift from Dan Andrews) and evaluated the ability of H-2K<sup>b</sup>NS2<sub>114</sub> and H-2K<sup>b</sup>PB1<sub>703</sub> tetramers to bind simultaneously to Ly49C. Indeed, both H-2K<sup>b</sup>NS2<sub>114</sub> and H-2K<sup>b</sup>PB1<sub>703</sub> tetramers were able to simultaneously bind Ly49C transfected, compared to untransfected, CHO cells (**Figure 19A, B**). To demonstrate that H-2K<sup>b</sup> binding was mediated directly by interaction with Ly49C, I added an anti-Ly49C/I mAb (clone 5E6) prior to H-2K<sup>b</sup> tetramer staining. The anti-Ly49C/I mAb is known to inhibit the interaction between Ly49C/I and MHC I (217, 222) and indeed tetramer binding was substantially diminished (although not abrogated) by addition the mAb (**Figure 19C-E**). It is possible that the inability to completely block H-2K<sup>b</sup> tetramer binding was due to the over-expression of Ly49C on CHO cell lines, and further experiments are warranted to attempt to inhibit the interaction with saturating levels of anti-Ly49C/I mAb. This demonstrates that H-2K<sup>b</sup> tetramers, even when refolded with human  $\beta_2m$  and expressing the H-2D<sup>b</sup>  $\alpha_3$  domain, are still capable of binding Ly49C. Accordingly, Ly49C was the prime candidate ligand responsible for mediating the H-2K reactivity observed in T cell populations from mice lacking H-2K<sup>b</sup>.

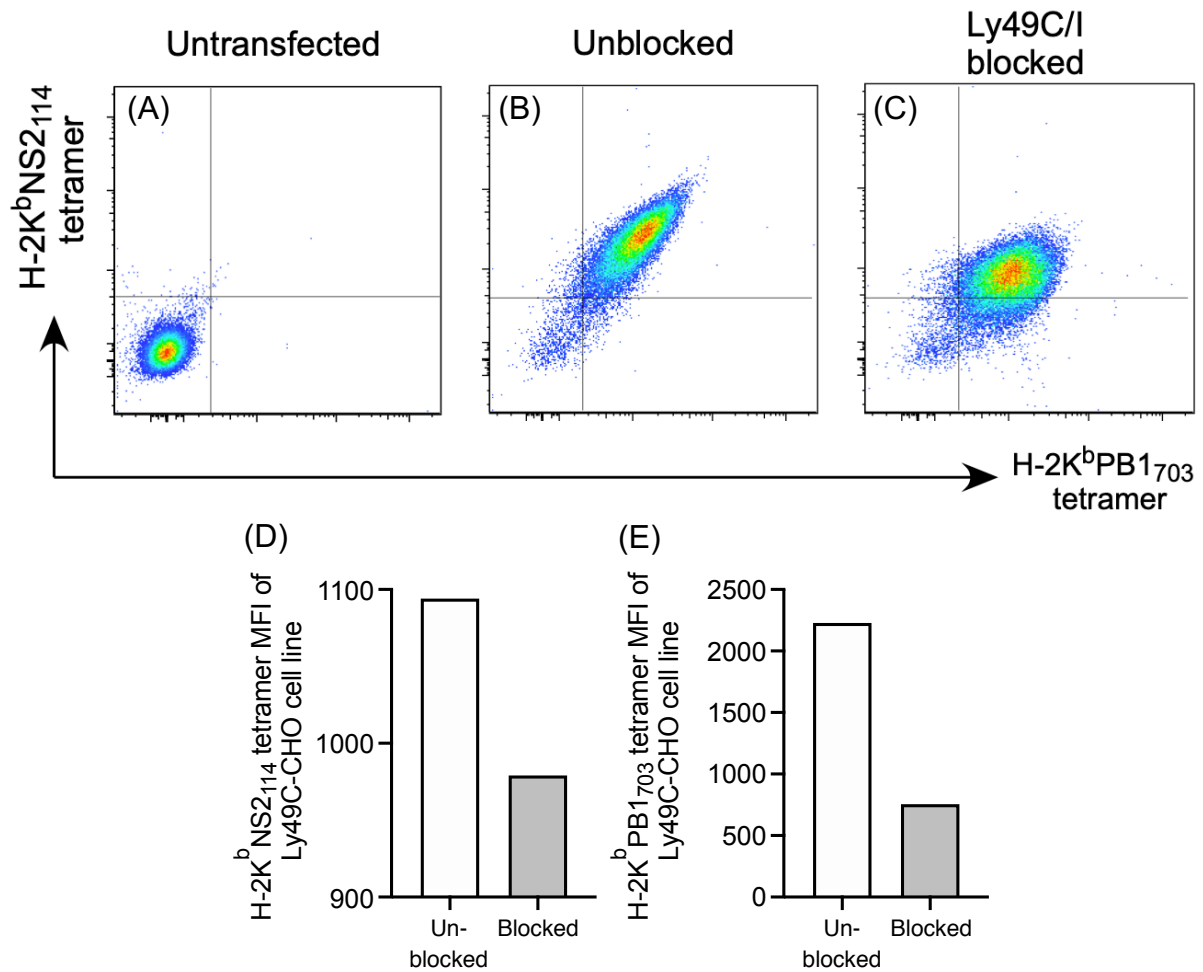


**Figure 19:** Binding of H-2K<sup>b</sup>NS2<sub>114</sub> and H-2K<sup>b</sup>PB1<sub>703</sub> tetramers to Ly49C-expressing CHO cell line. Representative dot plots showing Ly49C-CHO cell lines (A) unstained or (B, C) stained simultaneously with H-2K<sup>b</sup>NS2<sub>114</sub> and H-2K<sup>b</sup>PB1<sub>703</sub> tetramers. (C) Ly49C-CHO cell lines were stained with the anti-Ly49C/I (Clone: 5E6) blocking antibody prior to dual-H-2K<sup>b</sup> tetramer staining. The (D) H-2K<sup>b</sup>NS2<sub>114</sub> and (E) H-2K<sup>b</sup>PB1<sub>703</sub> tetramer staining MFI on Ly49C-CHO cell lines unblocked (white) or blocked (grey) with anti-Ly49C/I mAb. Cells are gated on events that are live Ly49C-CHO cells. These results are representative of a single experiment.

### 3.2.11. Ly49C/I/F/H blocking antibody failed to abrogate binding of H-2K<sup>b</sup>-reactive cells

Given that I had validated that Ly49C is able to bind to H-2K<sup>b</sup> tetramers in an *in vitro* system, I then tested whether a H-2K<sup>b</sup>-Ly49C interaction was mediating H-2K<sup>b</sup>-reactivity on *ex vivo* cells from H-2K<sup>b</sup><sup>-/-</sup> mice. In order to block this interaction, and any interaction between a broader spectrum of Ly49 family members and H-2K<sup>b</sup>, I used an anti-Ly49C/I/F/H mAb (Clone: 14B11). This antibody binds to a conserved site across four Ly49 family members: Ly49C, Ly49I, Ly49F and Ly49H, and has been previously shown to inhibit the interaction of multiple Ly49 molecules, including Ly49C, with the H-2K<sup>b</sup> molecule (206).

Dual H-2K<sup>b</sup>NS2<sub>114</sub> and H-2K<sup>b</sup>PB1<sub>703</sub> tetramer staining of cells from H-2K<sup>b</sup><sup>-/-</sup> mice showed the characteristic H-2K<sup>b</sup> binding as previously described (**Figure 20A**). The addition of the blocking anti-Ly49C/I/F/H mAb prior to dual tetramer enrichment failed to abrogate or even diminish the binding of H-2K-reactive cells to H-2K<sup>b</sup> tetramers (**Figure 20B, C**). Of note, H-2K-binding CD8 T cells were highly enriched for Ly49C/I/F/H<sup>+</sup> cells (**Figure 20D**), indicating that binding of H-2K<sup>b</sup> tetramers was at least coincident with expression of Ly49C/I/F/H molecules. The failure of the anti-Ly49C/I/F/H mAb to inhibit H-2K-reactivity raises two possible explanations: 1) that the binding of H-2K-reactive cells to H-2K<sup>b</sup> tetramer is not mediated by Ly49C, Ly49I, Ly49F or Ly49H or 2) that the anti-Ly49C/I/F/H mAb binds to Ly49C at a site that is distal to its interaction with H-2K. Further experiments are required to verify the blocking action of this particular antibody against the Ly49 molecules.

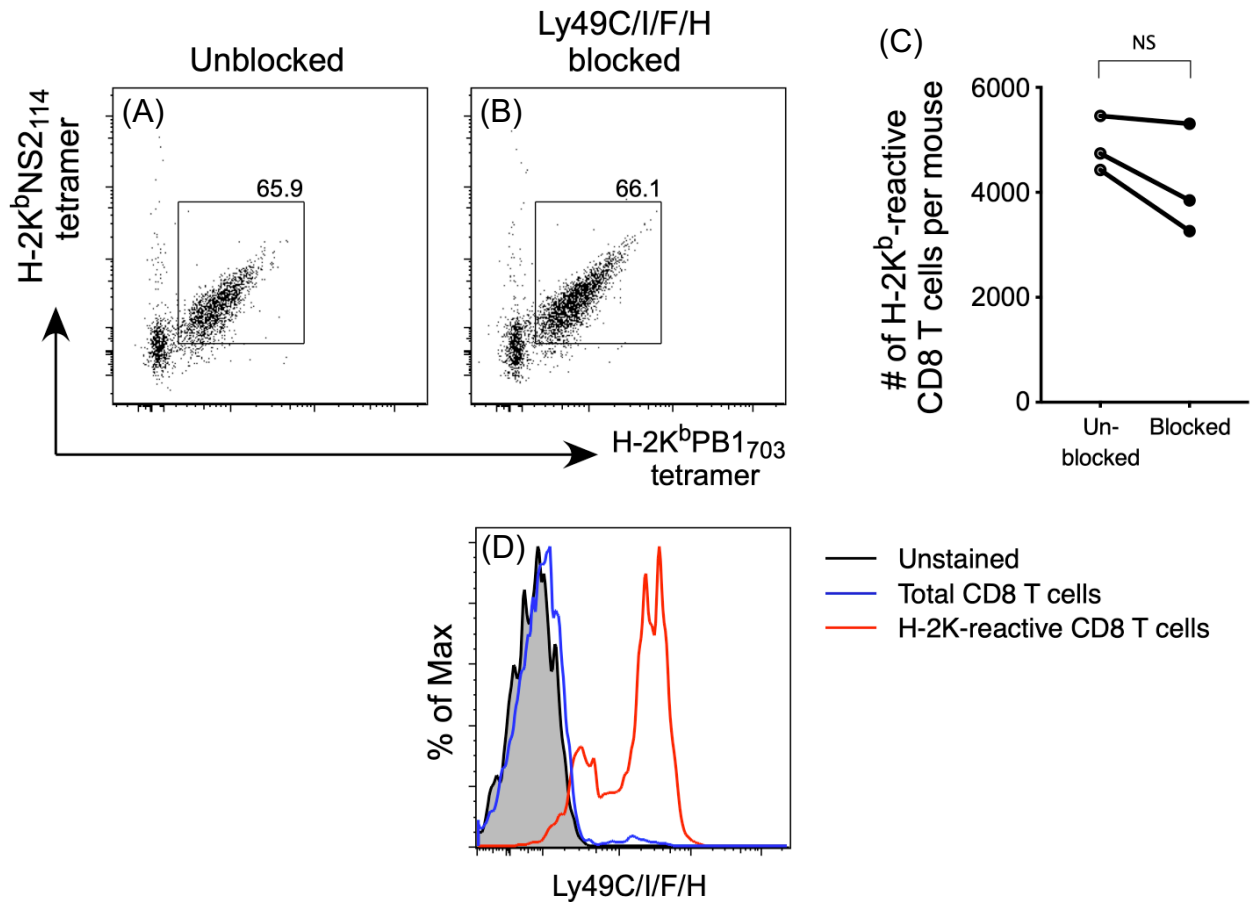


**Figure 20:** H-2K-reactive cells bound H-2K<sup>b</sup> tetramers despite the presence of a blocking anti-Ly49C/II/F/H mAb (clone: 14B11). Representative dot plots showing binding of H-2K<sup>b</sup>NS2<sub>114</sub> and H-2K<sup>b</sup>PB1<sub>703</sub> tetramers to live, B220<sup>-</sup>, F4/80<sup>-</sup>, CD3<sup>+</sup>, TCRβ<sup>+</sup>, CD8<sup>+</sup> T lymphocytes from H-2K<sup>b</sup><sup>-/-</sup> mice in the (A) presence of (B) absence of anti-Ly49C/II/F/H mAb. (C) The number of H-2K-reactive CD8 T cells in the absence or presence of the anti-Ly49C/II/F/H mAb blockade. (D) Representative histogram plot of Ly49C/II/F/H staining on H-2K-reactive and total CD8 T cells in H-2K<sup>b</sup><sup>-/-</sup> mice. NS indicates p > 0.05 (Mann Whitney test). These results are representative of 2 independent experiments with n = 3 per group.

### 3.3. Discussion

The interplay between MHC restriction and alloreactivity is a pivotal immune axis that controls rejection of MHC mismatched tissues, with clinical consequences such as transplant rejection, GvHD and GvL (186, 187). The capacity of a mismatched MHC molecule to impact on the selection of T cells specific for another MHC haplotype is of paramount importance to patients receiving a bone marrow transplant, making HLA matching between a donor and recipient during transplantation of high clinical importance. The HLA match between donor and recipient should be as close as possible at both MHCI and MHCII loci to minimize graft rejection and GvHD mediated by alloreactive T cells. On the other hand, a positive outcome of MHC mismatch during transplantation is GvL, where donor T cells facilitate the elimination of leukemic cells (187, 223). Both GvHD and GvL are clinically important outcomes mediated by alloreactive T cells. Therefore, a deeper understanding of the mechanisms and drivers of alloreactivity will contribute to our understanding of GvHD and GvL during HSCT.

Work performed during my BSc. (Hons) year addressed the question of whether an allomorphic MHCI molecule can mediate the selection of an alloreactive MHCI-restricted CD8 T cell population, and the functionality of that population. I identified the presence of a smaller, but reproducible population of naïve H-2D<sup>b</sup>PA<sub>224</sub>-specific CD8 T cells selected on the H-2D<sup>b</sup> molecule. However, alloreactive H-2D<sup>b</sup>PA<sub>224</sub>-specific CD8 T cells exhibited lower tetramer binding MFI than cells from WT mice despite similar TCR expression, suggesting that these cells had an intrinsically lower affinity for the H-2D<sup>b</sup>PA<sub>224</sub> tetramer. Alloreactive H-2D<sup>b</sup>PA<sub>224</sub>-specific CD8 T cells were non-

responsive when stimulated by the PA<sub>224</sub> peptide *in vitro*, indicating that they were poorly- or non-functional despite their capacity to bind to H-2D<sup>b</sup>PA<sub>224</sub>.

The first part of this chapter represented an extension of this project by further validating the capacity of alloreactive H-2D<sup>b</sup>PA<sub>224</sub>-specific TCRs to bind to H-2D<sup>b</sup>PA<sub>224</sub> *in vitro* and testing their response to cognate antigen *in vivo*. An alloreactive TCR H-2D<sup>b</sup>PA<sub>224</sub>-specific TCR expressed *in vitro* was able to bind H-2D<sup>b</sup>PA<sub>224</sub> tetramer but it exhibited a reduced H-2D<sup>b</sup>PA<sub>224</sub> tetramer MFI, suggestive of a lower tetramer binding capacity. Moreover, *in vivo* analysis of T cells responsiveness following peptide-pulsed DC vaccination demonstrated that alloreactive CD8 T cell failed to upregulate CD44 or expand, despite their ability to bind H-2D<sup>b</sup>PA<sub>224</sub>. Collectively, these data suggest that although selection on the H-2K<sup>b</sup> molecule can generate alloreactive H-2D<sup>b</sup>PA<sub>224</sub>-specific CD8 T cells, the binding affinity and subsequent functionality of these alloreactive CD8 T cells is limited.

Clonotypic analysis of alloreactive H-2D<sup>b</sup>PA<sub>224</sub>-specific TCRs revealed unaltered TRAV usage but diminished TRBV29 usage compared to H-2D<sup>b</sup>PA<sub>224</sub>-specific TCRs selected on the matched H-2D<sup>b</sup> molecule. This aligns with the crystal structure of the canonical “6218” H-2D<sup>b</sup>PA<sub>224</sub> TCR in complex with the H-2D<sup>b</sup>PA<sub>224</sub> molecule showing that the TCR $\alpha$  chain and CDR3 $\alpha$  loop dominates the contact with the PA<sub>224</sub> peptide, whilst the TCR $\beta$  chain interacts extensively with the H-2D<sup>b</sup> molecule (80). Thus, it follows that, with selection on a distinct MHCI molecule, the TCR $\beta$  repertoire is most likely to be affected. Precisely how the recognition has been altered by selection on a distinct MHCI molecule can only really be definitively resolved by structural resolution of the ternary structure of the alloreactive H-2D<sup>b</sup>PA<sub>224</sub>-specific TCR in complex with

the H-2D<sup>b</sup>PA<sub>224</sub> molecule. To that end, I am currently collaborating with structural biologist Jamie Rossjohn (Monash University) to solve the ternary structure of the alloreactive H-2D<sup>b</sup>PA<sub>224</sub>-specific TCR in complex with the H-2D<sup>b</sup>PA<sub>224</sub> molecule. A recent study by Gras et al (2016) revealed that the docking topology of a TCR-pMHC I is crucial for its function to permit optimal T cell signalling and activation (84). It is possible that the lack of alloreactive H-2D<sup>b</sup>PA<sub>224</sub> CD8 T cell activation shown in this study is the result of a non-conventional docking orientation of the alloreactive TCR to the pMHC I molecule. The alloreactive TCR docking topology may permit binding to pMHC I but be sub-optimal for subsequent T cell signalling and activation. In addition, to investigate the presence and function of analogous populations of alloreactive T cells in humans, I am collaborating with Paul Thomas from St. Jude Children's Research Hospital in Memphis, Tennessee, USA. The Thomas Lab has access to peripheral blood mononuclear cells (PBMCs) from patients who have undergone an MHC mismatched bone marrow transplant. CD8 T cells in these patients undergo selection on an HLA (recipient: HLA-X) that is distinct to the one expressed by their BM-derived cells (donor: HLA-Y). Thus, these patients have the potential for *in vivo* alloreactive CD8 T cell responses (HLA-Y-specific responses by HLA-X-restricted T cells). Cells from these patients will be analysed for frequency and functionality of viral epitope-specific cells restricted to the HLA from the transplant donor.

In the second part of this chapter, I observed H-2K<sup>b</sup> tetramer binding by cells from mice lacking H-2K<sup>b</sup>, that occurred independently of the TCR, the bound peptide, or the CD8 coreceptor. The cells were cross-reactive across multiple H-2K alleles regardless of the loaded peptide. One hypothesis was that this phenomenon was due to defective negative selection of pan-H-2K-reactive T cells in mice lacking the self-ligand H-2K<sup>b</sup>.

This was refuted when TCRs from H-2K-reactive cells were expressed *in vitro* and they were unable to bind to H-2K tetramer. I also showed that H-2K reactivity was enriched in activated/memory CD8 T cells, CD4 NKT cells, and NK cells. Based on the literature available, I deduced that the most likely candidate was a member of the Ly49 family. In particular, the Ly49C molecule is known to interact strongly with the H-2K<sup>b</sup> molecule (224). While I have shown that Ly49C was highly expressed on H-2K reactive cells, I was unable to verify that this molecule was responsible for the H-2K<sup>b</sup> reactivity observed in H-2K<sup>b/-</sup> and DKO mice.

The Ly49 family of receptors are innate MHC I receptors family highly expressed on NK and NKT cells (225). Coles et al (2000) have also detected the expression of multiple Ly49 family members (including Ly49C) on a polyclonal subset of memory phenotype CD8 T cells, but the expression is completely absent in conventional CD4 T cell populations (213). The Ly49 molecules are inhibitory receptors that regulate the activation of NK cells through detection of their ligand, MHC I, in a phenomenon known as the “missing-self” (reviewed in (226)). In this phenomenon, NK cells ubiquitously survey the periphery for normal levels of MHC I expression, which in turn inhibits NK cell activation when the Ly49 inhibitory molecules are engaged with MHC I. Down-regulation of MHC I molecules is a common escape mechanism employed by viruses to avoid detection from the immune system (227). Consequently, downregulation of MHC I is a key indicator of viral infection, which leads to loss of the inhibitory Ly49 interaction with MHC I molecules and hence NK cell activation. Activated NK cells then assist in mediating viral clearance *via* the secretion of anti-viral molecules: perforins, granzymes and cytokines such as IFN $\gamma$  and TNF (228). The binding of Ly49 to MHC I molecules occurs in a peptide-dependent, but not peptide-specific manner, where the

peptide is necessary to merely stabilize the MHCI molecules expressed on the surface of cells (206). In particular, Ly49C has been shown to interact strongly with H-2K<sup>b</sup> but it binds H-2D<sup>b</sup> poorly (206, 217), which fits with my observation of pan-H-2K binding in H-2K<sup>b</sup><sup>-/-</sup> mice but not pan-H-2D binding in the absence of H-2D<sup>b</sup>. Multiple crystal structures of Ly49 molecules binding to MHCI molecules have been solved to date. There is evidence from site-directed mutagenesis studies that Ly49C makes prominent contacts with residues on the  $\alpha_2$  and  $\alpha_3$  domains on both H-2K<sup>b</sup> and H-2D<sup>b</sup> and with  $\beta_2m$  (215, 218), again providing an explanation for my observation of H-2K tetramer binding even with the  $\alpha_3$  domain of H-2D<sup>b</sup> and refolded with human  $\beta_2m$ .

The Ly49 family of molecules can bind MHCI in two orientations: in *cis* (on the same cell) and in *trans* (on other cells) (216). Ly49C molecules are predominantly sequestered by H-2K<sup>b</sup> in *cis* to limit the number of free Ly49C molecules available for *trans* binding (229) to regulate NK cell activity by lowering the threshold for activation, making NK cells more sensitive to minute changes in MHCI expression in the periphery. Hence, the loss of H-2K<sup>b</sup> likely frees up Ly49C molecules, that now allows H-2K<sup>b</sup> tetramer binding in *trans*. My data is consistent with the hypothesis that the loss of endogenous H-2K<sup>b</sup> (in H-2K<sup>b</sup><sup>-/-</sup> and DKO mice) results in populations of Ly49C-expressing cells that can bind to H-2K tetramers regardless of the loaded peptide. While *cis* binding of MHCI by Ly49 molecules has been widely demonstrated on NK cells and NKT cells, there has been no demonstration of this in conventional CD8 $\alpha\beta$  T cells. By extension, this would suggest that the expression of Ly49C on conventional T cells may act in a similar fashion to suppress innate-like activation. In essence, the loss of H-2K<sup>b</sup> could potentially result in a lower activation threshold of memory CD8 T cells and NKT cells. While it remains to be formally demonstrated that the ligand for

H-2K tetramer binding is the Ly49C molecule, I will pursue this by blocking experiments such as those outlined here, using a range of different antibody clones with differential specificity for various Ly49 molecules.

The anti-Ly49C/I/F/H mAb (clone: 14B11) has been shown to inhibit the binding of Ly49C to the H-2K<sup>b</sup> molecule (206). However, the inclusion of the anti-Ly49C/I/F/H mAb prior to H-2K<sup>b</sup> tetramer-based magnetic enrichment failed to abrogate the binding of H-2K<sup>b</sup> tetramers to H-2K-reactive CD8 T cells. The alternative anti-Ly49C/I mAb (clone: 5E6) has also been shown to block the interaction of Ly49C to the H-2K<sup>b</sup> molecule (222). While I have successfully used the anti-Ly49C/I mAb to reduce H-2K-reactivity with a Ly49C-CHO cell line *in vitro*, it remains to be seen whether the anti-Ly49C/I mAb can also reduce H-2K-reactivity with H-2K-reactive cells from H-2K<sup>b</sup><sup>-/-</sup> mice. As it stands, the anti-Ly49C/I mAb appears to be a better candidate to inhibit any potential Ly49C-H-2K<sup>b</sup> interaction in H-2K<sup>b</sup><sup>-/-</sup> mice than the anti-Ly49C/I/F/H mAb.

The generation of MHC I monomers have traditionally substituted the mouse  $\beta_2m$  with the human  $\beta_2m$  fragment. Although the  $\beta_2m$  protein is highly conserved across different vertebrates with a 70% homology between humans and mice (48, 52, 230), the substitution of the mouse  $\beta_2m$  with the human  $\beta_2m$  fragment has been shown to abrogate non-specific binding by the Ly49 molecules in mice and reduce background staining with tetramer (210). It was intriguing that the H-2K<sup>b</sup> tetramers, refolded with the human  $\beta_2m$  fragment, still bound Ly49C molecules in the *in vitro* assay with the Ly49C-CHO cell line. This highlights the potential that H-2K<sup>b</sup> tetramers could in fact be binding Ly49C, even in WT mice, rather than an antigen-specific population of CD8 T cells.

In conclusion, in the absence of H-2K<sup>b</sup>, I have observed the binding of H-2K tetramers by a non-TCR ligand expressed on NK, NKT and memory phenotype CD8 T cells. I have identified the most likely ligand: the Ly49C molecule, that is predominantly sequestered by endogenous H-2K<sup>b</sup> in *cis*. I hypothesize that, in the absence of H-2K<sup>b</sup>, Ly49C is likely to be freely available to bind H-2K tetramers in *trans*, resulting in an inflated population of cells (particularly memory CD8 T cells) binding to H-2K tetramers in a non-TCR mediated interaction. If this hypothesis is accurate, this would be the first evidence of *cis* binding with an inhibitory NK cell receptor on CD8 T cells and, intriguingly, it may imply a similar role for the ligand in functionally suppressing conventional CD8 T cell activity.

#### ***4. The Impact of MHC Class I Dose on Development and Maintenance of the Polyclonal Naïve CD8 T cell Repertoire***

Xavier Y.X. Sng<sup>1</sup>, Jasmine Li<sup>2</sup>, Pirooz Zareie<sup>1</sup>, Lisa Assmus<sup>1,3,4</sup>, Jason Lee<sup>2</sup>, Claerwen M. Jones<sup>1</sup>, Stephen J. Turner<sup>2</sup>, Stephen R. Daley<sup>1</sup>, Kylie M. Quinn<sup>1,5\*</sup>, Nicole L. La Gruta<sup>1\*</sup>

<sup>1</sup> Department of Biochemistry and Molecular Biology, Monash Biomedicine Discovery Institute, Monash University, Clayton VIC 3800, Australia.

<sup>2</sup> Department of Microbiology, Monash Biomedicine Discovery Institute, Monash University, Clayton VIC 3800, Australia.

<sup>3</sup> Department of Microbiology and Immunology, University of Melbourne, The Peter Doherty Institute for Infection and Immunity, Melbourne, Victoria 3000, Australia.

<sup>4</sup> Institute of Experimental Immunology, University Hospital Bonn 53105, Bonn, Germany.

<sup>5</sup> Translational Immunology and Nanotechnology Program, School of Health and Biomedical Sciences, RMIT University, 3083, Australia

\* Correspondence: Nicole.la.gruta@monash.edu, Kylie.quinn@rmit.edu.au

## 4.1. Summary

Naïve CD8<sup>+</sup> T cell survival in the periphery is critically dependent on tonic T cell receptor (TCR) signaling through peptide + MHC class I (MHCI) recognition however little is known about how natural variation in MHCI levels impacts on the naïve CD8<sup>+</sup> T cell repertoire. Using mice that are hemizygous or homozygous for a single MHCI allele, we showed that, despite a reduction in peripheral CD8<sup>+</sup> T cell numbers of ~50% in MHCI hemizygous mice, MHCI levels had no notable impact on the rate of thymic generation or emigration of CD8 single positive (SP) T cells. Moreover, the peripheral T cell repertoire in hemizygous mice showed selective retention of T cell clonotypes with a greater competitive advantage, as evidenced by increased expression of CD5 and IL-7R $\alpha$ . The qualitative superiority of CD8<sup>+</sup> T cells retained in hemizygous mice was also seen during influenza A virus (IAV) infection, where epitope-specific CD8<sup>+</sup> T cells from hemizygous mice had higher avidity for pMHCI and increased cytokine polyfunctionality, despite a reduced response magnitude. Collectively, this study suggests that natural variation in MHCI expression levels has a notable and biologically relevant impact on the maintenance, but not generation, of the naïve CD8<sup>+</sup> T cell repertoire.

**Keywords:** MHC class I dose, hemizygous and homozygous MHCI expression, naïve CD8<sup>+</sup> T cells, T cell homeostasis, CD8<sup>+</sup> T cell development.

## 4.2. Introduction

The peripheral maintenance of naïve CD8<sup>+</sup> T cells is dependent on both tonic TCR-pMHC signalling (105, 231–233) and homeostatic IL-7 cytokine signaling (234–236). The impact of IL-7 dose on naïve CD8<sup>+</sup> T cell survival is well-defined. IL-7 is not only essential for naïve T cell survival – adoptive transfer of T cells into IL-7<sup>-/-</sup> mice or blockade of IL-7R $\alpha$  results in the loss of transferred T cells (235, 236) – but available IL-7 levels delimit the size of the naïve CD8<sup>+</sup> T cell pool. Constitutive expression of IL-7R $\alpha$  results in a reduced niche size because it limits the availability of IL-7 to the wider naïve T cell pool (237). Additionally, overexpression of IL-7 drives an increased number of naïve T cells (238, 239).

By comparison, relatively little is known about the role of MHC I levels in delimiting the size and quality of the naïve CD8<sup>+</sup> T cell pool. Certainly, the recognition of pMHC by naïve T cells must be specific to the selecting pMHC ligand (240, 241), and competition for pMHC ligands is evident under conditions of adoptive transfer of large numbers of precursor populations or TCR transgenic T cells with differing affinities (238, 241, 242). However, how physiological levels of MHC I expression, driven by homozygous or hemizygous allelic expression, control the generation, survival and homeostatic maintenance of endogenous naïve CD8<sup>+</sup> T cell populations remains unknown.

The relevance of this biological question to the human condition becomes evident when considering MHC polymorphism. A human individual can inherit and co-dominantly express up to 6 different MHC I genes (2 HLA-A, B and C genes from each

parent), with massive polymorphism across these HLA genes. As a consequence of the co-dominant expression of the HLA genes, individuals can be either homozygous or heterozygous at each of the HLA-A, B, and C gene loci. HLA heterozygosity is largely considered to be beneficial for protection from infections (243–246), while homozygosity has been associated with exacerbation of several autoimmune diseases (247–249). Despite this largely anecdotal evidence around the impact of MHC dose on protective and detrimental immune responses, there has been no detailed analysis of how physiological shifts in MHC levels, driven by hemizygous or homozygous gene expression, impact the development, peripheral maintenance and function of T cells.

Here, we have investigated the impact of MHC class I dose on the development and peripheral maintenance of polyclonal naïve CD8<sup>+</sup> T cells. We used a reductionist model in which mice are homozygous or hemizygous for one MHC I gene and lack expression of the other MHCI gene. We show that physiological levels of MHCI, like IL-7, delimit the peripheral CD8<sup>+</sup> T cell niche, largely by limiting peripheral survival rather than thymic export. Moreover, limiting the dose of MHCI resulted in the retention of qualitatively superior CD8<sup>+</sup> T cells. Thus, challenge with IAV elicited an antiviral CD8<sup>+</sup> T cell response that, while diminished in magnitude compared to MHCI homozygous mice, showed increased pMHCI avidity and cytokine functionality upon viral challenge. This study suggests that hemizygous MHCI expression does not result in a proportional loss of T cell efficacy.

### 4.3. Materials and Methods

#### Mice and Influenza A Virus Infection

Female C57BL/6 mice (6-8 weeks old) were bred and housed in specific-pathogen free conditions in the Monash Animal Research Platform (MARF) and the Animal Research Facility (ARL) at Monash University. H-2D<sup>b-/-</sup>, H-2K<sup>b-/-</sup>, and H-2K<sup>b-/-</sup>D<sup>b-/-</sup> mice (250) were obtained with permission from Institut Pasteur. H-2K<sup>b-/-</sup>D<sup>b+/-</sup> and H-2D<sup>b-/-</sup>K<sup>b+/-</sup> hemizygous mice were generated by crossing homozygous H-2D<sup>b-/-</sup> or H-2K<sup>b-/-</sup> mice with H-2D<sup>b-/-</sup>K<sup>b-/-</sup> double knockout mice. For influenza A virus infection, mice were anesthetized by isoflurane inhalation and infected intranasally with 1 x 10<sup>4</sup> plaque-forming-units of HKx31 or HKx31 NP-N5Q mutant (H3N2) in 30µL of PBS (251). All experimental procedures were approved and conducted under guidelines set by the Monash University Animal Ethics Committee.

#### Flow Cytometry

Spleen and thymus from naïve uninfected mice were harvested and processed into single cell suspensions for analysis. Tissues were labelled with fluorophore-conjugated antibodies from eBioscience, Biologend or BD Pharmingen. Antibodies to the following list of molecules were used: CD4 (GK1.5), CD8 $\alpha$  (53-6.7), CD8 $\beta$  (53-5.8), TCR $\beta$  (H57-597), CD103 (2E7), CD11b (M1/70), CD11c (N418), F4/80 (BM8), NK1.1 (PK136), B220 (RA3-6B2), CD44 (IM7), H-2K<sup>b</sup> (AF6-88.5), H-2D<sup>b</sup> (KH95), CD49d (R1-2), CD127 (A7R34), CD5 (REA421), IFN $\gamma$ , TNF (MP6-XT22), IL-2, V $\beta$ 2 (B20.6), V $\beta$ 4 (KT4), V $\beta$ 10 (B21.5), V $\beta$ 5.1 and V $\beta$ 5.2 (MP9-4), V $\beta$ 8.3 (1B3.3), V $\beta$ 8.1

and V $\beta$ 8.2 (MR5-2), V $\beta$ 13 (MR12-3), V $\beta$ 11 (RR3-15), V $\beta$ 9 (MR10-2), V $\beta$ 6 (RR4-7), V $\beta$ 17 (KJ23), V $\beta$ 3.1 (KJ25), V $\beta$ 7 (TR310) and V $\beta$ 14 (14-2). Biotinylated H-2D<sup>b</sup>PA<sub>224</sub> monomers were tetramerized with PE-conjugated streptavidin for identification of H-2D<sup>b</sup>PA<sub>224</sub>-specific CD8<sup>+</sup> T cells. The median fluorescence intensities (MFI) of CD5, TCR $\beta$  and CD127 (IL-7R $\alpha$ ) on cells from D<sup>b</sup>+/- mice were normalized to the corresponding MFIs from D<sup>b</sup>+/+ mice.

### **Magnetic enrichment and isolation of epitope-specific CD8<sup>+</sup> T cells**

Tetramer-based magnetic enrichment was performed to isolate and identify naïve H-2D<sup>b</sup>PA<sub>224</sub>-specific CD8<sup>+</sup> T cell precursors (137, 138, 252). Spleen and major lymph nodes (auxiliary, brachial, cervical, inguinal and mesenteric) were pooled from naïve mice and stained with phycoerythrin (PE)-labelled influenza-specific H-2D<sup>b</sup>PA<sub>224</sub> tetramers. Cells were washed to remove excess tetramer and incubated with anti-PE-conjugated magnetic microbeads (Miltenyi Biotec) and tetramer-bound cells were enriched over an LS column (Miltenyi Biotec) on a magnetic platform. Enriched cells were stained with a cocktail of conjugated antibodies to identify H-2D<sup>b</sup>PA<sub>224</sub>-specific CD8<sup>+</sup> T cells (tetramer<sup>+</sup> CD8 $\alpha$ <sup>+</sup> TCR $\beta$ <sup>+</sup>, CD11b<sup>-</sup>, CD11c<sup>-</sup>, B220<sup>-</sup>, F4/80<sup>-</sup> CD4<sup>-</sup>). Entire samples were acquired on a BD LSRFortessa X-20 for analysis or BD Influx for single-cell sorting for multiplex RT-PCR.

### Single-cell multiplex RT-PCR

Individual naïve D<sup>b</sup>PA<sub>224</sub>-specific CD8<sup>+</sup> T cells were sorted into 96-well plates following magnetic enrichment. Multiplex single-cell reverse transcription and PCR amplification of TCR $\alpha$  and TCR $\beta$  chains were performed using a panel of TCR  $\alpha$  chain variable region (TRAV)- and TCR  $\beta$  chain variable region (TRBV)-specific oligonucleotides as previously described (179). Briefly, mRNA was reverse transcribed into cDNA using the SuperScript III VILO cDNA Kit (ThermoFisher) and incubated at 25°C for 10 mins, 42°C for 120 mins then 85°C for 5 mins. Samples were then used in a 25 $\mu$ L nested PCR reaction including 1.5 U Taq DNA polymerase, 1x PCR buffer, 1.5 mM MgCl<sub>2</sub>, 0.25 mM dNTPs and panel of 24 TRAV-specific external sense primers and a TCR $\alpha$  chain constant region (TRAC)-specific external antisense primer, together with 19 TRBV external sense primers and a TCR  $\beta$  chain constant region (TRBC)-specific external antisense primer (each at 0.1 pmol/ $\mu$ L) at standard PCR conditions. For the second-round of nested PCR reaction, 2.5  $\mu$ L of the first-round PCR product was used in separate TRAV- and TRBV-specific PCRs using the same reaction mix describe above. However, a set of 24 TRAV-specific internal sense primers and an TRAC-specific internal antisense primer, or a set of 19 TRBV-specific internal sense primers and a TRBC-specific internal antisense primer were used. Products from the second-round PCR were subjected to gel electrophoresis and products were purified with ExoSAP-IT reagent. Purified products were used in Sanger sequencing reactions with internal TRAC- or TRBC-specific antisense primers. Sequenced TCR gene segments were assigned using the IMGT (International ImMunoGeneTics) database (253).

### **Intracellular Cytokine Staining**

For analyses of cytokine production, cells were stimulated *in vitro* for 5 hrs in the presence of GolgiPlug and were surface stained for CD4 and CD8. To assess cytokine production, cells were stained intracellularly for cytokines IFN $\gamma$ , TNF and IL-2 using the Cytofix/Cytoperm kit (BD Pharmingen). Data were analysed using FlowJo version 9.6 (FlowJo LLC, Ashland, OR), Pestle version 1.8 and SPICE version 5.3 (Mario Roederer, National Institutes of Health, Bethesda, MD).

### **Intravenous labelling of CD8<sup>+</sup> T cells in the thymic perivascular space**

This procedure was described previously (254, 255). Briefly, PE-conjugated anti-CD8 $\alpha$  (Biolegend, Clone 63.6-7) was injected intravenously (1  $\mu$ g per mouse), and mice were humanely euthanized 3-4 mins later. Mice were perfused with PBS to remove excess unbound antibody prior to thymus collection. Thymi from 4 mice were pooled, labelled cells were isolated from single-cell suspension with anti-PE microbeads (Miltenyi) before labelling for flow cytometry analysis. Anti-CD8 $\alpha$ :PE-labelled cells were further confirmed to be bona fide emigrating CD8<sup>+</sup> T cells by staining with anti-CD8 $\beta$ :PE-Cy7 (Biolegend, Clone YTS156.7.7) and anti-CD103:APC (Biolegend, Clone: 2E7), which is known to be increased on recent thymic emigrants in the blood.

### **Tetramer Dissociation**

Lymphocytes from H-2D<sup>b+/+</sup>K<sup>b-/-</sup> (H-2D<sup>b+/+</sup>) and H-2D<sup>b+/-</sup>K<sup>b-/-</sup> (H-2D<sup>b+/-</sup>) mice at day 10 post-IAV infection were stained with 5µg/mL of H-2D<sup>b</sup>PA<sub>224</sub>-PE tetramers for 1hr at room temperature. Cells were washed and incubated for various timepoints at 37°C with anti-H-2D<sup>b</sup>/K<sup>b</sup> antibody (28-8-6; Pharmingen) (25 µg/mL) to prevent tetramer rebinding. Cells were then washed and stained with anti-CD8 $\alpha$ , anti-TCR $\beta$  and anti-CD44 antibodies for flow cytometric analysis.

### **Statistical analyses**

GraphPad Prism (version 8.2.1) was used for all data analyses and arrangements. Pestle (version 1) and SPICE (version 5.35) were used for TRBV data analyses. The Mann Whitney *U* test or Student's 2-tailed unpaired *t* test (with Bonferroni's correction for multiple comparisons) was used for to determine significance for all individual statistical comparisons.

## 4.4. Results

### 4.4.1. Gene Dosage of MHC I Controls the Expression Level of Protein

To alter the abundance of MHC I expression *in vivo*, we generated MHC I hemizygous mice on the C57BL/6 (WT) background by crossing either H-2D<sup>b+/+</sup>K<sup>b-/-</sup> (D<sup>b+/+</sup>) or H-2D<sup>b-/-</sup>K<sup>b+/+</sup> (K<sup>b+/+</sup>) mice with H-2D<sup>b-/-</sup>K<sup>b-/-</sup> (double knockout (DKO)) mice (250). These crosses generated F<sub>1</sub> mice that were hemizygous for one MHC I gene and knocked-out for the other: H-2D<sup>b+/-</sup>K<sup>b-/-</sup> (D<sup>b+/-</sup>) and H-2D<sup>b-/-</sup>K<sup>b+/-</sup> (K<sup>b+/-</sup>), respectively. To verify that changes in MHC I dosage led to changes in MHC I protein expression, we quantified the level of MHC I expression on splenocytes from H-2D<sup>b</sup> and H-2K<sup>b</sup> homozygous (D<sup>b+/+</sup> and K<sup>b+/+</sup>) and hemizygous (D<sup>b+/-</sup> and K<sup>b+/-</sup>) mice. Both H-2D<sup>b</sup> and H-2K<sup>b</sup> homozygous mice showed similar levels of H-2D<sup>b</sup> and H-2K<sup>b</sup> protein expression to WT mice, demonstrating that the loss of one MHC I gene had no impact on expression of the other (**Figure 21A, B**) (250). However, cells from hemizygous H-2D<sup>b</sup> and H-2K<sup>b</sup> mice showed a 44% and 43% reduction in expression of H-2D<sup>b</sup> and H-2K<sup>b</sup>, respectively, relative to cells from WT mice and their homozygous counterparts (**Figure 21C, D**). These data confirm that the expression of distinct MHC I genes is independently regulated, and that MHC I gene dosage dictates the level of protein expressed on the cell surface.

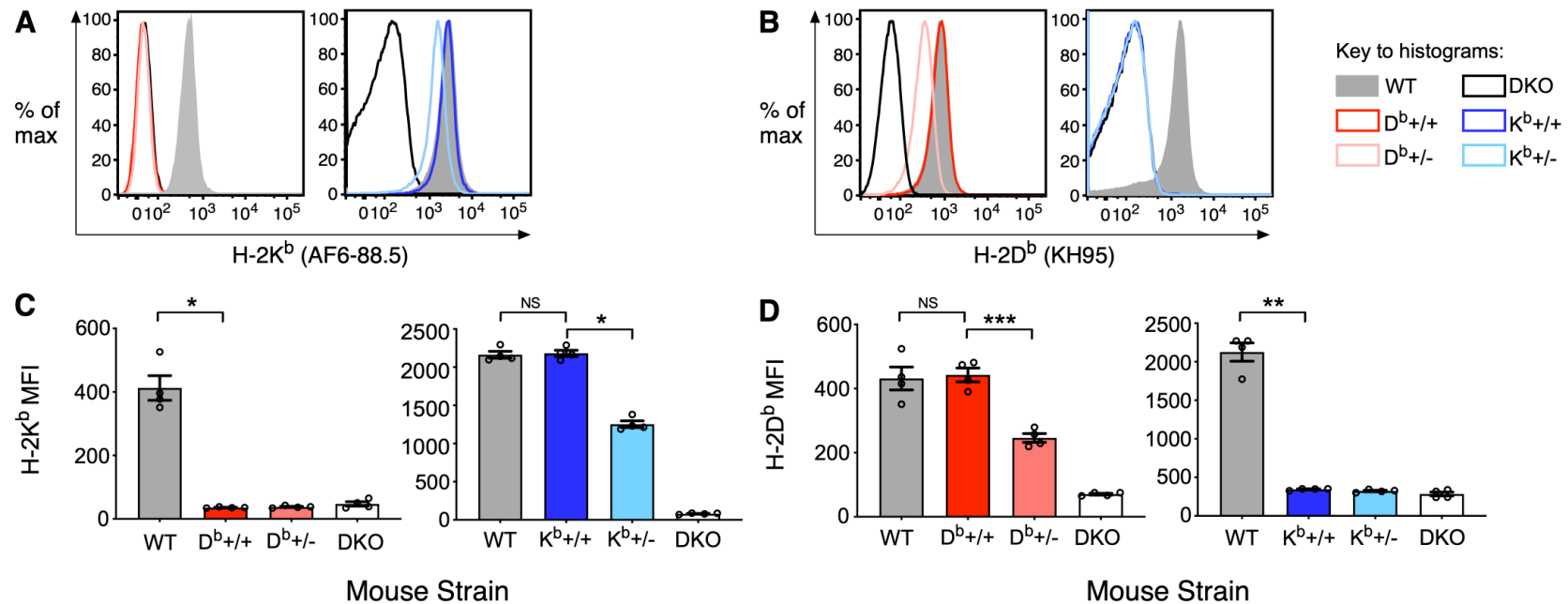


**Figure 21:** Expression of MHC I genes is independently regulated and dependent on gene dose. Surface expression of H-2K<sup>b</sup> (A, C) and H-2D<sup>b</sup> (B, D) was assessed on splenocytes from naïve WT, homozygous H-2D<sup>b</sup> (D<sup>b</sup>+/) and H-2K<sup>b</sup> (K<sup>b</sup>+/) mice, hemizygous H-2D<sup>b</sup> (D<sup>b</sup>+/-) and H-2K<sup>b</sup> (K<sup>b</sup>+/-) mice, and DKO mice. \*\*\*, p≤0.001; \*\*, p≤0.01; \*, p≤0.05; NS= not significant. Bars and error bars represent mean +/- standard error of the mean (SEM). Data are representative of 3 independent experiments with n = 4 mice per group.

#### 4.4.2. MHC I Expression Levels Control Peripheral Naïve CD8<sup>+</sup> T cell Number

To investigate the impact of altered MHC I expression on the size of the peripheral naïve CD8<sup>+</sup> T cell compartment, we enumerated splenic CD8<sup>+</sup> T cells in WT, homozygous, hemizygous and DKO mice. As shown previously (250), both H-2D<sup>b</sup> and H-2K<sup>b</sup> homozygous mice had an approximately 40%-60% reduction in CD8<sup>+</sup> T cell numbers (**Figure 22A**) compared to WT mice, with the loss of each MHC I gene reducing CD8<sup>+</sup> T cell numbers to a similar extent. The H-2D<sup>b</sup> and H-2K<sup>b</sup> hemizygous mice showed a further reduction in CD8<sup>+</sup> T cell numbers by 40% and 35%, respectively, relative to their homozygous counterparts. These data suggest that the level of MHC I expression determines the size of the peripheral CD8<sup>+</sup> T cell population in a dose-dependent manner. The number of peripheral CD4<sup>+</sup> T cells remained unchanged in homozygous and hemizygous mice compared to WT mice (**Supplementary 4.9.1**).

To determine whether reducing the level of MHC I led to the selective loss of particular CD8<sup>+</sup> T cell subsets, we classified the CD8<sup>+</sup> T cell population into three subsets based on the expression of CD44 and CD49d: phenotypically naïve (T<sub>N</sub>; CD44<sup>lo</sup>), virtual memory (T<sub>VM</sub>; CD44<sup>hi</sup>CD49d<sup>lo</sup>), and conventional memory (T<sub>MEM</sub>; CD44<sup>hi</sup>CD49d<sup>hi</sup>) T cells (**Figure 22B**) ((256, 257). While the numbers of T<sub>VM</sub> and T<sub>MEM</sub> cells remained relatively unchanged with altered MHC I expression, there was a significant reduction (37% for H-2D<sup>b</sup> hemizygous mice and 40% for H-2K<sup>b</sup> hemizygous mice) in the numbers of T<sub>N</sub> cells (**Figure 22C**). Thus, reduced MHC I expression selectively impacted on CD8<sup>+</sup> T<sub>N</sub> cells.

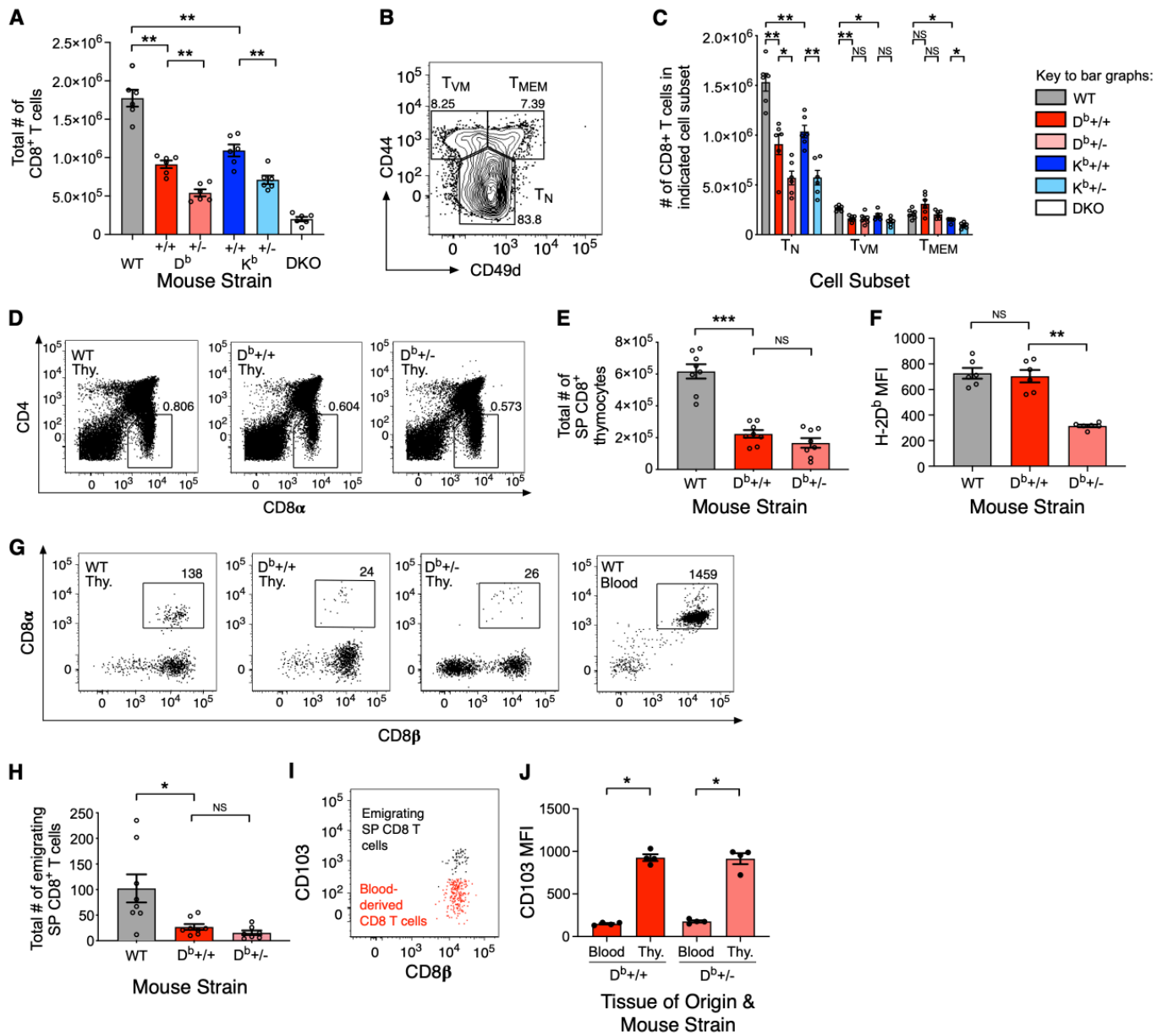


**Figure 22:** MHC I expression level delimits naïve CD8<sup>+</sup> T cell number in the periphery but not CD8<sup>+</sup> T cell development or thymic output. (A) Total splenic CD8<sup>+</sup> T cells from naïve WT, homozygous H-2D<sup>b</sup> and H-2K<sup>b</sup> mice, and hemizygous H-2D<sup>b</sup> and H-2K<sup>b</sup> mice and DKO mice. (B) Representative density plot of CD8<sup>+</sup> T cells that are T<sub>N</sub> (CD44<sup>lo</sup>), T<sub>VM</sub> (CD44<sup>hi</sup> CD49d<sup>lo</sup>) and T<sub>MEM</sub> (CD44<sup>hi</sup> CD49d<sup>hi</sup>) cells. Cells are gated on single, live, CD4<sup>-</sup> TCRβ<sup>+</sup> CD8<sup>+</sup> lymphocytes. (C) Number of splenic T<sub>N</sub>, T<sub>VM</sub>, and T<sub>MEM</sub> CD8<sup>+</sup> T cells from naïve WT, homozygous H-2D<sup>b</sup> and H-2K<sup>b</sup> mice, and hemizygous H-2D<sup>b</sup> and H-2K<sup>b</sup> mice (D) Representative dot plots of single, live, thymocytes from WT, homozygous H-2D<sup>b</sup> and hemizygous H-2D<sup>b</sup> mice. Cells are gated on single, live thymocytes. (E) Number of CD8<sup>+</sup> CD4<sup>-</sup> thymocytes and (F) MFI of H-2D<sup>b</sup> expression on thymocytes in WT, homozygous H-2D<sup>b</sup> and hemizygous H-2D<sup>b</sup> mice. (G) Representative dot plots of PE-enriched singlet, live, CD8 SP thymocytes from mice injected intravenously with anti-CD8α:PE, and then stained *ex vivo* with anti-CD8β. A representative stain of the blood is used as a positive control. Cells are gated on single live B220<sup>-</sup> CD4<sup>-</sup> CD11b<sup>-</sup> CD11c<sup>-</sup> F4/80<sup>-</sup> NK1.1<sup>-</sup> lymphocytes. (H) Total number of perivascular CD8 SP thymocytes based on dual-staining with CD8α and CD8β. (I) Representative dot plot (left) and collated data (right) showing CD103 expression of blood-derived CD8<sup>+</sup> T cells (red dots) and perivascular CD8 SP thymocytes (black dots). \*\*\*, p≤0.001; \*\*, p≤0.01; \*, p≤0.05; NS= not significant. Bars and error bars represent mean +/- SEM. These results are representative of 2 independent experiments with n = 4-8 per group.

#### 4.4.3. Reduction in naïve CD8<sup>+</sup> T cells in MHC I hemizygous mice is not due to reduced CD8<sup>+</sup> T cell generation or thymic output

The impact of altered MHC I expression levels on the numbers of T<sub>N</sub> cells could be the result of changes in thymic output and/or peripheral homeostatic maintenance. To explore these mechanisms, we focused on H-2D<sup>b</sup> homozygous and hemizygous mice, with validation of some key observations in H-2K<sup>b</sup> homozygous and hemizygous mice. An initial analysis of CD8 T cell generation in the thymus revealed a substantial reduction in mature CD8 single positive (SP) T cells in both H-2D<sup>b</sup> homozygous and hemizygous strains compared to WT controls, which is likely due to the loss of H-2K<sup>b</sup>-restricted CD8<sup>+</sup> T cells (**Figure 22D, E**). In contrast, we observed no difference in CD8 SP thymocytes between H-2D<sup>b</sup> homozygous and hemizygous mice (**Figure 22D, E**) despite a reduction in H-2D<sup>b</sup> expression in the thymi of hemizygous mice (**Figure 22F**). This illustrates that MHC I gene dosage does not impact on CD8<sup>+</sup> T cell generation in the thymus.

Mature SP T cells are thought to emigrate to the periphery at perivascular spaces at the corticomedullary junction (254, 255). Thus, to measure thymic emigration, we used an established method to identify and enumerate mature CD8 SP thymocytes in these perivascular spaces (**Supplementary 4.9.2**). An anti-CD8 $\alpha$ -PE antibody was injected intravenously into mice to label all blood-derived CD8<sup>+</sup> T cells, as well as emigrating CD8 SP thymocytes. Animals were sacrificed 3 minutes later and immediately perfused to deplete blood-derived CD8<sup>+</sup> T cells from the thymus. Emigrating CD8 SP thymocytes residing in the perivascular channels (anti-CD8 $\alpha$ -PE<sup>+</sup>) were magnetically enriched using PE-specific beads. Cells were subsequently co-stained with anti-

CD8 $\beta$ -APC and the number of dual-labelled cells was taken as an indication of the rate of thymocyte egress (**Supplementary 4.9.2**). There were significantly fewer emigrating CD8 SP thymocytes in both H-2D<sup>b</sup> homozygous and hemizygous mice compared to WT mice, but there was no difference in the number of emigrating CD8 SP thymocytes between H-2D<sup>b</sup> homozygous and hemizygous mice (**Figure 22G, H**). The identified cells were newly formed CD8 SP thymocytes (as opposed to contaminating blood cells) was verified by their high level of CD103 expression (**Figure 22I**) (258).

Collectively, while the loss of one MHC1 gene had a substantial effect on the development and emigration of mature CD8 SP T cells, these data show that the rate of thymic development and emigration of mature CD8 SP T cells were not substantially influenced by halving the expression of the remaining MHC gene. Thus, we conclude that the reduction in naïve CD8<sup>+</sup> T cell number in the periphery of MHC1 hemizygous mice is not a consequence of reduced thymic export.

#### 4.4.4. Qualitative changes in peripheral T cell repertoire from MHC I hemizygous mice

To determine whether the peripheral loss of CD8<sup>+</sup> T cells in MHC I hemizygous mice was selective or stochastic, we analysed the TCR repertoire. The global TRBV usage of naïve CD8<sup>+</sup> T cells was assessed by flow cytometry using a panel of V $\beta$ -specific antibodies in both the thymus and spleen of WT mice, and H-2D<sup>b</sup> homozygous and hemizygous mice. In the thymus, TRBV usage was surprisingly similar across all mouse strains. These data suggest firstly that thymic selection on H-2D<sup>b</sup> and H-2K<sup>b</sup> molecules does not drive overtly different TRBV usage (**Figure 23A, Supplementary 4.9.3A**) and supports our earlier data that CD8<sup>+</sup> T cell generation and thymic output are not influenced by MHC I dosage (**Figure 22D – I**). In contrast, analysis of TRBV usage in the spleen revealed significant differences in the usage of particular TRBVs by CD8<sup>+</sup> T cells from homozygous and hemizygous mice. In particular, H-2D<sup>b</sup> hemizygous mice showed a significant increase in the usage of TRBV16, TRBV24 and, most strikingly, TRBV29 (**Figure 23B**).

Of note, a similar pattern was seen when TRBV usage was assessed across H-2K<sup>b</sup> homozygous and hemizygous mice. There was no difference in the thymus (**Supplementary 4.9.3A**) but H-2K<sup>b</sup> hemizygous mice exhibited modest increases in TRBV16, TRBV24 and TRBV29 usage on peripheral T cells compared to their homozygous counterparts (**Supplementary 4.9.3B**). The TRBV repertoire of CD4<sup>+</sup> T cells in the periphery was not impacted by MHC I expression levels, indicating that these shifts are a consequence of altered peripheral CD8<sup>+</sup> T cell recognition of pMHC I (**Supplementary 4.9.4A, B**). These shifts in the peripheral TRBV repertoire usage

under conditions of reduced MHC I expression indicate that naïve CD8<sup>+</sup> T cell populations are selectively retained in a TCR dependent manner.

Selective retention of naïve CD8<sup>+</sup> T cells may be mediated by increased competition for the two major survival signals: TCR recognition of pMHC I and IL-7 signaling. Thus, we analysed markers denoting the capacity of the cells to compete for these signals. To evaluate pMHC I/TCR signalling, CD5 expression was assessed as an indicator of the strength of signal received through TCR recognition of pMHC I, and thus competitiveness for pMHC I binding (259–261) and TCR $\beta$  was assessed as a marker of TCR density. On CD8 SP thymocytes, there was no difference in CD5 or TCR $\beta$  expression between H-2D<sup>b</sup> homozygous and hemizygous mice (**Figure 23C, D**) suggesting that TCR/pMHC I signaling during thymic selection was unaltered. However, peripheral naïve CD8<sup>+</sup> T cells from H-2D<sup>b</sup> hemizygous mice showed significantly elevated expression of CD5, despite similar TCR levels as their homozygous counterparts (**Figure 23E, F**). CD5 expression was similarly increased on peripheral CD8<sup>+</sup> T cells from H-2K<sup>b</sup> hemizygous mice (**Supplementary 4.9.3C**) but CD5 levels were unchanged on peripheral CD4<sup>+</sup> T cells from H-2D<sup>b</sup> and H-2K<sup>b</sup> hemizygous mice (**Supplementary 4.9.4C, D**). To evaluate IL-7 signalling capacity, the expression of IL-7R $\alpha$  (CD127) was evaluated by flow cytometry. Expression of IL-7R $\alpha$  (CD127) was significantly upregulated on cells from mice that were hemizygous for either H-2D<sup>b</sup> (**Figure 23G**) or H-2K<sup>b</sup> (**Supplementary 4.9.3D**).

Collectively, these data indicate that naïve CD8<sup>+</sup> T cells with a higher capacity to bind self pMHC I and compete for IL-7 are preferentially maintained under conditions of

limited MHC I expression. As a result, MHC I dose substantially influences both the frequency and quality of peripheral naïve CD8<sup>+</sup> T cells.

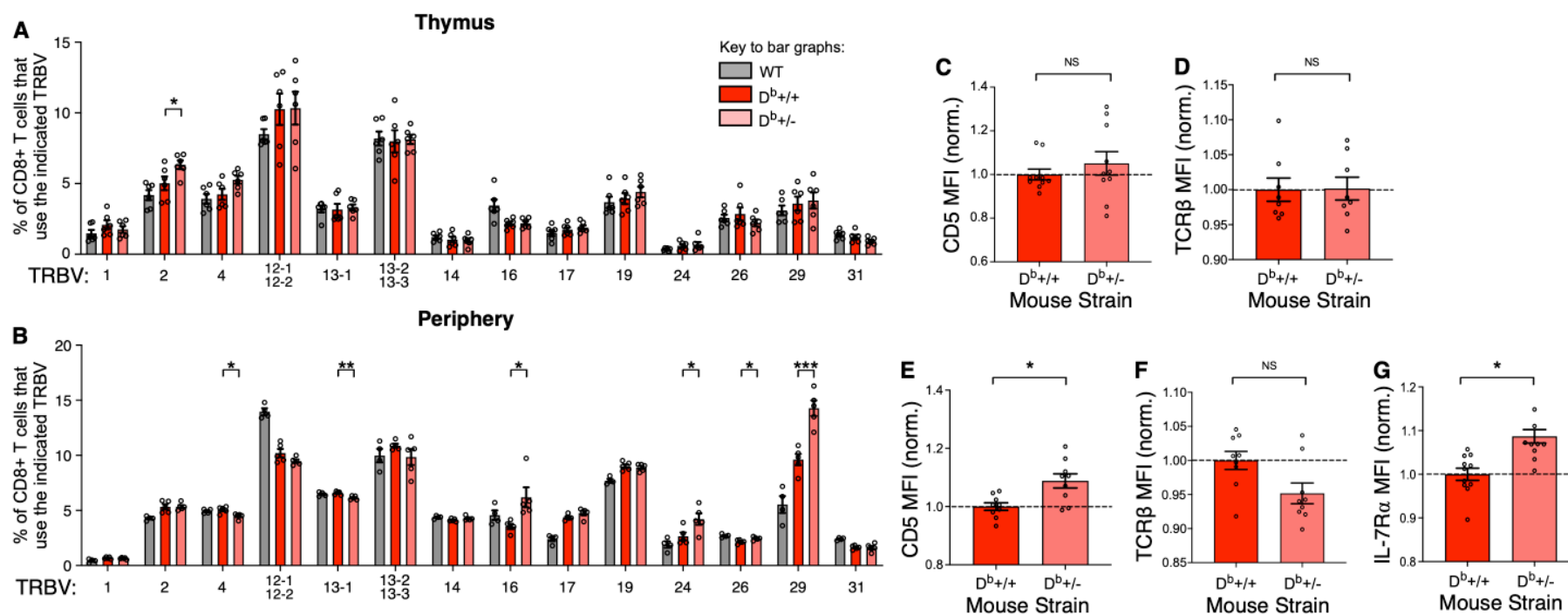


**Figure 23:** MHC I expression level influences the composition of the peripheral naïve CD8<sup>+</sup> T cell repertoire. TRBV usage was assessed by flow cytometry on (A) CD8 SP thymocytes and (B) peripheral splenic CD8<sup>+</sup> T cells from WT, homozygous H-2D<sup>b</sup> and hemizygous H-2D<sup>b</sup> mice. Normalized median fluorescence intensity (MFI) for (C) CD5 expression and (D) TCRβ expression on CD8 SP thymocytes. Normalized MFI for (E) CD5 expression, (F) TCRβ expression and (G) IL-7Rα expression on naïve splenic CD8<sup>+</sup> T cells. \*\*\*, p<sub>≤</sub>0.001; \*\*, p<sub>≤</sub>0.01; \*, p<sub>≤</sub>0.05; NS= not significant. Bars and error bars represent mean +/- SEM. These results are representative of 2 independent experiments with n = 4-6 mice per group (A, B) and pooled and normalized to D<sup>b</sup>/D<sup>b</sup> MFI (C-F).

#### 4.4.5. During IAV infection, CD8<sup>+</sup> T cells from MHC I Hemizygous Mice Exhibit Improved Functionality

To understand how the observed changes in the CD8<sup>+</sup> T cell repertoire in MHC I hemizygous mice might impact on an antigen-specific population, we took advantage of the pronounced increase in TRBV29 usage in H-2D<sup>b</sup> hemizygous mice. We have previously shown that CD8<sup>+</sup> T cells specific for the influenza A virus (IAV)-derived H-2D<sup>b</sup>-restricted acidic polymerase epitope (PA<sub>224-233</sub>) predominantly utilize TRBV29 in the naïve repertoire, and this is accentuated in the immune repertoire (137, 141, 149). This suggests that the naïve TRBV29<sup>+</sup> CD8<sup>+</sup> T cells that are preferentially retained in H-2D<sup>b</sup> hemizygous mice may confer superior H-2D<sup>b</sup>PA<sub>224</sub> recognition and activation.

To evaluate whether naïve TRBV29<sup>+</sup> H-2D<sup>b</sup>PA<sub>224</sub>-specific CD8<sup>+</sup> T cells are preferentially retained in H-2D<sup>b</sup> hemizygous mice, total H-2D<sup>b</sup>PA<sub>224</sub>-specific T cells from naïve H-2D<sup>b</sup> homozygous and hemizygous mice were enumerated and single cell sorted to assess TRBV29 expression *via* multiplex nested RT-PCR. H-2D<sup>b</sup> hemizygous mice had significantly fewer naïve H-2D<sup>b</sup>PA<sub>224</sub>-specific CD8<sup>+</sup> T cells than homozygous mice (**Figure 24A, B**), consistent with the reduction observed for total CD8<sup>+</sup> T cells (**Figure 22A**). Intriguingly, the reduction of naïve H-2D<sup>b</sup>PA<sub>224</sub>-specific CD8<sup>+</sup> T cells was mediated predominantly through loss of TRBV29<sup>-</sup> cells, while the number of TRBV29<sup>+</sup> cells was maintained (**Figure 24B**). Thus, while a similar proportion of the naïve H-2D<sup>b</sup>PA<sub>224</sub>-specific repertoire used TRBV29 in the WT and H-2D<sup>b</sup> homozygous mice, a significantly larger proportion of the repertoire used TRBV29<sup>+</sup> in the H-2D<sup>b</sup> hemizygous mice (**Figure 24C**). These data demonstrate that

the selective maintenance of cells under conditions of reduced MHC I expression impacts on naïve antigen-specific CD8<sup>+</sup> T cell populations.

To determine how the preferential retention of naïve TRBV29<sup>+</sup> H-2D<sup>b</sup>PA<sub>224</sub>-specific CD8<sup>+</sup> T cells impacted on the immune response to IAV infection, H-2D<sup>b</sup> homozygous and hemizygous mice were infected intranasally with IAV, and CD8<sup>+</sup> T cell responses to the dominant H-2D<sup>b</sup>PA<sub>224</sub> epitope were assessed 10 days post-infection. The H-2D<sup>b</sup>PA<sub>224</sub>-specific CTL response in H-2D<sup>b</sup> hemizygous mice was significantly reduced when compared to that observed in homozygous mice (**Figure 24D**), in line with reduced frequency of naïve cells. Analysis of TRBV usage in the epitope specific response showed that the magnitude of the TRBV29<sup>+</sup> response in hemizygous mice was not significantly affected, while the magnitude of responses generated by TRBV29<sup>-</sup> cells was significantly reduced (**Figure 24D**). This selective loss of the TRBV29<sup>-</sup> response to H-2D<sup>b</sup>PA<sub>224</sub> was confirmed after infection of mice with a recombinant IAV in which the competing co-dominant NP<sub>366-374</sub> epitope was removed *via* a single point mutation (N5Q) to prevent H-2D<sup>b</sup> binding (**Figure 24E**) (169, 173).

As a qualitative measure of functionality, we assessed the capacity of H-2D<sup>b</sup>PA<sub>224</sub>-specific CD8<sup>+</sup> T cells to secrete IFN $\gamma$ , TNF and IL-2 cytokines after short-term restimulation with the PA<sub>224</sub> peptide *ex vivo* (**Figure 24F**). The ability of CD8<sup>+</sup> T cells to simultaneously produce multiple cytokines has been correlated with more effective protection against virus infection (262, 263). H-2D<sup>b</sup> hemizygous mice preferentially retained multifunctional (3+) H-2D<sup>b</sup>PA<sub>224</sub>-specific CD8<sup>+</sup> T cells, capable of secreting all three cytokines, and showed a proportional loss of dual- (2+) and mono-functional (1+) CD8<sup>+</sup> T cells compared to H-2D<sup>b</sup> homozygous mice (**Figure 24G**). In addition,

after staining cells from H-2D<sup>b</sup> homozygous and hemizygous mice with H-2D<sup>b</sup>PA<sub>224</sub> tetramer, we assessed the relative rate of tetramer dissociation in the presence of an anti-H-2D<sup>b</sup> antibody. We found that H-2D<sup>b</sup>PA<sub>224</sub>-specific CD8<sup>+</sup> T cells from H-2D<sup>b</sup> hemizygous mice exhibited a slower dissociation rate, or higher avidity, relative to cells from H-2D<sup>b</sup> homozygous mice (**Figure 24H**).

Collectively, these data demonstrate that while the reduced expression of MHC I results in the loss of a substantial number of naïve H-2D<sup>b</sup>PA<sub>224</sub>-specific CD8<sup>+</sup> T cells, there is preferential retention of naïve CD8<sup>+</sup> T cells that are better able to respond to antigen following virus infection.

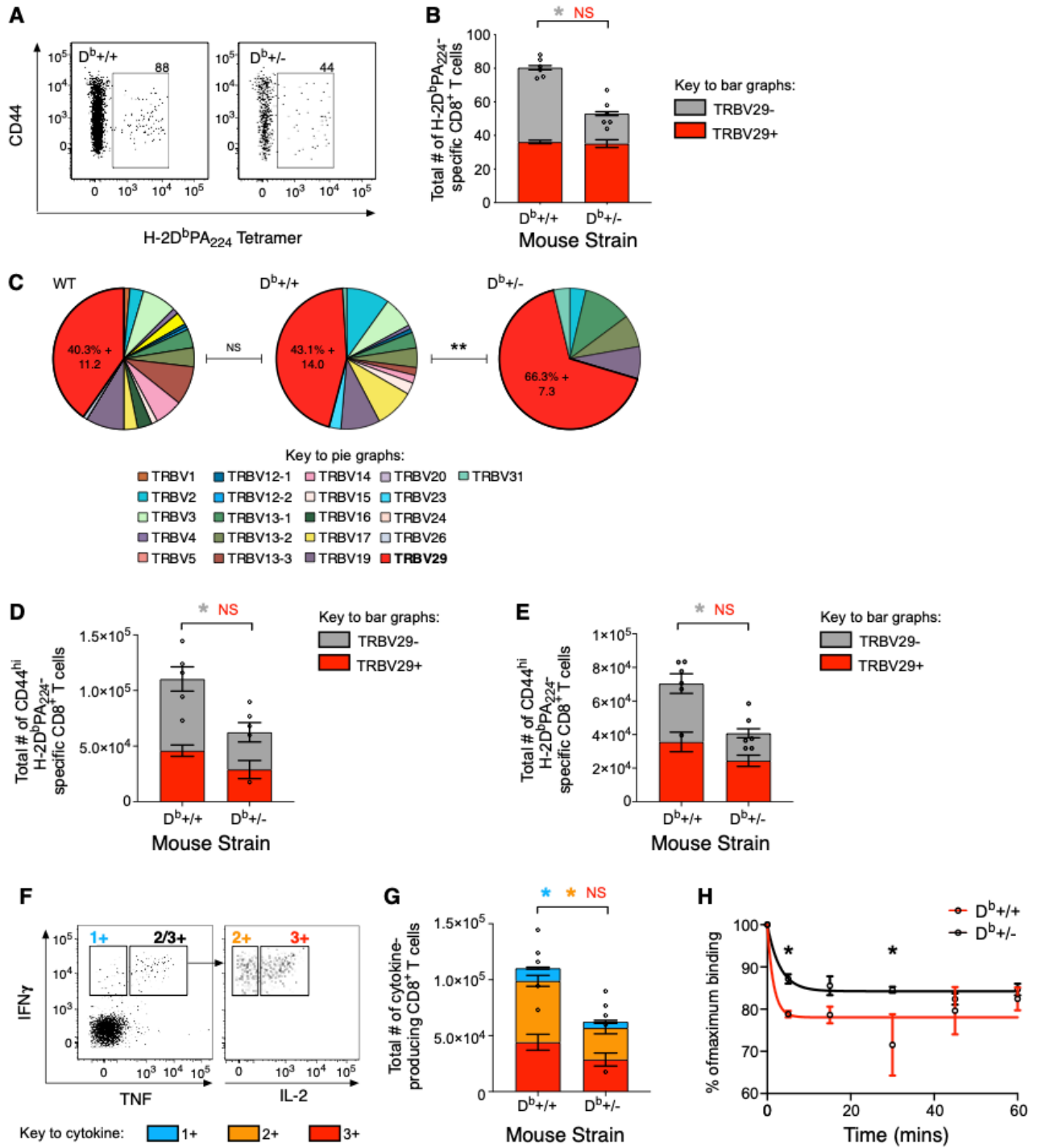


**Figure 24:** Reduced MHC I expression leads to alterations in IAV-specific naïve CD8<sup>+</sup> T cell repertoires and IAV-specific CD8<sup>+</sup> T cell immune responses. (A) Representative dot plots of naïve H-2D<sup>b</sup>PA<sub>224</sub> tetramer<sup>+</sup> CD8<sup>+</sup> T cells, gated on single live lymphocytes that are B220<sup>-</sup> CD4<sup>-</sup> CD11b<sup>-</sup> CD11c<sup>-</sup> F4/80<sup>-</sup> NK1.1<sup>-</sup> and CD8<sup>+</sup> T cells from pooled spleen and major lymph nodes of naïve H-2D<sup>b</sup> homozygous and hemizygous mice. (B) Numbers of naïve H-2D<sup>b</sup>PA<sub>224</sub>-specific CD8<sup>+</sup> T cells isolated from naïve H-2D<sup>b</sup> homozygous or hemizygous mice, with the proportion of TRBV29<sup>+</sup> cells indicated. (C) TRBV usage of naïve H-2D<sup>b</sup>PA<sub>224</sub>-specific CD8<sup>+</sup> T cells from naïve WT, H-2D<sup>b</sup> homozygous and hemizygous mice, where  $n = 133, 111,$  and  $27$  sequences from  $5, 3,$  and  $3$  mice for each mouse strain, respectively. Number of immune TRBV29<sup>+</sup> H-2D<sup>b</sup>PA<sub>224</sub>-specific CD8<sup>+</sup> T cells isolated from H-2D<sup>b</sup> homozygous and hemizygous mice after (D) HKx31 and (E) HKx31 NP-N5Q IAV infection, with the proportion of TRBV29<sup>+</sup> cells indicated. (F) Representative dot plots and (G) number of cytokine-producing H-2D<sup>b</sup>PA<sub>224</sub>-specific CD8<sup>+</sup> T cells isolated from H-2D<sup>b</sup> homozygous or hemizygous mice 10 days after HKx31 infection. (H) Kinetics of H-2D<sup>b</sup>PA<sub>224</sub> tetramer dissociation for splenic CD8<sup>+</sup> T cells on day 10 after primary HKx31 infection showing data points and line of best fit. \*\*\*,  $p \leq 0.001$ ; \*\*,  $p \leq 0.01$ ; \*,  $p \leq 0.05$ ; NS= not significant. Bars and error bars represent mean  $\pm$  SEM. These results are representative of 2-3 independent experiments with  $n = 5-6$

## 4.5. Discussion

Early studies investigating the role of MHC I in peripheral CD8<sup>+</sup> T cell maintenance demonstrated that pMHC I recognition in the periphery is essential for survival of naive CD8<sup>+</sup> T cells (105, 231–233). There is also compelling evidence, in models of adoptive transfer of TCR transgenic T cells and lymphopenic-induced models, for a level of competition amongst naïve CD8<sup>+</sup> T cells for tonic TCR-pMHC I signalling. Those T cells with higher affinity for self pMHC I compete better when pMHC I is limiting and thus exhibit a survival advantage (109, 242). However, these early studies typically transferred large numbers of cells with a single specificity, all competing for survival signals from the same pMHC I (240, 242) or they transferred large numbers of polyclonal cells into TCR transgenic mice (240, 242). Thus, it remained unclear from these early transfer experiments the extent to which endogenous, *in situ*, polyclonal CD8<sup>+</sup> T cell repertoires, which have an exceedingly small number of T cells specific for any given pMHC I (133, 137), normally compete for pMHC I at physiologically relevant levels of expression (driven by either homozygous or hemizygous expression of a particular MHC I allele). Here, we show that modulating the expression level of an MHC I molecule is sufficient to cause substantial changes in peripheral CD8<sup>+</sup> T cell number, independent of thymic generation and output. These changes arise in the periphery due to TCR-dependent competition that leads to selective loss of CD8<sup>+</sup> T cells expressing TCRs with low affinity for pMHC I. This peripheral selection directly influenced the ability of the CD8<sup>+</sup> T cells to respond to a viral challenge.

Other studies have also highlighted that affinity for selecting pMHC I in the thymus correlates with restricting pMHC I in the periphery and foreign pMHC I during challenge.

Studies with mice expressing a single pMHC have suggested that the signal driving positive selection in the thymus and survival in the periphery appears to be delivered by the same pMHCI complex (109, 111, 264). More recently, a correlation between the strength of signal received *via* recognition of self pMHC in the thymus and that received after recognition of foreign cognate pMHC has also been observed, indicating that the nature of the TCR-pMHCI interaction during positive selection programs an intrinsic T cell responsiveness to foreign pMHCI (260). Furthermore, MHC heterozygosity in mice have been demonstrated to confer better protection against viral infections by generating a diverse T cell repertoire (265). It is clear that the TRBV29<sup>+</sup> subset represent an optimal solution for TCR recognition of H-2D<sup>b</sup>PA<sub>224</sub>. TRBV29<sup>+</sup> cells represent ~ 40-50% of the H-2D<sup>b</sup>PA<sub>224</sub>-specific repertoire in naïve mice, but ~70% in the immune repertoire (137, 149), corresponding to a significant increase in avidity for pMHCI (144). The selective retention of this subset in the naïve H-2D<sup>b</sup>PA<sub>224</sub>-specific pool in H-2D<sup>b</sup> hemizygous mice therefore supports the idea that limiting tonic signaling by self pMHCI in the periphery results in the preferential survival of CD8<sup>+</sup> T cells that are not only more competitive for self-pMHCI (as evidenced by CD5 expression) but also for foreign cognate pMHCI.

It was striking that we observed no significant change in the number, egress, or phenotype of mature CD8 SP thymocytes from MHC I homozygous and hemizygous mice. Although not significant, we observed a trend for a very modest drop in SP and perivascular CD8<sup>+</sup> T cells in the thymus of H-2D<sup>b</sup> hemizygous mice. Given that our analysis represents a snapshot of the thymic microenvironment, it is possible that the accumulation of very modest changes may contribute to the effects observed in the periphery. However, in contrast to mature peripheral CD8<sup>+</sup> T cells, mature CD8 SP T

cells from H-2D<sup>b</sup> homozygous and hemizygous mice did not exhibit any change in either TRBV usage or CD5 expression. Thus, on balance our data indicates that MHCI gene dosage controls the homeostatic maintenance of CD8<sup>+</sup> T cells in the periphery and does not substantially impact CD8<sup>+</sup> T cell development in the thymus. This seems to stand in contrast with our understanding of thymic selection, as the density of specific pMHCI ligands has been shown to influence both positive and negative selection (266–268). However, it is supported by analyses of mice lacking the  $\beta 5i$  immunoproteasome subunit, in which there is a 25-50% reduction in MHCI levels. These mice showed no effect on CD8 SP cell numbers or TCR expression levels (269, 270). Collectively, our data suggest that MHCI levels in hemizygous mice are well above that which is required for normal thymic selection, allowing them to maintain the breadth of self pMHCI epitopes needed to support the production of a diverse CD8<sup>+</sup> T cell repertoire. The discrepancy between this and the limited ability to maintain cells in the periphery may be explained by the fact that thymocytes are more sensitive to TCR mediated signals than their mature peripheral counterparts (271, 272), or by the vastly increased numbers of CD8<sup>+</sup> T cells that must be maintained in the periphery.

With regard to the mechanisms that drive this preferential CD8<sup>+</sup> T cell retention, we observed elevated levels of CD5 and IL-7R $\alpha$  on cells that were selectively retained in the periphery of MHCI hemizygous mice. This indicates that CD8<sup>+</sup> T cells that are retained with reduced MHCI expression have a superior capacity to compete for both of the signals that are critical for naïve T cell survival; pMHCI and IL-7. Indeed, previous studies have demonstrated that CD5<sup>hi</sup> cells, as opposed to CD5<sup>lo</sup> cells, exhibit increased responsiveness to multiple cytokines, including IL-7, IL-2 and IL-15 (257, 260, 273). Moreover, a seminal study showed that CD4<sup>+</sup> and CD8<sup>+</sup> T cells

stimulated with strong, as opposed to weak, TCR signals subsequently exhibited heightened sensitivity to IL-7, IL-15 and IL-2 to promote survival (274), indicating a clear causal link between TCR sensitivity to pMHC and cytokine responsiveness. Of note, ageing causes a dramatic decline in naïve CD8<sup>+</sup> T cells but CD5<sup>+</sup> CD8<sup>+</sup> T cells are preferentially retained over the course of ageing in mice (136, 275). As a result, it would be of interest to evaluate whether heterozygote mice exhibit better retention of naïve CD8<sup>+</sup> T cells with age.

Our work is particularly relevant for understanding the impact of MHC I dose in the outbred human population. HLA heterozygosity in humans has been shown to confer a distinct advantage, based on multiple studies in which heterozygous individuals show superior viral control or protection from diseases including HIV, HSV1, HTLV-1 and HBV (243–246), or improved responses to checkpoint blockade immunotherapy in cancer patients (276), compared to homozygous individuals. This ‘heterozygote advantage’ is thought to be actively selected for through MHC-disassortative mating preferences (277–279) and is thought to be due to an increased capacity to respond to a broader array of epitopes. On the other hand, homozygosity of HLA genes has been positively correlated with the incidence and/or severity of several autoimmune diseases such as multiple sclerosis (247), celiac disease (248) and rheumatoid arthritis (249), suggesting that an increased dose of particular MHC molecules can augment T cell responses. These anecdotal findings appear, *prima facie*, to be contradictory, with HLA homozygosity associated with both poorer and augmented responses. However, we contend, in light of the data presented here, that while HLA homozygosity can result in a proportional increase in naïve T cell frequencies and immune responses, HLA hemi- or heterozygous individuals may selectively retain

naïve T cell populations that can generate qualitatively superior immune responses. As a result, HLA hemi- or heterozygous individuals may have two distinct immunological advantages that optimize pathogen control: i) they can respond to a broader array of epitopes and ii) they selectively retain qualitatively superior CD8<sup>+</sup> T cells.

Collectively, this study demonstrates that physiological variation in the expression of a given MHC I allele is a delimiter of peripheral CD8<sup>+</sup> T cell numbers, by regulating the survival signal accessible to mature peripheral T cells, but not T cell development. Moreover, this study provides clear evidence of clonal competition under physiological conditions of CD8<sup>+</sup> T cell composition and frequency, and MHC I expression, with limited MHC I expression driving selective survival of CD8<sup>+</sup> T cells with superior pMHC I recognition capacity. This work furthers our fundamental understanding of the nature of naïve CD8<sup>+</sup> T cell repertoires maintained by homozygous and heterozygous MHC allelic expression and thus has implications for understanding the impact of MHC I dose on homeostasis, disease and ageing.

## **4.6. Acknowledgements**

This work was supported by a Sylvia and Charles Viertel Senior Medical Research Fellowship, an Australian Research Council (ARC) Future Fellowship FT170100174, a National Health and Medical Research Council (NHMRC) Program grant APP1071916 (to N.L.L. and S.J.T.), an NHMRC Principal Research Fellowship (to S.J.T.) and a Monash University Biomedicine Discovery Scholarship (to X. Y. X. S.).

## **4.7. Author Contributions**

X. Y. X. S. performed the majority of experiments and analyzed data; N.L.L., K.M.Q., and S.R.D. designed the study and N.L.L., K.M.Q., and S.J.T. supervised the research; J.L., P.Z., L.A., C.M.J. and J.L performed key experiments and analyzed data; N.L.L., K.M.Q., and X. Y. X. S. wrote the initial draft of the manuscript and all authors participated in writing the final manuscript.

## **4.8. Competing Interests**

The authors declare no competing financial interests.

## 4.9. Supplementary Figures

### 4.9.1. Supplementary Figure 1

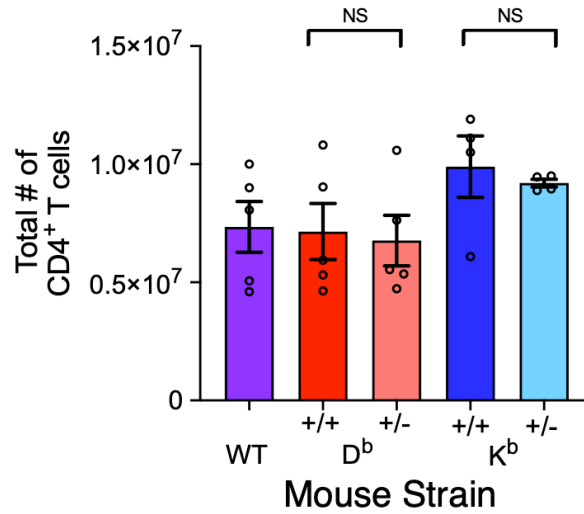


**Figure 25:** MHC I expression level does not influence peripheral CD4<sup>+</sup> T cell population. Total splenic CD4<sup>+</sup> T cells from naive WT, homozygous D<sup>b</sup> (D<sup>b</sup>/D<sup>b</sup>) and K<sup>b</sup> (K<sup>b</sup>/K<sup>b</sup>) mice, and hemizygous D<sup>b</sup> (D<sup>b</sup>/-) and K<sup>b</sup> (K<sup>b</sup>/-) mice. Results are representative of 2-3 independent experiments with  $n = 4-6$

4.9.2. Supplementary Figure 2

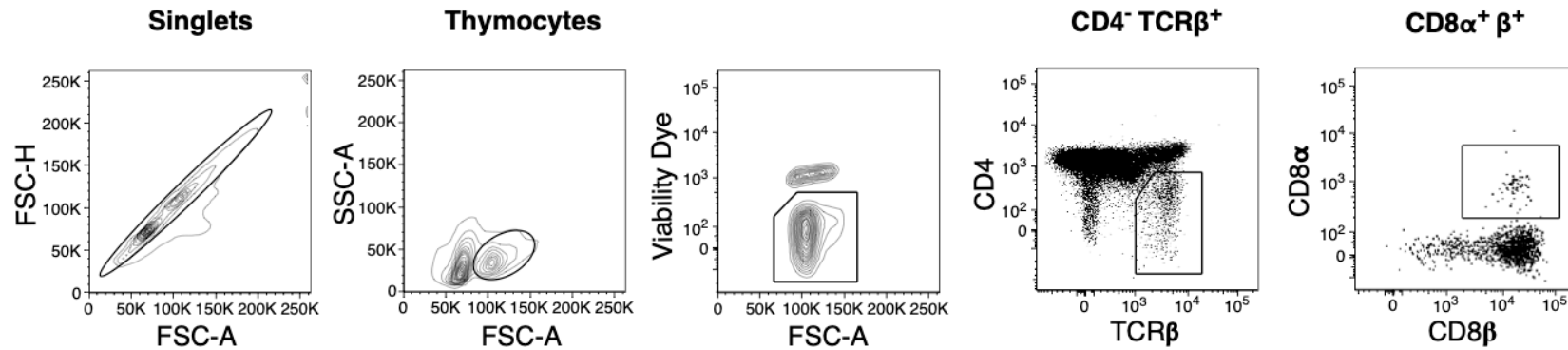


**Figure 26:** Gating strategy for perivascular CD8<sup>+</sup> thymocytes. WT, homozygous D<sup>b</sup> and hemizygous D<sup>b</sup> mice were injected intravenously with 1μg of PE-conjugated anti-CD8α antibody and mice were humanely euthanized 3-4 mins later. Mice were perfused with PBS to remove excess unbound antibody prior to thymus collection. Shown is the gating strategy for the identification of single cells, lymphocytes, live cells, CD4<sup>-</sup> TCRβ<sup>+</sup>, CD8α<sup>+</sup>, CD8β<sup>+</sup> perivascular thymocytes.

4.9.3. Supplementary Figure 3

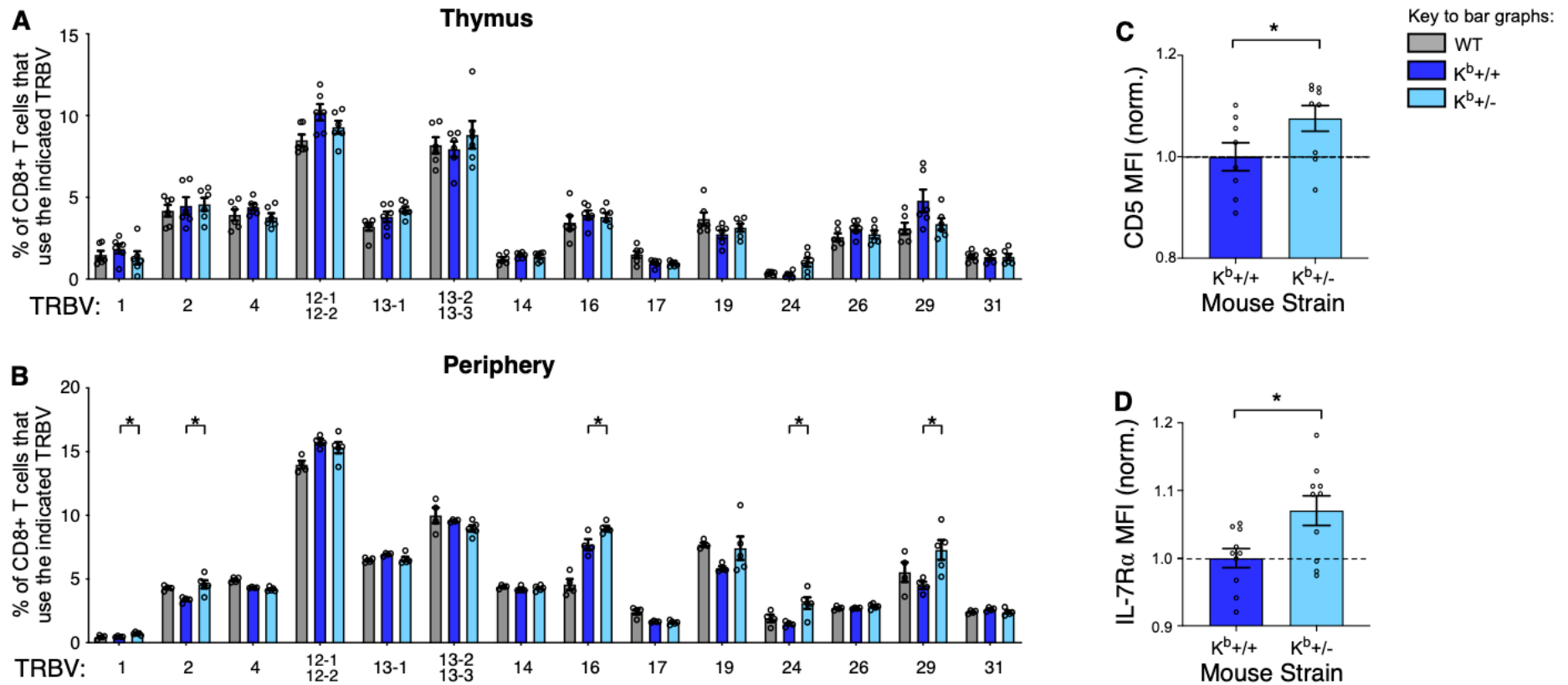


**Figure 27:** MHC I expression level influences the composition of the peripheral naive CD8<sup>+</sup> T cell repertoire. (A) TRBV usage on CD8 SP thymocytes and (B) peripheral splenic CD8<sup>+</sup> T cells of WT, homozygous  $K^b$ , and hemizygous  $K^b$  mice. (C) MFI of CD5 expression on naive splenic CD8<sup>+</sup> T cells. (D) MFI of CD127 expression of naive splenic CD8<sup>+</sup> T cells. \*\*\*,  $p < 0.001$ ; \*\*,  $p < 0.01$ ; \*,  $p < 0.05$ . These results are representative of 2 independent experiments with (A, B)  $n = 5-6$  and (C, D) were pooled and normalized to  $K^b_{+/+}$  MFI.

4.9.4. Supplementary Figure 4

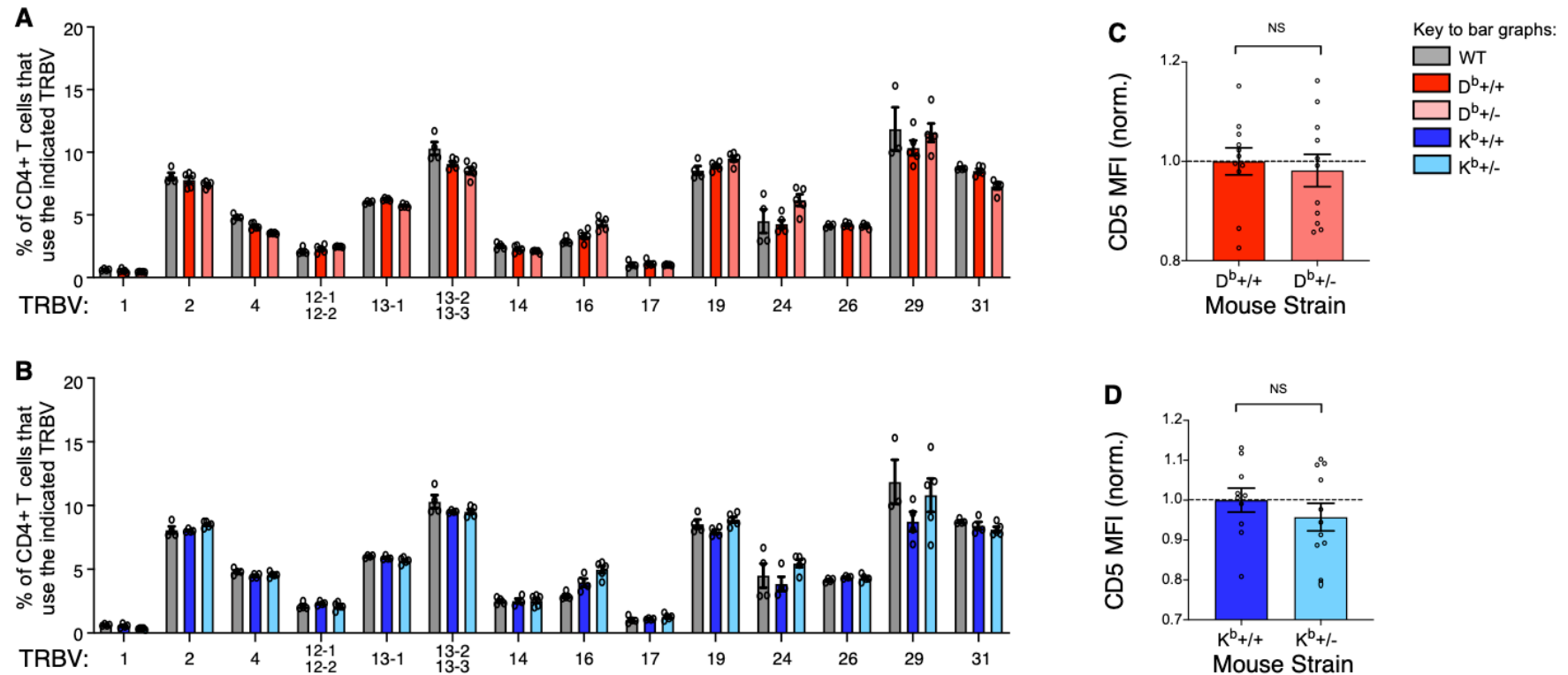


**Figure 28:** MHC I expression level does not influence the composition of the peripheral naive CD4<sup>+</sup> T cell repertoire. (A) TRBV usage on peripheral splenic CD4<sup>+</sup> T cells from WT, homozygous  $D^b$ , hemizygous  $D^b$ , and (B) WT, homozygous  $K^b$  and hemizygous  $K^b$  mice. MFI of CD5 expression on naive splenic CD4<sup>+</sup> T cells from (C)  $D^b/D^b$  and  $D^b/-$  mice, and (D)  $K^b/K^b$  and  $K^b/-$  mice. Results are representative of 2 independent experiments with (A, B)  $n = 4-6$ , and pooled and normalized to (C)  $D^b/+$  and (D)  $K^b/+$ .



## ***5. Analysis of Immunodomination in Anti-Viral CD8 T cell Responses During IAV Infection***

### **5.1. Introduction**

The overall magnitude of a polyclonal CD8 T cell response is governed in part by the dynamics of individual antigen-specific responses and their influence on each other. In particular, subdominant responses can be diminished by concurrent large or immunodominant responses (reviewed in (128)), in a phenomenon known as immunodomination. Various studies have provided evidence of immunodomination by showing that subdominant responses are augmented in the absence of other immunodominant pMHC complexes (246–249).

There have been various mechanisms proposed to underpin the phenomenon of immunodomination: 1) competition within CD8 T cell populations for access to pMHC, costimulatory signals and cytokines produced by APCs, 2) the preferential MHC presentation of certain epitopes over and above others, 3) the killing of APCs following activation of CD8 T cells of a particular specificity, and 4) the superior elimination of virus by early-responders (reviewed in (120, 246)). Of note, immunodomination can occur between CD8 T cells with either the same epitope specificity or distinct specificities.

Immunodomination occurs most readily within CD8 T cell populations with the same specificity. This is exemplified following the adoptive transfer of a large number of TCR transgenic cells CD8 T cells specific for Ovalbumin-derived H-2K<sup>b</sup>Ova<sub>257</sub> prior to infection with virus expressing this epitope. The presence of the TCR transgenic cells significantly diminished the magnitude of the endogenous H-2K<sup>b</sup>Ova<sub>257</sub>-specific CD8 T cell response during challenge (160, 163). The same effect was also seen following adoptive transfer of TCR transgenic CD8 T cells specific for the LCMV-derived H-2D<sup>b</sup>gp<sub>33</sub> epitope (161). Of note, the robust expansion of these TCR transgenic CD8 T cells had little effect on the concurrent responses from CD8 T cells of other specificities, suggesting that immunodomination within, rather than between, epitope specificities occurs more readily.

However, competition amongst CD8 T cell populations of different specificities has been shown to occur. Studies in multiple infection models have demonstrated that mutation and loss of one immunodominant epitope can lead to compensatory shifts in the immunodominance hierarchy (153, 162, 280–282). For example, Webby et al (2003) introduced point mutations into the immunodominant NP<sub>366</sub> and PA<sub>224</sub> epitopes in IAV, which abrogated presentation by the H-2D<sup>b</sup> molecule after infection (162). With loss of these immunodominant epitopes, they observed a compensatory increase in the otherwise subdominant H-2K<sup>b</sup>PB1<sub>703</sub>-specific CD8 T cell response. This effect was further exacerbated during secondary challenge, where the absence of H-2D<sup>b</sup>NP<sub>366</sub> and H-2D<sup>b</sup>PA<sub>224</sub>-specific CD8 T cell responses lead to a robust increase in the H-2K<sup>b</sup>PB1<sub>703</sub>-specific CD8 T cell response (280). As another example, Stock et al. (2006) introduced point mutations into the immunodominant gB<sub>498</sub> epitope from LCMV that again abrogated presentation by the H-2D<sup>b</sup> (283). This did not lead to a decrease in

the total magnitude of the anti-viral CD8 T cell response, suggesting that other CD8 T cell responses were compensating for the loss of the H-2D<sup>b</sup>gB<sub>498</sub>-specific response. Taken together, these studies suggest that there is a level of interaction across CD8 T cells populations of various specificities, where the presence of a particular CD8 T cell population suppresses the expansion of others. Thus, it is important to understand more precisely how the quantity and quality of other CD8 T cell responses are affected by the presence or absence of other anti-viral responses.

As described above, many murine studies of immunodomination have used reverse-engineering to generate viruses lacking specific epitopes to look at the impact across epitope specificities. However, the impact of the loss of one MHCI gene on remaining polyclonal CD8 T cell responses with regard to immunodominance hierarchies has been under-studied. Of note, one relevant study by ven der Most et al. (2003) demonstrated significant shifts in the immunodominance hierarchy following chronic LCMV infection with the loss of the H-2D<sup>b</sup> allele (153). The loss of H-2D<sup>b</sup>, which would otherwise present the immunodominant H-2D<sup>b</sup>NP<sub>396</sub> and H-2D<sup>b</sup>GP<sub>33</sub> epitopes, resulted in the significant increase in the size of otherwise subdominant responses to H-2K<sup>b</sup>GP<sub>34</sub>, H2K<sup>b</sup>NP<sub>205</sub>, H-2K<sup>b</sup>NP<sub>235</sub> and H-2K<sup>b</sup>GP<sub>118</sub> epitopes. While MHC allele-specific immunodomination was clearly demonstrated in this chronic model, the impact of MHC allele-specific immunodomination in an acute model of infection and during secondary responses has not been addressed.

Although immunodomination remains a key determinant of CD8 T cell response magnitude during infection (discussed in **Section 1.7.5**), the factors that govern immunodomination are still unclear. IAV infection of C57BL/6 mice represents a highly

controlled model within which to dissect these factors. C57BL/6 mice co-dominantly express both H-2D<sup>b</sup> and H-2K<sup>b</sup> MHCI molecules and IAV infection results in a highly reproducible CD8 T cell immunodominance hierarchy following both primary and secondary challenge. This CD8 T cell response is generated against both H-2D<sup>b</sup> and H-2K<sup>b</sup>-restricted IAV-derived peptides (164, 169, 171, 175). In this chapter, I tracked compensatory shifts in the magnitude and quality of the CD8 T cell response following IAV infection in mice lacking either H-2D<sup>b</sup> or H-2K<sup>b</sup> MHCI molecules to ascertain how CD8 T cell responses restricted to one MHCI molecule impact on responses to another.

## 5.2. Results

### 5.2.1. Modest compensation in the magnitude of H-2D<sup>b</sup>NP<sub>366</sub> response after HKx31 virus infection

In order to determine the impact of a non-restricting MHC I molecule on a MHC I-restricted CD8 T cell population during infection, I infected WT, H-2D<sup>b</sup><sup>-/-</sup> and H-2K<sup>b</sup><sup>-/-</sup> mice with the HKx31 strain of influenza A virus (IAV) and measured the magnitude of epitope-specific responses 10 days post-infection using tetramer staining. Primary IAV infection of C57BL/6 mice results in a well-characterized CD8 T cell immunodominance hierarchy; larger responses are targeted against the H-2D<sup>b</sup>NP<sub>366</sub> and H-2D<sup>b</sup>PA<sub>224</sub> epitopes (immunodominant), and smaller, but significant responses against H-2D<sup>b</sup>PB1-F<sub>262</sub>, H-2K<sup>b</sup>PB1<sub>703</sub> and H-2K<sup>b</sup>NS<sub>2114</sub> (subdominant) (141, 251). It was the magnitude of these five largest CD8 T cell responses that were tracked following IAV infection: H-2D<sup>b</sup>NP<sub>366</sub>, H-2D<sup>b</sup>PA<sub>224</sub>, H-2D<sup>b</sup>PB1-F<sub>262</sub> responses in WT and H-2K<sup>b</sup><sup>-/-</sup> mice, and H-2K<sup>b</sup>-restricted H-2K<sup>b</sup>NS<sub>2114</sub> and H-2K<sup>b</sup>PB1<sub>703</sub> responses in WT and H-2D<sup>b</sup><sup>-/-</sup> mice (**Table 16**). It should be noted that IAV infection also results in a host of other peptide-specific CD8 T cell responses, all of which induce reproducibly minor responses that were not tracked in this study (75).

**Table 16:** Amino acid sequences and MHCI restriction of IAV-derived epitopes investigated in this study

Peptide	Amino acid sequence	MHCI restriction
NP <sub>366-374</sub>	ASNENMETM	H-2D <sup>b</sup>
PA <sub>224-233</sub>	SSLENFRAYV	H-2D <sup>b</sup>
PB1-F2 <sub>62-70</sub>	LSLRNPILV	H-2D <sup>b</sup>
NS2 <sub>114-121</sub>	RTFSFQLI	H-2K <sup>b</sup>
PB1 <sub>703-711</sub>	SSYRRPVGI	H-2K <sup>b</sup>

First, I characterized of the number of CD8 T cells in the spleens and lungs of WT, H-2K<sup>b</sup><sup>-/-</sup> and H-2D<sup>b</sup><sup>-/-</sup> mice 10 days after HKx31 infection. In the spleens of uninfected mice, the loss of H-2K<sup>b</sup> and H-2D<sup>b</sup> reduced the number of peripheral CD8 T cells by approximately 40% and 60%, respectively, due to the loss of each of the CD8 T cell populations restricted to these alleles (**Section 4.4.2**) (250). In the spleen of IAV infected mice, the loss of one MHCI gene (H-2K<sup>b</sup> or H-2D<sup>b</sup>) resulted in a similar ~60% and ~45% reduction in CD8 T cell numbers (**Figure 29A**), which is most likely due to the lower starting number of naïve CD8 T cells. In contrast, in the lungs of IAV infected mice, there were similar numbers of CD8 T cells in WT, H-2K<sup>b</sup><sup>-/-</sup> and H-2D<sup>b</sup><sup>-/-</sup> mice (~1.5 x 10<sup>5</sup> CD8 T cells per mouse), all of which were significantly higher than uninfected WT mice (p = 0.016). This illustrates that the loss of one MHCI gene does not impair the recruitment of CD8 T cells to the site of infection (**Figure 29B**).

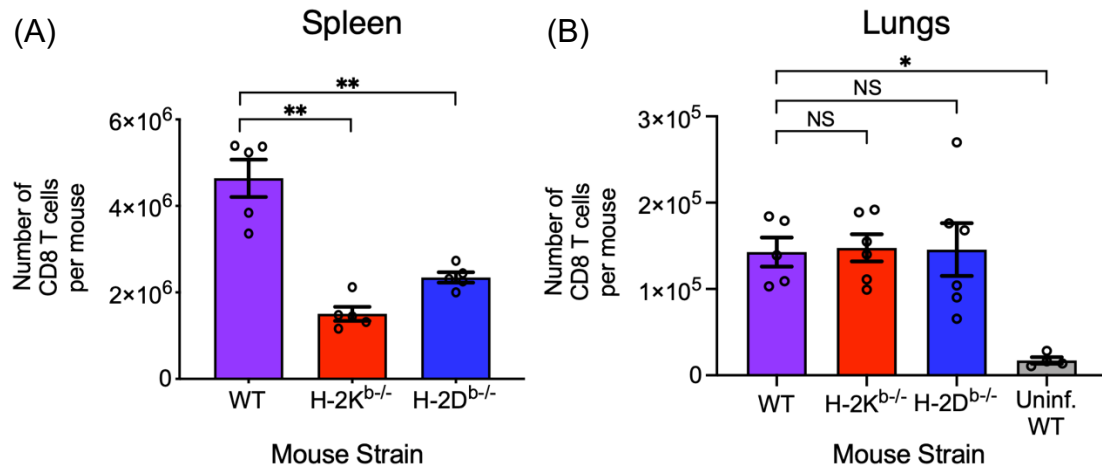


**Figure 29:** Absolute numbers of CD8 T cells in IAV-infected WT, H-2K<sup>b</sup><sup>-/-</sup> and H-2D<sup>b</sup><sup>-/-</sup> mice at day 10 post-infection. Total CD8 T cells were enumerated in the (A) spleen and (B) lungs of IAV-infected WT (purple), H-2K<sup>b</sup><sup>-/-</sup> (red) and H-2D<sup>b</sup><sup>-/-</sup> (blue) mice 10 days after IAV infection. The lungs of uninfected WT mice (grey) were used as a control. \*\* indicates  $p \leq 0.01$ , NS indicates  $p > 0.05$  (Mann-Whitney test). For all panels, lines and error bars represent mean +/- SEM. These results are representative of 3 independent experiments with  $n = 5$  per group.

In H-2D<sup>b</sup><sup>-/-</sup> mice, analysis of the IAV antigen-specific populations revealed a significant increase in the proportion of H-2K<sup>b</sup>NS<sub>2114</sub> and H-2K<sup>b</sup>PB<sub>1703</sub> CD8 T cells in both the spleens and lungs relative to WT mice (**Figure 30A, E**). However, the increase in frequency reflected only a trend for increased numbers of antigen-specific CD8 T cells (**Figure 30C, G**) that was not significant ( $p = 0.20$  for H-2K<sup>b</sup>NS<sub>2114</sub> and  $p = 0.30$  for H-2K<sup>b</sup>PB<sub>1703</sub> responses). In H-2K<sup>b</sup><sup>-/-</sup> mice, the frequency of H-2D<sup>b</sup>NP<sub>366</sub>-specific cells was significantly increased in the spleen ( $p = 0.0159$ ), but only showed an increase trend in the lungs, compared to WT mice (**Figure 30B, F**), and neither of which translated to significantly increased numbers of cells **Figure 30D, H**). In contrast, the frequency of H-2D<sup>b</sup>PA<sub>224</sub>- and H-2D<sup>b</sup>PB1-F<sub>262</sub>-specific CD8 T cells did not change in the spleen in H-2K<sup>b</sup><sup>-/-</sup> mice. In the lungs, however, there was a significant increase in frequency but not numbers of H-2D<sup>b</sup>PA<sub>224</sub>- and H-2D<sup>b</sup>PB1-F<sub>262</sub>-specific CD8 T cells

in H-2K<sup>b</sup><sup>-/-</sup> mice. Collectively, these data indicate that IAV infection of mice lacking either H-2K<sup>b</sup> or H-2D<sup>b</sup> does not appear to markedly or significantly alter the absolute magnitude of the remaining epitope-specific populations in the spleen and lungs following primary acute infection.

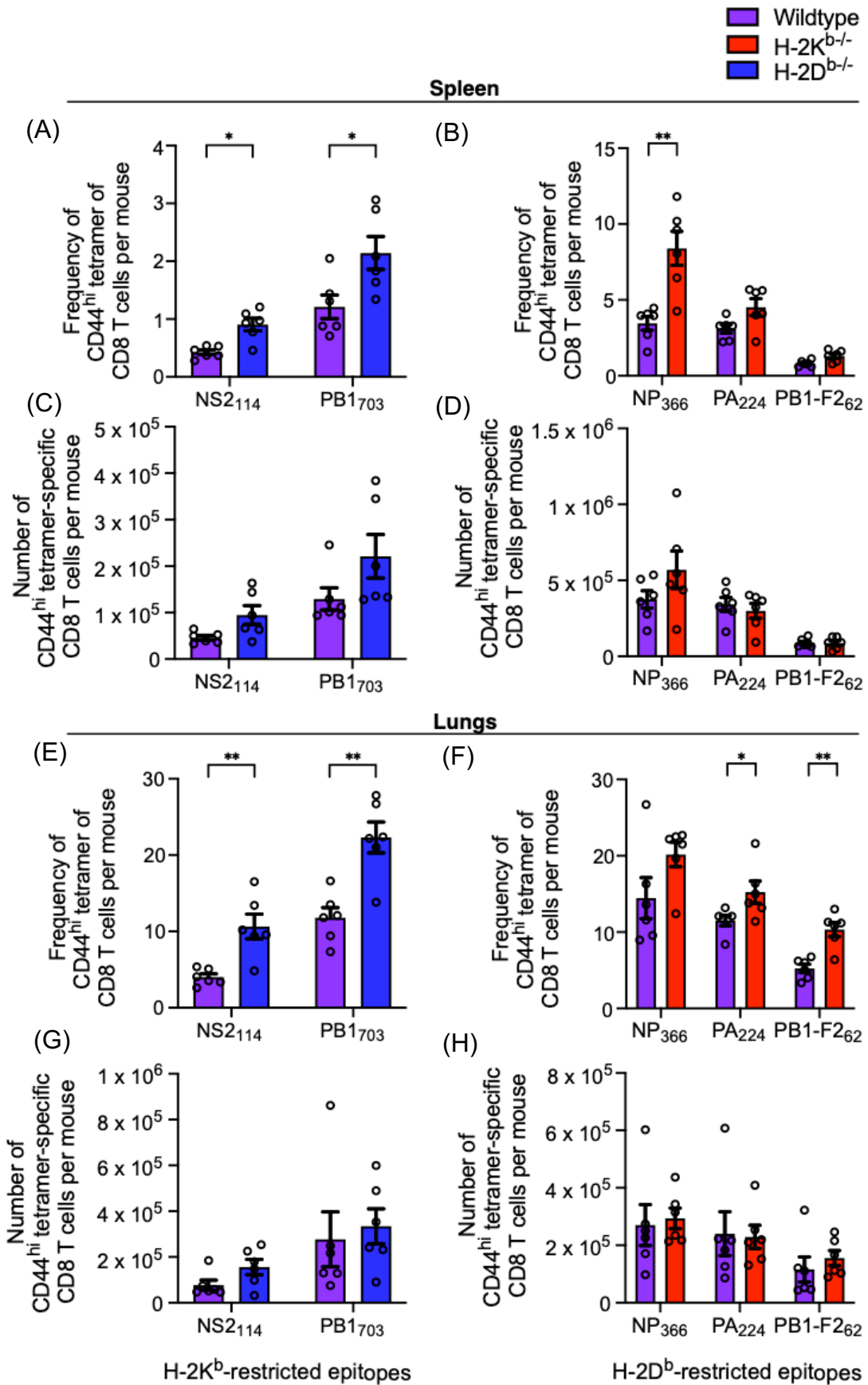


**Figure 30:** Magnitude of epitope-specific CD8 T cell responses after intranasal (i.n.) infection with  $10^4$  pfu of HKx31 virus. The frequency (A, B, E, F) and number (C, D, G, H) of H-2K<sup>b</sup>-restricted (A, C, E, G) and H-2D<sup>b</sup>-restricted (B, D, F, H) epitope-specific CD8 T cells were measured in the spleen (A, B, C, D) and lungs (E, F, G, H) of WT (purple), H-2D<sup>b/-</sup> (blue) and H-2K<sup>b/-</sup> (red) mice at 10 days post-infection. \*\* indicates  $p \leq 0.01$ , \* indicates  $p \leq 0.05$  (Mann-Whitney test). For all panels, lines and error bars represent mean  $\pm$  SEM. These results are representative of 2 independent experiments with  $n = 6$  mice per group

I then measured the functional capacity of antigen-specific CD8 T cell populations from H-2D<sup>b/-</sup> and H-2K<sup>b/-</sup> mice during an IAV-driven immune response by measuring the ability to secrete IFN $\gamma$ , TNF and IL-2. Simultaneous secretion of multiple cytokines has been previously shown to correlate with increased T cell-mediated immune protection (284). Splenocytes of infected mice were re-stimulated directly *ex vivo* for 5hrs with specific peptides and the level of IFN $\gamma$ , TNF and IL-2 was assessed by intracellular cytokine staining and flow cytometry (**Figure 31A**). I then used Boolean gating to identify CD8 T cells that were 1+ (producing a single cytokine, predominantly IFN $\gamma$ ) 2+ (producing two cytokines, predominantly IFN $\gamma$  and TNF) or 3+ (producing IFN $\gamma$ , TNF and IL-2).

In WT mice, each epitope-specific population exhibited distinct cytokine profiles after IAV infection. For the H-2D<sup>b</sup>-restricted responses, H-2D<sup>b</sup>NP<sub>366</sub>-specific CD8 T cells had a higher proportions of 1+ cells, while H-2D<sup>b</sup>PA<sub>224</sub> and H-2D<sup>b</sup>PB1-F2<sub>62</sub>-specific CD8 T cells had a higher proportion of 3+ cells (**Figure 31B**), as has been seen in previous studies (173, 251). For the H-2K<sup>b</sup>-restricted responses, H-2K<sup>b</sup>NS<sub>214</sub> and H-2K<sup>b</sup>PB1<sub>703</sub> CD8 T cells had a higher proportion of 1+ cells (**Figure 31C**), again as has been seen in previous studies (170).

When H-2D<sup>b</sup>-restricted cytokine responses were assessed in H-2K<sup>b/-</sup> mice, profiles were similar to WT mice (**Figure 31B**). Specifically, the proportions of 1+ cells was similar between WT and H-2K<sup>b/-</sup> mice for H-2D<sup>b</sup>NP<sub>366</sub>- (WT 42.5%, H-2K<sup>b/-</sup> 37.9%), H-2D<sup>b</sup>PA<sub>224</sub>- (WT 30.5%, H-2K<sup>b/-</sup> 24.5%) and H-2D<sup>b</sup>-PB1-F2<sub>62</sub>-specific CD8 T cells (WT 41.4%, H-2K<sup>b/-</sup> 35.7%). The proportions of 3+ cells were also similar for H-

2D<sup>b</sup>NP<sub>366</sub><sup>-</sup> (WT 24.4%, H-2K<sup>b/-</sup> 26.5%), H-2D<sup>b</sup>PA<sub>224</sub><sup>-</sup> (WT 40.5%, H-2K<sup>b/-</sup> 43.1%) and H-2D<sup>b</sup>PB1-F2<sub>62</sub>-specific CD8 T cells (WT 30.7%, H-2K<sup>b/-</sup> 30.1%) (**Figure 31B**).

When H-2K<sup>b</sup>-restricted cytokine responses were assessed in H-2D<sup>b/-</sup> mice, profiles were again similar to WT mice (**Figure 31C**). Specifically, the proportion of 1+ CD8 T cells in H-2K<sup>b</sup>NS2<sub>114</sub> (WT 59.6%, H-2D<sup>b/-</sup> 61.8%) and H-2K<sup>b</sup>PB1<sub>703</sub> (WT 71.1%, H-2D<sup>b/-</sup> 65.5%), and 3+ CD8 T cells in H-2K<sup>b</sup>NS2<sub>114</sub> (WT 18.3%, H-2D<sup>b/-</sup> 21.9%) and H-2K<sup>b</sup>PB1<sub>703</sub> (WT 9.7%, H-2D<sup>b/-</sup> 9.1%) populations were similar (**Figure 31C**).

These data therefore demonstrate that the loss of H-2K<sup>b</sup> and H-2D<sup>b</sup> does not result in the qualitative compensation of H-2D<sup>b</sup>- and H-2K<sup>b</sup>-restricted responses, respectively. This is consistent with the absence of any significant quantitative shift in epitope-specific CD8 T cell responses (**Figure 30**). Collectively, this demonstrates that the loss of a non-restricting MHC I did not have a significant impact on quantitative or qualitative features of epitope-specific CD8 T cell responses during IAV infection.

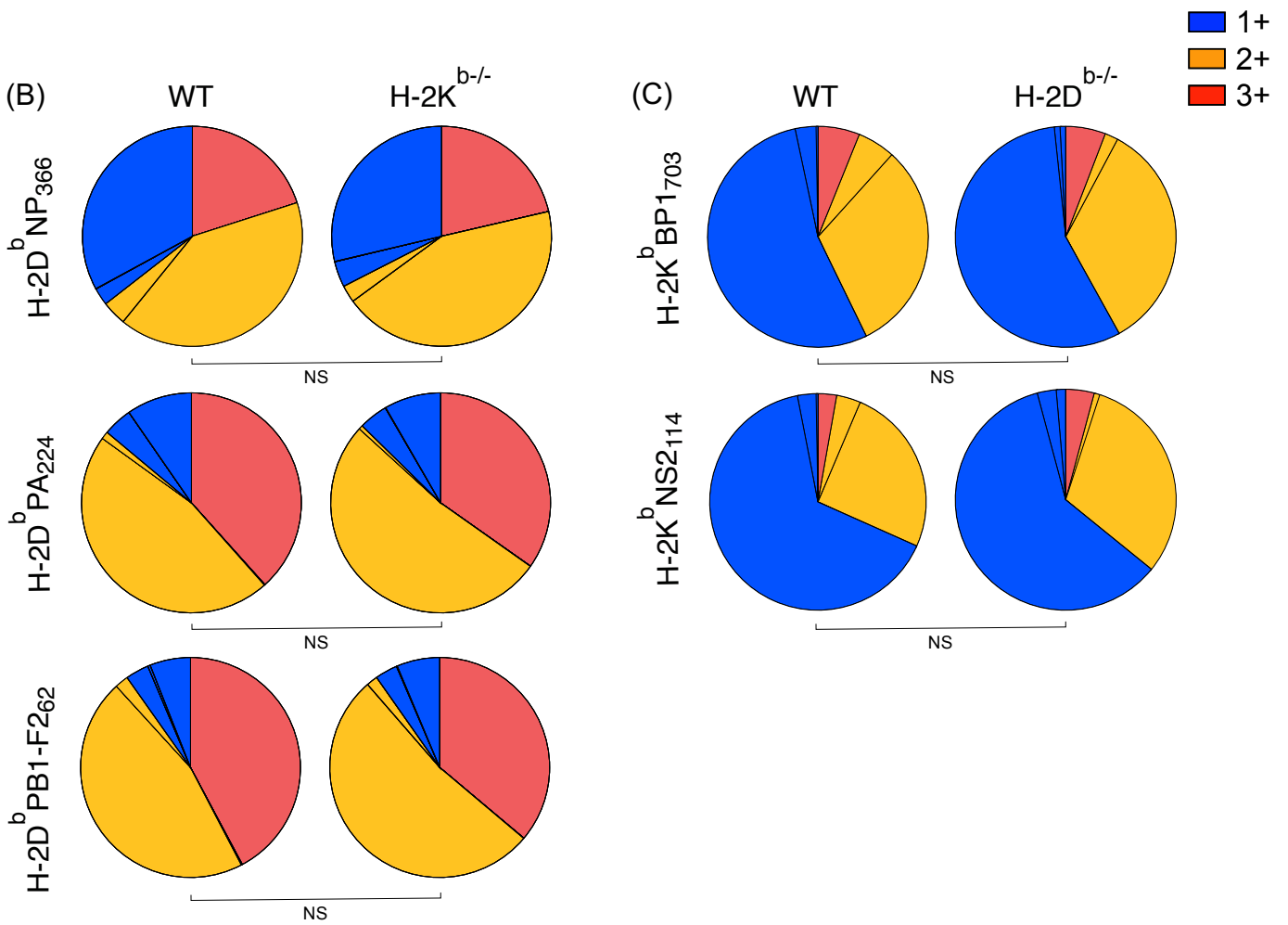
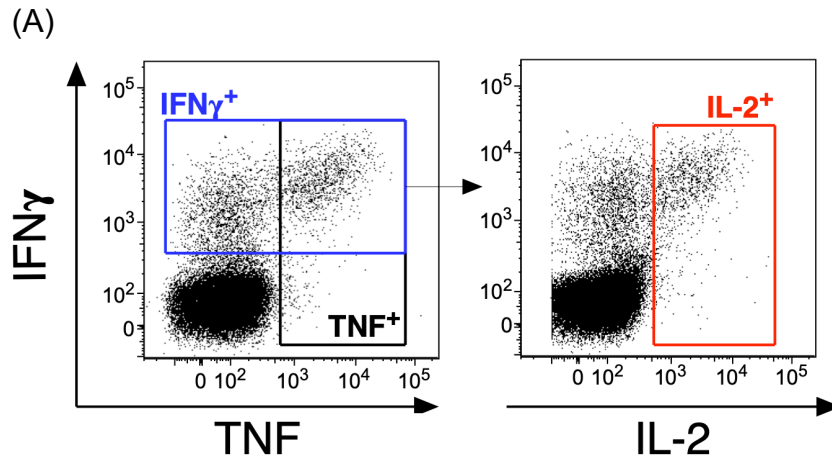


**Figure 31:** Cytokine production by epitope-specific CD8 T cells at 10 days after i.n. infection with  $10^4$  pfu HKx31 virus. (A) Representative dot plot of cytokine-producing H-2D<sup>b</sup>NP<sub>366</sub>-specific CD8 T cells isolated from WT mice. Splenocytes from infected (A and B) WT, (A) H-2K<sup>b/-</sup> and (B) H-2D<sup>b/-</sup> mice were re-stimulated for 5hrs with NP<sub>366</sub>, PA<sub>224</sub>, PB1-F2<sub>62</sub>, PB1<sub>703</sub> or NS2<sub>114</sub> peptides directly *ex vivo* 10 days post-infection. Colours represent the secretion of a single cytokine (predominantly IFN $\gamma$ ) (blue), two cytokines (predominantly IFN $\gamma$  and TNF) (orange) and all three cytokines (red). Cells are gated on single live, CD4<sup>-</sup>, CD8<sup>+</sup> lymphocytes. NS indicates  $p > 0.05$  (Wilcoxon rank sum test). These results are representative of 2 independent experiments with  $n = 6$  per group.

### 5.2.2. Compensation by the immunodominant H-2D<sup>b</sup>NP<sub>366</sub> and H-2K<sup>b</sup>Ova<sub>257</sub> CD8

#### T cell responses in mice lacking the alternative MHC gene, after primary acute infection with IAV-Ova virus

One limitation with the WT IAV infection lies in the fact that the H-2K<sup>b</sup>-restricted responses are all subdominant, and therefore removal of these may be insufficient to drive compensatory H-2D<sup>b</sup>-restricted responses and where minor shifts in the magnitude of these small responses (in the absence of H-2D<sup>b</sup>) may fall below our limit of detection. To better assess the effect of H-2D<sup>b</sup> on H-2K<sup>b</sup>-restricted responses, I used IAVs that have been engineered to express an H-2K<sup>b</sup>-restricted immunodominant epitope derived from ovalbumin (OVA<sub>257-264</sub>, SIINFEKL) in the neuraminidase stalk (HKx31-Ova and PR8-Ova) (163).

Because the HKx31 and PR8 IAVs are serologically distinct but share the same internal ribonucleoprotein components (284), mice can be primed and challenged with these strains (**Figure 32A**) for analysis of secondary CD8 T cell responses against conserved internal antigens (165) in the absence of cross-protective antibody responses. This is particularly advantageous in the study of immunodomination since secondary responses may amplify any modest differences in CD8 T cell epitope-specific populations that are seen after primary responses.

Infection with either HKx31-Ova or PR8-Ova gives rise to an immunodominant H-2K<sup>b</sup>Ova<sub>257</sub>-specific CD8 T cell response similar to the magnitude of the H-2D<sup>b</sup>NP<sub>366</sub>-specific response and larger than the response directed toward H-2D<sup>b</sup>PA<sub>224</sub> following both primary and secondary challenge with Ova<sub>257</sub>-expressing IAV (163). I therefore

used the OVA<sub>257</sub>-expressing IAVs to study the impact of an immunodominant H-2K<sup>b</sup>-restricted response on H-2D<sup>b</sup> restricted responses, and *vice versa*, during the acute primary, long term memory, and secondary response to infection.

Weight loss, used to indicate the severity of infection, was similar across WT, H-2K<sup>b</sup><sup>-/-</sup> and H-2D<sup>b</sup><sup>-/-</sup> mice following both primary and secondary infection with IAV-Ova, with all groups showing moderate weight loss over the course of infection, and full recovery of their original weight at days 10 and 7 after primary and secondary infection, respectively (**Figure 32B, C**). This indicates that the loss of IAV-specific CD8 T cells that are restricted by one or the other MHC I molecule does not impair the ability to recover from IAV infection.

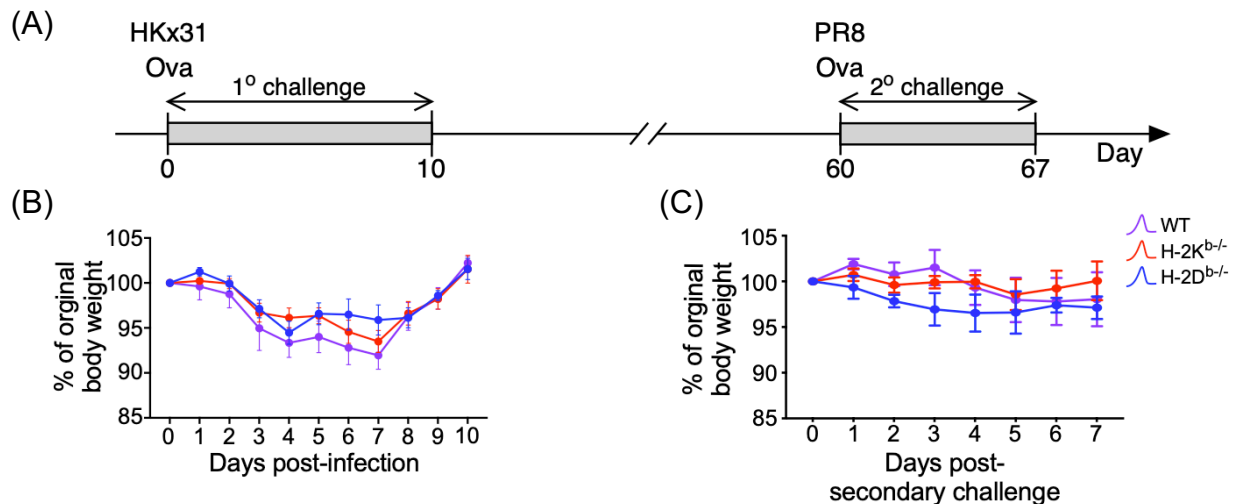


**Figure 32:** Timeline and weight loss following i.n. primary and i.n. secondary challenge with HKx31-Ova and PR8-Ova IAV, respectively. (A) Mice were primed i.n. with 10<sup>4</sup> pfu of HKx31-Ova and rechallenged i.n. with 10<sup>3</sup> pfu of PR8-Ova virus at 60 days post-infection. Analysis of the primary and secondary immune responses were performed 10 and 7 days post-primary or -secondary challenge, respectively. (B) Percentage of original body weight at day 0 of WT (purple), H-2K<sup>b</sup><sup>-/-</sup> (red) and H-2D<sup>b</sup><sup>-/-</sup> (blue) mice following primary and secondary IAV infection. These results are representative of 2 independent experiments with *n* = 5 per group.

I then measured the peak magnitude of epitope-specific CD8 T cell responses following primary challenge with HKx31-Ova. In the spleens and lungs of H-2D<sup>b-/-</sup> mice, there was no significant change in either the frequency or number of H-2K<sup>b</sup>NS2<sub>114</sub> and H-2K<sup>b</sup>PB1<sub>703</sub>-specific CD8 T cells after infection (**Figure 33A, C, E, G**). There was, however, a striking 3- to 4-fold increase in the frequency and number of H-2K<sup>b</sup>Ova<sub>257</sub>-specific CD8 T cells in both the spleen and lung of H-2D<sup>b-/-</sup> mice compared to WT mice (**Figure 33A, C, E, G**). This demonstrates that the loss of the H-2D<sup>b</sup>-restricted responses, including the immunodominant H-2D<sup>b</sup>NP<sub>366</sub>- and H-2D<sup>b</sup>PA<sub>224</sub>-specific responses, resulted in preferential compensation by the immunodominant H-2K<sup>b</sup>Ova<sub>257</sub> response.

In the spleens of H-2K<sup>b-/-</sup> mice, there was a significant increase in the frequencies and a trend for increased numbers (although not significant) for all H-2D<sup>b</sup>-restricted epitope-specific CD8 T cell populations analysed (**Figure 33B, D**). The loss of H-2K<sup>b</sup> appeared to drive a more marked increase in the H-2D<sup>b</sup>NP<sub>366</sub> specific population, compared to the H-2D<sup>b</sup>PA<sub>224</sub> or H-2D<sup>b</sup>-PB1-F2<sub>62</sub> specific populations. A similar result was observed in the lungs of infected animals (**Figure 33F, H**), with a greater impact of H-2K<sup>b</sup> loss on H-2D<sup>b</sup>NP<sub>366</sub>-specific, compared to H-2D<sup>b</sup>PA<sub>224</sub>- and H-2D<sup>b</sup>PB1-F2<sub>62</sub>-specific CD8 T cell responses. Collectively, these data suggest that the immunodominant H-2D<sup>b</sup>NP<sub>366</sub> response is modestly more susceptible than other H-2D<sup>b</sup>-restricted responses to immunodomination by H-2K<sup>b</sup> responses.

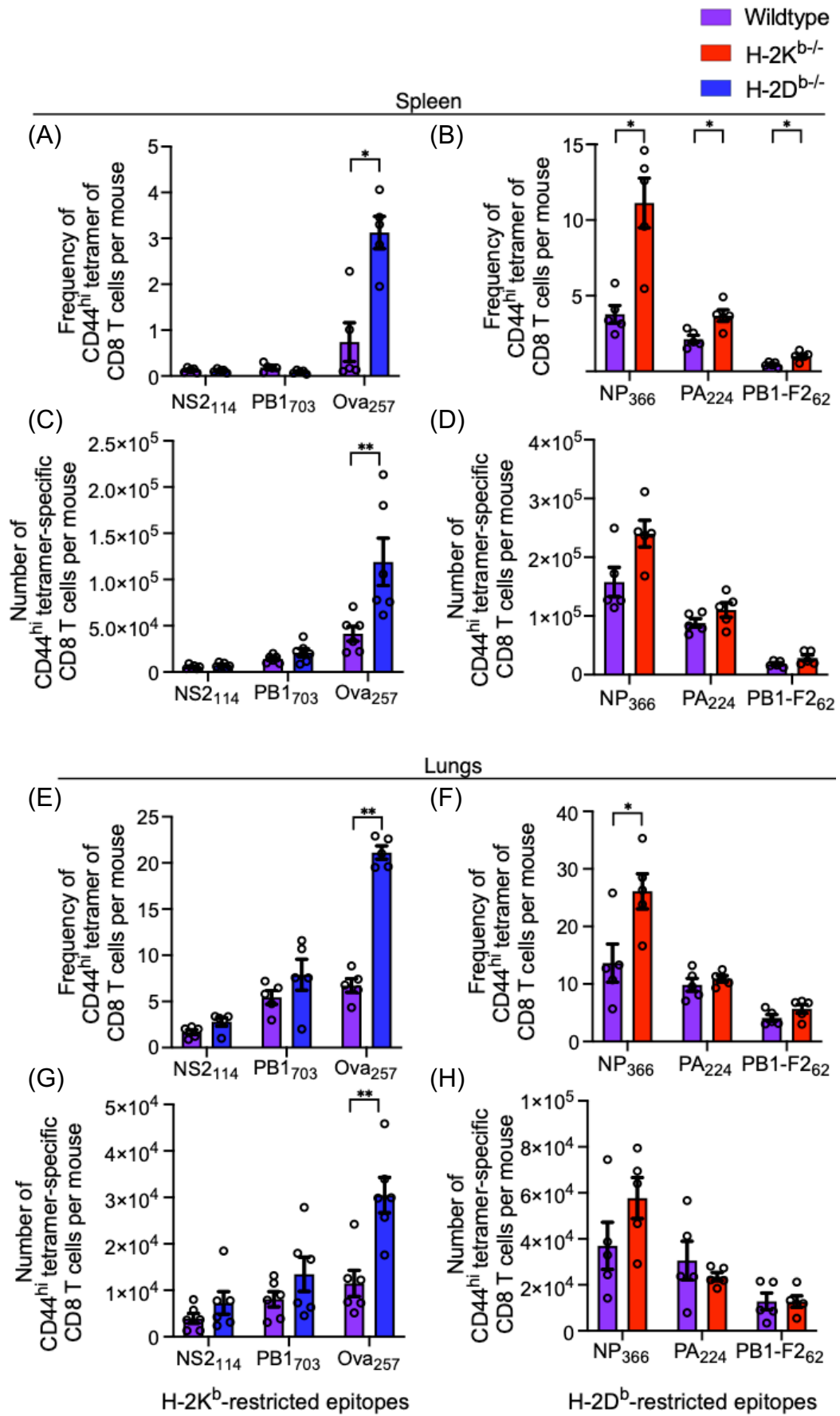


**Figure 33:** Magnitude of epitope-specific CD8 T cell responses after i.n. infection with  $10^4$  pfu of HKx31-Ova virus. The frequency (A, B, E, F) and number (C, D, G, H) of H-2K<sup>b</sup>- (A, C, E, G) and H-2D<sup>b</sup> (B, D, F, H) epitope-specific CD8 T cells were measured in the spleen (A, B, C, D) and lungs (E, F, G, H) of WT (purple), H-2D<sup>b/-</sup> (blue) and H-2K<sup>b/-</sup> (red) mice 10 days post-infection. \*\* indicates  $p \leq 0.01$ , \* indicates  $p \leq 0.05$ . For all panels, lines and error bars represent mean  $\pm$  SEM. These results are representative of 2 independent experiments with  $n = 5$  per group.

---

### 5.2.3. Impaired IAV-specific CD8 T cell memory formation in mice lacking H-2D<sup>b</sup>, but not H-2K<sup>b</sup>

I next assessed the relative ability of CD8 T cells to form memory populations in the presence or absence of the non-restricting MHCI molecule. WT, H-2K<sup>b</sup><sup>-/-</sup> and H-2D<sup>b</sup><sup>-/-</sup> mice were infected with HKx31-Ova virus and memory CD8 T cell populations were assessed 60 days later.

In the spleens of H-2D<sup>b</sup><sup>-/-</sup> mice, the frequency of H-2K<sup>b</sup>NS2<sub>114</sub>, H-2K<sup>b</sup>PB1<sub>703</sub> and H-2K<sup>b</sup>Ova<sub>257</sub>-specific CD8 T cells in the spleen was comparable to WT mice (**Figure 34A**), despite the observation of markedly higher frequencies of H-2K<sup>b</sup>Ova<sub>257</sub>-specific CD8 T cells at day 10 (**Figure 33A**). In the lungs, the frequency of all of the epitope-specific populations was significantly reduced in H-2D<sup>b</sup><sup>-/-</sup> mice relative to WT mice (**Figure 34E**). When numbers of epitope-specific CD8 T cells were assessed, there was a significant reduction for all epitope-specificities in both the spleen and lung for H-2D<sup>b</sup><sup>-/-</sup> mice compared to WT mice (**Figure 33C, G**). Thus, despite an augmented effector response, particularly in the H-2K<sup>b</sup>Ova<sub>257</sub>-specific CD8 T cell population, H-2K<sup>b</sup>-restricted memory formation was drastically impaired in the absence of H-2D<sup>b</sup>.

By contrast, in the spleens of H-2K<sup>b</sup><sup>-/-</sup> mice, the frequencies of H-2D<sup>b</sup>NP<sub>366</sub>- (WT 0.3%, H-2K<sup>b</sup><sup>-/-</sup> 0.9%), H-2D<sup>b</sup>PA<sub>224</sub>- (WT 0.1%, H-2K<sup>b</sup><sup>-/-</sup> 0.4%) and H-2D<sup>b</sup>PB1-F<sub>262</sub>- (WT 0.07%, H-2K<sup>b</sup><sup>-/-</sup> 0.2%) specific CD8 T cells were all significantly increased in the spleen (**Figure 34B**). These populations also trended towards an increase in the lungs (H-2D<sup>b</sup>NP<sub>366</sub>: WT 2.8%, H-2K<sup>b</sup><sup>-/-</sup> 5.2%; H-2D<sup>b</sup>PA<sub>224</sub>: WT 1.7%, H-2K<sup>b</sup><sup>-/-</sup> 2.3%; H-2D<sup>b</sup>PB1-F<sub>262</sub> WT 0.7%, H-2K<sup>b</sup><sup>-/-</sup> 1.9%) (**Figure 34F**), largely recapitulating the relative

differences observed during the effector response (**Figure 30B, F**). Despite this, the loss of H-2K<sup>b</sup> did not alter the absolute number of epitope-specific memory CD8 T cells in either the spleen or lung (**Figure 34D, H**). Taken together, this highlights a distinct variation in the biology of H-2D<sup>b</sup> and H-2K<sup>b</sup>, with H-2D<sup>b</sup> selectively influencing the memory formation of H-2K<sup>b</sup>-restricted memory populations to a larger extent than H-2K<sup>b</sup> influences the H-2D<sup>b</sup>-restricted memory population.

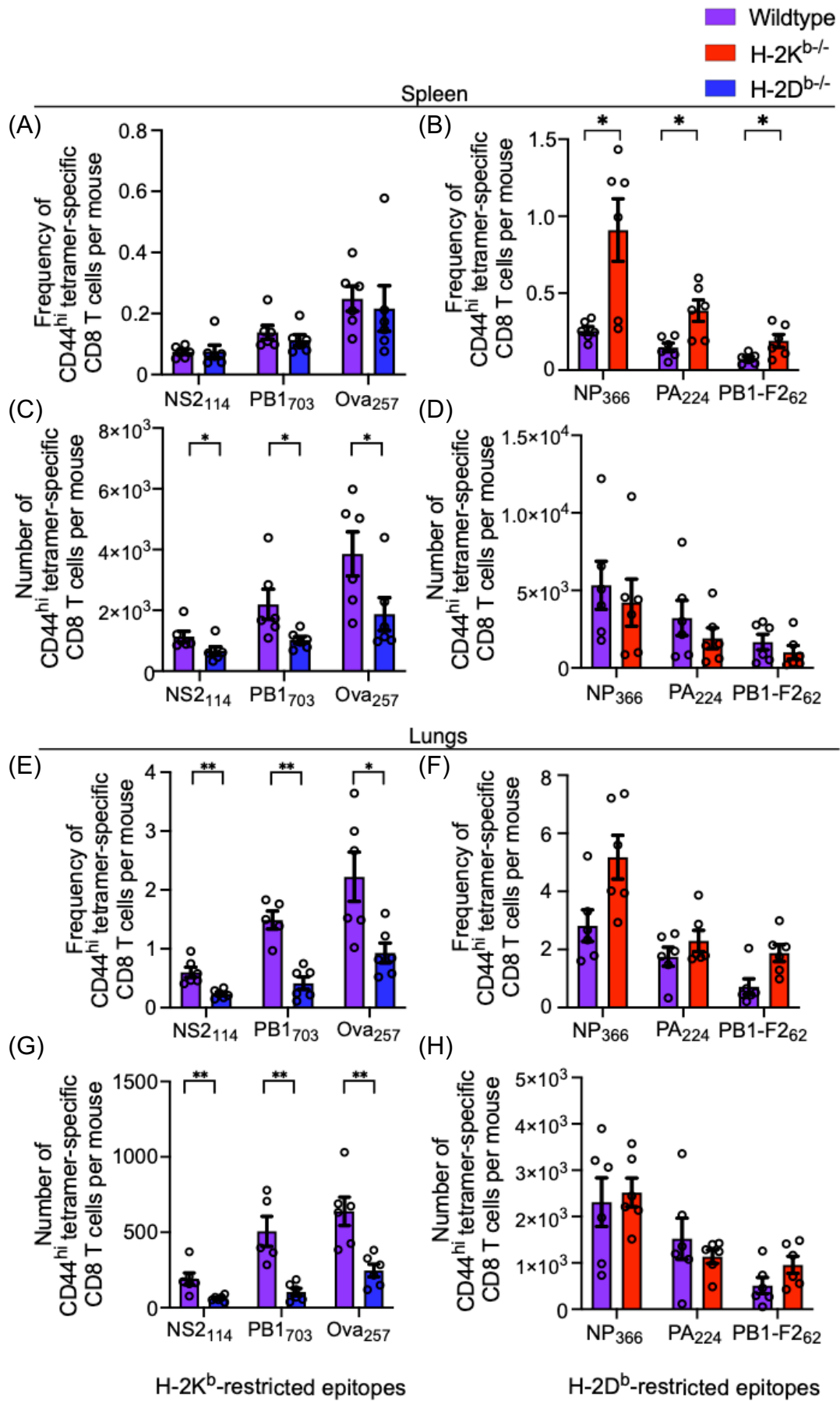


**Figure 34:** Magnitude of epitope-specific memory CD8 T cell populations 60 days after i.n. primary acute infection with  $10^4$  pfu of HKx31-Ova virus. The frequency (A, B, E, F) and number (C, D, G, H) of H-2K<sup>b</sup>- (A, C, E, G) and H-2D<sup>b</sup> (B, D, F, H) epitope-specific CD8 T cells were measured in the spleen (A, B, C, D) and lungs (E, F, G, H) of WT (purple), H-2D<sup>b/-</sup> (blue) and H-2K<sup>b/-</sup> (red) 60 days post-infection. \*\* indicates  $p \leq 0.01$ , \* indicates  $p \leq 0.05$  (Mann Whitney test). For all panels, lines and error bars represent mean +/- SEM. These results are representative of 3 independent experiments with  $n = 6$  per group.

#### 5.2.4. The H-2K<sup>b</sup>Ova<sub>257</sub>-specific CD8 T cell response is markedly augmented in H-2D<sup>b/-</sup> mice after secondary challenge with PR8-Ova virus

I then assessed the ability of IAV-primed WT, H-2K<sup>b/-</sup> and H-2D<sup>b/-</sup> mice to mount secondary responses when challenged with PR8-Ova virus. Mice were primed with HKx31-Ova virus then challenged with PR8-Ova 60 days later, and analysed 7 days post-secondary infection.

In WT mice, the immunodominant H-2D<sup>b</sup>NP<sub>366</sub> and H-2K<sup>b</sup>Ova<sub>257</sub>-specific CD8 T cell responses comprised most of the secondary CD8 T cell response (**Figure 35C, D, G, H**). As has been observed previously, the H-2D<sup>b</sup>PA<sub>224</sub>-specific CD8 T cell response becomes subdominant and the H-2K<sup>b</sup>NS<sub>2114</sub><sup>-</sup>, H-2K<sup>b</sup>PB1<sub>703</sub><sup>-</sup> and H-2D<sup>b</sup>PB1-F<sub>262</sub>-specific CD8 T cell responses remain subdominant following secondary infection (171).

In the spleens of H-2D<sup>b/-</sup> mice, the frequencies and numbers of H-2K<sup>b</sup>PB1<sub>703</sub> and H-2K<sup>b</sup>Ova<sub>257</sub><sup>-</sup>, but not H-2K<sup>b</sup>NS<sub>2114</sub><sup>-</sup>-specific CD8 T cells, were significantly increased in the spleen compared to WT mice (**Figure 35A, C**). In the lungs, while the frequencies of H-2K<sup>b</sup>PB1<sub>703</sub><sup>-</sup>, H-2K<sup>b</sup>NS<sub>2114</sub><sup>-</sup> and H-2K<sup>b</sup>Ova<sub>257</sub>-specific CD8 T cells were significantly increased (**Figure 35E**), only the number of H-2K<sup>b</sup>Ova<sub>257</sub>-specific CD8 T cells was significantly increased in H-2D<sup>b/-</sup> mice compared to WT mice (**Figure 35G**).

In the spleens of H-2K<sup>b/-</sup> mice, the frequencies of H-2D<sup>b</sup>NP<sub>366</sub>, H-2D<sup>b</sup>PA<sub>224</sub> and H-2D<sup>b</sup>PB1-F<sub>262</sub>-specific CD8 T cells were significantly increased in the spleen (**Figure 35B**), but the absolute number of cells was comparable to WT mice (**Figure 35D**). In

the lungs, the frequency and number of epitope-specific CD8 T cells was again comparable to WT mice (**Figure 35F, H**).

Of note, there was a marked 5- to 10-fold increase in the frequency and number of H-2K<sup>b</sup>Ova<sub>257</sub>-specific CD8 T cells in the spleens and lungs of H-2D<sup>b/-</sup> mice compared to WT mice following secondary challenge. This is notable as these cells have expanded dramatically during the secondary response, despite their impaired ability to form a memory population in H-2D<sup>b/-</sup> mice (**Figure 34A, C, E, G**). Given the low number of H-2K<sup>b</sup>Ova<sub>257</sub>-specific CD8 T cells in H-2D<sup>b/-</sup> mice at the memory timepoint, these cells must expand to an even larger extent, thereby amplifying the effect of compensation on secondary H-2K<sup>b</sup>Ova<sub>257</sub>-specific CD8 T cell responses. This also suggests that there is a qualitative shift in memory H-2K<sup>b</sup>Ova<sub>257</sub>-specific CD8 T cells with the loss of H-2D<sup>b</sup>.

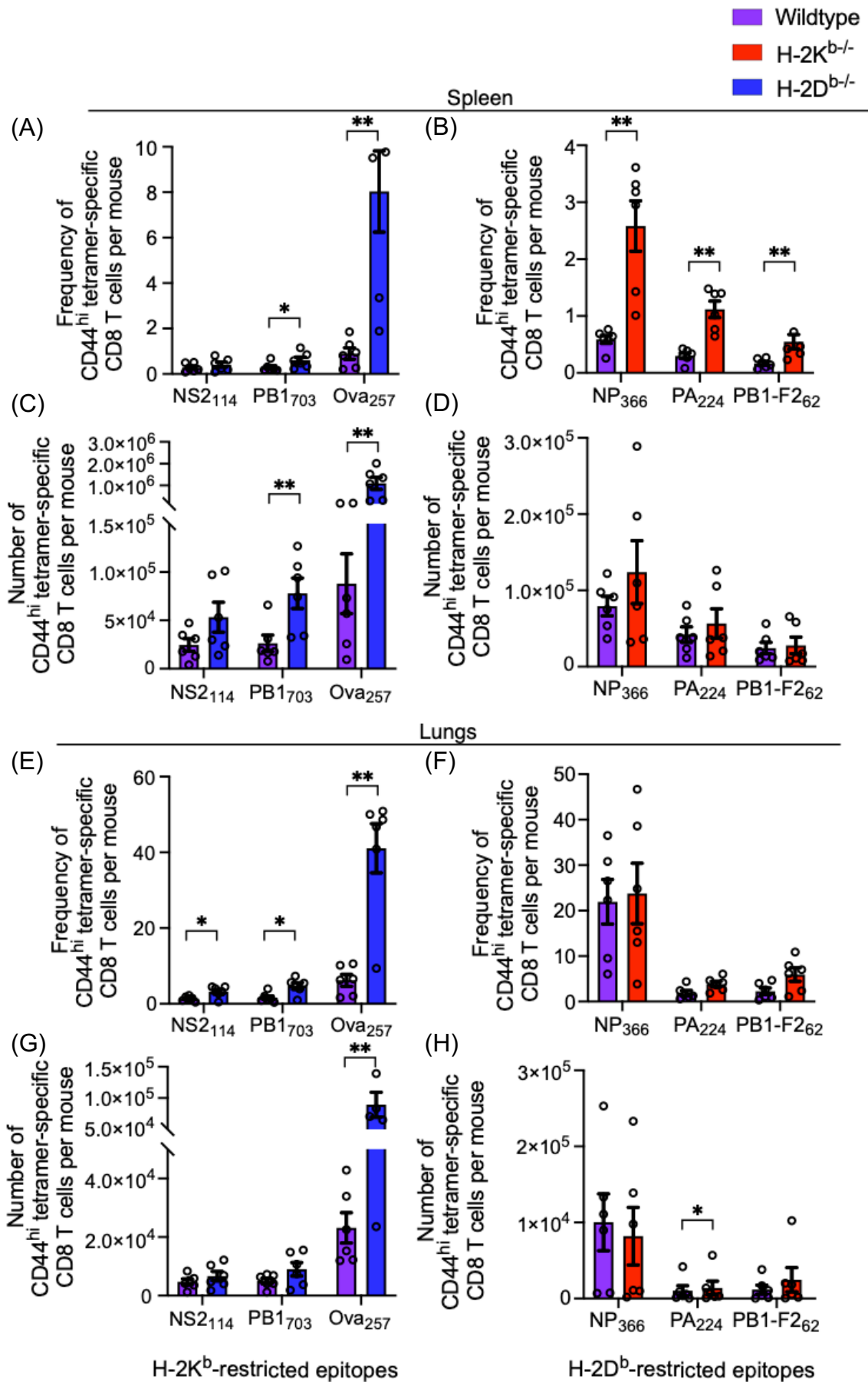


**Figure 35:** Magnitude of epitope-specific CD8 T cell responses after i.n. prime and i.n. challenge with  $10^4$  pfu of HKx31-Ova and  $10^4$  pfu of PR8-Ova viruses, respectively. The frequency (A, B, E, F) and number (C, D, G, H) of H-2K<sup>b</sup>- (A, C, E, G) and H-2D<sup>b</sup> (B, D, F, H) epitope-specific CD8 T cells were measured in the spleen (A, B, C, D) and lungs (E, F, G, H) of WT (purple), H-2D<sup>b/-</sup> (blue) and H-2K<sup>b/-</sup> (red) mice 7 days post-secondary infection. \*\* indicates  $p \leq 0.01$ , \* indicates  $p \leq 0.05$ . For all panels, lines and error bars represent mean +/- SEM. These results are representative of 2 independent experiments with  $n = 6$  per group.

### 5.2.5. Quality of compensatory H-2D<sup>b</sup>NP<sub>366</sub> and H-2K<sup>b</sup>Ova<sub>257</sub> responses are similar to those observed in WT mice following IAV-Ova infection

To assess one aspect of the quality of epitope-specific CD8 T cells, I measured their ability to produce cytokines after short term peptide re-stimulation, as previously described (**Section 5.2.1**). I took lymphocytes from spleens and lungs of mice at days 10 (peak primary) or 60 (memory) after HKx31-Ova infection, and 7 days after PR8-Ova infection (peak secondary) and measured IFN $\gamma$ , TNF and IL-2 cytokine production.

At peak primary infection with HKx31-Ova, the proportions of 1+ and 3+ CD8 T cells were similar for H-2D<sup>b</sup>NP<sub>366</sub><sup>-</sup>, H-2D<sup>b</sup>PA<sub>224</sub><sup>-</sup> and H-2D<sup>b</sup>PB1-F<sub>262</sub> in the spleen and lung of H-2K<sup>b</sup><sup>-/-</sup> mice as compared to WT mice (**Figure 36A, C**). Likewise, the proportions of 1+ and 3+ CD8 T cells were similar for H-2K<sup>b</sup>PB1<sub>703</sub> and H-2K<sup>b</sup>NS<sub>2114</sub> in the spleens and lungs of H-2D<sup>b</sup><sup>-/-</sup> mice compared to WT mice (**Figure 36B, D**). This is also consistent with observations with the parental HKx31 (**Figure 31**) and it indicates that the inclusion of the Ova<sub>257</sub> epitope during IAV infection does not alter the cytokine profile of IAV epitope-specific responses.

At peak primary infection for H-2K<sup>b</sup>Ova<sub>257</sub>-specific CD8 T cells in WT mice, the frequencies of 1+ and 3+ cells (**Figure 36B, D**) were similar to that seen in previous studies (163). In H-2D<sup>b</sup><sup>-/-</sup> mice, the frequencies of 1+ and 3+ cells were similar to WT mice, indicating that the quality of H-2K<sup>b</sup>Ova<sub>257</sub>-specific responses is unaffected by the loss of H-2D<sup>b</sup>-restricted responses during HKx31-Ova infection (**Figure 36B, D**).

Finally, when cytokine profiles were assessed at memory and peak secondary, they also did not differ based on the absence of H-2D<sup>b</sup> or H-2K<sup>b</sup> (data not shown).

Taken together, these data indicate that the loss of one MHCI molecule does not impact on the cytokine profile of the remaining CD8 T cells during primary, memory or secondary responses. This is striking for the H-2K<sup>b</sup>Ova<sub>257</sub>-specific responses, as it demonstrates that the loss of H-2D<sup>b</sup> affects the magnitude of the response but not the quality of the response, as assessed by cytokine production.

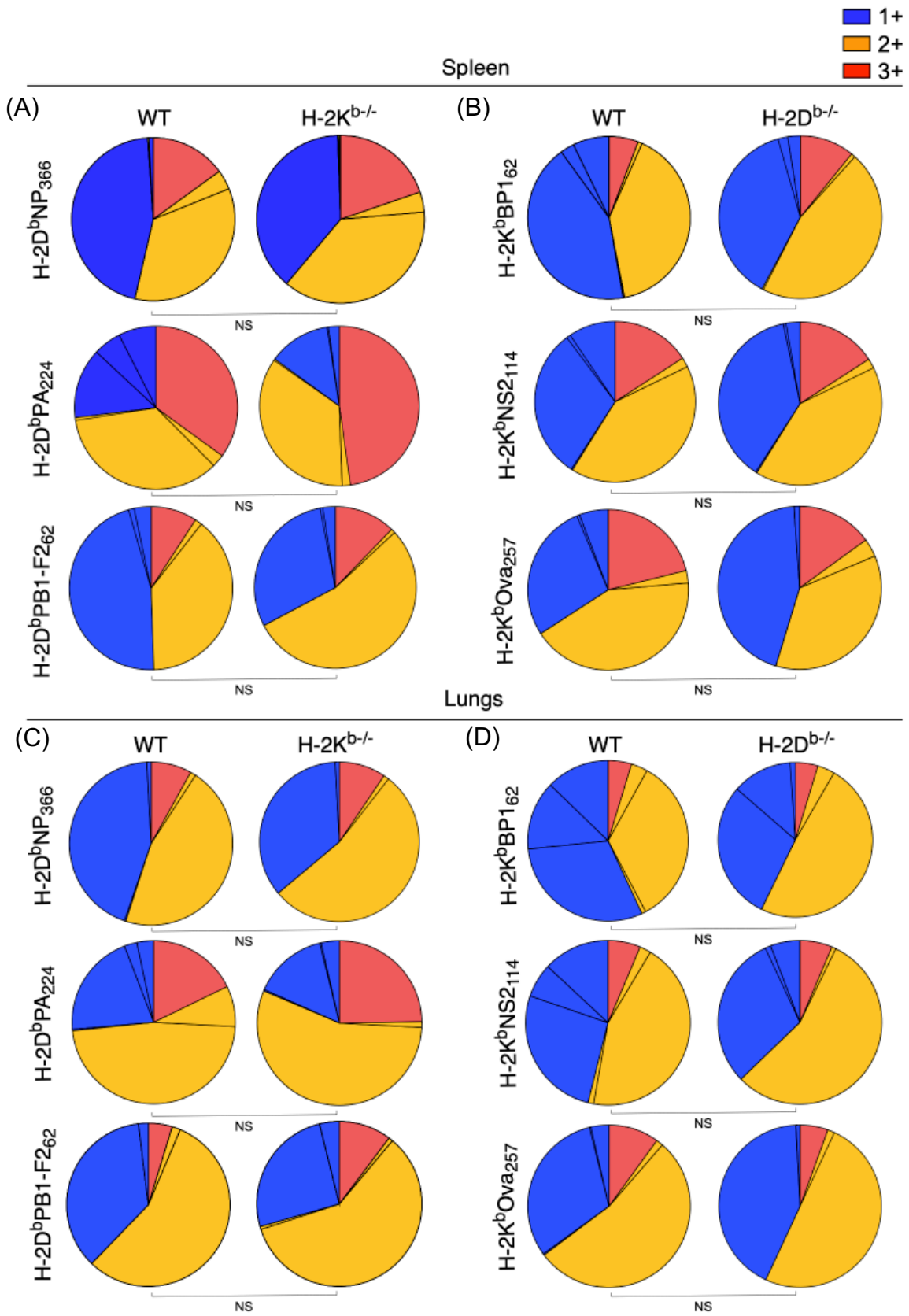


**Figure 36:** Cytokine production by epitope-specific CD8 T cell responses after i.n. infection with  $10^4$  pfu HKx31-Ova virus. Lymphocytes from the (A and B) spleen and (C and D) lungs of infected (A-D) WT, (A and C) H-2K<sup>b/-</sup> and (B and D) H-2D<sup>b/-</sup> mice were re-stimulated with H-2D<sup>b</sup>NP<sub>366</sub>, H-2D<sup>b</sup>PA<sub>224</sub>, H-2D<sup>b</sup>PB1-F<sub>262</sub>, H-2K<sup>b</sup>PB1<sub>703</sub>, H-2K<sup>b</sup>NS<sub>2114</sub> or H-2K<sup>b</sup>Ova<sub>257</sub> directly *ex vivo* 10 days post-infection. Colours represent the secretion of a single cytokine (blue), two cytokines (orange) and all three cytokines (red). NS indicates  $p > 0.05$  (Wilcoxon rank sum test). These results are representative of 2 independent experiments with  $n = 5$  per group.

To assess another measure of quality, I quantified the amount of IFN $\gamma$  produced on a per cell basis in H-2K<sup>b</sup>Ova<sub>257</sub>- and H-2D<sup>b</sup>NP<sub>366</sub>-specific CD8 T cells using the MFI of IFN $\gamma$  at the peak of primary and secondary response.

Similar to the cytokine profiles (**Figure 36**), the IFN $\gamma$  MFI of H-2K<sup>b</sup>OVA<sub>257</sub>-specific CD8 T cells in the spleen and lungs after both primary and secondary IAV challenge was not significantly different across both WT and H-2D<sup>b/-</sup> mice (**Figure 37A, C**). In addition, the IFN $\gamma$  MFIs of H-2D<sup>b</sup>NP<sub>366</sub>-specific CD8 T cells in the spleen and lungs was not significantly different across WT and H-2K<sup>b/-</sup> mice (**Figure 37B, D**). This further indicates that the loss of one MHC I molecule results in a quantitative, but not qualitative compensation by some CD8 T cell restricted by the alternative MHC I.

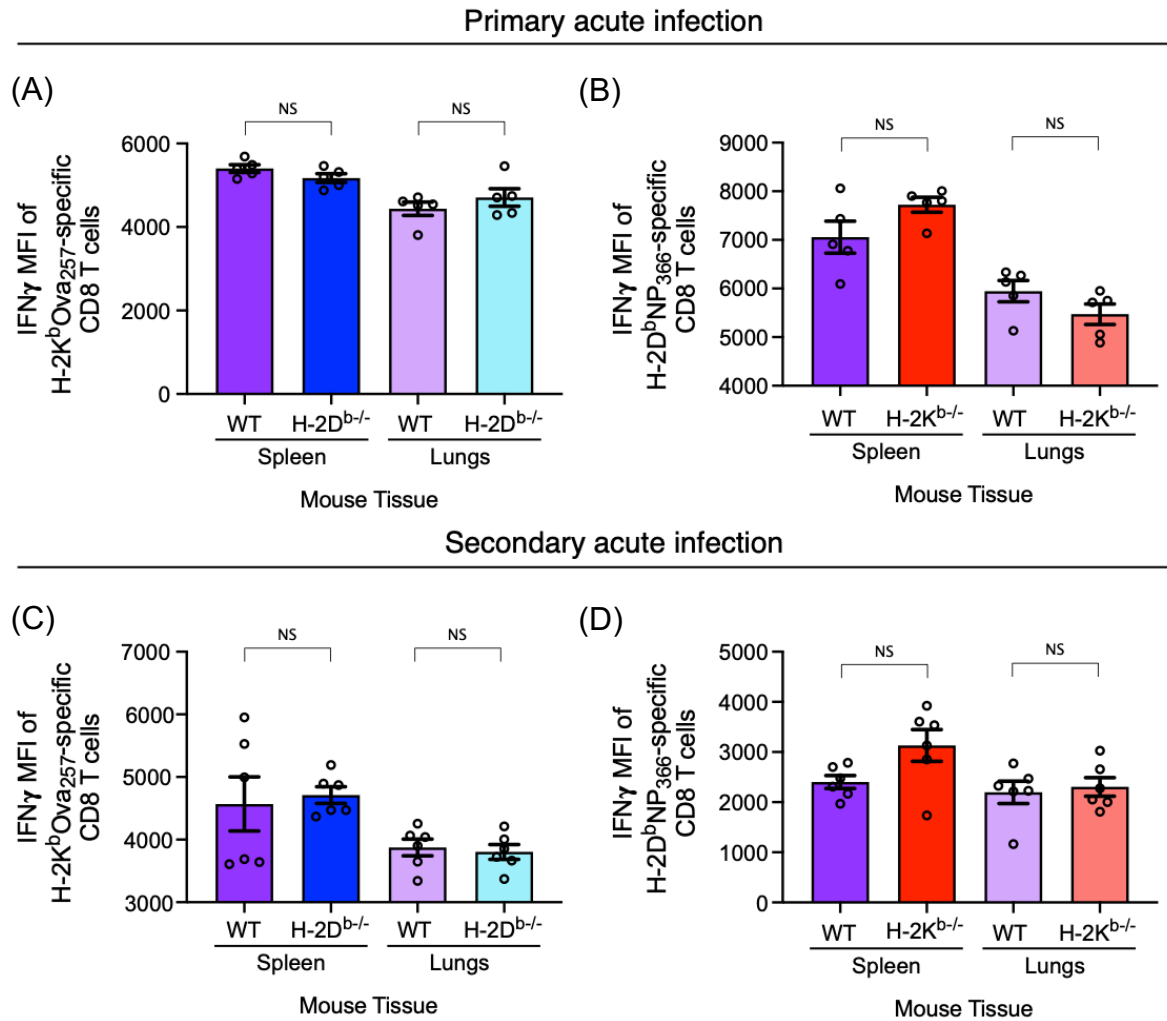


**Figure 37:** MFI of IFN $\gamma$  production by H-2K<sup>b</sup>Ova<sub>257</sub>- and H-2D<sup>b</sup>NP<sub>366</sub>-specific CD8 T cells after Ova<sub>257</sub> and NP<sub>366</sub> peptide stimulation respectively. IFN $\gamma$  MFI the spleen (dark purple, blue and red) and lungs (pale purple, blue and red) of WT (purple), H-2D<sup>b-/-</sup> (blue) and H-2K<sup>b-/-</sup> (red) mice after stimulation with (A, C) Ova<sub>257</sub> and (B, D) NP<sub>366</sub> peptide (A, B) 10 days post-HKx31-Ova infection and (C, D) 7 days post-PR8-Ova infection. \*\* indicates  $p \leq 0.01$ , \* indicates  $p \leq 0.05$ , NS indicates  $p > 0.05$ . For all panels, lines and error bars represent mean  $\pm$  SEM. These results are representative of 2 independent experiments with  $n = 5$  or 6 per group.

### 5.2.6. Diminished capacity of H-2K<sup>b</sup>Ova<sub>257</sub>-specific CD8 T cells in H-2D<sup>b</sup><sup>-/-</sup> mice is not influenced by the proportion of MPECs and SLECs.

As previously discussed in **Section 5.2.3**, the formation of the H-2K<sup>b</sup>Ova<sub>257</sub> memory population after primary IAV infection was diminished in the absence of the H-2D<sup>b</sup> molecule. The decline in the size of the memory population was observed in both the spleen and lungs of H-2D<sup>b</sup><sup>-/-</sup> mice compared to WT mice despite having an expanded number of effector H-2K<sup>b</sup>Ova<sub>257</sub>-specific CD8 T cell population following primary and secondary infection with the IAV virus (**Figure 38A, B**).

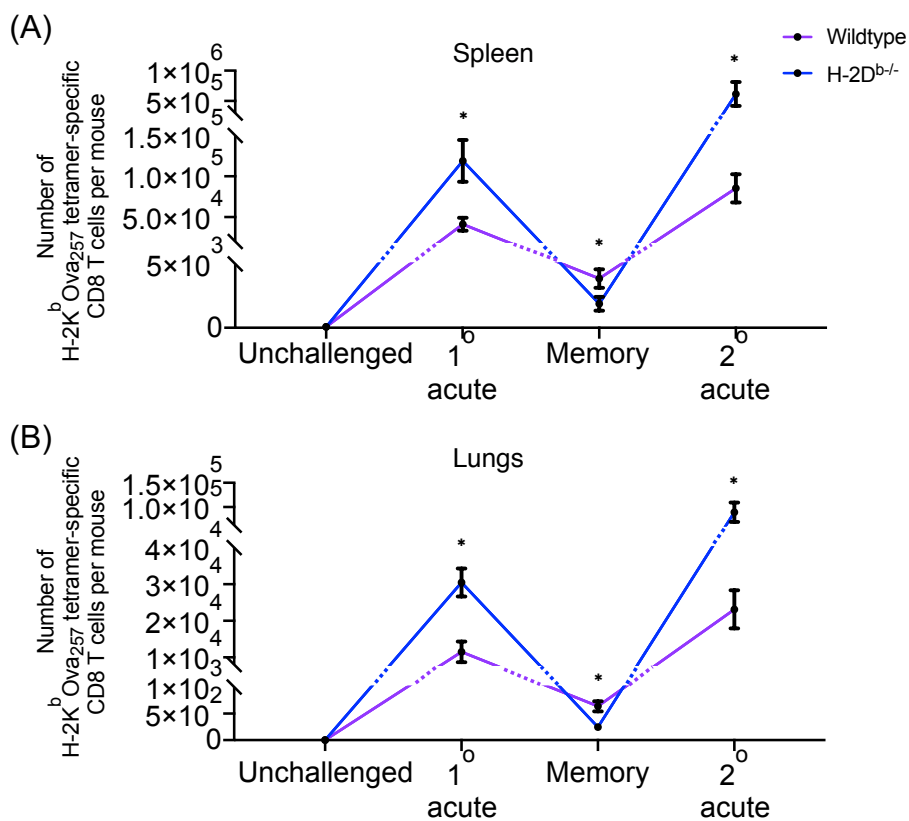


**Figure 38:** Kinetics of H-2K<sup>b</sup>Ova<sub>257</sub>-specific CD8 T cell response after IAV infection. The number of H-2K<sup>b</sup>Ova<sub>257</sub>-specific CD8 T cells in the (A) spleen and (B) lungs of WT (purple) and H-2D<sup>b</sup><sup>-/-</sup> (blue) mice after primary acute, memory and secondary acute timepoints. For all timepoints, points and error bars represent mean +/- SEM. \* indicates  $p \leq 0.05$  (Mann Whitney test). These results are representative of 2-3 independent experiments with  $n = 5-6$  per group.

Given the impaired development of memory populations in H-2D<sup>b/-</sup> mice, I assessed the memory potential of effector H-2K<sup>b</sup>Ova<sub>257</sub>-specific cells using expression of killer cell lectin-like receptor sub-family G member (KLRG1) and IL-7 receptor (CD127) at day 10 post-primary infection. KLRG1<sup>lo</sup>CD127<sup>hi</sup> CD8 T cells have been defined as memory-precursor effector cells (MPECs), which are effector cells that have a greater potential to persist into memory populations (183, 285). KLRG1<sup>hi</sup>CD127<sup>lo</sup> CD8 T cells are defined as short-lived effector cells (SLECs), which are highly differentiated effector cells that undergo apoptosis following viral clearance. I hypothesized that there would be fewer H-2K<sup>b</sup>Ova<sub>257</sub>-specific MPECs in H-2D<sup>b/-</sup> mice, which would lead to decreased memory cell formation.

In IAV-infected WT mice, H-2K<sup>b</sup>Ova<sub>257</sub>-specific CD8 T cells predominantly exhibited the MPEC phenotype in both the spleen and lungs (spleen 48.6%; lungs 33.5%) (**Figure 39A, B**), while a minor proportion of H-2K<sup>b</sup>Ova<sub>257</sub>-specific effector CD8 T cells exhibited the SLEC phenotype (spleen 11.1%; lungs 7.2%). In IAV-infected H-2D<sup>b/-</sup> mice, there was a no significant difference in the proportion of MPECs or SLECs in both the spleen and lungs compared to WT mice (**Figure 39A, B**), although there was a consistent minor trend for fewer MPECs. It is possible that a minor decrease in MPECs may have a pronounced effect on the generation of the memory pool (285). However, previous studies have also suggested that the MPEC and SLEC phenotype is not a good predictor of memory potential in the C57BL/6 model of IAV infection (183, 184).

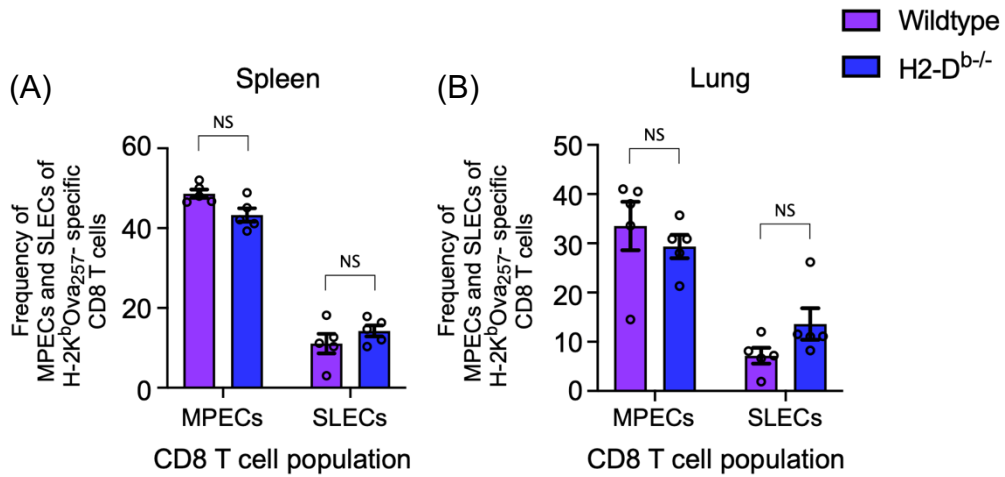


**Figure 39:** Proportion of MPECs and SLECs in the H-2K<sup>b</sup>Ova<sub>257</sub>-specific CD8 T cell population 10 days after i.n. primary acute infection with 10<sup>4</sup> pfu HKx31-Ova. H-2K<sup>b</sup>Ova<sub>257</sub>-specific effector CD8 T cells were subdivided into MPECs (KLRG1<sup>lo</sup>CD127<sup>hi</sup>) and SLECs (KLRG1<sup>hi</sup>CD127<sup>lo</sup>) in the (A) spleen and (B) lungs of WT (purple) and H-2D<sup>b/-</sup> (blue) mice. Bars and error bars represent mean +/- SEM. ns indicates p > 0.05 (Mann Whitney test). This result is generated from a single experiment with n = 5 per group.

### 5.2.7. Unaltered H-2K<sup>b</sup>Ova<sub>257</sub> presentation with the lack of H-2D<sup>b</sup>

One key determinant of CD8 T cell response magnitude is the level of antigen presented on the surface of APCs, where more presented antigen can boost the CD8 T cell response (269, 270). To determine whether the increase in H-2K<sup>b</sup>Ova<sub>257</sub>-specific responses in IAV-infected H-2D<sup>b/-</sup> mice was a consequence of increased level of H-2K<sup>b</sup>Ova<sub>257</sub> epitope presentation on APCs, I measured the level of H-2K<sup>b</sup>Ova<sub>257</sub> presented on APCs 5 days after primary IAV infection of WT and H-2D<sup>b/-</sup> mice using an antibody specific for the H-2K<sup>b</sup>Ova<sub>257</sub> complex (25-D1.16). Dendritic cells (DCs) from the spleen and lungs of WT and H-2D<sup>b/-</sup> mice at 7 days after HKx31-Ova infection were stained with the antibody and H-2K<sup>b</sup>Ova<sub>257</sub> presentation analysed by flow cytometry.

Following primary infection with the HKx31-Ova virus, DCs were identified in the spleen of WT and H-2D<sup>b/-</sup> mice by the co-expression of CD11c and MHCII (I-A<sup>b</sup>). Analysis of the level of H-2K<sup>b</sup>Ova<sub>257</sub> presentation on the DC surface showed no significant difference in MFI either in the spleen (**Figure 40A**) or lungs (**Figure 40B**) (spleen and lungs  $p = 0.7$ ). These data suggest that there was no significant difference in H-2K<sup>b</sup>Ova<sub>257</sub> presentation with the loss of H-2D<sup>b</sup> at day 5 after infection. As a result, the compensatory increase in the magnitude of the H-2K<sup>b</sup>Ova<sub>257</sub>-specific response is not likely to be driven by differences in antigen presentation.

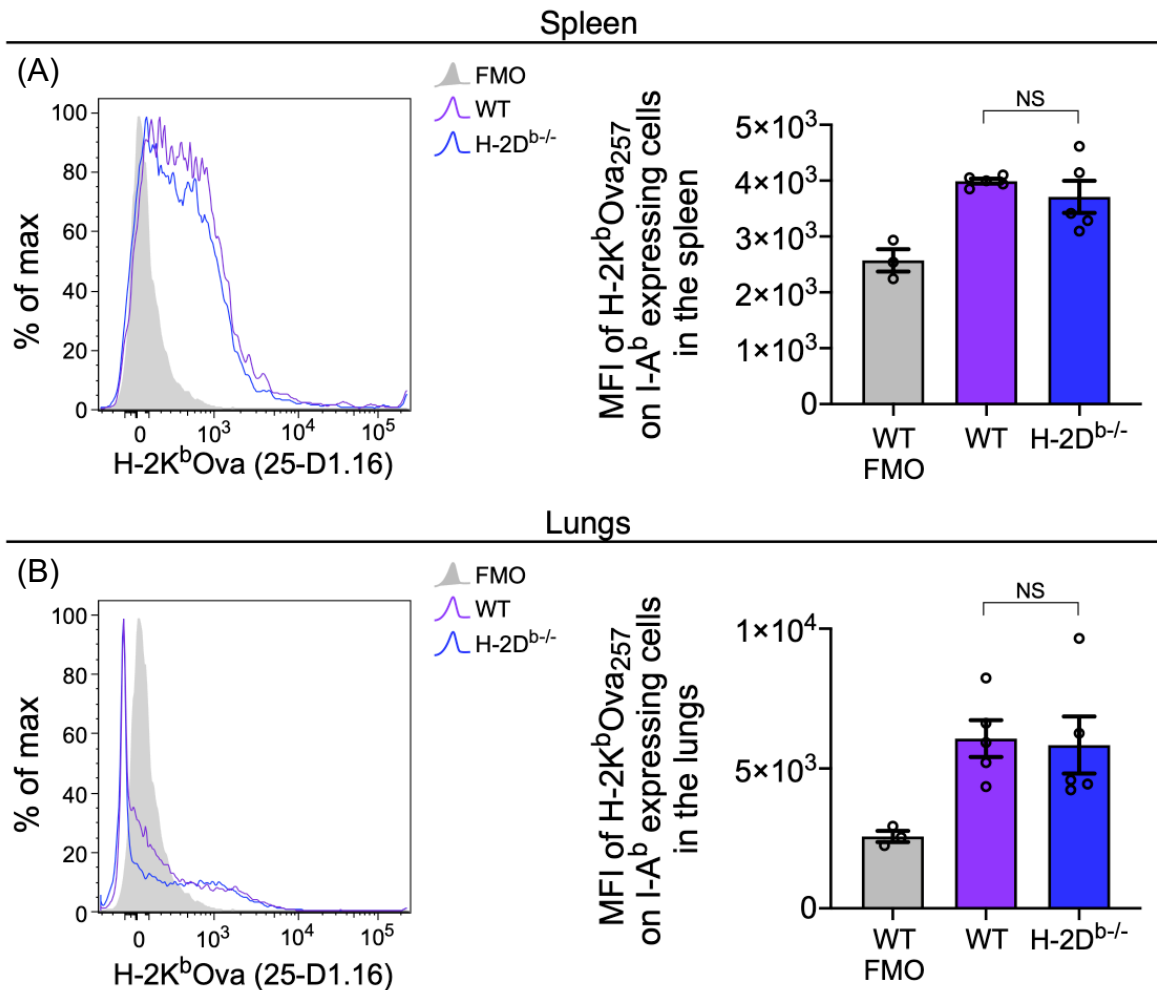


**Figure 40:** Similar presentation of H-2K<sup>b</sup>Ova<sub>257</sub> on DCs from WT and H-2D<sup>b-/-</sup> mice following HKx31-Ova infection. Representative histogram MFI summary plots of H-2K<sup>b</sup>Ova: PE-Cy7 expression in the (A) spleen and (B) lungs of WT (purple) and H-2D<sup>b-/-</sup> (blue) mice. ns indicates  $p > 0.05$  (Mann Whitney test). Cells are live, CD11c<sup>+</sup>, I-A<sup>b</sup><sup>+</sup> DCs. For all panels, lines and error bars represent mean  $\pm$  SEM. These results are representative of 2 independent experiments with  $n = 4$  or 5 per group.

**5.2.8. The compensatory increase in the H-2K<sup>b</sup>Ova<sub>257</sub>-specific CD8 T cell response is driven by augmented recruitment of naïve cells in H-2D<sup>b/-</sup> mice**

Another key determinant of CD8 T cell response magnitude is the efficiency of recruitment from the pool of circulating naïve epitope-specific CD8 T cells (137). To measure the efficiency of recruitment of H-2K<sup>b</sup>Ova<sub>257</sub>-specific CD8 T cells after IAV infection, I tracked the early divisions of these cells using BrdU, a thymidine analog that can be incorporated into dividing cells as previously described (137). Briefly, mice were infected intranasally with the HKx31-Ova virus and administered BrdU in drinking water at days 5 and 6 post-infection. Spleens and lungs of mice were harvested at day 7 post-infection for analysis of recruitment and division of epitope-specific CD8 T cells (**Figure 41**). Epitope-specific CD8 T cell populations were isolated using tetramer-based magnetic enrichment and naïve (CD62L<sup>hi</sup>CD44<sup>lo</sup>) and activated (CD62L<sup>lo</sup>CD44<sup>hi</sup>) were analysed for BrdU incorporation. Both H-2K<sup>b</sup>Ova<sub>257</sub>- and H-2K<sup>b</sup>PB1<sub>703</sub>-specific populations were analysed to compare two epitope-specific populations that are differentially impacted by the loss of the H-2D<sup>b</sup>, exhibiting either robust or no increase in number, respectively.

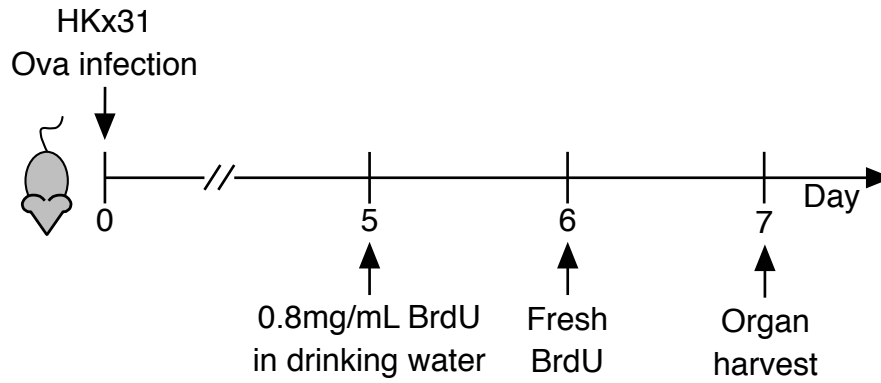


**Figure 41:** Schematic of BrdU treatment strategy. WT and H-2D<sup>b/-</sup> mice were infected i.n. with HKx31-Ova then administered BrdU in drinking water from day 5 post-infection. Mice were killed and spleen and peripheral lymph nodes were harvested at day 7 post-infection for analysis of early cell division.

To measure the efficiency of recruitment of naïve epitope-specific CD8 T cells, I enumerated H-2K<sup>b</sup>Ova<sub>257</sub>- and H-2K<sup>b</sup>PB1<sub>703</sub>-specific CD8 T cells that had retained a naïve phenotype (CD62L<sup>hi</sup>CD44<sup>lo</sup>) and that were undivided (BrdU<sup>-</sup>).

For H-2K<sup>b</sup>PB1<sub>703</sub>-specific CD8 T cells, there are reported to be ~308 naïve CD8 T cells in WT mice (136). In IAV infected WT mice, most of the H-2K<sup>b</sup>PB1<sub>703</sub>-specific CD8 T cells had been recruited by day 7, with an average of 73 cells remaining unrecruited (**Figure 42A, E**). In IAV infected H-2D<sup>b/-</sup> mice, an average of ~64 cells remained unrecruited by day 7 (**Figure 42B, E**). These data suggested that loss of H-2D<sup>b</sup> did not have an impact on the recruitment of naïve H-2K<sup>b</sup>PB1<sub>703</sub>-specific CD8 T cells into the immune response. This is also consistent with an unchanged magnitude of the H-2K<sup>b</sup>PB1<sub>703</sub>-specific CD8 T cell response in H-2D<sup>b/-</sup> mice (**Figure 33C**).

For H-2K<sup>b</sup>Ova<sub>257</sub>-specific CD8 T cells, there are reported to be ~130 naïve CD8 T cells in WT mice (133, 138). In IAV infected WT mice, most H-2K<sup>b</sup>Ova<sub>257</sub>-specific CD8 T

cells had again been recruited by day 7, with an average of ~40 cells remaining unrecruited (**Figure 42C, E**). In contrast, in IAV infected H-2D<sup>b/-</sup> mice, there were significantly fewer cells remaining unrecruited, at an average of ~16 cells (**Figure 42D, E**). These data suggested that loss of H-2D<sup>b</sup> leads to an increase in recruitment of naïve H-2K<sup>b</sup>Ova<sub>257</sub>-specific CD8 T cells following IAV infection, consistent with the increased magnitude of the naïve H-2K<sup>b</sup>Ova<sub>257</sub>-specific CD8 T cell response.

To determine if there were specific characteristics of naïve CD8 T cells that remained unrecruited, I assessed expression levels of CD5. CD5 can be used to indicate the TCR affinity for both self-pMHC I as well as foreign cognate pMHC I molecules (260). Unrecruited cells that were H-2K<sup>b</sup>Ova<sub>257</sub>-specific, but not H-2K<sup>b</sup>-PB1<sub>703</sub>-specific, cells had a significantly lower MFI for CD5 in H-2D<sup>b/-</sup> mice when compared to WT mice (**Figure 42F**). These data indicate that the increased recruitment of naïve H-2K<sup>b</sup>Ova<sub>257</sub>-specific CD8 T cells is facilitated by recruitment of CD5<sup>hi</sup> cells with higher affinity for antigen.

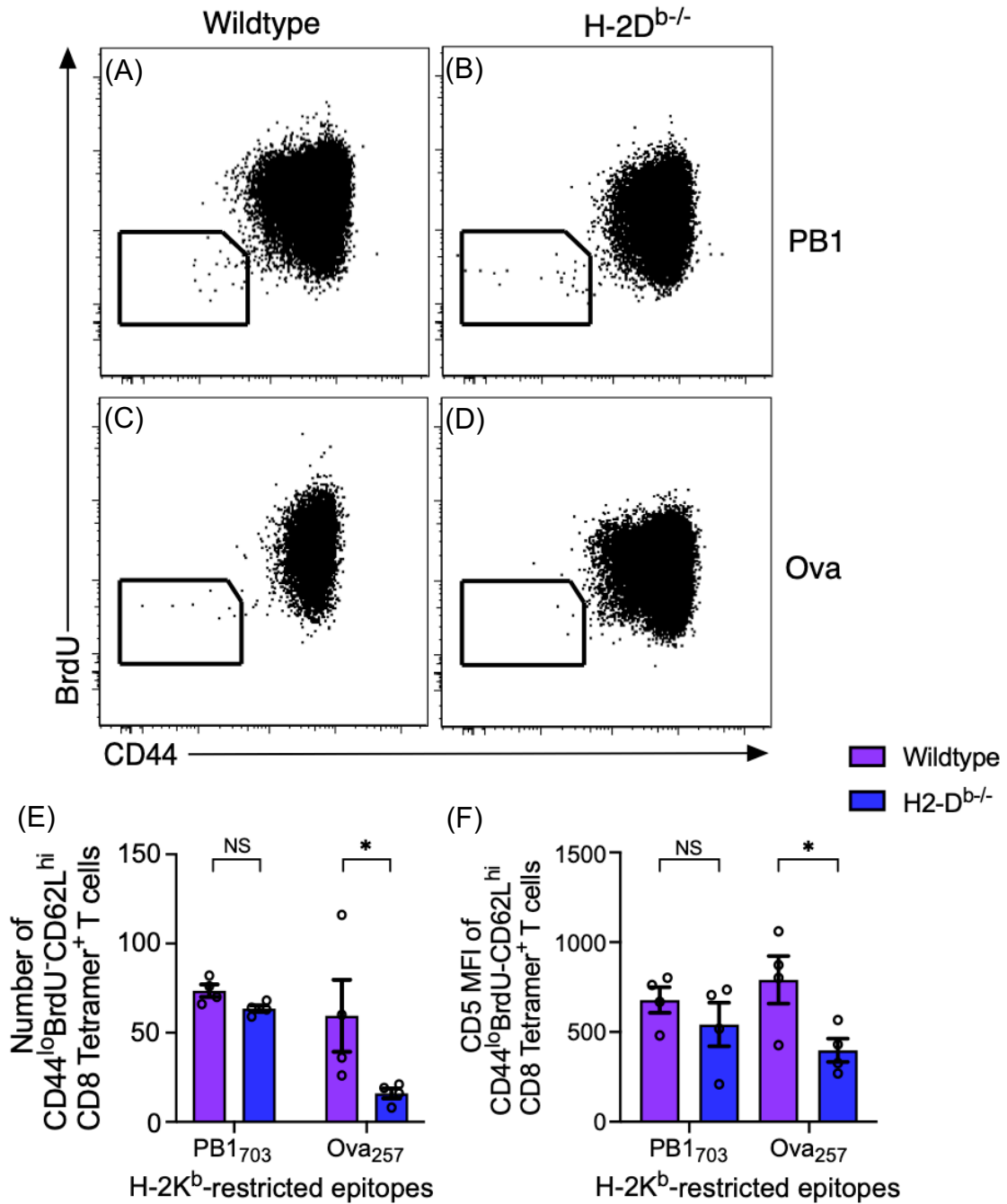


**Figure 42:** Increased recruitment of H-2K<sup>b</sup>Ova<sub>257</sub>-specific CD8 T cells in the absence of H-2D<sup>b</sup>. (A) Representative dot plots of WT (A, C) and H-2D<sup>b/-</sup> (B, D) splenocytes that were magnetically enriched using H-2K<sup>b</sup>PB1<sub>703</sub> (A, B) and H-2K<sup>b</sup>Ova<sub>257</sub> (C, D) tetramers. Data shows BrdU incorporation vs CD44 expression on live, CD19<sup>-</sup>, F4/80<sup>-</sup>, TCRβ<sup>+</sup>, CD4<sup>-</sup>, CD8<sup>+</sup> tetramer<sup>+</sup>, CD62L<sup>hi</sup> lymphocytes after tetramer-based magnetic enrichment. (E) Number and (F) CD5 MFI of CD62L<sup>hi</sup>CD44<sup>lo</sup>BrdU<sup>-</sup> naïve H-2K<sup>b</sup>PB1<sub>703</sub> H-2K<sup>b</sup>Ova<sub>257</sub>-specific CD8 T cells in WT (purple) and H-2D<sup>b/-</sup> (blue) mice at day 7 post-infection. \* indicates p ≤ 0.05, ns indicates p > 0.05 (Mann-Whitney test). Bars and error bars represent mean ± SEM. These results are representative of 2 independent experiments with n = 4 per group.

### 5.3. Discussion

This study has defined the relative capacity of different epitope-specific responses to compensate for the loss of responses restricted by another MHCI following IAV infection. Briefly, the loss of H-2K<sup>b</sup>-restricted responses following infection with an IAV-Ova virus, resulted in a modest, but reproducible compensation in the magnitude of the immunodominant H-2D<sup>b</sup>NP<sub>366</sub>-specific CD8 T cell response after primary infection. In contrast, the loss of H-2D<sup>b</sup>-restricted responses led to a striking increase in the magnitude of the H-2K<sup>b</sup>Ova<sub>257</sub>-specific CD8 T cell response after primary challenge. This compensatory response was amplified by up to 10-fold after secondary infection, despite a reduction in memory cells. Despite the increase in magnitude of H-2D<sup>b</sup>NP<sub>366</sub>- and H-2K<sup>b</sup>Ova<sub>257</sub>-specific CD8 T cell responses with the loss of H-2K<sup>b</sup> and H-2D<sup>b</sup> respectively, this did not reflect a qualitative change in these epitope-specific CD8 T cells. The cytokine profiles and MPEC/SLEC profiles of all epitope-specific CD8 T cell populations remained unaltered despite the loss of H-2D<sup>b</sup> or H-2K<sup>b</sup>. The compensatory increase in the magnitude of the H-2K<sup>b</sup>Ova<sub>257</sub>-specific response was due, at least in part, to enhanced recruitment of the relatively high affinity cells from the naïve pool, however there was no evidence that this was driven by increased H-2K<sup>b</sup>Ova<sub>257</sub> presentation in the absence of H-2D<sup>b</sup>. Overall, I observed modest compensation by remaining CD8 T cell responses with the loss of one MHCI molecule, with immunodominant responses compensating to a greater extent than subdominant responses. This indicates that there is a level of flexibility in immunodominant populations, providing a better capacity to compensate for the loss of other CD8 T cell responses.

Immunodomination is a biological phenomenon that can be a key determinant of CD8 T cell response magnitude and it may also be relevant to a number of physiological scenarios, including 1) immune escape, 2) MHCI downregulation during infection and 3) interactions between diverse HLA alleles in outbred human populations. During viral infection, prominent epitopes can become mutated, which allows mutant viral variants to “escape” detection by the immune system (286–289). This occurs during many viral infections, including the human immunodeficiency virus (HIV), hepatitis C virus, herpes simplex virus (HSV) and influenza A virus (IAV). This loss of immunodominant epitopes during immune escape could potentially decrease immunodomination of other epitope-specific responses. During viral infection, MHCI can also be downregulated by certain viruses, such as HSV and IAV, with preferential downregulation of specific HLA genes and alleles (290, 291). Selective MHCI downregulation may again potentially reduce an immunodominant epitope-specific response restricted by one MHC complex which may then reduce immunodomination of responses restricted by other MHC genes. Finally, humans express a vast number of HLA allelic variants across the population, with 18,694 HLA Class I alleles known to date (292). An understanding of the effect of individual MHCI-specific responses on the magnitude or quality of other non-restricted CD8 T cell responses is essential to predict the magnitude and quality of CD8 T cell responses in individuals with a specific HLA haplotype. Therefore, to more effectively manage immune escape, MHCI downregulation and HLA diversity during viral infection, it is critical to understand immunodomination and the complexities of the interaction between CD8 T cell responses restricted by different MHC genes.

The insertion of the Ova<sub>257</sub> peptide (SIINFEKL) into the neuraminidase stalk of the influenza A virus introduces an H-2K<sup>b</sup>-restricted immunodominant response in C57BL/6 mice (163). The introduction of the Ova<sub>257</sub>-epitope was shown to modestly decrease the H-2D<sup>b</sup>PA<sub>224</sub>-specific CD8 T cell response during infection (163). This suggests that the H-2D<sup>b</sup>PA<sub>224</sub>-specific response is more sensitive to the introduction of H-2K<sup>b</sup>Ova<sub>257</sub>-specific responses. Intriguingly, the removal of the global H-2K<sup>b</sup>-restricted responses (including the H-2K<sup>b</sup>Ova<sub>257</sub>) resulted in compensation by one immunodominant epitope, H-2D<sup>b</sup>NP<sub>366</sub>, but not H-2D<sup>b</sup>PA<sub>224</sub>. On the other hand, the complete removal of the global H-2D<sup>b</sup>-restricted responses resulted in the significant compensation in magnitude of H-2K<sup>b</sup>Ova<sub>257</sub>-specific responses, but not other H-2K<sup>b</sup>-restricted responses. I have shown that the H-2K<sup>b</sup>Ova<sub>257</sub>-specific response, which is highly immunodominant, is more sensitive to the loss of other two immunodominant responses when compared to the subdominant H-2K<sup>b</sup>NS<sub>214</sub> and H-2K<sup>b</sup>PB<sub>1703</sub> responses.

It appears that the immunodominant H-2K<sup>b</sup>Ova<sub>257</sub>- and H-2D<sup>b</sup>NP<sub>366</sub>-, but not H-2D<sup>b</sup>PA<sub>224</sub>-specific responses, are more sensitive to immunodomination and therefore more able to compensate in the absence of other MHC-restricted responses. This is contrary to previous studies where they observed compensation by subdominant responses in the absence of other immunodominant responses (162, 280, 281). On the contrary, CD8 T cells that generate immunodominant responses during infection express TCRs of higher affinity. It is likely that the TCR properties of immunodominant CD8 T cell responses, at least in the model of IAV, provide them with the capacity to compensate for the loss of other CD8 T cell responses. Furthermore, the capacity of immunodominant responses to expand is amplified by the total loss of other MHCI-

restricted responses (144, 148). In particular, H-2K<sup>b</sup>Ova<sub>257</sub>-specific CD8 T cells expanded to a greater extent following secondary infection from a diminished pool of memory population. To this end, a detailed analysis of the rate of expansion following primary and secondary infection is warranted to address this hypothesis.

The recruitment of epitope-specific naïve CD8 T cells into the immune response is a well-established determinant of CD8 T cell response magnitude (137, 293). The comprehensive recruitment of naïve H-2D<sup>b</sup>NP<sub>366</sub>- and H-2D<sup>b</sup>PA<sub>224</sub>-specific CD8 T cells into the immune response correlates strongly with their immunodominance during IAV infection, while the partial recruitment of H-2D<sup>b</sup>PB1-F<sub>262</sub> correlates with a subdominant response (137). It is possible that subdominant responses are incapable of expanding further due to limitations in their intrinsic ability to respond to antigen. This is supported by previous studies that have shown that subdominant responses have an overall lower TCR affinity for its cognate antigen (147). Despite high levels of peptide presentation during infection (75), subdominant responses are incapable of forming large magnitude of responses, suggesting that they are limited in their capacity to respond likely due to their lower TCR affinity. The increased magnitude of H-2K<sup>b</sup>Ova<sub>257</sub>-specific CD8 T cells in H-2D<sup>b</sup><sup>-/-</sup> mice also correlated with better recruitment of naïve CD8 T cells into the immune response in WT mice. BrdU analysis showed an incomplete recruitment of naïve H-2K<sup>b</sup>Ova<sub>257</sub>-specific CD8 T cells when H-2D<sup>b</sup> is present, suggesting that there is a set point in the effector response during an infection, where there is a fixed number of effector CD8 T cells that can be present in the immune response. This may represent a mechanism to prevent excessive accumulation of activated CD8 T cells. Excessive accumulation could result in bystander killing of other

cells and could lead to clinical manifestations, such as autoimmunity and immunopathology (reviewed in (294)).

A strong correlation has been previously described between the naïve precursor frequency and the magnitude of T cell responses for multiple models of infections (reviewed in (128, 133)). This correlation, however, does not apply during IAV infection where there is an inverse correlation between naïve precursor frequency and the immunodominance hierarchy (137). The present study makes the assumption that the loss of H-2D<sup>b</sup> has no influence on the selection and maintenance of the naïve H-2K<sup>b</sup>-restricted population. This assumption was based on the data generated in **Section 3.2.1**, where the loss of H-2K<sup>b</sup> had negligible impact on the frequency of naïve H-2D<sup>b</sup>PA<sub>224</sub>-specific CD8 T cells. However, it will be important to verify that loss of H-2D<sup>b</sup> similarly has no impact on the frequency of naïve H-2K<sup>b</sup>Ova<sub>257</sub>-specific CD8 T cells. Additionally, given the increased recruitment from the H-2K<sup>b</sup>Ova<sub>257</sub>-specific response, it will be important to characterize the qualitative differences in the H-2K<sup>b</sup>Ova<sub>257</sub>-specific TCR $\alpha\beta$  repertoire in both naïve and immune WT and H-2D<sup>b</sup><sup>-/-</sup> mice. While I did not find evidence that the loss of H-2K<sup>b</sup> influenced naïve H-2D<sup>b</sup>PA<sub>224</sub>-specific CD8 T cell selection (**Section 3.2.1**), there may be distinct mechanisms that govern naïve H-2K<sup>b</sup>Ova<sub>257</sub>-specific CD8 T cell selection with the loss of H-2D<sup>b</sup>.

One striking observation from this study is that memory formation of all H-2K<sup>b</sup> restricted responses was impaired in the absence of H-2D<sup>b</sup>. I hypothesised that this impairment was due to a reduction in MPECs and increased SLECs frequency, but this was not the case. The size of the memory population that persists after an infection is influenced by multiple factors including 1) antigen dose, 2) duration of antigen

presentation, 3) co-stimulatory signalling and 4) cytokines, such as IL-2, IL-12 and type I IFNs, provided by DCs and CD4 T cells (295–297). Others and I have shown that the loss of H-2D<sup>b</sup> or H-2K<sup>b</sup> has no influence on the number of CD4 T cells (**Section 4.9.1**; (250)), suggesting that memory formation impairment is not due to a loss of CD4 T cells. However, a detailed characterization of the different DC subsets and the level of antigen presented is warranted to determine whether the loss of H-2D<sup>b</sup> impacts on DC cytokine secretion or antigen presentation.

Finally, I observed an amplification of compensation following the secondary infection, which has been observed in other systems (280). This amplification was in spite of the decreased memory pool, suggesting that the memory H-2K<sup>b</sup>Ova<sub>257</sub>-specific CD8 T cells generated in H-2D<sup>b</sup><sup>-/-</sup> mice are higher quality, possibly with higher affinity for H-2K<sup>b</sup>Ova<sub>257</sub>. Thus, the compensatory increase in the effector response did not correspond to the size of the memory CD8 T cell pool, however the diminished memory pool was able to drive a significantly larger recall response after challenge indicative of a qualitatively superior functional capacity, compared to that generated in WT mice.

Taken together, this study has tracked how the immune response compensates for the absence of an MHCI molecule and provides a deeper understanding of mechanisms that govern the generation of polyclonal primary, memory and secondary CD8 T cell responses. This study is particularly relevant for understanding human responses, where a wide repertoire of HLA alleles is expressed. The presence or absence of certain HLA alleles may lead to immunodomination on remaining CD8 T cell responses during infection. In addition, the loss of key epitopes during viral mutation, or virus-induced MHCI downregulation, may selectively remove the

suppression on certain CD8 T cell responses and allow the ability of remaining responses to mount an effective CD8 T cell response during infection.

## **6. Concluding Remarks**

MHC genes exhibit the highest degree of polymorphism known in higher vertebrates (298), with up to 18,697 different HLA Class I alleles alone within the human population (299). Phylogenetic analyses of the MHC genes in humans and mice have shown that the individual genes and alleles have evolved over time to accumulate mutations localized predominantly within the peptide-binding cleft (190, 300). The accumulation of mutations within the peptide-binding cleft has enabled different MHC molecules to present distinct repertoires of peptides to T cells (301). The diversity of repertoires across MHC alleles confers an advantage in an outbred population, where individuals likely present distinct peptide repertoires from each other and the population is more likely to contain an individual capable of presenting a protective epitope (302). The structure of the MHC molecule is also crucial for its function (298), which is exemplified by the fact that, despite the vast number of MHC allelic variants, MHC molecules share up to 93% structural homology (195). While MHC alleles are structurally homologous, distinct MHC alleles drive development of distinct populations of T cells in a phenomenon known as MHC restriction.

MHC restriction implies that MHC molecules play a dominant role in modulating selection of TCR repertoires but the exact interactions that govern the selection process are still being defined. Specifically, it is unclear how T cell selection is shaped by 1) TCR interactions with MHC molecules, 2) TCR interactions with self-peptides presented by MHC molecules and 3) the net effect of both interactions. The MHC

molecule clearly plays a fundamental role in T cell selection, where T cells expressing TCRs with affinity for MHC but not self-antigen are able to mature and circulate in the periphery (reviewed in (303–305)). MHC allelic differences can influence the TCR repertoire directly, by biasing the TCR repertoire to accommodate contacts with the MHC molecule, or indirectly, due to the distinct peptide repertoire loaded on the MHC molecule. In humans, studies have shown a strong correlation between TCR V-region bias (distinct TRAV and TRBV usage) and variations in the MHC locus (306–308). In addition, the TCR residues that were predominantly responsible for the association with MHC variation were focused on the TCR-MHC interface. This suggests that HLA haplotypes play a significant role in skewing the peripheral TCR repertoire to shape MHC reactivity. In addition, there are studies that showed unique peptide-binding modalities that confers TCR-pMHC specificities (196, 309, 310), in line with the hypothesis that the TCR repertoire is, at least, partially shaped by interactions with the peptide. However, whether the TCR repertoire is skewed to facilitate direct contacts with the MHC molecule, or the unique peptide repertoire loaded by distinct MHC molecules cannot be dissected here.

Given the complexity of MHC allelic variants and their clear relationship to T cell selection, it is essential to gain more insight into the MHC determinants that influence T cell biology. This PhD project has explored the influence of MHC I expression on CD8 T cell populations and can be broadly grouped into the influence on CD8 T cell selection (**Chapter 3**), homeostatic maintenance (**Chapter 4**) and activation during infection (**Chapter 5**).

This thesis has provided a detailed examination of alloreactive CD8 T cell populations (**Chapter 3**), by assessing the capacity of an alternative MHCI molecule to mediate the selection of an epitope-specific CD8 T cell population. I characterised the binding capacity and function of a population of alloreactive H-2D<sup>b</sup>PA<sub>224</sub>-specific CD8 T cells that were selected on the mismatched H-2K<sup>b</sup> molecule compared to the matched H-2D<sup>b</sup> molecule. The presence of these alloreactive CD8 T cells has clinical consequences in conditions such as transplant rejection, GvHD and GvL. It also highlights that there is a level of similarity between MHC allelic variants that is capable of mediating the selection of an alloreactive T cell population. Of note, alloreactive CD8 T cells often appear to recognize multiple MHCI molecules (196, 197), which implies that they are recognizing highly conserved structural features of MHC molecules. Previous studies have assessed alloreactivity in the CD4 T cell population, where antigen-specific CD4 T cells can be selected on allelic variants of the MHCII genes in allomorphic mice (200). They also demonstrated a level of similarity across multiple MHCII molecules sufficient to mediate the selection of alloreactive CD4 T cells, so similarities in MHC clearly contributes to the selection of alloreactive T cells in general.

One key outstanding question is whether selection of alloreactive H-2D<sup>b</sup>PA<sub>224</sub>-specific CD8 T cell population is only mediated by similarities in H-2K<sup>b</sup> and H-2D<sup>b</sup>, or whether the selecting self-peptide presented on H-2K<sup>b</sup> also contributes. This can only be determined with identification of the selecting self-peptide, which is technically challenging. However, we can define how alloreactive T cells bind to foreign-derived epitopes loaded onto allogeneic MHC by solving the crystal structure of the alloreactive TCR in complex with H-2D<sup>b</sup>PA<sub>224</sub>. Since contacts mediate foreign-derived

epitopes may reflect contacts on self-derived epitopes that mediated positive selection (311, 312), the resolved crystal structure will likely provide insights into the specific interactions mediating the positive selection of alloreactive TCRs. This in turn will provide insights into how differences between MHC molecules influence cognate pMHC recognition.

The data presented in this thesis also highlights that there is a distinction between alloreactive cells that are capable of binding tetramer and those that were capable of being activated by allogeneic MHC. The alloreactive population detected in my study was incapable of responding to antigen stimulation both *in vitro* and *in vivo* (**Figure 6, 8**), as compared to cells selected on matched MHCI. Our data therefore suggests that the vast majority of alloreactive cells that bind to allogeneic MHC do not respond to stimulation by becoming activated in our systems. However, the existence of GvHD and GvL suggests that some alloreactive cells must be capable of becoming activated. To account for these observations, I advance 3 possible, not mutually exclusive, scenarios; 1) that alloreactive cells capable of becoming activated by allogeneic MHC are very rare, 2) that different antigen targets may have differing frequencies of alloreactive cells capable of both binding and being activated by allogeneic MHC and/or 3) that our *in vitro* and *in vivo* model systems are not sufficiently sensitive to drive or detect activation of alloreactive T cells. To explore these 3 scenarios, I would perform a number of experiments. Firstly, alloreactive T cells that are capable of activation may be rare due to an increased frequency of atypical TCR-pMHC docking topologies that do not permit optimal TCR signalling required for T cell activation (**Figure 43**) (84, 313). With regards to GvHD, I speculate that pathogenic alloreactive T cells happen to bind allogeneic pMHC molecules in a conventional orientation, which

permits them to expand and cause disease. Hence, if I am able to define the crystal structure of a number of alloreactive TCRs in complex with an allogeneic pMHC molecule, this will both define the frequency of atypical binding topology and identify key binding residues for alloreactive T cell populations. This knowledge may enable us to detect naive alloreactive T cells and may enable us to identify targets for TCR blockade or specific depletion during GvHD to control disease. Secondly, I could assess the frequency and activation capacity of alloreactive cells for other antigen specificities, to see if the capacity for activation of alloreactive cells is a function of the target peptide. Finally, I should test the activation of alloreactive T cells in an allogeneic transplantation model, which may more closely model the conditions that support activation of alloreactive cells in GvHD.

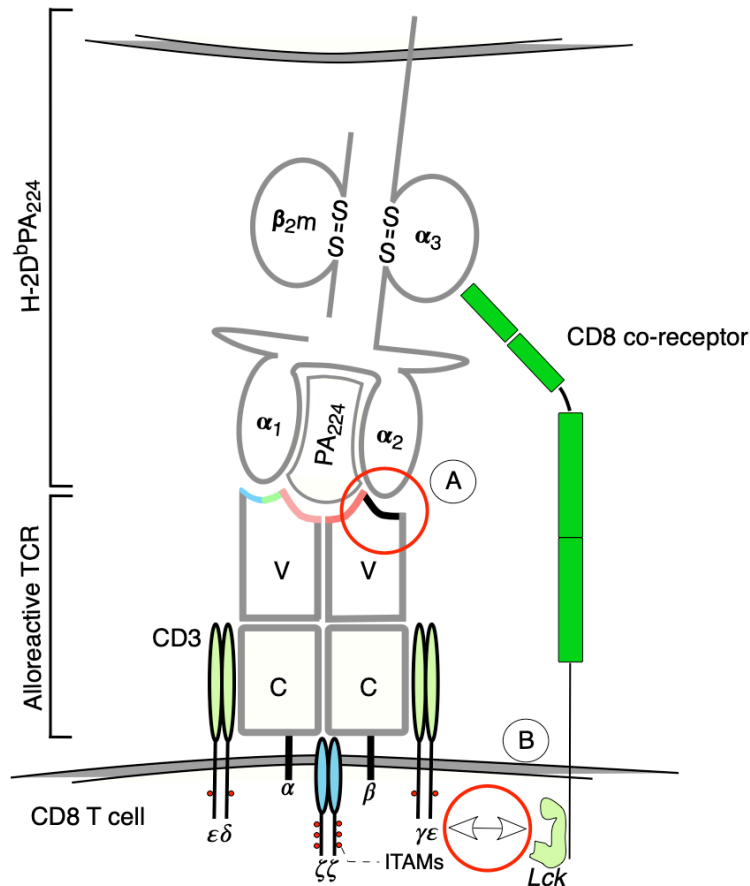


**Figure 43:** Schematic diagram of alloreactive H-2D<sup>b</sup>PA<sub>224</sub>-specific TCR in complex with H-2D<sup>b</sup>PA<sub>224</sub>. (A) Altered TCRβ usage and/or (B) atypical TCR-pMHC I docking topology permits binding, but may not be optimal for CD8 docking, TCR signalling and activation of alloreactive H-2D<sup>b</sup>PA<sub>224</sub>-specific CD8 T cells.

One outstanding question arising from this observation is whether alloreactive H-2D<sup>b</sup>PA<sub>224</sub>-specific CD8 T cell population are capable of responding to H-2D<sup>b</sup>PA<sub>224</sub> during a physiological immune response. To model an immune response *in vitro*, I first expanded the cells with anti-CD3. This is a robust TCR cross-linking stimulus, which may have driven activation induced non-responsiveness (201), resulting in these cells being refractory to further TCR signalling. To model an immune response *in vivo*, I used DC vaccination with activated peptide-loaded WT BMDCs in NK cell-depleted mice (**Section 3.2.3**). However, DC vaccination has been shown to elicit a poor CD8

T cell response in multiple models of infection (314–318), including IAV infection (147). The overall poor efficacy of DC vaccination combined with the lowered affinity of the alloreactive H-2D<sup>b</sup>PA<sub>224</sub>-specific TCRs for its cognate antigen (**Figure 6**) may have resulted in the impaired responses observed in this study. Hence, it is entirely plausible that alloreactive H-2D<sup>b</sup>PA<sub>224</sub>-specific CD8 T cells are capable of responding to H-2D<sup>b</sup>PA<sub>224</sub>, but that the sensitivity of the assays used to detect responses here (DC vaccination and *in vitro* expansion/stimulation) were insufficient to detect it.

Another outstanding question is whether alloreactive CD8 T cells found in mice that only express H-2K<sup>b</sup> (H-2D<sup>b</sup><sup>-/-</sup> mice) are also capable of being generated in mice that express H-2D<sup>b</sup> (i.e. WT mice). I could confirm this if public clonotypes were seen the TCR repertoire of H-2D<sup>b</sup>PA<sub>224</sub>-specific CD8 T cells from both H-2D<sup>b</sup><sup>-/-</sup> mice and WT mice, but I did not observe such sequences. However, a more definitive result on this question would require more sequences to ensure deeper coverage of the diverse TCR repertoire.

Alloreactive CD8 T cells in WT mice are not only positively selected on an alternative MHCI molecule, but they may also be negatively selected differently in the presence of other MHCI molecules. As a result, the identification of alloreactive CD8 T cells in mice expressing multiple MHCI genes is not an accurate representation of the positive selection processes of alloreactive T cell populations. To address these two issues, I would aim to use bone marrow chimeras (319) generated using irradiated H-2K<sup>b</sup><sup>-/-</sup> mice or H-2D<sup>b</sup><sup>-/-</sup> mice reconstituted with bone marrow from WT mice. This will allow the positive selection of H-2D<sup>b</sup>PA<sub>224</sub>-specific CD8 T cells on either matched H-2D<sup>b</sup> or mismatched H-2K<sup>b</sup>, because positive selection is mediated exclusively by cortical

thymic epithelial cells, and negative selection on both H-2K<sup>b</sup> and H-2D<sup>b</sup> derived from WT bone marrow. In this way, I could directly assess the impact of positive selection on a mismatched MHCI as compared to a matched MHCI, in the presence of multiple ligands for negative selection. Characterisation of alloreactive H-2D<sup>b</sup>PA<sub>224</sub>-specific CD8 T cells in these chimeric mice will provide a better understanding of precisely how MHC shapes the repertoire of epitope-specific CD8 T cells. In addition, chimeric mice would express H-2D<sup>b</sup> in the periphery, which would allow the generation of an endogenous IAV response during infection, providing a useful tool to assess alloreactive TCR-dependent functionality.

While the expression of particular MHCI molecules in the thymus is paramount for CD8 T cell development, the effect of MHCI expression levels on thymic selection is understudied. Despite modulating the amount of MHCI expressed in hemizygous mice (H-2D<sup>b+/-</sup>K<sup>b-/-</sup> and H-2D<sup>b-/-</sup>K<sup>b+/-</sup>), thymic development and output were unaffected with limiting MHCI levels (**Chapter 4**). This may be due to a known degree of flexibility in the selection process, whereby the TCR avidity threshold for selection adapts to the global average TCR avidity threshold in an individual (320). As a result, if MHCI expression levels in the thymus are globally reduced, relative signalling threshold for selection would also be reduced, to result similar development and output thymocytes. As such, MHCI expression in the thymus is still sufficient to generate peripheral T cells. However, it is possible that T cells with autoreactive TCRs are more likely to survive selection with the adapted TCR avidity threshold. It would therefore be informative to evaluate susceptibility to autoimmune disease and to assess the frequency of cells with more autoreactive TCRs, such as T cells reactive to self-antigen and natural Tregs, in hemizygous mice.

Despite normal thymic development and output, MHCI expression levels influenced the size of the naïve CD8 T cell pool in the periphery (**Chapter 4**). During maintenance, naïve CD8 T cells require tonic signalling *via* the transient TCR-pMHCI interaction, which can potentiate IL-7 signalling and promote naïve T cell survival (105, 321). The number of naïve CD8 T cells in circulation decreases by approximately 50% in hemizygous mice, suggesting that the level of MHCI expressed delimits the number of naïve CD8 T cells that can be maintained in the periphery. Perhaps unsurprisingly, naïve CD8 T cells in hemizygous mice express TCRs of higher self-reactivity (based on their CD5 MFI) and higher expression of the IL-7 receptor  $\alpha$  chain. They also exhibited superior functional capacity to secrete cytokines during infection as homozygous mice. This suggests that reducing the level of MHCI signalling leads to selective survival of the ‘fittest’ T cells, that are most sensitive to both MHCI and IL-7 signalling and that are most functional during an immune response.

Humans co-dominantly express individual MHCIa genes (HLA-A, -B and -C) on both chromosomes. Up to six independent MHCIa allele-specific naïve CD8 T cell populations can be maintained in each individual. The vast number of HLA alleles in the population (253, 299) and such heterozygosity at the HLA loci provides a selective advantage. Heterozygosity at the HLA locus has also been correlated with superior viral control and protection from diseases including HIV (246, 322), HSV1 (244) and HTLV-1 (245), and improved checkpoint blockade immunotherapy (276) compared to homozygous individuals. This is known as the “heterozygote advantage” and it has been assumed to reflect that a larger repertoire of peptides can be presented on MHC molecules in heterozygotes during infection (50). On the other hand, homozygosity of

the HLA genes can positively correlate with severity in autoimmune diseases such as multiple sclerosis (247), celiac disease (323) and rheumatoid arthritis (249). Therefore, MHC I heterozygosity may have conferred a selective advantage during evolution, by mediating a delicate balance during CD8 T cell immunity: to both ensure effective viral control and clearance, as well as preventing autoimmune diseases in humans.

As a result, this work allows me to propose a model, where homozygous and heterozygous individuals may have similar numbers of total CD8 T cells, but heterozygosity at all three MHC I $\alpha$  genes enables the selection and maintenance of six distinct repertoires of MHC I $\alpha$ -restricted CD8 T cells (**Figure 44**). As a result, the CD8 T cell repertoire in heterozygous individuals can engage with a broader array of peptides during infection and neoantigens during cancer, which increases the likelihood of generating a protective response. In addition and as previously outlined, CD8 T cells in heterozygous individuals would have TCRs with higher affinity for self (and possibly foreign) peptides, they would be more sensitive to the homeostatic survival cytokine IL-7 and secrete more IFN $\gamma$ , TNF and IL-2 during infection (**Figure 44**). Thus, despite reducing the number of CD8 T cells specific for a given pMHC I, my work suggests that heterozygosity likely retains CD8 T cells with superior functionality, as well as increasing the breadth of epitope presentation. As a result, heterozygosity at the HLA locus in humans may confer dual advantages to augment the breadth and quality of CD8 T cell immunity during infection.

MHC haplotype restriction							TCR affinity	IL-7R $\alpha$ level	Cytokine Functionality
Gene	A	B	C	A	B	C			
Allele	1	1	1	2	2	2			
Naive CD8 T cell population							High	High	IFN $\gamma$ , TNF and IL-2
							Low	Low	IFN $\gamma$ only

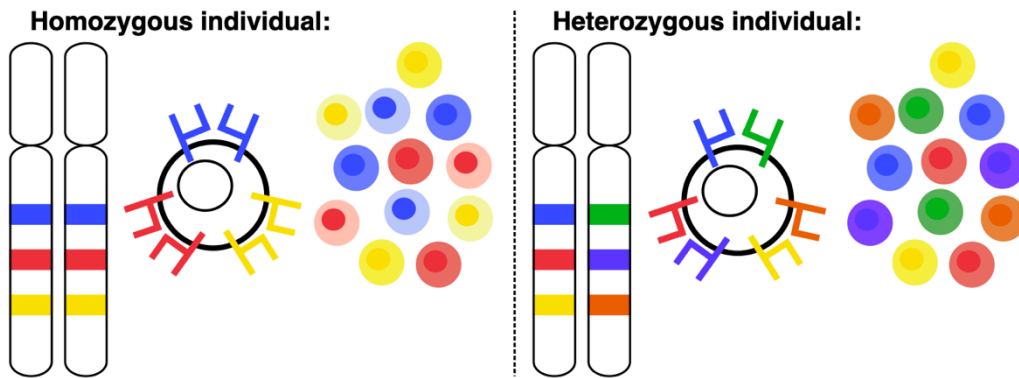


**Figure 44:** Heterozygosity and homozygosity at the HLA locus impacts the quality of peripheral naïve CD8 T cells. Homozygosity at the HLA locus results in a naïve CD8 T cell repertoire with more low affinity TCRs than heterozygous individuals. Heterozygosity at the HLA locus results in six different CD8 T cell repertoires with the same overall number of naïve T cells but more diversity of MHC haplotype restriction, more high affinity TCRs, increased sensitivity to IL-7 and increased cytokine multifunctionality after activation.

This thesis also provided an in-depth analysis of the interactions between CD8 T cells of different specificities, specifically how the loss of one MHC I molecule influences remaining CD8 T cell populations during an infection (**Chapter 5**).

The impact of immunodomination across distinct MHC I $\alpha$  alleles is readily observed and is highly relevant in humans. One example of this occurs during IAV infection in HLA-B\*0801<sup>+</sup> individuals, where the HLA-B\*0801-restricted NP<sub>383</sub> epitope typically generates a subdominant but measurable CD8 T cell response (283). However, in individuals that co-express the HLA-B\*2705 allele, the frequency of HLA-B\*0801-

NP<sub>383</sub>-specific CD8 T cells is threefold lower on average (324, 325). This is thought to be due to competition for presentation of overlapping epitopes by HLA-B80801 (NP<sub>383-391</sub>) and HLA-B\*2705 (NP<sub>381-388</sub>) (326). Similarly, during IAV infection in HLA-A\*0201<sup>+</sup> individuals, the CD8 T cell response against the HLA-A\*0201-NP<sub>44</sub> epitope is threefold higher in individuals that do not co-express HLA-B27 or HLA-A03 (323). This suggests that the HLA-A\*0201-NP<sub>44</sub>-specific CD8 T cell response is somehow suppressed by HLA-B27 and/or HLA-A03. Analogous findings are seen in hepatitis C virus (HCV)-infected patients, where a number of HLA-A2 epitopes are used to predict CD8 T cell responses during HCV infection (292). However, only a minority of the population (~45%) have detectable HCV-specific responses to these HLA-A2 epitopes in the presence of other HLA alleles (326). These observations are suggestive of immunodomination, where the presence and/or absence of certain HLA alleles can modify other HLA-restricted responses during infection.

In animal studies, the loss of immunodominant responses can result in compensation by subdominant responses (156, 272), suggesting that sub-dominant responses were otherwise suppressed by the presence of immunodominant epitopes. Intriguingly, I observed compensation by the immunodominant H-2D<sup>b</sup>NP<sub>366</sub>- and H-2K<sup>b</sup>Ova<sub>257</sub>-specific CD8 T cell responses, rather than subdominant responses, with the loss of H-2K<sup>b</sup> and H-2D<sup>b</sup>, respectively. This suggests that, in this IAV infection model, subdominant responses are intrinsically programmed to respond in an inferior way even with the loss of an entire MHCI-restricted population. This is supported by the finding that subdominant CD8 T cell populations have more low avidity CD8 T cells, leading to a lower magnitude response during infection, while CD8 T cells that give rise to immunodominant responses are comprised predominantly of high avidity TCRs,

leading to greater expansion (147). One could postulate that if immunodominant responses are immunodominant because of a superior capacity to respond, their ability to compensate for the loss of an entire MHCI-restricted response could be increased over sub-dominant responses after infection (147). Although subdominant responses have been shown to increase in magnitude following the elimination of other IAV-specific epitopes during infection (162, 280, 281), subdominant responses in mice lacking one MHCI-restricted population were comparable to WT mice, suggesting that there are other factors driving the immunodominance hierarchy. Hence, whether the capacity of immunodominant responses to compensate for the absence of other MHCI-restricted responses holds true across other systems remains to be investigated. This work is relevant to providing a deeper understanding of the determinants mediating an effective CD8 T cell response, especially in vaccine design where the efficacy of vaccination may vary across individuals with the diverse combinations of HLA that can be expressed in the population. Additionally, this work suggests that vaccine design should be targeted towards immunodominant, rather than subdominant MHCI-restricted epitopes given their capacity to expand further, especially with the vast diversity of HLA alleles expressed in the human population.

Finally, I identified a population of cells, including memory CD8 T cells, NKT cells and NK cells that bind H-2K, but not H-2D<sup>b</sup>, tetramers in the absence of H-2K<sup>b</sup> (**Chapter 3**). This interaction is not TCR-mediated but I propose that it is mediated through the interaction of H-2K tetramers with the Ly49C molecule. Ly49C has been shown to interact strongly with H-2K<sup>b</sup> and it has also been demonstrated to bind H-2D<sup>b</sup> poorly (206, 217), which highlights that there are differences in the basic biology of distinct MHC molecules. The Ly49 family of receptors are expressed on NK cell populations

and play an inhibitory role in regulating NK cell activation through detection of their ligand, MHCI, in a phenomenon known as the “missing-self” (226). Ly49C molecules are predominantly sequestered by H-2K<sup>b</sup> in *cis*, limiting the number of Ly49C available for *trans* binding, making NK cells more sensitive to minute changes in MHCI expression by lowering the activation threshold (216, 221). Ly49C has also been shown to be expressed on memory CD8 T cell subsets (213), with its expression correlating with increased sensitivity to IL-15 and antigen-independent proliferative capacity (327), but the precise function of the Ly49C molecule on memory CD8 T cells is unclear. The phenotype of Ly49C<sup>+</sup> memory CD8 T cells is similar to the virtual memory CD8 T cell subset, which is highly sensitivity to IL-15 and accumulates with age (257). This suggests that the identified population of H-2K<sup>b</sup>-binding CD8 T cells could in fact be virtual memory T cells. Since the loss of H-2K<sup>b</sup> (in H-2K<sup>b</sup><sup>-/-</sup> and DKO mice) likely frees up Ly49C molecules available for *trans* binding, the non-antigen specific activation threshold for Ly49C<sup>+</sup> CD8 T cells may be lowered in the absence of H-2K<sup>b</sup>. If the molecule mediating the H-2K<sup>b</sup> binding is verified to be Ly49C, it may act in a similar way on these conventional CD8 T cells as it does on NK cells, that is to inhibit functionality. Therefore, I postulate that in the absence of H-2K<sup>b</sup>, with a deficit in *cis* binding of Ly49C, the T cells may have a decreased activation threshold and this could drive a virtual memory-like phenotype. Accordingly, a thorough investigation of the activation state, or stimulation threshold of Ly49C<sup>+</sup> CD8 T cell populations in the presence or absence of H-2K<sup>b</sup>, will provide a deeper understanding of the function of Ly49C on CD8 T cells.

Overall, this thesis has expanded our understanding of MHCI determinants regulating CD8 T cell selection, homeostatic maintenance and activation. While there is a general

understanding of the roles played by individual MHCI molecules in these processes, there is still a lack of understanding in how the similarities and differences between MHCI molecules influence CD8 T cell populations. The consequences are perhaps most apparent in the CD8 T cell populations that the MHCI molecules selected for in the thymus and maintain in the periphery. Furthermore, this thesis provided a mechanistic explanation as to how gene dosage influence CD8 T cell maintenance and function and expands our understanding of how MHC heterozygosity may provide an advantage during human evolution. Finally, while it has been widely accepted that cell-mediated components are crucial to induce a T cell response in vaccination, differential HLA genes expressed in each individual is a major complication to vaccine design. Thus, it is critical to understand how CD8 T cell responses restricted by different MHC molecules impact on one another, so that optimal MHC restricted peptide repertoires may be selected for future vaccine strategies. In summary, this thesis provides information that has advanced our fundamental understanding of precisely how changes in the nature and abundance of MHCI determines effective CD8 T cell immunity during infection.



## **7. Bibliography**

1. Janeway, C. A., and R. Medzhitov. 2002. Innate immune recognition. *Annu Rev Immunol* 20: 197–216.
2. Matzinger, P. 1998. An innate sense of danger. *Semin Immunol* 10: 399–415.
3. Zhang, X., and D. Mosser. 2008. Macrophage activation by endogenous danger signals. *J Pathology* 214: 161–178.
4. Schaefer, L. 2014. Complexity of Danger: The diverse nature of damage-associated molecular patterns. *J Biol Chem* 289: 35237–35245.
5. Iwasaki, A., and R. Medzhitov. 2015. Control of adaptive immunity by the innate immune system. *Nat Immunol* 16: 343–353.
6. Daëron, M. 1997. Fc receptor biology. *Annu Rev Immunol* 15: 203–234.
7. Luckheeram, R. V., R. Zhou, A. D. Verma, and B. Xia. 2012. CD4<sup>+</sup>T cells: differentiation and functions. *Clin Dev Immunol* 2012: 925135.
8. Quinn, K. M., R. S. McHugh, F. J. Rich, L. M. Goldsack, G. W. de Lisle, B. M. Buddle, B. Delahunt, and J. R. Kirman. 2006. Inactivation of CD4<sup>+</sup> CD25<sup>+</sup> regulatory T cells during early mycobacterial infection increases cytokine production but does not affect pathogen load. *Immunol Cell Biol* 84: 467–474.

9. Marshall, N. B., and S. L. Swain. 2011. Cytotoxic CD4 T cells in antiviral immunity. *J Biomed Biotechnology* 2011: 954602.
10. Wong, P., and E. G. Pamer. 2003. CD8 T cell responses to infectious pathogens. *Annu Rev Immunol* 21: 29–70.
11. Lowin, B., M. Hahne, C. Mattmann, and J. Tschopp. 1994. Cytolytic T-cell cytotoxicity is mediated through perforin and Fas lytic pathways. *Nature* 370: 650–652.
12. Kagi, D., F. Vignaux, B. Ledermann, K. Burki, V. Depraetere, S. Nagata, H. Hengartner, and P. Golstein. 1994. Fas and perforin pathways as major mechanisms of T cell-mediated cytotoxicity. *Science* 265: 528–530.
13. Liu, C.-C., C. M. Walsh, and J. D.-E. Young. 1995. Perforin: structure and function. *Immunol Today* 16: 194–201.
14. Peters, P. J., J. Borst, V. Oorschot, M. Fukuda, O. Krähenbühl, J. Tschopp, J. W. Slot, and H. J. Geuze. 1991. Cytotoxic T lymphocyte granules are secretory lysosomes, containing both perforin and granzymes. *J Exp Medicine* 173: 1099–1109.
15. Heusel, J. W., R. L. Wesselschmidt, S. Shresta, J. H. Russell, and T. J. Ley. 1994. Cytotoxic lymphocytes require granzyme B for the rapid induction of DNA fragmentation and apoptosis in allogeneic target cells. *Cell* 76: 977–987.
16. Wheelock, E. F. 1965. Interferon-like virus-inhibitor induced in human leukocytes by phytohemagglutinin. *Science* 149: 310–311.

17. Carswell, E. A., L. J. Old, R. L. Kassel, S. Green, N. Fiore, and B. Williamson. 1975. An endotoxin-induced serum factor that causes necrosis of tumors. *Proc National Acad Sci* 72: 3666–3670.
18. Lefranc, M.-P. 2003. IMGT, the international ImMunoGeneTics database ®. *Nucleic Acids Res* 31: 307–310.
19. La Gruta, N. L. L., S. Gras, S. R. Daley, P. G. Thomas, and J. Rossjohn. 2018. Understanding the drivers of MHC restriction of T cell receptors. *Nat Rev Immunol* 18: 467–478.
20. Schatz, D. G., M. A. Oettinger, and D. Baltimore. 1989. The V(D)J recombination activating gene, RAG-1. *Cell* 59: 1035–1048.
21. Cabaniols, J.-P., N. Fazilleau, A. Casrouge, P. Kourilsky, and J. M. Kanellopoulos. 2001. Most  $\alpha/\beta$  T cell receptor diversity is due to terminal deoxynucleotidyl transferase. *J Exp Medicine* 194: 1385–1390.
22. Davis, M. M., and P. J. Bjorkman. 1988. T cell antigen receptor genes and T cell recognition. *Nature* 334: 395–402.
23. Lythe, G., R. E. Callard, R. L. Hoare, and C. Molina-Paris. 2016. How many TCR clonotypes does a body maintain? *J Theor Biol* 389: 214–224.

24. Zarnitsyna, V. I., B. D. Evavold, L. N. Schoettle, J. N. Blattman, and R. Antia. 2013. Estimating the diversity, completeness, and cross-reactivity of the T cell repertoire. *Front Immunol* 4: 485.
25. Krangel, M. S. 2009. Mechanics of T cell receptor gene rearrangement. *Curr Opin Immunol* 21: 133–9.
26. Brazin, K. N., R. J. Mallis, A. Boeszoermyeni, Y. Feng, A. Yoshizawa, P. A. Reche, P. Kaur, K. Bi, R. E. Hussey, J. S. Duke-Cohan, L. Song, G. Wagner, H. Arthanari, M. J. Lang, and E. L. Reinherz. 2018. The T cell antigen receptor  $\alpha$  transmembrane domain coordinates triggering through regulation of bilayer immersion and CD3 subunit associations. *Immunity* 49: 829–841.
27. Marrack, P., J. P. Scott-Browne, S. Dai, L. Gapin, and J. W. Kappler. 2008. Evolutionarily conserved amino acids that control TCR-MHC interaction. *Annu Rev Immunol* 26: 171–203.
28. Stewart-Jones, G. B. E., A. J. McMichael, J. I. Bell, D. I. Stuart, and E. Y. Jones. 2003. A structural basis for immunodominant human T cell receptor recognition. *Nat Immunol* 4: 657–633
29. Meuer, S. C., O. Acuto, R. E. Hussey, J. C. Hodgdon, K. A. Fitzgerald, S. F. Schlossman, and E. L. Reinherz. 1983. Evidence for the T3-associated 90K heterodimer as the T cell antigen receptor. *Nature* 303: 808-810.

30. Wucherpfennig, K. W., E. Gagnon, M. J. Call, E. S. Huseby, and M. E. Call. 2010. Structural biology of the T cell receptor: insights into receptor assembly, ligand recognition, and initiation of signaling. *Csh Perspect Biol* 2: a005140.
31. Dong, D., L. Zheng, J. Lin, B. Zhang, Y. Zhu, N. Li, S. Xie, Y. Wang, N. Gao, and Z. Huang. 2019. Structural basis of assembly of the human T cell receptor–CD3 complex. *Nature* 573: 546–552.
32. Moran, A. E., and K. A. Hogquist. 2012. T cell receptor affinity in thymic development. *Immunology* 135: 261–267.
33. Shah, D. K., and J. C. Zúñiga-Pflücker. 2014. An overview of the intrathymic intricacies of T cell development. *J Immunol* 192: 4017–4023.
34. Rothenberg, E. V. 1992. The development of functionally responsive T cells. *Adv Immunol* 51: 85–214.
35. Shortman, K. 1992. Cellular aspects of early T cell development. *Curr Opin Immunol* 4: 140–146.
36. Ordentlich, P., A. Lin, C.-P. Shen, C. Blaumueller, K. Matsuno, S. Artavanis-Tsakonas, and T. Kadesch. 1998. Notch inhibition of E47 supports the existence of a novel signaling pathway. *Mol Cell Biol* 18: 2230–2239.

37. Sasai, Y., R. Kageyama, Y. Tagawa, R. Shigemoto, and S. Nakanishi. 1992. Two mammalian helix-loop-helix factors structurally related to *Drosophila* hairy and enhancer of split. *Gene Dev* 6: 2620–2634.
38. Tanigaki, K., M. Tsuji, N. Yamamoto, H. Han, J. Tsukada, H. Inoue, M. Kubo, and T. Honjo. 2004. Regulation of  $\alpha\beta/\gamma\delta$  T cell lineage commitment and peripheral T cell responses by Notch/RBP-J signaling. *Immunity* 20: 611–622.
39. Kreslavsky, T., M. Gleimer, M. Miyazaki, Y. Choi, E. Gagnon, C. Murre, P. Sicinski, and H. von Boehmer. 2012.  $\beta$ -selection-induced proliferation is required for  $\alpha\beta$  T cell differentiation. *Immunity* 37: 840–853.
40. Xu, Y., L. Davidson, F. W. Alt, and D. Baltimore. 1996. Function of the pre-T cell receptor alpha chain in T cell development and allelic exclusion at the T cell receptor beta locus. *Proc National Acad Sci* 93: 2169–2173.
41. Pang, S. S., R. Berry, Z. Chen, L. Kjer-Nielsen, M. A. Perugini, G. F. King, C. Wang, S. H. Chew, N. L. La Gruta, N. K. Williams, T. Beddoe, T. Tiganis, N. P. Cowieson, D. I. Godfrey, A. W. Purcell, M. C. J. Wilce, J. McCluskey, and J. Rossjohn. 2010. The structural basis for autonomous dimerization of the pre-T cell antigen receptor. *Nature* 467: 844–8.
42. Yamasaki, S., E. Ishikawa, M. Sakuma, K. Ogata, K. Sakata-Sogawa, M. Hiroshima, D. L. Wiest, M. Tokunaga, and T. Saito. 2005. Mechanistic basis of pre-T cell receptor-mediated autonomous signaling critical for thymocyte development. *Nat Immunol* 7: 67–75.

43. Yang, X., and R. A. Mariuzza. 2015. Pre-T cell receptor binds MHC: implications for thymocyte signaling and selection. *Proc National Acad Sci USA* 112: 8166–7.
44. Alam, S. M., I. N. Crispe, and N. R. J. Gascoigne. 1995. Allelic exclusion of mouse T cell receptor  $\alpha$  chains occurs at the time of thymocyte TCR up-regulation. *Immunity* 3: 449–458.
45. Gascoigne, N. R. J., and S. M. Alam. 1999. Allelic exclusion of the T cell receptor  $\alpha$ -chain: developmental regulation of a post-translational event. *Semin Immunol* 11: 337–347.
46. Boyd, R., I. Kozieradzki, A. Chidgey, H. W. Mittrücker, D. Bouchard, E. Timms, K. Kishihara, C. J. Ong, D. Chui, J. D. Marth, T. W. Mak, and J. M. Penninger. 1998. Receptor-specific allelic exclusion of TCRV alpha-chains during development. *J Immunol* 161: 1718–27.
47. Breuning, M. H., E. M. van den Berg-Loonen, L. F. Bernini, J. B. Bijlsma, E. van Loghem, P. M. Khan, and L. E. Nijenhuis. 1977. Localization of HLA on the short arm of chromosome 6. *Hum Genet* 37: 131–139.
48. Güssow, D., R. Rein, I. Ginjaar, F. Hochstenbach, G. Seemann, A. Kottman, and H. L. Ploegh. 1987. The human beta 2-microglobulin gene. Primary structure and definition of the transcriptional unit. *J Immunol* 139: 3132–8.
49. Marsh, S. G. 2018. Nomenclature for factors of the HLA system, updated September 2018. *HLA* 92: 354–371.

50. Penn, D. J., K. Damjanovich, and W. K. Potts. 2002. MHC heterozygosity confers a selective advantage against multiple-strain infections. *Proc National Acad Sci* 99: 11260–11264.
51. Andrews, P. W., and E. A. Boyse. 1978. Mapping of an H-2-linked gene that influences mating preference in mice. *Immunogenetics* 6: 265–268.
52. Cox, D. R., J. A. Sawicki, D. Yee, E. Appella, and C. J. Epstein. 1982. Assignment of the gene for beta 2-microglobulin ( $\beta_2m$ ) to mouse chromosome 2. *Proc National Acad Sci* 79: 1930–1934.
53. Reeve, E. 1989. Genetic variants and strains of the laboratory mouse, 2nd edition. Edited by Mary Lyon and Anthony Searle. Oxford University Press. 1989. *Genet Res* 54: 239–240.
54. Neefjes, J., M. L. M. Jongsma, P. Paul, and O. Bakke. 2011. Towards a systems understanding of MHC class I and MHC class II antigen presentation. *Nat Rev Immunol* 11: 823–836.
55. Strominger, J. L., W. Ferguson, A. Fuks, M. Giphart, J. Kaufman, D. Mann, H. Orr, P. Parham, R. Robb, and C. Terhorst. 1978. Isolation and structure of HLA antigens. *Birth Defects Orig Article Ser* 14: 235–46.
56. Coligan, J. E., T. J. Kindt, H. Uehara, J. Martinko, and S. G. Nathenson. 1981. Primary structure of a murine transplantation antigen. *Nature* 291: 35–39.

57. Zijlstra, M., M. Bix, N. E. Simister, J. M. Loring, D. H. Raulet, and R. Jaenisch. 2010. Beta 2-microglobulin deficient mice lack CD4-8<sup>+</sup> cytolytic T cells. 1990. *J Immunol* 184: 4587–91.
58. Fremont, D. H., W. A. Hendrickson, P. Marrack, and J. Kappler. 1996. Structures of an MHC class II molecule with covalently bound single peptides. *Science* 272: 1001–1004.
59. Bjorkman, P. J., M. A. Saper, B. Samraoui, W. S. Bennett, J. L. Strominger, and D. C. Wiley. 1987. Structure of the human class I histocompatibility antigen, HLA-A2. *Nature* 329: 506–512.
60. Adams, E. J., and A. M. Luoma. 2013. The adaptable major histocompatibility complex (MHC) fold: structure and function of nonclassical and MHC class I-like molecules. *Annu Rev Immunol* 31: 529–561.
61. Falk, K., O. Rötzschke, S. Stevanović, G. Jung, and H.-G. Rammensee. 1991. Allele-specific motifs revealed by sequencing of self-peptides eluted from MHC molecules. *Nature* 351: 290–296.
62. Nuchtern, J. G., W. E. Biddison, and R. D. Klausner. 1990. Class II MHC molecules can use the endogenous pathway of antigen presentation. *Nature* 343: 74–76.
63. Stern, L. J., I. Potoличchio, and L. Santambrogio. 2006. MHC class II compartment subtypes: structure and function. *Curr Opin Immunol* 18: 64–69.

64. Zhu, Y., A. Y. Rudensky, A. L. Corper, L. Teyton, and I. A. Wilson. 2003. Crystal structure of MHC class II I-A<sup>b</sup> in complex with a human CLIP peptide: prediction of an I-A<sup>b</sup> peptide-binding motif. *J Mol Biol* 326: 1157–1174.
65. Yewdell, J., Bennink, and Y. Hosaka. 1988. Cells process exogenous proteins for recognition by cytotoxic T lymphocytes. *Science* 239: 637–640.
66. Ritz, U., and B. Seliger. 2001. The transporter associated with antigen processing (TAP): structural integrity, expression, function, and its clinical relevance. *Mol Med* 7: 149–158.
67. Wright, C. A., P. Kozik, M. Zacharias, and S. Springer. 2004. Tapasin and other chaperones: models of the MHC class I loading complex. *Biol Chem* 385: 763–778.
68. Hewitt, E. W. 2003. The MHC class I antigen presentation pathway: strategies for viral immune evasion. *Immunology* 110: 163–169.
69. Gaczynska, M., K. L. Rock, and A. L. Goldberg. 1993.  $\gamma$ -Interferon and expression of MHC genes regulate peptide hydrolysis by proteasomes. *Nature* 365: 264–267.
70. Aki, M., N. Shimbara, M. Takashina, K. Akiyama, S. Kagawa, T. Tamura, N. Tanahashi, T. Yoshimura, K. Tanaka, and A. Ichihara. 1994. Interferon-gamma induces different subunit organizations and functional diversity of proteasomes. *J Biochem* 115: 257–69.
71. Driscoll, J., M. G. Brown, D. Finley, and J. J. Monaco. 1993. MHC-linked LMP gene products specifically alter peptidase activities of the proteasome. *Nature* 365: 262–264.

72. Kincaid, E. Z., J. W. Che, I. York, H. Escobar, E. Reyes-Vargas, J. C. Delgado, R. M. Welsh, M. L. Karow, A. J. Murphy, D. M. Valenzuela, G. D. Yancopoulos, and K. L. Rock. 2011. Mice completely lacking immunoproteasomes show major changes in antigen presentation. *Nat Immunol* 13: 129–35.
73. Mishto, M., J. Liepe, K. Textoris-Taube, C. Keller, P. Henklein, M. Weberruß, B. Dahlmann, C. Enenkel, A. Voigt, U. Kuckelkorn, M. P. H. Stumpf, and P. M. Kloetzel. 2014. Proteasome isoforms exhibit only quantitative differences in cleavage and epitope generation. *Eur J Immunol* 44: 3508–3521.
74. Zanker, D., and W. Chen. 2014. Standard and immunoproteasomes show similar peptide degradation specificities. *Eur J Immunol* 44: 3500–3503.
75. Wu, T., J. Guan, A. Handel, D. C. Tschärke, J. Sidney, A. Sette, L. M. Wakim, X. Y. X. Sng, P. G. Thomas, N. P. Croft, A. W. Purcell, and N. L. La Gruta. 2019. Quantification of epitope abundance reveals the effect of direct and cross-presentation on influenza CTL responses. *Nat Comm* 10: 2846.
76. Xu, H., and D. R. Littman. 1993. A kinase-independent function of Lck in potentiating antigen-specific T cell activation. *Cell* 74: 633–643.
77. Cole, D. K., K. M. Miles, F. Madura, C. J. Holland, A. J. A. Schauenburg, A. J. Godkin, A. M. Bulek, A. Fuller, H. J. E. Akpovwa, P. G. Pymm, N. Liddy, M. Sami, Y. Li, P. J. Rizkallah, B. K. Jakobsen, and A. K. Sewell. 2014. T-cell receptor (TCR)-peptide specificity overrides affinity-enhancing TCR-major histocompatibility complex interactions. *J Biol Chem* 289: 628–638.

78. Merwe, P. A. van der, and S. J. Davis. 2003. Molecular interactions mediating T cell antigen recognition. *Annu Rev Immunol* 21: 659–684.
79. Stone, J. D., A. S. Chervin, and D. M. Kranz. 2009. T-cell receptor binding affinities and kinetics: impact on T-cell activity and specificity. *Immunology* 126: 165–176.
80. Day, E. B., C. Guillonneau, S. Gras, N. L. La Gruta, D. A. A. Vignali, P. C. Doherty, A. W. Purcell, J. Rossjohn, and S. J. Turner. 2011. Structural basis for enabling T cell receptor diversity within biased virus-specific CD8<sup>+</sup> T cell responses. *Proc National Acad Sci* 108: 9536–9541.
81. Garcia, K. C., J. J. Adams, D. Feng, and L. K. Ely. 2009. The molecular basis of TCR germline bias for MHC is surprisingly simple. *Nat Immunol* 10: 143–147.
82. Yin, Y., X. X. Wang, and R. A. Mariuzza. 2012. Crystal structure of a complete ternary complex of T-cell receptor, peptide-MHC, and CD4. *Proc National Acad Sci USA* 109: 5405–10.
83. Li, Y., Y. Yin, and R. A. Mariuzza. 2013. Structural and biophysical insights into the role of CD4 and CD8 in T cell activation. *Front Immunol* 4: 206.
84. Gras, S., J. Chadderton, C. M. Del Campo, C. Farenc, F. Wiede, T. M. Josephs, X. Y. X. Sng, M. Mirams, K. A. Watson, T. Tiganis, K. M. Quinn, J. Rossjohn, and N. L. La Gruta. 2016. Reversed T cell receptor docking on a major histocompatibility class I complex limits involvement in the immune response. *Immunity* 45: 749-760.

85. Beringer, D. X., F. S. Kleijwegt, F. Wiede, A. R. van der Slik, K. L. Loh, J. Petersen, N. L. Dudek, G. Duinkerken, S. Laban, A. Joosten, J. P. Vivian, Z. Chen, A. P. Uldrich, D. I. Godfrey, J. McCluskey, D. A. Price, K. J. Radford, A. W. Purcell, T. Nikolic, H. H. Reid, T. Tiganis, B. O. Roep, and J. Rossjohn. 2015. T cell receptor reversed polarity recognition of a self-antigen major histocompatibility complex. *Nat Immunol* 16: 1153–1161.
86. Buslepp, J., H. Wang, W. E. Biddison, E. Appella, and E. J. Collins. 2003. A Correlation between TCR V $\alpha$  Docking on MHC and CD8 Dependence Implications for T Cell Selection. *Immunity* 19: 595–606.
87. Hahn, M., M. J. Nicholson, J. Pyrdol, and K. W. Wucherpfennig. 2005. Unconventional topology of self peptide–major histocompatibility complex binding by a human autoimmune T cell receptor. *Nat Immunol* 6: 490-796.
88. Brownlie, R. J., and R. Zamoyska. 2013. T cell receptor signalling networks: branched, diversified and bounded. *Nat Rev Immunol* 13: 257–269.
89. Starr, T. K., S. C. Jameson, and K. A. Hogquist. 2003. Positive and negative selection of T cells. *Annu Rev Immunol* 21: 139–176.
90. Jameson, S. C., K. A. Hogquist, and M. J. Bevan. 1995. Positive Selection of Thymocytes. *Annu Rev Immunol* 13: 93–126.
91. Yates, A. J. 2014. Theories and quantification of thymic selection. *Front Immunol* 5: 13.

92. Linette, G. P., M. J. Grusby, S. M. Hedrick, T. H. Hansen, L. H. Glimcher, and S. J. Korsmeyer. 1994. Bcl-2 is upregulated at the CD4+ CD8+ stage during positive selection and promotes thymocyte differentiation at several control Points. *Immunity* 1: 197–205.
93. R. M. Zinkernagel and P. C. Doherty. 1974. Restriction of *in vitro* T cell-mediated cytotoxicity in lymphocytic choriomeningitis within a syngeneic or semiallogeneic system. *Nature* 248: 701–702
94. Daley, S. R., D. Y. Hu, and C. C. Goodnow. 2013. Helios marks strongly autoreactive CD4+ T cells in two major waves of thymic deletion distinguished by induction of PD-1 or NF- $\kappa$ B. *J Exp Medicine* 210: 269–85.
95. Stritesky, G. L., Y. Xing, J. R. Erickson, L. A. Kalekar, X. Wang, D. L. Mueller, S. C. Jameson, and K. A. Hogquist. 2013. Murine thymic selection quantified using a unique method to capture deleted T cells. *Proc National Acad Sci USA* 110: 4679–84.
96. Mathis, D., and C. Benoist. 2009. AIRE. *Annu Rev Immunol* 27: 287–312.
97. Kyewski, B., and L. Klein. 2006. A central role for central tolerance. *Annu Rev Immunol* 24: 571–606.
98. Klein, L., M. Hinterberger, G. Wirnsberger, and B. Kyewski. 2009. Antigen presentation in the thymus for positive selection and central tolerance induction. *Nat Rev Immunol* 9: 833–844.

99. van Meerwijk, J. P., S. Marguerat, R. K. Lees, R. N. Germain, B. J. Fowlkes, and R. H. MacDonald. 1997. Quantitative impact of thymic clonal deletion on the T cell repertoire. *J Exp Medicine* 185: 377–384.
100. Shortman, K., D. Vremec, and M. Egerton. 1991. The kinetics of T cell antigen receptor expression by subgroups of CD4+8+ thymocytes: delineation of CD4+8+3(2+) thymocytes as post-selection intermediates leading to mature T cells. *J Exp Medicine* 173: 323–332.
101. Huesmann, M., B. Scott, P. Kisielow, and H. von Boehmer. 1991. Kinetics and efficacy of positive selection in the thymus of normal and T cell receptor transgenic mice. *Cell* 66: 533–540.
102. Boyman, O., C. Ramsey, D. M. Kim, J. Sprent, and C. D. Surh. 2008. IL-7/anti-IL-7 mAb complexes restore T cell development and induce homeostatic T cell expansion without lymphopenia. *J Immunol* 180: 7265–7275.
103. Rathmell, J. C., E. A. Farkash, W. Gao, and C. B. Thompson. 2001. IL-7 enhances the survival and maintains the size of naive T cells. *J Immunol* 167: 6869–6876.
104. Mendoza, A., V. Fang, C. Chen, M. Serasinghe, A. Verma, J. Muller, V. S. Chaluvadi, M. L. Dustin, T. Hla, O. Elemento, J. E. Chipuk, and S. R. Schwab. 2017. Lymphatic endothelial S1P promotes mitochondrial function and survival in naive T cells. *Nature* 546: 158–161.

105. Tanchot, C., F. A. Lemonnier, B. Péronau, A. A. Freitas, and B. Rocha. 1997. Differential requirements for survival and proliferation of CD8 naïve or memory T cells. *Science* 276: 2057–2062.
106. Almeida, A. R. M., B. Rocha, A. A. Freitas, and C. Tanchot. 2005. Homeostasis of T cell numbers: from thymus production to peripheral compartmentalization and the indexation of regulatory T cells. *Semin Immunol* 17: 239–249.
107. Stefanová, I., J. R. Dorfman, and R. N. Germain. 2002. Self-recognition promotes the foreign antigen sensitivity of naive T lymphocytes. *Nature* 420: 429–434.
108. Dzhagalov, I., A. Dunkle, and Y.-W. He. 2008. The anti-apoptotic Bcl-2 family member Mcl-1 promotes T lymphocyte survival at multiple stages. *J Immunol* 181: 521–528.
109. Ernst, B., D.-S. Lee, J. M. Chang, J. Sprent, and C. D. Surh. 1999. The peptide ligands mediating positive selection in the thymus control T cell survival and homeostatic proliferation in the periphery. *Immunity* 11: 173–181.
110. Goldrath, A. W., and M. J. Bevan. 1999. Selecting and maintaining a diverse T cell repertoire. *Nature* 402: 35005508.
111. Goldrath, A. W., and M. J. Bevan. 1999. Low-affinity ligands for the TCR drive proliferation of mature CD8<sup>+</sup> T cells in lymphopenic hosts. *Immunity* 11: 183–190.

112. Kieper, W. C., and S. C. Jameson. 1999. Homeostatic expansion and phenotypic conversion of naïve T cells in response to self-peptide/MHC ligands. *Proc National Acad Sci* 96: 13306–13311.
113. Boer, R. J. D., and A. S. Perelson. 2013. Quantifying T lymphocyte turnover. *J Theor Biol* 327: 45–87.
114. Parretta, E., G. Cassese, A. Santoni, J. Guardiola, A. Vecchio, and F. D. Rosa. 2008. kinetics of *in vivo* proliferation and death of memory and naïve CD8 T cells: parameter estimation based on 5-bromo-2'-deoxyuridine incorporation in spleen, lymph nodes, and bone marrow. *J Immunol* 180: 7230–7239.
115. Rane, S., T. Hogan, B. Seddon, and A. J. Yates. 2018. Age is not just a number: Naive T cells increase their ability to persist in the circulation over time. *PLOS Biol* 16: e2003949.
116. Belz, G. T., N. S. Wilson, C. M. Smith, A. M. Mount, F. R. Carbone, and W. R. Heath. 2006. Bone marrow-derived cells expand memory CD8<sup>+</sup> T cells in response to viral infections of the lung and skin. *Eur J Immunol* 36: 327–335.
117. Jung, S., D. Unutmaz, P. Wong, G.-I. Sano, K. D. los Santos, T. Sparwasser, S. Wu, S. Vuthoori, K. Ko, F. Zavala, E. G. Pamer, D. R. Littman, and R. A. Lang. 2002. *In vivo* depletion of CD11c<sup>+</sup> dendritic cells abrogates priming of CD8<sup>+</sup> T cells by exogenous cell-associated antigens. *Immunity* 17: 211–220.
118. Zammit, D. J., L. S. Cauley, Q.-M. Pham, and L. Lefrançois. 2005. Dendritic cells maximize the memory CD8 T cell response to infection. *Immunity* 22: 561–570.

119. Haring, J. S., V. P. Badovinac, and J. T. Harty. 2006. Inflaming the CD8+ T cell response. *Immunity* 25: 19–29.
120. Mescher, M. F., J. M. Curtsinger, P. Agarwal, K. A. Casey, M. Gerner, C. D. Hammerbeck, F. Popescu, and Z. Xiao. 2006. Signals required for programming effector and memory development by CD8+ T cells. *Immunol Rev* 211: 81–92.
121. Hodge, J. W., H. Sabzevari, A. G. Yafal, L. Gritz, M. G. Lorenz, and J. Schlom. 1999. A triad of costimulatory molecules synergize to amplify T cell activation. *Cancer Res* 59: 5800–7.
122. Dubey, C., M. Croft, and S. L. Swain. 1995. Costimulatory requirements of naive CD4+ T cells. ICAM-1 or B7-1 can co-stimulate naive CD4 T cell activation but both are required for optimum response. *J Immunol* 155: 45–57.
123. Parra, E., A. G. Wingren, G. Hedlund, T. Kalland, and M. Dohlsten. 1997. The role of B7-1 and LFA-3 in costimulation of CD8+ T cells. *J Immunol* 158: 637–42.
124. Wingren, A. G., E. Parra, M. Varga, T. Kalland, H.-O. Sjogren, G. Hedlund, and M. Dohlsten. 1995. T cell activation pathways: B7, LFA-3, and ICAM-1 shape unique T cell profiles. *Crit Rev Immunol* 15: 235–253.
125. Curtsinger, J. M., J. O. Valenzuela, P. Agarwal, D. Lins, and M. F. Mescher. 2005. Cutting edge: Type I IFNs provide a third signal to CD8 T cells to stimulate clonal expansion and differentiation. *J Immunol* 174: 4465–4469.

126. Curtsinger, J. M., C. S. Schmidt, A. Mondino, D. C. Lins, R. M. Kedl, M. K. Jenkins, and M. F. Mescher. 1999. Inflammatory cytokines provide a third signal for activation of naive CD4<sup>+</sup> and CD8<sup>+</sup> T cells. *J Immunol* 162: 3256–62.
127. Parrish-Novak, J., S. R. Dillon, A. Nelson, A. Hammond, C. Sprecher, J. A. Gross, J. Johnston, K. Madden, W. Xu, J. West, S. Schrader, S. Burkhead, M. Heipel, C. Brandt, J. L. Kuijper, J. Kramer, D. Conklin, S. R. Presnell, J. Berry, F. Shiota, S. Bort, K. Hambly, S. Mudri, C. Clegg, M. Moore, F. J. Grant, C. Lofton-Day, T. Gilbert, F. Raymond, A. Ching, L. Yao, D. Smith, P. Webster, T. Whitmore, M. Maurer, K. Kaushansky, R. D. Holly, and D. Foster. 2000. Interleukin 21 and its receptor are involved in NK cell expansion and regulation of lymphocyte function. *Nature* 408: 57–63.
128. Tschärke, D. C., N. P. Croft, P. C. Doherty, and N. L. La Gruta. 2015. Sizing up the key determinants of the CD8<sup>+</sup> T cell response. *Nat Rev Immunol* 15: 705–716.
129. Roy-Proulx, G., M. Meunier, A. Lanteigne, S. Brochu, and C. Perreault. 2001. Immunodomination results from functional differences between competing CTL. *Eur J Immunol* 31: 2284–2292.
130. Chen, W., K. Pang, K.-A. Masterman, G. Kennedy, S. Basta, N. Dimopoulos, F. Hornung, M. Smyth, J. R. Bennink, and J. W. Yewdell. 2004. Reversal in the Immunodominance Hierarchy in Secondary CD8<sup>+</sup> T Cell Responses to Influenza A Virus: Roles for Cross-Presentation and Lysis-Independent Immunodomination. *J Immunol* 173: 5021–5027.

131. Choi, E. Y., G. J. Christianson, Y. Yoshimura, T. J. Sproule, N. Jung, S. Joyce, and D. C. Roopenian. 2002. Immunodominance of H60 is caused by an abnormally high precursor T cell pool directed against its unique minor histocompatibility antigen peptide. *Immunity* 17: 593–603.
132. Badovinac, V. P., J. S. Haring, and J. T. Harty. 2007. Initial T cell receptor transgenic cell precursor frequency dictates critical aspects of the CD8<sup>+</sup> T cell response to infection. *Immunity* 26: 827–841.
133. Jenkins, M. K., and J. J. Moon. 2012. The role of naive T cell precursor frequency and recruitment in dictating immune response magnitude. *J Immunol* 188: 4135–4140.
134. Tschärke, D. C., G. Karupiah, J. Zhou, T. Palmore, K. R. Irvine, S. M. M. Haeryfar, S. Williams, J. Sidney, A. Sette, J. R. Bennink, and J. W. Yewdell. 2005. Identification of poxvirus CD8<sup>+</sup> T cell determinants to enable rational design and characterization of smallpox vaccines. *J Exp Medicine* 201: 95–104.
135. Flesch, I. E. A., W.-P. Woo, Y. Wang, V. Panchanathan, Y.-C. Wong, N. L. La Gruta, T. Cukalac, and D. C. Tschärke. 2010. Altered CD8<sup>+</sup> T Cell immunodominance after vaccinia virus infection and the naive repertoire in inbred and F1 mice. *J Immunol* 184: 45–55.
136. Quinn, K. M., S. G. Zaloumis, T. Cukalac, W.-T. Kan, X. Y. X. Sng, M. Mirams, K. A. Watson, J. M. McCaw, P. C. Doherty, P. G. Thomas, A. Handel, and N. L. La Gruta. 2016. Heightened self-reactivity associated with selective survival, but not expansion, of naïve virus-specific CD8<sup>+</sup> T cells in aged mice. *Proc National Acad Sci* 113: 1333–1338.

137. La Gruta, N. L., W. T. Rothwell, T. Cukalac, N. G. Swan, S. A. Valkenburg, K. Kedzierska, P. G. Thomas, P. C. Doherty, and S. J. Turner. 2010. Primary CTL response magnitude in mice is determined by the extent of naive T cell recruitment and subsequent clonal expansion. *J Clin Invest* 120: 1885–1894.
138. Obar, J. J., K. M. Khanna, and L. Lefrançois. 2008. Endogenous naive CD8<sup>+</sup> T cell precursor frequency regulates primary and memory responses to infection. *Immunity* 28: 859–69.
139. Schmidt, J., A. K. N. Iversen, S. Tenzer, E. Gostick, D. A. Price, V. Lohmann, U. Distler, P. Bowness, H. Schild, H. E. Blum, P. Klenerman, C. Neumann-Haefelin, and R. Thimme. 2012. Rapid antigen processing and presentation of a protective and immunodominant HLA-B\*27-restricted hepatitis C virus-specific CD8<sup>+</sup> T cell epitope. *PLOS Pathogen* 8: e1003042.
140. Iglesias, M. C., O. Briceno, E. Gostick, A. Moris, C. Meaudre, D. A. Price, M.-N. Ungeheuer, A. Saez-Cirion, R. Mallone, and V. Appay. 2012. Immunodominance of HLA-B27-restricted HIV KK10-specific CD8(+) T-cells is not related to naïve precursor frequency. *Immunol Lett* 149: 119–22.
141. Belz, G. T., P. G. Stevenson, and P. C. Doherty. 2000. Contemporary analysis of MHC-related immunodominance hierarchies in the CD8<sup>+</sup> T cell response to influenza A viruses. *J Immunol* 165: 2404–2409.
142. Ruckwardt, T. J., A. M. W. Malloy, E. Gostick, D. A. Price, P. Dash, J. L. McClaren, P. G. Thomas, and B. S. Graham. 2011. Neonatal CD8 T cell hierarchy is distinct from adults

and is influenced by intrinsic T cell properties in respiratory syncytial virus infected mice. *PLOS Pathogen* 7: e1002377.

143. Malherbe, L., C. Hausl, L. Teyton, and M. G. McHeyzer-Williams. 2004. Clonal selection of helper T cells is determined by an affinity threshold with no further skewing of TCR binding properties. *Immunity* 21: 669–679.

144. Cukalac, T., J. Chadderton, A. Handel, P. C. Doherty, S. J. Turner, P. G. Thomas, and N. L. La Gruta. 2014. Reproducible selection of high avidity CD8+ T cell clones following secondary acute virus infection. *Proc National Acad Sci* 111: 1485–1490.

145. McHeyzer-Williams, L. J., J. F. Panus, J. A. Mikszta, and M. G. McHeyzer-Williams. 1999. Evolution of antigen-specific T cell receptors *in vivo*: Pre-immune and antigen-driven selection of preferred complementarity-determining region 3 (CDR3) motifs. *J Exp Medicine* 189: 1823–1838.

146. Zehn, D., S. Y. Lee, and M. J. Bevan. 2009. Complete but curtailed T-cell response to very low-affinity antigen. *Nature* 458: 211–214.

147. Cukalac, T., J. Chadderton, W. Zeng, J. G. Cullen, W. T. Kan, P. C. Doherty, D. C. Jackson, S. J. Turner, and N. L. La Gruta. 2014. The influenza virus-specific CTL immunodominance hierarchy in mice is determined by the relative frequency of high-avidity T cells. *J Immunol* 192: 4061–4068.

148. Busch, D. H., and E. G. Pamer. 1999. T cell affinity maturation by selective expansion during infection. *J Exp Medicine* 189: 701–710.

149. Cukalac, T., W. Kan, P. Dash, J. Guan, K. M. Quinn, S. Gras, P. G. Thomas, and N. L. La Gruta. 2015. Paired TCR $\alpha\beta$  analysis of virus-specific CD8<sup>+</sup> T cells exposes diversity in a previously defined 'narrow' repertoire. *Immunol Cell Biol* 93: 804–814.
150. Turner, S. J., G. Diaz, R. Cross, and P. C. Doherty. 2003. Analysis of clonotype distribution and persistence for an influenza virus-specific CD8<sup>+</sup> T cell response. *Immunity* 18: 549–559.
151. Wensveen, F. M., K. P. J. M. van Gisbergen, I. A. M. Derks, C. Gerlach, T. N. Schumacher, R. A. W. van Lier, and E. Eldering. 2010. Apoptosis threshold set by Noxa and Mcl-1 after T cell activation regulates competitive selection of high-affinity clones. *Immunity* 32: 754–765.
152. Hildeman, D. A., Y. Zhu, T. C. Mitchell, P. Bouillet, A. Strasser, J. Kappler, and P. Marrack. 2002. Activated T cell death *in vivo* mediated by proapoptotic Bcl-2 family member Bim. *Immunity* 16: 759–767.
153. Most, R. G. van der, K. Murali-Krishna, J. G. Lanier, E. J. Wherry, M. T. Puglielli, J. N. Blattman, A. Sette, and R. Ahmed. 2003. Changing immunodominance patterns in antiviral CD8 T-cell responses after loss of epitope presentation or chronic antigenic stimulation. *Virology* 315: 93–102.
154. Purcell, A. W., N. P. Croft, and D. C. Tscharke. 2016. Immunology by numbers: quantitation of antigen presentation completes the quantitative milieu of systems immunology! *Curr Opin Immunol* 40: 88–95.

155. Rutigliano, J. A., T. J. Ruckwardt, J. E. Martin, and B. S. Graham. 2007. Relative dominance of epitope-specific CD8<sup>+</sup> T cell responses in an F1 hybrid mouse model of respiratory syncytial virus infection. *Virology* 362: 314–319.
156. Luciani, F., M. T. Sanders, S. Oveissi, K. C. Pang, and W. Chen. 2013. Increasing viral dose causes a reversal in CD8<sup>+</sup> T cell immunodominance during primary influenza infection due to differences in antigen presentation, T cell avidity, and precursor numbers. *J Immunol* 190: 36–47.
157. Yewdell, J. W., L. C. Antón, and J. R. Bennink. 1996. Defective ribosomal products (DRiPs): a major source of antigenic peptides for MHC class I molecules? *J Immunol* 157: 1823–6.
158. Zanker, D. J., S. Oveissi, D. C. Tschärke, M. Duan, S. Wan, X. Zhang, K. Xiao, N. A. Mifsud, J. Gibbs, L. Izzard, D. Dlugolenski, P. Faou, K. L. Laurie, N. Vigneron, I. G. Barr, J. Stambas, B. J. V. den Eynde, J. R. Bennink, J. W. Yewdell, and W. Chen. 2019. Influenza A virus infection induces viral and cellular defective ribosomal products encoded by alternative reading frames. *J Immunol* 202: 3370–3380.
159. Kedl, R. M., B. C. Schaefer, J. W. Kappler, and P. Murrack. 2001. T cells down-modulate peptide-MHC complexes on APCs *in vivo*. *Nat Immunol* 3: 27–32.
160. Kedl, R. M., W. A. Rees, D. A. Hildeman, B. Schaefer, T. Mitchell, J. Kappler, and P. Murrack. 2000. T cells compete for access to antigen-bearing antigen-presenting Cells. *J Exp Medicine* 192: 1105–1114.

161. Butz, E. A., and M. J. Bevan. 1998. Massive expansion of antigen-specific CD8<sup>+</sup> T cells during an acute virus infection. *Immunity* 8: 167–175.
162. Webby, R. J., S. Andreansky, J. Stambas, J. E. Rehg, R. G. Webster, P. C. Doherty, and S. J. Turner. 2003. Protection and compensation in the influenza virus-specific CD8<sup>+</sup> T cell response. *Proc National Acad Sci* 100: 7235–7240.
163. Jenkins, M. R., R. Webby, P. C. Doherty, and S. J. Turner. 2006. Addition of a prominent epitope affects influenza A virus-specific CD8<sup>+</sup> T cell immunodominance hierarchies when antigen is limiting. *J Immunol* 177: 2917–2925.
164. Mintern, J. D., S. Bedoui, G. M. Davey, J. M. Moffat, P. C. Doherty, and S. J. Turner. 2009. Transience of MHC Class I-restricted antigen presentation after influenza A virus infection. *Proc National Acad Sci* 106: 6724–6729.
165. Effros, R. B., P. C. Doherty, W. Gerhard, and J. Bennink. 1977. Generation of both cross-reactive and virus-specific T-cell populations after immunization with serologically distinct influenza A viruses. *J Exp Medicine* 145: 557–568.
166. Heiny, A. T., O. Miotto, K. N. Srinivasan, A. M. Khan, G. L. Zhang, V. Brusic, T. W. Tan, and J. T. August. 2007. Evolutionarily conserved protein sequences of influenza A viruses, avian and human, as vaccine targets. *PLOS One* 2: e1190.
167. Townsend, A., J. Bastin, H. Bodmer, G. Brownlee, J. Davey, F. Gotch, K. Gould, I. Jones, A. McMichael, J. Rothbard, and G. Smith. 1989. Recognition of influenza virus

---

proteins by cytotoxic T lymphocytes. *Philosophical Transactions Royal Soc Lond Ser B Biological Sci* 323: 527–33.

168. Townsend, A. R. M., J. Rothbard, F. M. Gotch, G. Bahadur, D. Wraith, and A. J. McMichael. 2006. The epitopes of influenza nucleoprotein recognized by cytotoxic T lymphocytes can be defined with short synthetic peptides. 1986. *J Immunol* 176: 5141–50.

169. La Gruta, N. L., K. Kedzierska, K. Pang, R. Webby, M. Davenport, W. Chen, S. J. Turner, and P. C. Doherty. 2006. A virus-specific CD8<sup>+</sup> T cell immunodominance hierarchy determined by antigen dose and precursor frequencies. *Proc National Acad Sci USA* 103: 994–999.

170. Belz, G. T., W. Xie, and P. C. Doherty. 2001. Diversity of epitope and cytokine profiles for primary and secondary influenza A virus-specific CD8<sup>+</sup> T cell responses. *J Immunol* 166: 4627–4633.

171. Belz, G. T., W. Xie, J. D. Altman, and P. C. Doherty. 2000. A previously unrecognized H-2D<sup>b</sup>-restricted peptide prominent in the primary influenza A virus-specific CD8<sup>+</sup>T cell response is much less apparent following secondary challenge. *J Virol* 74: 3486–3493.

172. Maryanski, J. L., C. V. Jongeneel, P. Bucher, J.-L. Casanova, and P. R. Walker. 1996. Single-cell PCR analysis of TCR repertoires selected by antigen *in vivo*: a high magnitude CD8 response is comprised of very few clones. *Immunity* 4: 47–55.

173. La Gruta, N. L. L., P. G. Thomas, A. I. Webb, M. A. Dunstone, T. Cukalac, P. C. Doherty, A. W. Purcell, J. Rossjohn, and S. J. Turner. 2008. Epitope-specific TCR $\beta$  repertoire

diversity imparts no functional advantage on the CD8<sup>+</sup> T cell response to cognate viral peptides. *Proc National Acad Sci* 105: 2034–2039.

174. Kedzierska, K., S. J. Turner, and P. C. Doherty. 2004. Conserved T cell receptor usage in primary and recall responses to an immunodominant influenza virus nucleoprotein epitope. *Proc National Acad Sci* 101: 4942–4947.

175. Kedzierska, K., V. Venturi, K. Field, M. P. Davenport, S. J. Turner, and P. C. Doherty. 2006. Early establishment of diverse T cell receptor profiles for influenza-specific CD8<sup>+</sup>CD62L<sup>hi</sup> memory T cells. *Proc National Acad Sci* 103: 9184–9189.

176. Deckhut, A. M., W. Allan, A. McMickle, M. Eichelberger, M. A. Blackman, P. C. Doherty, and D. L. Woodland. 1993. Prominent usage of V beta 8.3 T cells in the H-2D<sup>b</sup>-restricted response to an influenza A virus nucleoprotein epitope. *J Immunol* 151: 2658–66.

177. Brander, C., K. E. Hartman, A. K. Trocha, N. G. Jones, R. P. Johnson, B. Korber, P. Wentworth, S. P. Buchbinder, S. Wolinsky, B. D. Walker, and S. A. Kalams. 1998. Lack of strong immune selection pressure by the immunodominant, HLA-A\*0201-restricted cytotoxic T lymphocyte response in chronic human immunodeficiency virus-1 infection. *J Clin Invest* 101: 2559–2566.

178. Koenderman, L. 2019. Inside-Out Control of Fc-Receptors. *Front Immunol* 10: 544.

179. Dash, P., J. L. McClaren, T. H. Oguin, W. Rothwell, B. Todd, M. Y. Morris, J. Becksfort, C. Reynolds, S. A. Brown, P. C. Doherty, and P. G. Thomas. 2011. Paired analysis of TCR $\alpha$  and TCR $\beta$  chains at the single-cell level in mice. *J Clin Invest* 121: 288–295.

180. Jin, D., and J. Sprent. 2018. GM-CSF culture revisited: preparation of bulk populations of highly pure dendritic cells from mouse bone marrow. *J Immunol* 201: 3129–3139.
181. Lutz, M. B., N. Kukutsch, A. L. J. Ogilvie, S. Rößner, F. Koch, N. Romani, and G. Schuler. 1999. An advanced culture method for generating large quantities of highly pure dendritic cells from mouse bone marrow. *J Immunol Methods* 223: 77–92.
182. Kim, A., Y.-W. Noh, K. D. Kim, Y. S. Jang, Y.-K. Choe, and J.-S. Lim. 2004. Activated natural killer cell-mediated immunity is required for the inhibition of tumor metastasis by dendritic cell vaccination. *Exp Mol Medicine* 36: 428–443.
183. Ye, F., J. Turner, and E. Flaño. 2012. Contribution of pulmonary KLRG1<sup>high</sup> and KLRG1<sup>low</sup> CD8 T cells to effector and memory responses during influenza virus infection. *J Immunol* 189: 5206–5211.
184. Shane, H. L., K. L. Reagin, and K. D. Klonowski. 2018. The respiratory environment diverts the development of antiviral memory CD8 T cells. *J Immunol* 200: 3752–3761.
185. Suchin, E. J., P. B. Langmuir, E. Palmer, M. H. Sayegh, A. D. Wells, and L. A. Turka. 2001. Quantifying the frequency of alloreactive T cells *in vivo*: new answers to an old question. *J Immunol* 166: 973–981.
186. Shlomchik, W. D. 2007. Graft-versus-host disease. *Nat Rev Immunol* 7: 340–352.
187. Kolb, H.-J. 2008. Graft-versus-leukemia effects of transplantation and donor lymphocytes. *Blood* 112: 4371–4383.

188. Rocha, P. N., T. J. Plumb, S. D. Crowley, and T. M. Coffman. 2003. Effector mechanisms in transplant rejection. *Immunol Rev* 196: 51–64.
189. Felix, N. J., and P. M. Allen. 2007. Specificity of T-cell alloreactivity. *Nat Rev Immunol* 7: 942–953.
190. Pullen, J. K., R. M. Horton, Z. L. Cai, and L. R. Pease. 1992. Structural diversity of the classical H-2 genes: K, D, and L. *J Immunol* 148: 953–67.
191. Huseby, E. S., J. White, F. Crawford, T. Vass, D. Becker, C. Pinilla, P. Marrack, and J. W. Kappler. 2005. How the T cell repertoire becomes peptide and MHC specific. *Cell* 122: 247–260.
192. Zerrahn, J., W. Held, and D. H. Raulet. 1997. The MHC reactivity of the T cell repertoire prior to positive and negative Selection. *Cell* 88: 627–636.
193. Bevan, M. J. 1984. High determinant density may explain the phenomenon of alloreactivity. *Immunol Today* 5: 128–30.
194. Kaye, J., and C. A. Janeway. 1984. The Fab fragment of a directly activating monoclonal antibody that precipitates a disulfide-linked heterodimer from a helper T cell clone blocks activation by either allogeneic Ia or antigen and self-Ia. *J Exp Med* 159: 1397–1412.

195. Chelvanayagam, G., I. B. Jakobsen, X. Gao, and S. Easteal. 1996. Structural comparison of major histocompatibility complex class I molecules and homology modelling of five distinct human leukocyte antigen-A alleles. *Protein Eng Des Sel* 9: 1151–1164.
196. Wang, Y., N. K. Singh, T. T. Spear, L. M. Hellman, K. H. Piepenbrink, R. H. McMahan, H. R. Rosen, C. W. V. Kooi, M. I. Nishimura, and B. M. Baker. 2017. How an alloreactive T-cell receptor achieves peptide and MHC specificity. *Proc National Acad Sci* 114: E4792–E4801.
197. Felix, N. J., D. L. Donermeyer, S. Horvath, J. J. Walters, M. L. Gross, A. Suri, and P. M. Allen. 2007. Alloreactive T cells respond specifically to multiple distinct peptide-MHC complexes. *Nat Immunol* 8: 388–397.
198. Obst, R., N. Netuschil, K. Klopfer, S. Stevanović, and H.-G. Rammensee. 2000. The role of peptides in T cell alloreactivity is determined by self–major histocompatibility complex molecules. *J Exp Medicine* 191: 805–812.
199. Lechler, R. I., G. Lombardi, J. R. Batchelor, N. Reinsmoen, and F. H. Bach. 1990. The molecular basis of alloreactivity. *Immunol Today* 11: 83–88.
200. Chu, H. H., J. J. Moon, K. Takada, M. Pepper, J. A. Molitor, T. W. Schacker, K. A. Hogquist, S. C. Jameson, and M. K. Jenkins. 2009. Positive selection optimizes the number and function of MHCII-restricted CD4+ T cell clones in the naive polyclonal repertoire. *Proc National Acad Sci* 106: 11241–11245.

201. Tham, E. L., and M. F. Mescher. 2002. The Poststimulation Program of CD4 Versus CD8 T Cells (Death Versus Activation-Induced Non-responsiveness). *J Immunol* 169: 1822–1828.
202. Moine, A. L., M. Goldman, and D. Abramowicz. 2002. Multiple pathways to allograft rejection. *Transplantation* 73: 1373–1381.
203. Rosenberg, A. S., and A. Singer. 1992. Cellular basis of skin allograft rejection: an *in vivo* model of immune-mediated tissue destruction. *Annu Rev Immunol* 10: 333–360.
204. Hellmann, D., and J. Stobo. 1982. The autologous mixed lymphocyte reaction. *Arthritis Rheumatism* 25: 121–125.
205. Weksler, M. E., C. E. Moody, and R. W. Kozak. 1981. The autologous mixed-lymphocyte reaction. *Adv Immunol* 31: 271–312.
206. Hanke, T., H. Takizawa, C. W. McMahon, D. H. Busch, E. G. Pamer, J. D. Miller, J. D. Altman, Y. Liu, D. Cado, F. A. Lemonnier, P. J. Bjorkman, and D. H. Raulet. 1999. Direct assessment of MHC class I binding by seven Ly49 inhibitory NK cell receptors. *Immunity* 11: 67–77.
207. Salter, R. D., R. J. Benjamin, P. K. Wesley, S. E. Buxton, T. P. J. Garrett, C. Clayberger, A. M. Krensky, A. M. Norment, D. R. Littman, and P. Parham. 1990. A binding site for the T cell co-receptor CD8 on the  $\alpha_3$  domain of HLA-A2. *Nature* 345: 41–46.

208. Salter, R. D., A. M. Norment, B. P. Chen, C. Clayberger, A. M. Krensky, D. R. Littman, and P. Parham. 1989. Polymorphism in the  $\alpha_3$  domain of HLA-A molecules affects binding to CD8. *Nature* 338: 345–347.
209. Norment, A. M., D. R. Littman, P. Parham, R. D. Salter, and V. H. Engelhard. 1988. Cell-cell adhesion mediated by CD8 and MHC class I molecules. *Nature* 336: 79.
210. Michaëlsson, J., A. Achour, A. Rölle, and K. Kärre. 2001. MHC class I recognition by NK receptors in the Ly49 family is strongly influenced by the  $\beta_2$ -microglobulin subunit. *J Immunol* 166: 7327–7334.
211. Wooldridge, L., H. A. van den Berg, M. Glick, E. Gostick, B. Laugel, S. L. Hutchinson, A. Milicic, J. M. Brenchley, D. C. Douek, D. A. Price, and A. K. Sewell. 2005. Interaction between the CD8 coreceptor and major histocompatibility complex class I stabilizes T cell receptor-antigen complexes at the cell surface. *J Biol Chem* 280: 27491–27501.
212. Borg, N. A., K. S. Wun, L. Kjer-Nielsen, M. C. J. Wilce, D. G. Pellicci, R. Koh, G. S. Besra, M. Bharadwaj, D. I. Godfrey, J. McCluskey, and J. Rossjohn. 2007. CD1d–lipid-antigen recognition by the semi-invariant NKT T cell receptor. *Nature* 448: 44–49.
213. Coles, M. C., C. W. McMahon, H. Takizawa, and D. H. Raulet. 2000. Memory CD8 T lymphocytes express inhibitory MHC-specific Ly49 receptors. *Eur J Immunol* 30: 236–244.
214. Gapin, L., J. L. Matsuda, C. D. Surh, and M. Kronenberg. 2001. NKT cells derive from double-positive thymocytes that are positively selected by CD1d. *Nat Immunol* 2: 971–978.

215. Dam, J., R. Guan, K. Natarajan, N. Dimasi, L. K. Chlewicki, D. M. Kranz, P. Schuck, D. H. Margulies, and R. A. Mariuzza. 2003. Variable MHC class I engagement by Ly49 natural killer cell receptors demonstrated by the crystal structure of Ly49C bound to H-2K<sup>b</sup>. *Nat Immunol* 4: 1213–1222.
216. Scarpellino, L., F. Oeschger, P. Guillaume, J. D. Coudert, F. Lévy, G. Leclercq, and W. Held. 2007. Interactions of Ly49 Family Receptors with MHC Class I Ligands in *trans* and *cis*. *J Immunol* 178: 1277–1284.
217. Brennan, J., G. Mahon, D. L. Mager, W. A. Jefferies, and F. Takei. 1996. Recognition of class I major histocompatibility complex molecules by Ly49: specificities and domain interactions. *J Exp Med* 183: 1553–1559.
218. Tormo, J., K. Natarajan, D. H. Margulies, and R. A. Mariuzza. 1999. Crystal structure of a lectin-like natural killer cell receptor bound to its MHC class I ligand. *Nature* 402: 623–631.
219. Wang, J., M. C. Whitman, K. Natarajan, J. Tormo, R. A. Mariuzza, and D. H. Margulies. 2001. Binding of the natural killer cell inhibitory receptor Ly49A to its major histocompatibility complex class I ligand. *J Biol Chem* 277: 1433–1442.
220. Matsumoto, N., M. Mitsuki, K. Tajima, W. M. Yokoyama, and K. Yamamoto. 2001. The functional binding site for the C-type lectin-like natural killer cell receptor Ly49A spans three domains of its major histocompatibility complex class I ligand. *J Exp Medicine* 193: 147–158.

221. Doucey, M.-A., L. Scarpellino, J. Zimmer, P. Guillaume, I. F. Luescher, C. Bron, and W. Held. 2004. *Cis* association of Ly49A with MHC class I restricts natural killer cell inhibition. *Nat Immunol* 5: 328–336.
222. Yu, Y. Y. L., T. George, J. R. Dorfman, J. Roland, V. Kumar, and M. Bennett. 1996. The role of Ly49A and 5E6(Ly49C) molecules in hybrid resistance mediated by murine natural killer cells against normal T cell blasts. *Immunity* 4: 67–76.
223. Alyea, E. P. 2008. Modulating graft-versus-host disease to enhance the graft-versus-leukemia effect. *Best Pract Res Cl Ha* 21: 239–250.
224. Garcia, K. C., M. Degano, R. L. Stanfield, A. Brunmark, M. R. Jackson, P. A. Peterson, L. Teyton, and I. A. Wilson. 1996. An  $\alpha\beta$  T cell receptor structure at 2.5Å and its orientation in the TCR-MHC complex. *Science* 274: 209–219.
225. Maeda, M., S. Lohwasser, T. Yamamura, and F. Takei. 2001. Regulation of NKT Cells by Ly49: analysis of primary NKT cells and generation of NKT cell line. *J Immunol* 167: 4180–4186.
226. Shifrin, N., D. H. Raulet, and M. Ardolino. 2014. NK cell self-tolerance, responsiveness and missing self-recognition. *Semin Immunol* 26: 138–44.
227. Huard, B., and K. Früh. 2000. A role for MHC class I down-regulation in NK cell lysis of herpes virus-infected cells. *Eur J Immunol* 30: 509–515.

228. Reefman, E., J. G. Kay, S. M. Wood, C. Offenhäuser, D. L. Brown, S. Roy, A. C. Stanley, P. C. Low, A. P. Manderson, and J. L. Stow. 2010. Cytokine secretion is distinct from secretion of cytotoxic granules in NK cells. *J Immunol* 184: 4852–4862.
229. Held, W., and R. A. Mariuzza. 2008. Cis interactions of immunoreceptors with MHC and non-MHC ligands. *Nat Rev Immunol* 8: 269–278.
230. Li, L., M. Dong, and X.-G. Wang. 2016. The implication and significance of beta 2 microglobulin: A conservative multifunctional regulator. *Chinese Med J-peking* 129: 448–455.
231. Labrecque, N., L. S. Whitfield, R. Obst, C. Waltzinger, C. Benoist, and D. Mathis. 2001. How much TCR does a T cell need? *Immunity* 15: 71–82.
232. Polic, B., D. Kunkel, A. Scheffold, and K. Rajewsky. 2001. How T cells deal with induced TCR ablation. *Proc National Acad Sci* 98: 8744–8749.
233. Seddon, B., and R. Zamoyska. 2002. TCR and IL-7 receptor signals can operate independently or synergize to promote lymphopenia-induced expansion of naïve T cells. *J Immunol* 169: 3752–3759.
234. Schluns, K. S., W. C. Kieper, S. C. Jameson, and L. Lefrançois. 2000. Interleukin-7 mediates the homeostasis of naïve and memory CD8 T cells *in vivo*. *Nat Immunol* 1: 426–432.

235. Tan, J. T., E. Dudl, E. LeRoy, R. Murray, J. Sprent, K. I. Weinberg, and C. D. Surh. 2001. IL-7 is critical for homeostatic proliferation and survival of naïve T cells. *Proc National Acad Sci* 98: 8732–8737.
236. Vivien, L., C. Benoist, and D. Mathis. 2001. T lymphocytes need IL-7 but not IL-4 or IL-6 to survive *in vivo*. *Int Immunol* 13: 763–768.
237. Park, J.-H., Q. Yu, B. Erman, J. S. Appelbaum, D. Montoya-Durango, H. L. Grimes, and A. Singer. 2004. Suppression of IL7Ralpha transcription by IL-7 and other pro-survival cytokines: a novel mechanism for maximizing IL-7-dependent T cell survival. *Immunity* 21: 289–302.
238. Kieper, W. C., J. T. Tan, B. Bondi-Boyd, L. Gapin, J. Sprent, R. Ceredig, and C. D. Surh. 2002. Overexpression of interleukin (IL)-7 leads to IL-15-independent generation of memory phenotype CD8+ T Cells. *J Exp Medicine* 195: 1533–1539.
239. Mertsching, E., C. Burdet, and R. Ceredig. 1995. IL-7 transgenic mice: analysis of the role of IL-7 in the differentiation of thymocytes *in vivo* and *in vitro*. *Int Immunol* 7: 401–414.
240. Kieper, W. C., J. T. Burghardt, and C. D. Surh. 2004. A Role for TCR affinity in regulating naive T cell homeostasis. *J Immunol* 172: 40–44.
241. Moses, C. T., K. M. Thorstenson, S. C. Jameson, and A. Khoruts. 2003. Competition for self-ligands restrains homeostatic proliferation of naïve CD4 T cells. *Proc National Acad Sci* 100: 1185–1190.

- 
242. Troy, A. E., and H. Shen. 2003. Cutting edge: homeostatic proliferation of peripheral T lymphocytes is regulated by clonal competition. *J Immunol* 170: 672–676.
243. Tang, J., C. Costello, I. P. M. Keet, C. Rivers, S. Leblanc, E. Karita, S. Allen, and R. A. Kaslow. 1999. HLA class I homozygosity accelerates disease progression in human immunodeficiency virus type 1 infection. *AIDS Res Hum Retrov* 15: 317–324.
244. Seppänen, M., M. Lokki, T. Timonen, M. Lappalainen, H. Jarva, A. Järvinen, S. Sarna, V. Valtonen, and S. Meri. 2001. Complement C4 deficiency and HLA homozygosity in patients with frequent intraoral herpes simplex virus type 1 infections. *Clin Infect Dis* 33: 1604–1607.
245. Jeffery, K. J. M., A. A. Siddiqui, M. Bunce, A. L. Lloyd, A. M. Vine, A. D. Witkover, S. Izumo, K. Usuku, K. I. Welsh, M. Osame, and C. R. M. Bangham. 2000. The influence of HLA class I alleles and heterozygosity on the outcome of human T cell lymphotropic virus type I infection. *J Immunol* 165: 7278–7284.
246. Carrington, M., G. W. Nelson, M. P. Martin, T. Kissner, D. Vlahov, J. J. Goedert, R. Kaslow, S. Buchbinder, K. Hoots, and S. J. O'Brien. 1999. HLA and HIV-1: heterozygote advantage and B\*35-Cw\*04 disadvantage. *Science* 283: 1748–1752.
247. Barcellos, L. F., J. R. Oksenberg, A. B. Begovich, E. R. Martin, S. Schmidt, E. Vittinghoff, D. S. Goodin, D. Pelletier, R. R. Lincoln, P. Bucher, A. Swerdlin, M. A. Pericak-Vance, J. L. Haines, S. L. Hauser, and M. S. G. Group. 2003. HLA-DR2 dose effect on susceptibility to multiple sclerosis and influence on disease course. *Am J Hum Genetics* 72: 710–716.

248. Kupfer, S. S., and B. Jabri. 2012. Pathophysiology of celiac disease. *Gastrointest Endosc Clin North Am* 22: 639–60.
249. Weyand, C. M., and J. J. Goronzy. 2000. Association of MHC and rheumatoid arthritis: HLA polymorphisms in phenotypic variants of rheumatoid arthritis. *Arthritis Res* 2: 212.
250. Pérarnau, B., M. Saron, B. R. S. Martin, N. Bervas, H. Ong, M. J. Soloski, A. G. Smith, J. M. Ure, J. E. Gairin, and F. A. Lemonnier. 1999. Single H2K<sup>b</sup>, H2D<sup>b</sup> and double H2K<sup>b</sup>D<sup>b</sup> knockout mice: peripheral CD8<sup>+</sup> T cell repertoire and anti-lymphocytic choriomeningitis virus cytolytic responses. *Eur J Immunol* 29: 1243–1252.
251. La Gruta, N. L., S. J. Turner, and P. C. Doherty. 2004. Hierarchies in cytokine expression profiles for acute and resolving influenza virus-specific CD8<sup>+</sup> T cell responses: correlation of cytokine profile and TCR avidity. *J Immunol* 172: 5553–5560.
252. Moon, J. J., H. H. Chu, M. Pepper, S. J. McSorley, S. C. Jameson, R. M. Kedl, and M. K. Jenkins. 2007. Naive CD4<sup>+</sup> T cell frequency varies for different epitopes and predicts repertoire diversity and response magnitude. *Immunity* 27: 203–213.
253. Lefranc, M.-P., V. Giudicelli, P. Duroux, J. Jabado-Michaloud, G. Folch, S. Aouinti, E. Carillon, H. Duvergey, A. Houles, T. Paysan-Lafosse, S. Hadi-Saljoqi, S. Sasorith, G. Lefranc, and S. Kossida. 2014. IMGT®, the international ImMunoGeneTics information system® 25 years on. *Nucleic Acids Res* 43: D413-22.

- 
254. Ruscher, R., R. L. Kummer, Y. J. Lee, S. C. Jameson, and K. A. Hogquist. 2017. CD8 $\alpha$  intraepithelial lymphocytes arise from two main thymic precursors. *Nat Immunol* 18: 771–779.
255. Zachariah, M. A., and J. G. Cyster. 2010. Neural crest–derived pericytes promote egress of mature thymocytes at the corticomedullary junction. *Science* 328: 1129–1135.
256. Haluszczak, C., A. D. Akue, S. E. Hamilton, L. D. S. Johnson, L. Pujanauski, L. Teodorovic, S. C. Jameson, and R. M. Kedl. 2009. The antigen-specific CD8<sup>+</sup> T cell repertoire in unimmunized mice includes memory phenotype cells bearing markers of homeostatic expansion. *J Exp Medicine* 206: 435–48.
257. Quinn, K. M., A. Fox, K. L. Harland, B. E. Russ, J. Li, T. H. O. Nguyen, L. Loh, M. Olshanksy, H. Naeem, K. Tsyganov, F. Wiede, R. Webster, C. Blyth, X. Y. X. Sng, T. Tiganis, D. Powell, P. C. Doherty, S. J. Turner, K. Kedzierska, and N. L. La Gruta. 2018. Age-related decline in primary CD8<sup>+</sup> T cell responses is associated with the development of senescence in virtual memory CD8<sup>+</sup> T cells. *Cell Reports* 23: 3512–3524.
258. Staton, T. L., B. Johnston, E. C. Butcher, and D. J. Campbell. 2004. Murine CD8<sup>+</sup> recent thymic emigrants are  $\alpha$ E integrin-positive and CC chemokine ligand 25 responsive. *J Immunol* 172: 7282–7288.
259. Azzam, H. S., A. Grinberg, K. Lui, H. Shen, E. W. Shores, and P. E. Love. 1998. CD5 expression is developmentally regulated by T cell receptor (TCR) signals and TCR avidity. *J Exp Medicine* 188: 2301–2311.

260. Fulton, R. B., S. E. Hamilton, Y. Xing, J. A. Best, A. W. Goldrath, K. A. Hogquist, and S. C. Jameson. 2015. The TCR's sensitivity to self peptide-MHC dictates the ability of naïve CD8+ T cells to respond to foreign antigens. *Nat Immunol* 16: 107–117.
261. Mandl, J. N., J. P. Monteiro, N. Vrisekoop, and R. N. Germain. 2013. T cell-positive selection uses self-ligand binding strength to optimize repertoire recognition of foreign antigens. *Immunity* 38: 263–274.
262. Seder, R. A., P. A. Darrah, and M. Roederer. 2008. T cell quality in memory and protection: implications for vaccine design. *Nat Rev Immunol* 8: 247–258.
263. Almeida, J. R., D. A. Price, L. Papagno, Z. A. Arkoub, D. Sauce, E. Bornstein, T. E. Asher, A. Samri, A. Schnuriger, I. Theodorou, D. Costagliola, C. Rouzioux, H. Agut, A.-G. Marcelin, D. Douek, B. Autran, and V. Appay. 2007. Superior control of HIV-1 replication by CD8+ T cells is reflected by their avidity, polyfunctionality, and clonal turnover. *J Exp Medicine* 204: 2473–2485.
264. Viret, C., F. S. Wong, and C. A. Janeway. 1999. Designing and maintaining the mature TCR repertoire. *Immunity* 10: 559–568.
265. Messaoudi, I., J. A. G. Patiño, R. Dyal, J. LeMaout, and J. Nikolich-Žugich. 2002. Direct link Between MHC polymorphism, T cell avidity, and diversity in immune defence. *Science* 298: 1797–1800.
266. Delaney, J. R., Y. Sykulev, H. N. Eisen, and S. Tonegawa. 1998. Differences in the level of expression of class I major histocompatibility complex proteins on thymic epithelial

and dendritic cells influence the decision of immature thymocytes between positive and negative selection. *Proc National Acad Sci* 95: 5235–5240.

267. Römermann, D., W. R. Heath, J. Allison, B. Bayer, Y. Sorge, J. F. A. P. Miller, and M. W. Hoffmann. 2001. Ligand density determines the efficiency of negative selection in the thymus. *Transplantation* 72: 305–311.

268. Sebzda, E., V. Wallace, J. Mayer, R. Yeung, T. Mak, and P. Ohashi. 1994. Positive and negative thymocyte selection induced by different concentrations of a single peptide. *Science* 263: 1615–1618.

269. Fehling, H., W. Swat, C. Laplace, R. Kuhn, K. Rajewsky, U. Muller, and H. von Boehmer. 1994. MHC class I expression in mice lacking the proteasome subunit LMP-7. *Science* 265: 1234–1237.

270. Tomaru, U., S. Konno, S. Miyajima, R. Kimoto, M. Onodera, S. Kiuchi, S. Murata, A. Ishizu, and M. Kasahara. 2019. Restricted expression of the thymoproteasome is required for thymic selection and peripheral homeostasis of CD8<sup>+</sup> T cells. *Cell Reports* 26: 639-651.

271. Davey, G. M., S. L. Schober, B. T. Endrizzi, A. K. Dutcher, S. C. Jameson, and K. A. Hogquist. 1998. Preselection thymocytes are more sensitive to T cell receptor stimulation than mature T cells. *J Exp Medicine* 188: 1867–1874.

272. Peterson, D. A., R. J. DiPaolo, O. Kanagawa, and E. R. Unanue. 1999. Cutting edge: negative selection of immature thymocytes by a few peptide-MHC complexes: differential sensitivity of immature and mature T cells. *J Immunol* 162: 3117–20.

273. Cho, J.-H., H.-O. Kim, C. D. Surh, and J. Sprent. 2010. T cell receptor-dependent regulation of lipid rafts controls naive CD8+ T cell homeostasis. *Immunity* 32: 214–26.
274. Gett, A. V., F. Sallusto, A. Lanzavecchia, and J. Geginat. 2003. T cell fitness determined by signal strength. *Nat Immunol* 4: 355–360.
275. Rudd, B. D., V. Venturi, G. Li, P. Samadder, J. M. Ertelt, S. S. Way, M. P. Davenport, and J. Nikolich-Zugich. 2011. Nonrandom attrition of the naive CD8+ T-cell pool with aging governed by T-cell receptor:pMHC interactions. *Proc National Acad Sci USA* 108: 13694–9.
276. Chowell, D., L. G. T. Morris, C. M. Grigg, J. K. Weber, R. M. Samstein, V. Makarov, F. Kuo, S. M. Kendall, D. Requena, N. Riaz, B. Greenbaum, J. Carroll, E. Garon, D. M. Hyman, A. Zehir, D. Solit, M. Berger, R. Zhou, N. A. Rizvi, and T. A. Chan. 2017. Patient HLA class I genotype influences cancer response to checkpoint blockade immunotherapy. *Science* 359: 582–587.
277. Dandine-Roulland, C., R. Laurent, I. Dall’Ara, B. Toupance, and R. Chaix. 2019. Genomic evidence for MHC disassortative mating in humans. *Proc Royal Soc B Biological Sci* 286: 20182664.
278. Potts, W. K., C. J. Manning, and E. K. Wakeland. 1991. Mating patterns in seminatural populations of mice influenced by MHC genotype. *Nature* 352: 619–621.
279. Ober, C., L. R. Weitkamp, N. Cox, H. Dytch, D. Kostyu, and S. Elias. 1997. HLA and Mate Choice in Humans. *Am J Hum Genetics* 61: 497–504.

280. Thomas, P. G., S. A. Brown, R. Keating, W. Yue, M. Y. Morris, J. So, R. J. Webby, and P. C. Doherty. 2007. Hidden epitopes emerge in secondary influenza virus-specific CD8+ T cell responses. *J Immunol* 178: 3091–3098.
281. Andreansky, S. S., J. Stambas, P. G. Thomas, W. Xie, R. J. Webby, and P. C. Doherty. 2005. Consequences of immunodominant epitope deletion for minor influenza virus-specific CD8+ T cell Responses. *J Virol* 79: 4329–4339.
282. Newberg, M. H., K. J. McEvers, D. A. Gorgone, M. A. Lifton, S. H. C. Baumeister, R. S. Veazey, J. E. Schmitz, and N. L. Letvin. 2006. Immunodomination in the evolution of dominant epitope-specific CD8+ T lymphocyte responses in simian immunodeficiency virus-infected rhesus monkeys. *J Immunol* 176: 319–328.
283. Huet, S., D. F. Nixon, J. B. Rothbard, A. Townsend, S. A. Ellis, and A. J. McMichael. 1990. Structural homologies between two HLA B27-restricted peptides suggest residues important for interaction with HLA B27. *Int Immunol* 2: 311–316.
284. Chen, C., R. W. Compans, and P. W. Choppin. 1971. Parainfluenza virus surface projections: glycoproteins with haemagglutinin and neuraminidase activities. *J Gen Virol* 11: 53–58.
285. Kaech, S. M., J. T. Tan, E. J. Wherry, B. T. Konieczny, C. D. Surh, and R. Ahmed. 2003. Selective expression of the interleukin 7 receptor identifies effector CD8 T cells that give rise to long-lived memory cells. *Nat Immunol* 4: 1191–1198.

286. Stock, A. T., C. M. Jones, W. R. Heath, and F. R. Carbone. 2006. CTL response compensation for the loss of an immunodominant class I-restricted HSV-1 determinant. *Immunol Cell Biol* 84: 543–550.
287. Burton, D. R., R. C. Desrosiers, R. W. Doms, W. C. Koff, P. D. Kwong, J. P. Moore, G. J. Nabel, J. Sodroski, I. A. Wilson, and R. T. Wyatt. 2004. HIV vaccine design and the neutralizing antibody problem. *Nat Immunol* 5: 233–236.
288. Goulder, P. J. R., R. E. Phillips, R. A. Colbert, S. McAdam, G. Ogg, M. A. Nowak, P. Giangrande, G. Luzzi, B. Morgana, A. Edwards, A. J. McMichael, and S. Rowland-Jones. 1997. Late escape from an immunodominant cytotoxic T lymphocyte response associated with progression to AIDS. *Nat Med* 3: 212–217.
289. Hahn, Y. S. 2003. Subversion of immune responses by hepatitis C virus: immunomodulatory strategies beyond evasion? *Curr Opin Immunol* 15: 443–449.
290. Koutsakos, M., H. E. G. McWilliam, T. E. Aktepe, S. Fritzlar, P. T. Illing, N. A. Mifsud, A. W. Purcell, S. Rockman, P. C. Reading, J. P. Vivian, J. Rossjohn, A. G. Brooks, J. M. Mackenzie, J. D. Mintern, J. A. Villadangos, T. H. O. Nguyen, and K. Kedzierska. 2019. Downregulation of MHC class I expression by influenza A and B viruses. *Front Immunol* 10: 1158.
291. Orr, M. T., K. H. Edelmann, J. Vieira, L. Corey, D. H. Raulet, and C. B. Wilson. 2005. Inhibition of MHC class I is a virulence factor in herpes simplex virus infection of mice. *PLOS Pathogen* 1: e7.

292. Cerny, A., J. G. McHutchison, C. Pasquinelli, M. E. Brown, M. A. Brothers, B. Grabscheid, P. Fowler, M. Houghton, and F. V. Chisari. 1995. Cytotoxic T lymphocyte response to hepatitis C virus-derived peptides containing the HLA A2.1 binding motif. *J Clin Invest* 95: 521–530.
293. Heijst, J. W. J. van, C. Gerlach, E. Swart, D. Sie, C. Nunes-Alves, R. M. Kerkhoven, R. Arens, M. Correia-Neves, K. Schepers, and T. N. M. Schumacher. 2009. Recruitment of antigen-specific CD8<sup>+</sup> T cells in response to infection is markedly efficient. *Science* 325: 1265–1269.
294. Fujinami, R. S., M. G. von Herrath, U. Christen, and J. L. Whitton. 2006. Molecular Mimicry, Bystander Activation, or Viral Persistence: Infections and Autoimmune Disease. *Clin Microbiol Rev* 19: 80–94.
295. Xiao, Z., K. A. Casey, S. C. Jameson, J. M. Curtsinger, and M. F. Mescher. 2009. Programming for CD8 T cell memory development requires IL-12 or type I IFN. *J Immunol* 182: 2786–2794.
296. Feau, S., R. Arens, S. Togher, and S. P. Schoenberger. 2011. Autocrine IL-2 is required for secondary population expansion of CD8<sup>+</sup> memory T cells. *Nat Immunol* 12: 908–913.
297. Northrop, J. K., R. M. Thomas, A. D. Wells, and H. Shen. 2006. Epigenetic remodeling of the IL-2 and IFN- $\gamma$  loci in memory CD8 T cells is influenced by CD4 T cells. *J Immunol* 177: 1062–1069.
298. Klein, J. 1982. Histocompatibility antigens, structure and function. 221–239.

299. Robinson, J., D. J. Barker, X. Georgiou, M. A. Cooper, P. Flicek, and S. G. E. Marsh. 2019. IPD-IMGT/HLA Database. *Nucleic Acids Res. Published ahead of print.*
300. Bitarello, B. D., R. dos S. Francisco, and D. Meyer. 2015. Heterogeneity of dN/dS ratios at the classical HLA class I genes over divergence time and across the allelic phylogeny. *J Mol Evol* 82: 38–50.
301. Bleek, G. M. van, and S. G. Nathenson. 1991. The structure of the antigen-binding groove of major histocompatibility complex class I molecules determines specific selection of self-peptides. *Proc National Acad Sci* 88: 11032–11036.
302. Borghans, J. A. M., J. B. Beltman, and R. J. D. Boer. 2004. MHC polymorphism under host-pathogen coevolution. *Immunogenetics* 55: 732–739.
303. Gascoigne, N. R. J., V. Rybakin, O. Acuto, and J. Brzostek. 2016. TCR signal strength and T cell development. *Annu Rev Cell Dev Bi* 32: 327–348.
304. Kisielow, P. 2019. How does the immune system learn to distinguish between good and evil? The first definitive studies of T cell central tolerance and positive selection. *Immunogenetics* 71: 513–518.
305. Klein, L., B. Kyewski, P. M. Allen, and K. A. Hogquist. 2014. Positive and negative selection of the T cell repertoire: what thymocytes see (and don't see). *Nat Rev Immunol* 14: 377–91.

306. Sharon, E., L. V. Sibener, A. Battle, H. B. Fraser, K. C. Garcia, and J. K. Pritchard. 2016. Genetic variation in MHC proteins is associated with T cell receptor expression biases. *Nat Genet* 48: 995–1002.
307. Gao, K., L. Chen, Y. Zhang, Y. Zhao, Z. Wan, J. Wu, L. Lin, Y. Kuang, J. Lu, X. Zhang, L. Tian, X. Liu, and X. Qiu. 2019. Germline-encoded TCR-MHC contacts promote TCR V gene bias in umbilical cord blood T cell repertoire. *Front Immunol* 10: 2064.
308. Emerson, R. O., W. S. DeWitt, M. Vignali, J. Gravley, J. K. Hu, E. J. Osborne, C. Desmarais, M. Klinger, C. S. Carlson, J. A. Hansen, M. Rieder, and H. S. Robins. 2017. Immunosequencing identifies signatures of cytomegalovirus exposure history and HLA-mediated effects on the T cell repertoire. *Nat Genet* 49: 659–665.
309. Simpson, A. A., F. Mohammed, M. Salim, A. Tranter, A. B. Rickinson, H. J. Stauss, P. A. H. Moss, N. M. Steven, and B. E. Willcox. 2011. Structural and energetic evidence for highly peptide-specific tumor antigen targeting *via* allo-MHC restriction. *Proc National Acad Sci USA* 108: 21176–81.
310. Huseby, E. S., F. Crawford, J. White, P. Marrack, and J. W. Kappler. 2006. Interface-disrupting amino acids establish specificity between T cell receptors and complexes of major histocompatibility complex and peptide. *Nat Immunol* 7: 1191–1199.
311. Alam, S. M., G. M. Davies, C. M. Lin, T. Zal, W. Nasholds, S. C. Jameson, K. A. Hogquist, N. R. J. Gascoigne, and P. J. Travers. 1999. Qualitative and quantitative differences in T cell receptor binding of agonist and antagonist ligands. *Immunity* 10: 227–237.

312. Liu, C.-P., F. Crawford, P. Marrack, and J. Kappler. 1998. T cell positive selection by a high density, low affinity ligand. *Proc National Acad Sci* 95: 4522–4526.
313. Adams, J. J., S. Narayanan, B. Liu, M. E. Birnbaum, A. C. Kruse, N. A. Bowerman, W. Chen, A. M. Levin, J. M. Connolly, C. Zhu, D. M. Kranz, and K. C. Garcia. 2011. T cell receptor signaling is limited by docking geometry to peptide-major histocompatibility complex. *Immunity* 35: 681–93.
314. Enk, A. H., H. Jonuleit, J. Saloga, and J. Knop. 1997. Dendritic cells as mediators of tumor-induced tolerance in metastatic melanoma. *Int J Cancer* 73: 309–316.
315. Gabrilovich, D. I., H. L. Chen, K. R. Girgis, H. T. Cunningham, G. M. Meny, S. Nadaf, D. Kavanaugh, and D. P. Carbone. 1996. Production of vascular endothelial growth factor by human tumors inhibits the functional maturation of dendritic cells. *Nat Med* 2: 1096–1103.
316. Merad, M., T. Sugie, E. G. Engleman, and L. Fong. 2002. *In vivo* manipulation of dendritic cells to induce therapeutic immunity. *Blood* 99: 1676–1682.
317. Nestle, F. O., G. Burg, J. Fähr, T. Wrone-Smith, and B. J. Nickoloff. 1997. Human sunlight-induced basal-cell-carcinoma-associated dendritic cells are deficient in T cell co-stimulatory molecules and are impaired as antigen-presenting cells. *Am J Pathology* 150: 641–51.
318. Thurnher, M., C. Radmayr, R. Ramoner, S. Ebner, G. Böck, H. Klocker, N. Romani, and G. Bartsch. 1996. Human renal-cell carcinoma tissue contains dendritic cells. *Int J Cancer* 68: 1–7.

319. Zinkernagel, R. M., and A. Althage. 1999. On the role of thymic epithelium vs. bone marrow-derived cells in repertoire selection of T cells. *Proc National Acad Sci* 96: 8092–8097.
320. Stojakovic, M., L. I. Salazar-Fontana, Z. Tatari-Calderone, V. P. Badovinac, F. R. Santori, D. Kovalovsky, D. Sant'Angelo, J. T. Harty, and S. Vukmanovic. 2008. Adaptable TCR avidity thresholds for negative selection. *J Immunol* 181: 6770–6778.
321. Takada, K., and S. C. Jameson. 2009. Self-class I MHC molecules support survival of naive CD8 T cells, but depress their functional sensitivity through regulation of CD8 expression levels. *J Exp Medicine* 206: 2253–2269.
322. Apps, R., Y. Qi, J. M. Carlson, H. Chen, X. Gao, R. Thomas, Y. Yuki, G. Q. D. Prete, P. Goulder, Z. L. Brumme, C. J. Brumme, M. John, S. Mallal, G. Nelson, R. Bosch, D. Heckerman, J. L. Stein, K. A. Soderberg, M. A. Moody, T. N. Denny, X. Zeng, J. Fang, A. Moffett, J. D. Lifson, J. J. Goedert, S. Buchbinder, G. D. Kirk, J. Fellay, P. McLaren, S. G. Deeks, F. Pereyra, B. Walker, N. L. Michael, A. Weintrob, S. Wolinsky, W. Liao, and M. Carrington. 2013. Influence of HLA-C expression level on HIV control. *Science* 340: 87–91.
323. Murray, J. A., S. B. Moore, C. T. van Dyke, B. D. Lahr, R. A. Dierkhising, A. R. Zinsmeister, L. J. Melton, C. M. Kroning, M. El-Yousseff, and A. J. Czaja. 2007. HLA DQ gene dosage and risk and severity of celiac disease. *Clin Gastroenterol H* 5: 1406–1412.
324. Boon, A. C. M., G. de Mutsert, R. A. M. Fouchier, K. Sintricolaas, A. D. M. E. Osterhaus, and G. F. Rimmelzwaan. 2004. Preferential HLA usage in the influenza virus-specific CTL response. *J Immunol* 172: 4435–4443.

325. Boon, A. C. M., G. de Mutsert, Y. M. F. Graus, R. A. M. Fouchier, K. Sintnicolaas, A. D. M. E. Osterhaus, and G. F. Rimmelzwaan. 2002. The magnitude and specificity of influenza A virus-specific cytotoxic T lymphocyte responses in humans is related to HLA-A and -B phenotype. *J Virol* 76: 582–590.
326. Lauer, G. M., K. Ouchi, R. T. Chung, T. N. Nguyen, C. L. Day, D. R. Purkis, M. Reiser, A. Y. Kim, M. Lucas, P. Klenerman, and B. D. Walker. 2002. Comprehensive analysis of CD8+ T cell responses against hepatitis C virus reveals multiple unpredicted specificities. *J Virol* 76: 6104–6113.
327. Kägi, D., B. Ledermann, K. Bürki, R. M. Zinkernagel, and H. Hengartner. 1996. Molecular mechanisms of lymphocyte-mediated cytotoxicity and their role in immunological protection and pathogenesis *in vivo*. *Annu Rev Immunol* 14: 207–232.

## 8. Appendices

### 8.1. Peptides

Lyophilised peptides (Genscript Biotech Corp, Nanjing, China) had a minimum purity of 70%, and were reconstituted to 100 $\mu$ M in HBSS and stored at -80°C until use (**Table 17**).

**Table 17:** Peptides used in the studies described in this thesis.

Abbreviation	Protein	Amino acid sequence	MHC Restriction
NP <sub>366-374</sub>	Nucleoprotein	ASNENMETM	H-2D <sup>b</sup>
PA <sub>224-233</sub>	Acidic polymerase	SSELENFRAYV	H-2D <sup>b</sup>
PB1 <sub>703-711</sub>	Polymerase subunit B1	SSYRRPVGI	H-2K <sup>b</sup>
PB1-F2 <sub>62-70</sub>	Polymerase subunit B1 – Frameshift 2	LSLRNPILV	H-2D <sup>b</sup>
NS2 <sub>114-120</sub>	Non-structural protein 2	RTFSFQLI	H-2K <sup>b</sup>
Ova <sub>257-263</sub>	Ovalbumin	SIINFEKL	H-2K <sup>b</sup>

## 8.2. Antibodies

Rat anti-mouse monoclonal antibodies used in this study for flow cytometry are listed below (**Table 18**).

**Table 18:** Mouse-specific antibodies used for flow cytometry analyses

Antibody	Clone	Fluorophore conjugate	Manufacturer
Anti-B220	RA3-6B2	FITC, Pacific Blue	eBioscience
Anti-BrdU	BU20A	FITC	Invitrogen
Anti-CD3	145-2C11	BV711	BD
Anti-CD4	GK1.5	AF700, PerCP-Cy5.5, BUV395	BD
Anti-CD5	REA421	PerCP-Vio700	Miltenyi Biotech
Anti-CD8 $\alpha$	53-6.7	BUV395, Pacific Blue, PE	Biolegend
Anti-CD8 $\beta$	53-5.8	PE-Cy7	Biolegend
Anti-CD11a	2D7	PE-Cy7	Biolegend
Anti-CD11b	M1/70	FITC, Pacific blue	eBioscience
Anti-CD11c	N418	FITC, Pacific blue	eBioscience
Anti-CD19	6D5	Pacific Blue	Biolegend
Anti-CD44	IM7	APC-Cy7, PE-Cy7	BD
Anti-CD49d	R1-2	AF647	Biolegend
Anti-CD62L	MEL-14	BV570, FITC	BD
Anti-CD103	2E7	APC	Biolegend
Anti-CD122	TM-b1	PE	BD
Anti-CD127	A7R34	PE	eBioscience
Anti-F4/80	BM8	FITC, Pacific Blue	eBioscience
Anti-Granzyme B	GB11	AF647	Biolegend
Anti-H-2D <sup>b</sup>	KH95	FITC, PE	Biolegend
Anti-H-2K <sup>b</sup>	AF6-88.5	FITC, PE	Biolegend
Anti-H-2K <sup>b</sup> :SIINFEKL	25-D1.16	PE-Cy7	eBioscience
Anti-I-A <sup>b</sup>	AF6-120.1	FITC, Pacific Blue	BD
Anti-IFN $\gamma$	-	FITC	BD
Anti-IL-2	-	PE	BD
Anti-KLRG1	2F1	FITC	eBioscience
Anti-Ly49C//F/H	14B11	FITC	eBioscience
Anti-NK1.1	PK136	FITC, Pacific Blue	BD

*Appendices*

Anti-TCRbeta	H57-597	APC-Cy7	BD
Anti-TNF	MP6-XT22	APC	Biolegend
Anti-PD1	29.F.1A12	PerCP-Cy5.5	Biolegend
Anti-Vβ2	B20.6	FITC, PE	BD
Anti-Vβ3.1	KJ25	FITC, PE	BD
Anti-Vβ4	KT4	FITC, PE	BD
Anti-Vβ5.1, 5.2	MR9-4	FITC, PE	BD
Anti-Vβ6	RR4-7	FITC, PE	BD
Anti-Vβ7	TR310	FITC, PE	BD
Anti-Vβ8.1, 8.2	MR5-2	FITC, PE	BD
Anti-Vβ8.3	1B3.3	FITC, PE	BD
Anti-Vβ9	MR10-2	FITC, PE	BD
Anti-Vβ10	B21.5	FITC, PE	BD
Anti-Vβ11	RR3-15	FITC, PE	BD
Anti-Vβ12	MR11-1	FITC, PE	BD
Anti-Vβ13	MR12-3	FITC, PE	BD
Anti-Vβ14	14-2	FITC, PE	BD
Anti-Vβ17	KJ23	FITC, PE	BD

### 8.3. Medias and Buffers

#### **Complete Roswell Park Memorial Institute media (cRPMI)**

RPMI 1640 media (Gibco) supplemented with 10% FCS, 2mM L-glutamine, 1mM MEM sodium pyruvate, 100µM MEM non-essential amino acids, 5mM HEPES buffer solution, 55µM 2-mercaptoethanol, 100U/mL penicillin (all Gibco) and 100µg/mL streptomycin (Invitrogen).

#### **Complete Dulbecco's Modified Eagle's Medium (cDMEM)**

DMEM media (Gibco) supplemented with 10% FCS, 2mM L-glutamine, 1mM MEM sodium pyruvate, 100µM MEM non-essential amino acids, 5mM HEPES buffer solution, 55µM 2-mercaptoethanol, 100U/mL penicillin (all Gibco) and 100µg/mL streptomycin (Invitrogen).

#### **Complete Iscove's Modified Dulbecco's Medium (cIMDM)**

IMDM media (Gibco) supplemented with 10% FCS, 2mM L-glutamine, 1mM MEM sodium pyruvate, 100µM MEM non-essential amino acids, 5mM HEPES buffer solution, 55µM 2-mercaptoethanol, 100U/mL penicillin (all Gibco) and 100µg/mL streptomycin (Invitrogen).

#### **Fc Block**

2.4G2 supernatant (**Section 2.5.1**) with 1% normal mouse serum and 1% normal rat serum (Stem cell technologies, Vancouver, Canada). Fc block was diluted 1:2 in MACS buffer for use.

### **Hanks buffered salt solution (HBSS)**

HBSS was purchased from the Media Preparation Unit from the Biomedicine Discovery Institute at Monash University, Clayton campus.

### **Lung digestion media**

Lung digest media was made with 2.5mg/mL of Type I collagenase (Gibco) and 105U/mL of recombinant DNase I (Sigma-Aldrich) in RPMI-1640 media.

### **MACS buffer**

PBS with 0.5% BSA and 2mM EDTA.

### **Red Blood Cell Lysing Buffer Hybri-Max™**

Red blood cell lysing buffer Hybri-Max™ was purchased from Sigma-Aldrich (St. Louis, Missouri, USA).

### **70% Percoll density gradient media**

70% Percoll density gradient media was made with 63% Percoll® (Sigma-Aldrich), 7% 10x PBS, 30% 1x PBS and 2mM EDTA.

## 8.4. PCR Primers for Multiplex RT-PCR

Primers directed against the mouse TCR sequence were previously designed and described (Table 19, 16). All primers were synthesized by Sigma-Aldrich and reconstituted to a final concentration of 5pmol/μL in Ultrapure Distilled Water (Invitrogen) and stored at -20°C until use.

**Table 19:** Mouse multiplex primer sequences for amplifying the CDR3 $\alpha$  region by single-cell multiplex RT-PCR<sup>1</sup>.

Primer	External Forward <sup>2</sup>	Internal Forward <sup>2</sup>
TRAV1	GCACATACAGCACCTCAG	AACGTGAAGGCCAAGC
TRAV2	CCACCAGGGACCACAG	ACTCTGAGCCTGCCCT
TRAV3	GGCGAGCAGGTGGAG	GCCCTCCTCACCTGAG
TRAV4	TCTGSTCTGAGATGCAATTTT	GGITIMAGGAACAAAGGAGAAT
TRAV5-1/5-4(D)	CTTCCYTTGGTATAAGCAAGA	ATYCGTTCAAATATGGAAAGAAA
TRAV6-1/6-2	CAGATGCAAGGTCAAGTGAC	GGAGAAGGTCCACAGCTC
TRAV6-3/6-4	AAGGTCCACAGCTCCTTC	CAACTGCCAACAACAAGG
TRAV6(D)-5	CTTCTCTGACTGTGAACTGTTC	CAGTACCCAACCCTGTTCTG
TRAV6-6	AGATTCCGTGACTCAAACAG	ACGGCTGGCCAGAAG
TRAV6(D/N)-7	GCCTCAAGGGACAAAGAG	AAAGGAAGCAGCAGAGG
TRAV7	AGAAGGTRCAGCAGAGCCCAGAATC	CAKGRCYTCYYTCAACTGCAC
TRAV8	TGAAAYTGYAGTTACAAGAC	TAATCTTAATACGTTCAAATGAG
TRAV9	CTCKSTGSAGCTGAGATGCAA	CAGYTKCTCCTCAAGTACTAT
TRAV10	GGAGAGAAGGTTCGAGCAAC	GAGGGAGACAGCGCTG
TRAV11	AAGACCCAAGTGGAGCAG	AACAGGACACAGGCAAAG
TRAV12	GACCCAGAMRGAAGGCCTG	GCTGAACWGCACCTATCAG
TRAV12-4	GGGAGGAGCAATGGAGATGG	CAGTGACCCAGAAGGAAGG
TRAV13	TCCTTGTTCTGCAGG	TGCAGTGGTTTTACCAA
TRAV14	GCAGCAGGTGAGACAAAG	CTCTGACAGTCTGGGAAGG
TRAV15	CTGSAYTGTTTCATATRAGACAAGT	TTAGTGGAGAGATGGTTTT
TRAV16	GTACAAGCAAACAGCAAGTG	ATTATTCTCTGAACTTTCAGAAGC
TRAV17	CAGTCCGTGGACCAGC	TATGAAGGAGCCTCCCTG
TRAV18	CAAGATTTCACTGCACG	TACTGGTACCGACAGGTC
TRAV19	CAAGTTAAACAAAGCTCTCCATC	GCTGACTGTTCAAGAGGGA
TRAV21	GTGCACTTGCCCTGTAGC	AATAGTATGGCTTTCCTGGC
Primer	External Reverse <sup>2</sup>	Internal Reverse <sup>2</sup>
TRAC	GGCATCACAGGGAACG	GCACATTGATTTGGGAGTC

<sup>1</sup> Primer sequences were obtained from (179).

<sup>2</sup> Primer sequences are 5' → 3'

*Appendices*

**Table 20:** Mouse multiplex primer sequences for amplifying the CDR3 $\beta$  region by single-cell multiplex RT-PCR<sup>1</sup>.

<b>Primer</b>	<b>External Forward<sup>2</sup></b>	<b>Internal Forward<sup>2</sup></b>
TRBV1	TACCACGTGGTCAAGCTG	GTATCCCTGGATGAGCTG
TRBV2	CAGTATCTAGGCCACAATGC	GGACAATCAGACTGCCTC
TRBV3	CCCAAAGTCTTACAGATCCC	GATATGGGGCAGATGGTG
TRBV4	GACGGCTGTTTTCCAGAC	CAGGTGGGAAATGAAGTG
TRBV5	GGTATAAACAGAGCGCTGAG	GCCAGAGCTCATGTTTCTC
TRBV12	GGGGTTGTCCAGTCTCC	CCAGCAGATTCTCAGTCC
TRBV13	GCTGCAGTCACCCAAAG	GTA CTGGTATCGGCAGGAC
TRBV14	GCAGTCCTACAGGAAGGG	GGTATCAGCAGCCCAGAG
TRBV15	GAGTTACCCAGACACCCAG	GTGTGAGCCAGTTTCAGG
TRBV16	CCTAGGCACAAGGTGACAG	GAAGCAACTCTGTGGTGTG
TRBV17	GAAGCCAAACCAAGCAC	GAACAGGGAAAGCTGACAC
TRBV19	GATTGGTCAGGAAGGGC	GGTACCGACAGGATTCAG
TRBV20	GGATGGAGTGTCAAGCTG	GCTTGGTATCGTCAATCG
TRBV23	CTGCAGTTACACAGAAGCC	GCCAGGAAGCAGAGATG
TRBV24	CAGACTCCACGATACCTGG	GCACACTGCCTTTTACTGG
TRBV26	GGTGAAAGGGCAAGGAC	GAGGTGTATCCCTGAAAAGG
TRBV29	GCTGGAATGTGGACAGG	GTA CTGGTATCGACAAGACCC
TRBV30	CCTCCTCTACCAAAGCC	GGACATCTGTCAAAGTGGC
TRBV31	CTAACCTCTACTGGTACTGGCAG	CTGTTGGCCAGGTAGAGTC
<b>Primer</b>	<b>External Reverse<sup>2</sup></b>	<b>Internal Reverse<sup>2</sup></b>
TRBC	CCAGAAGGTAGCAGAGACCC	CCTCCTTGCCATTCACCCAC

<sup>1</sup> Primer sequences were obtained from (179).

<sup>2</sup> Primer sequences are 5' → 3'

## 8.5. Alloreactive H-2D<sup>b</sup>PA<sub>224</sub>-specific TCR sequences from H-2D<sup>b/-</sup> mice

**Table 21:** *Ex vivo* analysis of paired and unpaired TCR CDR3 amino acid residues from naïve H-2D<sup>b</sup>PA<sub>224</sub>-specific CD8 T cells from H-2D<sup>b/-</sup> mice (M1-M6). Data was generated and reproduced from my BSc. (Hons) work for the purpose of this current study.

TRBV	CDR3β	TRBJ	Length aa	TRAV	CDR3α	TRAJ	Length aa	Frequency <sup>1</sup>					
								M 1	M 2	M 3	M 4	M 5	M 6
2	SQEWQGTNTEV	1-1	11	7	LSNYNVL	21	7	1	-	-	-	-	-
2	SQDWTYEQ	2-7	8	12	SVGSGGSNYKL	53	11	-	-	1	-	-	-
2	SQELGGLAEQ	2-1	10	12	TGNNYAQGL	26	9	-	-	-	-	1	-
4	RQYEQ	2-7	5	9	SQNYNQGKL	23	9	1	-	-	-	-	-
12	SPPDWGAPETL	2-3	11	3	SGTGGYKV	12	8	-	-	1	-	-	-
12	SRQGNSDY	1-2	8	14	SASYGNEKI	18	9	-	-	-	-	-	1
12	SLGLGQDTQ	2-5	9	19	GSNYGNEKI	48	9	-	1	-	-	-	-
13	SETGANGQL	2-2	9	9	SPYNYAQGL	26	9	-	-	-	-	1	-
14	RDYAEQ	2-1	6	6	GDPGTNTGKL	27	10	-	-	-	1	-	-
15	SLAMHEQ	2-7	7	6	GEGAGNKL	17	8	-	-	-	-	-	1
16	SLEGLAGDTL	2-4	10	13	GNNYAQGL	26	8	-	-	1	-	-	-
19	SIGGAV	1-1	6	12	STSSGQKL	16	8	-	-	-	-	1	-
20	REGSPSYEQ	2-7	9	16	REDSGYNKL	11	9	-	-	-	1	-	-
23	SQGIDAETL	2-3	9	7	SNMGYKL	9	7	1	-	-	-	-	-
29	WGSSYEQ	2-7	7	6	GDGSNYQL	33	8	-	-	-	-	-	1
29	SFGDTV	1-4	6	6	GDSGSWQL	22	8	-	-	1	-	-	-
29	WGYEQ	2-7	5	6	SGGSNYKL	53	8	-	-	1	-	-	-
29	SSSGGYTEV	1-1	9	10	PSSGSWQL	22	8	-	-	-	-	-	1
2	SQELGGSSYEQ	2-7	11					-	-	1	-	-	-
3	GDRGLEQ	2-7	7					-	-	1	-	-	-
3	SAGQDYEQ	2-7	8					-	-	1	-	-	-
12	SHTEV	1-1	5					-	-	1	-	-	-
12	SLSGRRRAEQ	2-1	10					-	-	1	-	-	-
12	SLPGSYAEQ	2-1	9					-	-	-	-	-	1
13	LGRARQDTQ	2-5	9					-	-	1	-	-	-
13	SDKAWGSAETL	2-3	11					-	-	1	-	-	-
13	SDWGGGAEQ	2-1	9					-	-	-	-	-	1
29	WGYEQ	2-7	5					-	-	1	-	-	-
31	TLWGGAGAETL	2-3	11					-	-	1	-	-	-
				6	SDGGNMGYKL	9	10	-	-	-	-	-	1
				6	GDPGSGWQL	22	9	-	-	-	1	-	-

\* Sequence in red was selected for *in vitro* expression.